



The Growth and Evolution of Polygonal fault tiers

Daniel Ashley Morgan

Submitted in partial fulfilment of the requirements for the degree of PhD

School of Earth and Ocean Sciences,
Cardiff University

DECLARATION

This work has not been submitted in substance for any other degree or award at this or any other university or place of learning, nor is being submitted concurrently in candidature for any degree or other award.

Signed (candidate) Date

STATEMENT 1

This thesis is being submitted in partial fulfillment of the requirements for the degree of PhD

Signed (candidate) Date

STATEMENT 2

This thesis is the result of my own independent work/investigation, except where otherwise stated.

Other sources are acknowledged by explicit references. The views expressed are my own.

Signed (candidate) Date

STATEMENT 3

I hereby give consent for my thesis, if accepted, to be available online in the University's Open Access repository and for inter-library loan, and for the title and summary to be made available to outside organisations.

Signed (candidate) Date

STATEMENT 4: PREVIOUSLY APPROVED BAR ON ACCESS

I hereby give consent for my thesis, if accepted, to be available online in the University's Open Access repository and for inter-library loans **after expiry of a bar on access previously approved by the Academic Standards & Quality Committee.**

Signed (candidate) Date

Dedicated to my Parents and Siblings,

Irrepressible and tenacious, a source of inspiration and motivation during this piece
of work. The masters of getting shit done.

Adfyd a ddwg wybodaeth, a gwybodaeth ddoethineb.

Acknowledgements

This PhD has been the subject of my attention for the last three and a half years and has been the making of me as an individual. There are a huge number of people that I want to thank for all their help and support.

Firstly, I wish to thank my supervisor, Joe. You took a chance on me when I emailed you back in 2010 asking about some coal based research (quite how we got from coal to polygonal faulting is still a mystery!). You kept me on when the coal project collapsed and have made me into the scientist I am today. I also want to say massive thank you to my partner Rachel and my family for the motivation, encouragement, and occasional kick up the arse when needed! None of this would be possible without you and I am truly blessed to have you all in my life. Even if I am a gravel monkey...

I have met a number of awesome people along the way, too many to mention in one page. I would like to thank Gwen Pettigrew, Chris Wild, Alodie Bubeck, Ben Manton, Davide Gamboa, Ana Maia, Iqbal Hajana, Olluchi and all my office mates and fellow PhD students for the fieldwork, the nights out, the guidance, the laughs and for generally making the 3D lab and Cardiff a great place to work. I also would like to thank Tom Blenkinsop and Tiago Alves for the proof reading and guidance on matters geological and PhD in the last eighteen months, your input and help really got me over the finish-line.

I was also fortunate enough to do some teaching at Cardiff and in USW. I want to thank Ian Skilling, Rich Walker and Richard Lisle for the opportunity and a big thank you to all the guys I taught for putting up with my droning on, I learnt a lot from the experience and it has made me a better geologist and was immense fun to be involved with.

Gorau adnabod, d'adnabod dy hun

Thesis Abstract

Polygonal faults are layer-bound arrays of normal faults confined to specific stratigraphic intervals called tiers. Typically hosted in fine-grained sediments, polygonal faults are thought to have the potential for fluid leakage and represent a potential seal bypass mechanism. Integral to understanding the impact of polygonal faults on regional top seal is timing and evolution of polygonal fault tiers. Whilst there are numerous studies imaging and describing polygonal faults in numerous basins around the world, very few specifically consider the growth of polygonal faults. Additionally, very few polygonal fault studies examine the evolution of fault hierarchies and how these hierarchies accommodate strain and deformation within the tier.

This study examines two wedge-shaped polygonal fault tiers on different passive margins. The first polygonal fault tier studied is from offshore Angola and is hosted in sediment thickness of less 500 m, in Plio-Pleistocene claystones. The second tier examined is from the Modgunn Arch, Norwegian Margin and is hosted in a sequence of siliceous oozes and claystones of Eocene to Pliocene age, up to 1200 m in thickness. This study uses the differences in sediment ages to compare and contrast polygonal fault tiers at different stages of evolution and aims to examine common features between young and mature tiers in order to constrain tier evolution.

This study considers two aspects of polygonal fault growth. Firstly it considers the utility of perturbations in polygonal fault tiers around features of the base of the tier. These perturbations have the potential to be a useful proxy for elucidating the nucleation position of polygonal faults in the tier. The second aspect of polygonal fault tier evolution reviews the mechanisms that control organisation hierarchies within a tier and examines the role of linkage in creating large master polygonal faults.

The results of this thesis show that the polygonal faults can initiate at low temperatures and low pressures, in sediment thickness of 100 m or less. Moreover, it can be demonstrated that polygonal fault tips propagate preferentially upwards with basal tips pinned by a mechanical boundary at the base of the tier and lateral tips pinned by early forming branchline intersections. The transition from shallow to deep burial shows that polygonal fault hierarchies are naturally forming and may relate to variation in the propagation rate of polygonal faults within the tier. With increasing burial, there

is an increased likelihood of branchline interaction. Branchline interaction can occur laterally with lateral tips abutting against other faults in the network. Vertical abutments occur where upwardly propagating tips interact to form triangular abutments and are a key mechanism forcing in the organisation of polygonal faults and growth of Master faults. Both abutment styles also impact the spatial distribution of displacement maxima. Polygonal fault tiers also show subtle spatial variability in orientation and linkage mechanisms that can be attributed to the distribution and magnitude of far field stresses as well as the early fault dimensions. This thesis also presents a primie facie case for diachrony in polygonal fault growth driven by variations in sediment loading and branchline linkage complexity. Overall, this thesis describes and accounts for some key behaviours of incipient polygonal faults tiers.

Contents

1	Introduction.....	1
1.1	Rationale	2
1.2	Polygonal fault growth and evolution	2
1.2.1	Polygonal fault genesis mechanisms.....	3
1.2.2	The evolution of polygonal fault tiers	11
1.2.3	Interaction between polygonal faults and topographic features.....	18
1.3	Aims of the thesis	23
1.4	Thesis structure	24
2	Database and Methods.....	26
2.1	Introduction.....	27
2.2	3D Seismic data	27
2.2.1	<i>Data acquisition.....</i>	27
2.2.2	<i>Data processing</i>	29
2.2.3	<i>Wavelet polarity, phase and seismic resolution</i>	31
2.2.4	<i>Geophysics of studied datasets</i>	35
2.3	Seismic mapping.....	36
2.3.1	<i>Horizon picking methodology</i>	36
2.3.2	<i>ASAP picking technique</i>	36
2.4	Analytical techniques.....	39
2.4.1	<i>The polygonal fault problem</i>	39
2.4.2	<i>Statistical analysis.....</i>	50
3	Regional Geology	51
3.1	Offshore Angola	52
3.1.1	<i>Basin Evolution</i>	52
3.1.2	<i>The structural evolution of the Lower Congo Basin</i>	56
3.1.3	<i>Occurrences of polygonal faults on the West African margin</i>	59
3.2	Norwegian Margin	61
3.2.1	<i>Structural evolution of the Vøring and Møre basins</i>	61
3.2.2	<i>Post rift sedimentation and tectonic inversion</i>	66
3.2.3	<i>Distribution of polygonal faults on the Norwegian Margin.....</i>	69
4	The controls on the development of Master polygonal faults within a single polygonal fault tier	71
4.1	Introduction.....	72
4.2	Regional seismic stratigraphy	74
4.2.1	Rogaland Group (H10-H9)	74
4.2.2	Brygge Fm. (H9-H4).....	74

4.2.3	Kai Formation (H4-H1)	76
4.3	Fault populations of the Modgunn Arch region.....	76
4.3.1	Displacement Distributions.....	78
4.3.2	Fault populations.....	82
4.3.3	Preferred orientation of polygonal faults	85
4.4	Discussion.....	87
4.4.1	Timing polygonal fault growth	87
4.4.2	Evolution of Master polygonal faults.....	90
4.5	Conclusions.....	94
5	The thin end of the wedge: determining early polygonal fault growth and tier evolution from shallowly buried polygonal faults	96
5.1	Introduction.....	97
5.2	Seismic stratigraphy	99
5.2.1	Reflection units	99
5.2.2	Sedimentation rates	99
5.3	PFS in a wedge shape geometry.....	102
5.3.1	The geometry and evolution of polygonal fault hosting body	102
5.3.2	The geometry of the polygonal fault tier.....	106
5.3.3	Polygonal fault displacement	114
5.4	Discussion.....	122
5.4.1	Polygonal fault nucleation	122
5.4.2	Blind or syn-sedimentary growth in polygonal fault tiers?.....	130
5.4.3	Kinematic evidence for polygonal fault propagation.....	131
5.4.4	Polygonal fault organisation	132
5.4.5	Tier boundaries	134
5.5	Conclusions.....	137
6	The origin of radial polygonal faults around hydrothermal vent complexes	139
6.1	Introduction.....	140
6.2	Results: Radial faults around HTVC's	144
6.2.1	Interpretation of BR1	144
6.2.2	Morphology of the mounded structures on the tier base horizon.....	148
6.2.3	Impact of the HTVCs on nearby faults	153
6.3	Discussion.....	159
6.3.1	Radial fault formation through differential compaction	164
6.4	Conclusions.....	172
7	Origin of concentric fault patterns around pockmarks and the implications for polygonal fault growth.....	173
7.1	Introduction.....	174

7.2	Geological Background.....	175
7.2.1	Seismic stratigraphy	175
7.2.2	Pockmarks near the base of the polygonal fault tier	177
7.3	Polygonal fault patterns.....	182
7.3.1	Plan view expression of ‘background’ polygonal faults	182
7.3.2	‘Background’ polygonal faults in cross section	183
7.4	Discussion.....	193
7.4.1	Evidence for early nucleation	193
7.4.2	Stress anisotropy due to buried pockmarks.....	196
7.4.3	Implications for polygonal fault growth	199
7.5	Conclusions.....	201
8	Discussion.....	203
8.1	Introduction.....	204
8.2	The significance of small-scale perturbation patterns in polygonal fault tiers	204
8.2.1	<i>Sources of anisotropy.....</i>	205
8.3	Nucleation and evolution of tiers	207
8.3.1	<i>Nucleation</i>	209
8.3.2	<i>Tier boundaries</i>	214
8.3.3	<i>Tier boundary classification</i>	219
8.3.4	<i>Polygonal fault scaling</i>	224
8.4	Polygonal fault tier evolution.....	229
8.4.1	<i>Stage 1: Growth</i>	229
8.4.2	<i>Stage 2: Restriction</i>	232
8.4.3	<i>Stage 3: Break-out</i>	232
9	Conclusions.....	235
9.1	Introduction.....	236
9.2	The interaction between polygonal faults and features at the base of the tier.	236
9.3	Propagation and organisation of polygonal faults	237
9.4	Fault Organisation	238
9.5	Recommendations for future work	239
References.....		240

1 Introduction

1.1 Rationale

Polygonal faults are arrays of layer-bound, normal faults that form laterally extensive arrays (Cartwright, 2011). Polygonal fault arrays have been found in numerous 3D surveys (Cartwright, 2011) from all over the world and now in outcrop (Tewksbury et al., 2014) (Fig. 1.1). The origins of polygonal faults are widely accepted to be non-tectonic (Cartwright et al., 2003), and the mechanism that forms them has been widely debated (see section 1.2.1 for summary). The term ‘tier’ was first ascribed to polygonal faults to describe the layer bound geometry of non-tectonic normal faults by Cartwright (1994). The term, tier, refers to a cross sectional view through a polygonal fault network whereby the polygonal faults are constrained to a particular sequence of reflections. The concept of polygonal fault tiers, although widely used, has not been rigorously investigated. The studies that do examine tiers examine the impact of sand within the tier facies and have since suggested that polygonal fault tiers may be defined in part, by lithological variation. Many examples have shown polygonal faults can be influenced by the presence of deep marine sand channels (Cartwright, 2011; Jackson et al., 2014; Lonergan and Cartwright, 1999; Möller et al., 2004), changes in clay mineralogy (Cartwright and Dewhurst, 1998; Dewhurst et al., 1999) and by transitions from clay to limestone (Ostanin et al., 2012). The work on the interaction between polygonal faults and sandstone channels is of particular interest. The work of Jackson et al. (2014) and Cartwright (2011) suggests that polygonal faults decouple where sands are present. In contrast, Cartwright and Lonergan (1999) and Möller et al. (2004) suggest that polygonal faults can help to not only constrain the position where channels form, but also aid in the erosion of the banks. A review by Cartwright (2011) takes the term tier a stage further by providing schematic diagrams of an idealised, complex and wedge shaped tier as well as suggesting a fault hierarchy.

There are several very pronounced gaps within polygonal fault literature. To date, no study has explicitly considered the growth of polygonal faults, in particular the relative timing of when nucleation and growth occurs relative to the sediment thickness. Given that polygonal fault arrays are susceptible to changes in regional stress (e.g. Ostanin et al., 2012), local tectonic stress (e.g. Carruthers et al., 2013; Hansen et al., 2004) and stress generated around structures within the tier (e.g. Andresen and Huuse, 2011; Hansen et al., 2005; Imbert, 2009). Examination of the

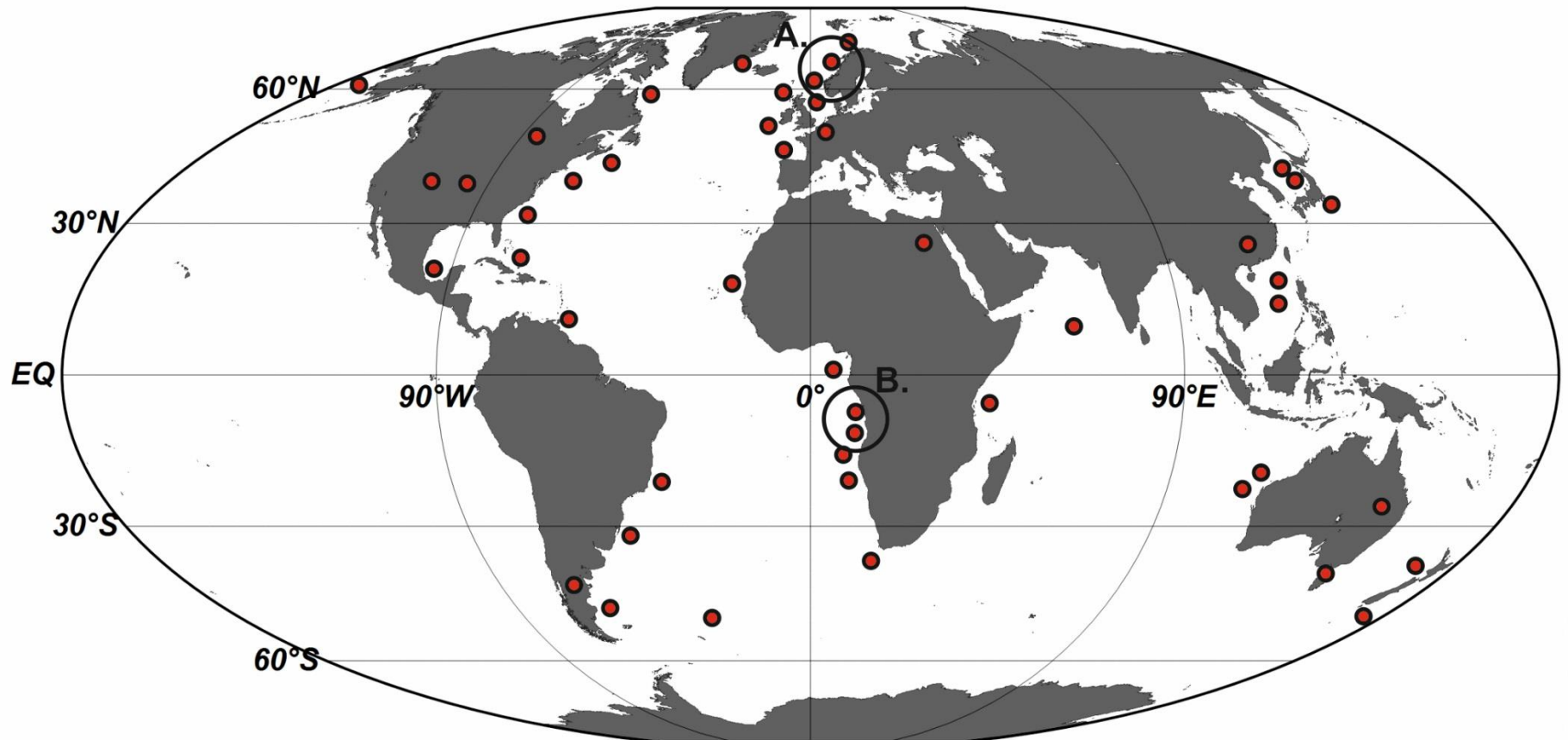


Figure 1.1: Global map showing the locations of polygonal fault arrays redrawn and updated from Cartwright, (2011). A and B refer to the locations of polygonal fault arrays studied in this thesis. The base map was produced from Ocean Data View 4, Schlitzer R., Ocean Data View, <http://odv.awi.de>, 2014.

stratigraphic position of fault pattern perturbations, as suggested in Cartwright (2011), could provide a useful proxy for constraining nucleation position and timing. Despite a wide range of studies conducted on polygonal fault arrays, no study has specifically considered the implications of perturbations of stress on timing the evolution of polygonal fault tier formation or for polygonal fault growth.

The temporo-spatial evolution of a polygonal tier, in particular the evolution of organisational hierarchies common within polygonal faults (see examples in Gay et al., 2004; Cartwright, 2011; Ostanin et al., 2012; Seebek et al., 2015) has not been considered. Additionally, the wedge shaped tier as a concept is somewhat misleading, as the ‘wedge shape’ depends largely on the scale on which the tier is imaged by the seismic survey and the directionality of the line of section. If a line was to be drawn parallel to the contours of a given wedge, the pattern geometry is likely to change to match either the ideal or complex tier geometry depending on the complexity of the planform pattern. There is also no clear definition as to what constitutes an upper and lower tier boundary, or indeed how contiguous the fault pattern has to be. Given that examples of polygonal fault patterns can extend for up to 2,000,000km² (Cartwright, 2011), it is likely that pattern changes over the areal extent are common. The presence of sub-tiers within a tier was suggested by Cartwright (1994) from the polygonal fault arrays in the Palaeogene of the North Sea and is yet to be investigated further.

This thesis aims to examine the evolution of fault organisation within polygonal fault tiers and examine the significance of local perturbation in polygonal fault patterns. These two aspects of polygonal fault tier development will give important clues about the evolution of polygonal fault tiers by constraining how much burial is needed to allow polygonal faults to nucleate in a sediment column, based on the relationship between perturbation patterns at the base of the tier and associated thickness changes over structures. By examining the impact that evolving mechanical conditions, such as changing regional stresses and diagenesis, have on tier development, this thesis will give important clues as to how polygonal fault hierarchies develop.

1.2 Polygonal fault growth and evolution

Polygonal fault arrays have been the subject of study for over twenty five years, yet despite this, there are still fundamental questions remaining regarding polygonal fault

tier formation. The proceeding section summarises the key findings of polygonal fault research since their first discovery through to the present day.

1.2.1 Polygonal fault genesis mechanisms

Polygonal fault genesis is the most widely studied and debated aspect of polygonal fault arrays. There are to date, six genesis mechanisms, the following sections examine the chronology of polygonal fault research, including their genesis mechanisms from first discovery to the modern day.

*1.2.1.1 *First discovery to the late 90's**

Polygonal fault arrays have been the subject of continued study for the last twenty years. The first study conducted on polygonal fault arrays (then termed layer-bound faults) was conducted by Henriet et al., (1991, 1989) on clay tectonic features in 2D seismic and outcrop in the Ypresian clays of Belgium and the southern North Sea. The origin of the clay tectonic features was attributed to density inversion where under-compacted and overpressured muds created a series of low amplitude folds, which in turn, create fractures and faults in sealing units that allow the overpressure to be released (Fig. 1.2). This release of overpressure and pore pressure collapse, compacts the previously overpressured clays. With the advent of 3D seismic data, polygonal faults were described in 3D seismic surveys from the North Sea (Cartwright, 1994a, 1994b). The genesis mechanism of these polygonal fault arrays was also attributed to overpressure release following hydrofracturing in the Lower Miocene sediments by a mechanism similar to that proposed by Henriet et al. (1989, 1991).

During the mid to late 1990s, polygonal fault genesis was attributed to volumetric contraction of sediments. Cartwright and Lonergan (1996) first suggested volumetric contraction based on radial line length restorations. These restorations showed that line balancing techniques for polygonal faults suggested a laterally isotropic strain. Cartwright and Lonergan, (1996) suggest that as polygonal fault arrays in the Lower Miocene of the North Sea are so pervasive, the mechanism to form them is internal, governed by pore fluid pressure increases or tensile stresses generated by pore

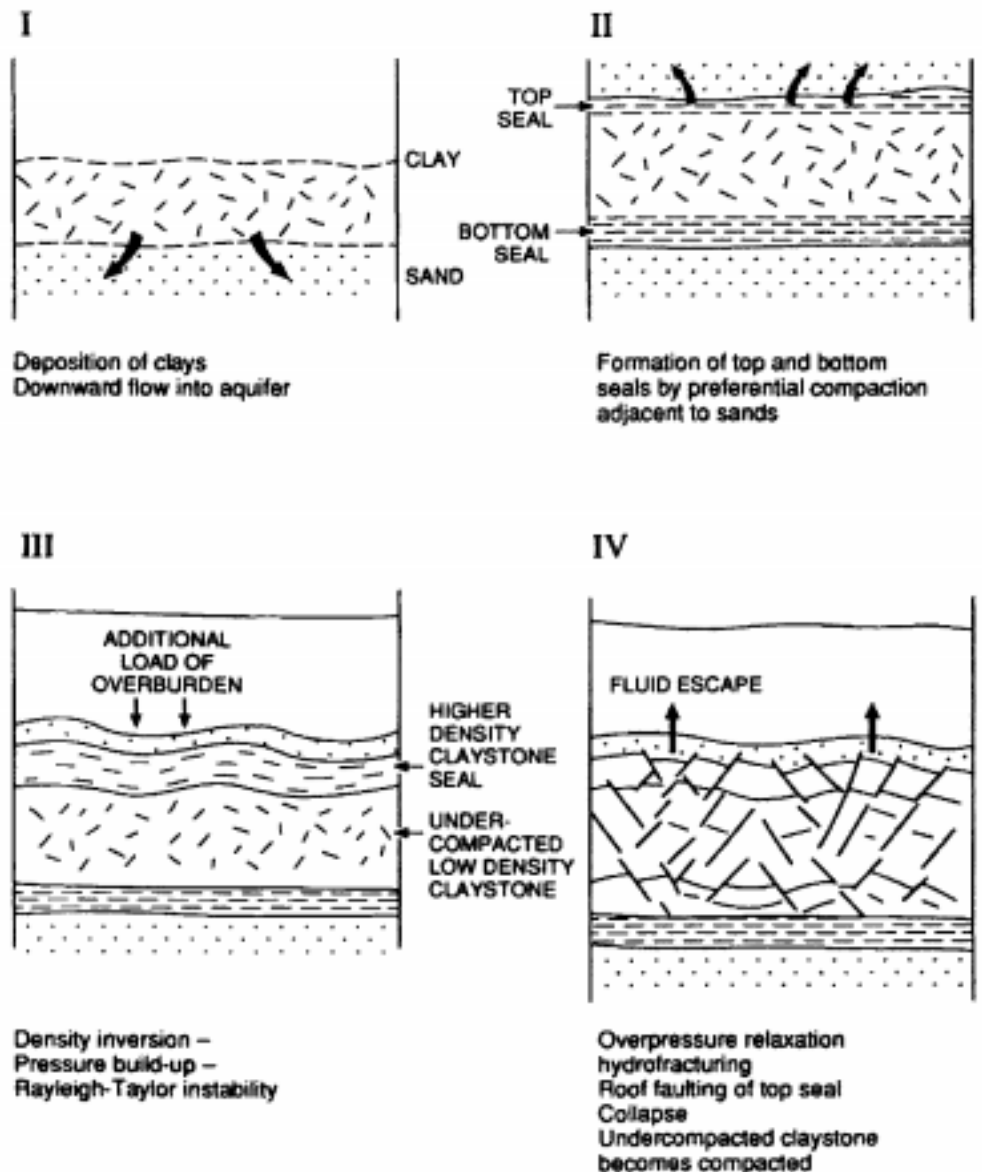


Figure 1.2: From Cartwright *et al.* (2003) a simplified sketch of the evolutionary diagram from Henriet *et al.* (1989). Stage I describes the deposition of clays, Stage II describes the sealing and pressure build-up. Stage III marks the onset of density inversion under loading. The final stage (Stage IV) overpressure is released by hydrofracturing and compaction of the clays.

pressure loss. Importantly, the conditions for polygonal faulting were not considered to be the result of far-field tectonic stress. Later work by Cartwright and Dewhurst, (1998) reviewed 28 examples of polygonal fault arrays using 2D and 3D seismic data. Cartwright and Dewhurst (1998) found that all polygonal fault arrays are found within ultra-fine to fine grained marine sediment sequences, rich in clay, with low porosity and high permeability. Further to this, Cartwright and Dewhurst (1998) conclude that type locations of North Sea, UK and Eromanga Basin, Australia, develop through a process of bed-length contraction termed syneresis (Fig. 1.3). Syneresis was the focus of a study by Dewhurst et al. (1999), who used both seismic and well data to reconcile the micro-scale variation in clay facies with the seismic expression of polygonal faults. Dewhurst et al. (1998) showed that the polygonal fault arrays in the North Sea are hosted within a smectite-rich sequence of rocks. Dewhurst et al. (1999) noted that high smectite percentages ($>60\%$) and large proportion of fine grain sizes (80% at $<2\mu\text{m}$), were coincident with regions of high strain in a polygonal fault tier.

1.2.1.2 Polygonal fault genesis 2000 to 2010

The polygonal fault genesis debate intensified during the early 2000s. A study by Watterson et al. (2000) studied a polygonal fault tier in an onshore survey in the Lake Hope region of Australia. Watterson et al. (2000) noted two important features in the survey; the presence of anticlinal folds in the hanging walls and synclinal folds in the footwalls of the polygonal faults cells and the low density zone at the base of the polygonal fault tier. The folds are contained within a fault ‘cell’ and are asymmetrical with the antiforms occupying 14% of the cell space. This geometry was suggested by Watterson et al. (2000) to be geometrically similar to density inversion structures in analogues on a variety of scales. Watterson et al. (2000) concluded that this observation coupled with the low-density layer are more indicative of a polygonal fault array generated by gravitational overturning as opposed to syneresis. The findings of this study were the subject of debate by James (2000), who suggested that the anticlinal folding is more suggestive of flexure between beds on a common hanging wall between conjugate faults, rather than being related to diapirism.

The polygonal fault genesis argument was further intensified by Goult, (2001a, 2001b). Goult (2001b) suggested that syneresis was not needed to explain genesis of polygonal fault arrays. The intrinsic mechanical properties of polygonal fault hosting lithologies is conducive to compaction failure as the fine-grained rocks and sediments

have exceptionally low coefficient of friction. Goult (2001a) summarises the early work of Cartwright and Dewhurst (1998) Dewhurst et al. (1999) and Watterson et al. (2000) and suggests that both density inversion and syneresis need not be invoked to explain polygonal faulting. Goult (2001a) suggests that polygonal faulting can be explained using 1D consolidation and soil mechanics. Goult (2001b) builds upon this and suggests a theoretical model using the Eocene London Clay as proxy to the Lower Tertiary units of the North Sea. Goult (2001b) demonstrates that the London Clay has a low angle of shearing resistance ($\varphi = <8^\circ$) and low residual shear resistance ($\mu_r = 0.14$). Goult (2001b) infers that sediments on a level surface, undergoing pure vertical compaction, with no horizontal strain (K_0) can reach the Mohr-Coulomb failure envelope and produce shear failure due to their intrinsically low mechanical strength. Goult (2001a, 2001b) did however concede that the mechanism only applied once fractures had developed. A review of polygonal fault genesis mechanisms by Cartwright et al. (2003) summarised the merits and caveats of all the leading polygonal fault genesis mechanisms including gravity sliding, density inversion, syneresis and gravitational loading. Cartwright et al. (2003) concluded that despite the differences between each mechanism, there were emerging themes of early development, compaction and pore fluid expulsion.

Two separate studies by Hibscher et al., (2003) and Hansen et al., (2004) demonstrated that polygonal faults could be hosted within chalks as well as within clays. Hibscher et al. (2003) reviewed a number of intra-formational structures within chalks of the Paris Basin, France and East Anglia, UK. These structures, in addition to being found exclusively within the chalk, exhibit a diverse range of fault and fracture strikes. Hibscher et al. (2003) propose that the observed deformation may be polyphase and explained by changing stress orientations through time or that the deformation is from a single phase of polygonal fault formation, driven by syneresis. Based on the layer bound nature of the structures and the multi azimuthal strikes, these chalk faults were tentatively compared with polygonal faults. A second seismic study also described polygonal faults in chalks from the Eastern Canadian margin (Hansen et al., 2004). Hansen et al. (2004) suggest that despite the variation in lithology between their study and the earlier work of Cartwright and Dewhurst (1998) and

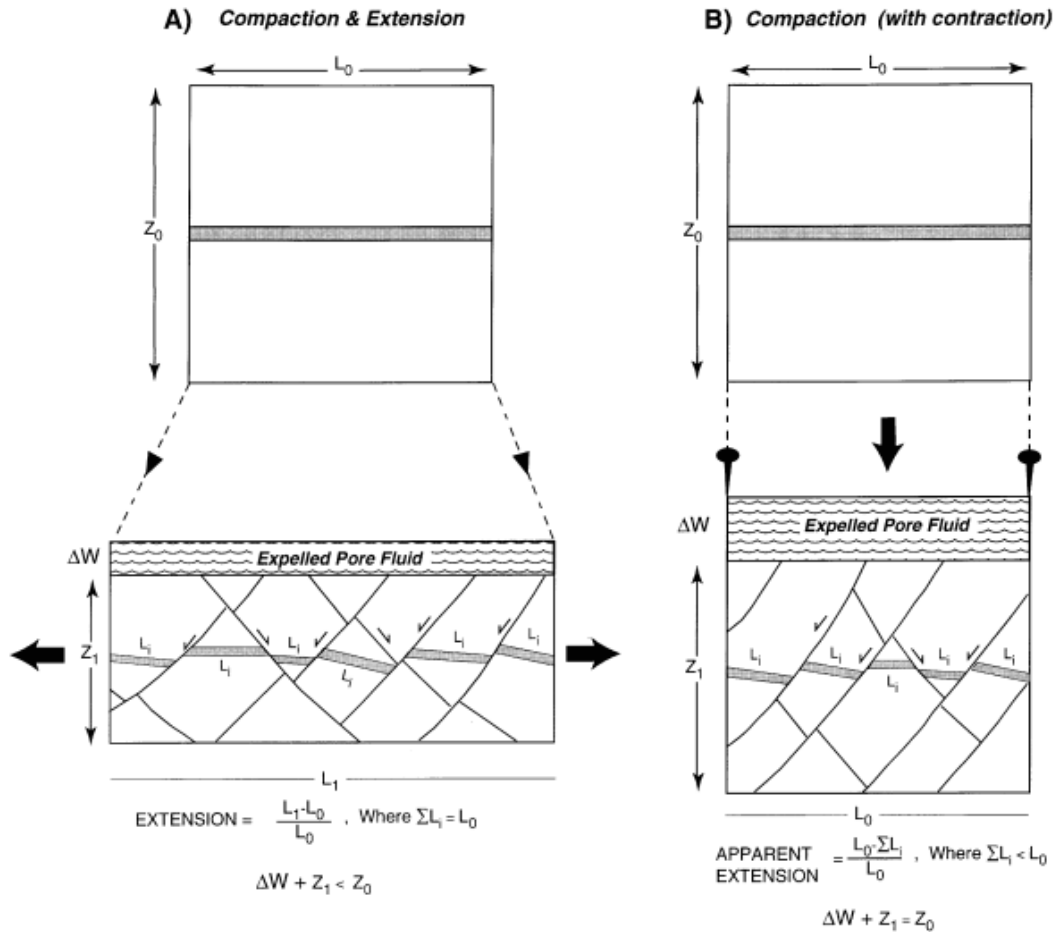


Figure 1.3: From Cartwright et al. (1996), a schematic diagram comparing two potential mechanisms to explain the deformation seen in Tertiary polygonal faults from the North Sea. Case A considers compaction and net extension and B compaction and contraction. As no extension is observed in the polygonal fault arrays of the North Sea the deformation can be accommodated by bed length contraction (syneresis).

Dewhurst et al. (1999), the presence of polygonal faults in chalks would suggest a common mechanism, in this case, a mechanism of syneresis. In an attempt to reconcile the debate between low coefficients of friction and syneresis, Goult and Swarbrick (2005) used geomechanical modelling to try to test how low coefficients of friction could cause polygonal faulting. Goult and Swarbrick (2005) used the formation integrity test to estimate the minimum horizontal stress value and used computer-modelled outputs from ShaleQuant, which reviews the wireline log responses, to estimate vertical stress from four wells in the North Sea. Goult and Swarbrick (2005) were able to estimate the ratio between vertical and horizontal stress (k) and demonstrate that the Tertiary clays in the tested wells have low coefficients of residual friction ($\mu_r = <0.13$). These low coefficients of friction are thought to be indicative of fault development. This work was critiqued by James (2006), who argued that estimating horizontal minimum stress from leak-off tests creates an over-estimation of K_0 values as leak-off tests were the result of overpressured horizons. James (2006) also suggests that polygonal fault growth occurs under shallow burial and so overpressure and pore pressure are likely to be reduced. James (2006) also critiques the use of K_0 as the polygonal faults accommodate strain internally through compaction and dilation around fault tips, the system cannot be considered ‘at rest’ as implied in K_0 conditions. Goult and Swarbrick (2006) counter the criticisms of James (2006) and assert that the leak-off test method is correct. Goult and Swarbrick (2006) agree that whilst polygonal fault initiation takes place at shallow depths, there was circumstantial evidence indicating polygonal fault activity at greater burial depths. Goult and Swarbrick (2006) also point out that nucleation and development can be separate processes operating in the subsurface. Furthermore, the values recorded by Goult and Swarbrick (2005) are representative of present day conditions that allow fault growth, and not initiation conditions.

In a review by Goult, (2008) all current polygonal fault initiation mechanisms were reviewed in light of prior studies (Gay et al., 2004; Hansen et al., 2004; Hibscher et al., 2003; Watrus et al., 2003), using syneresis or shrinkage as the initiation mechanism in polygonal faults. Goult (2008) notes that whilst syneresis has been observed in a variety of lithofacies and water salinities, laboratory experiments of syneresis in clays, show that syneresis occurs in clays with very high porosities and where there

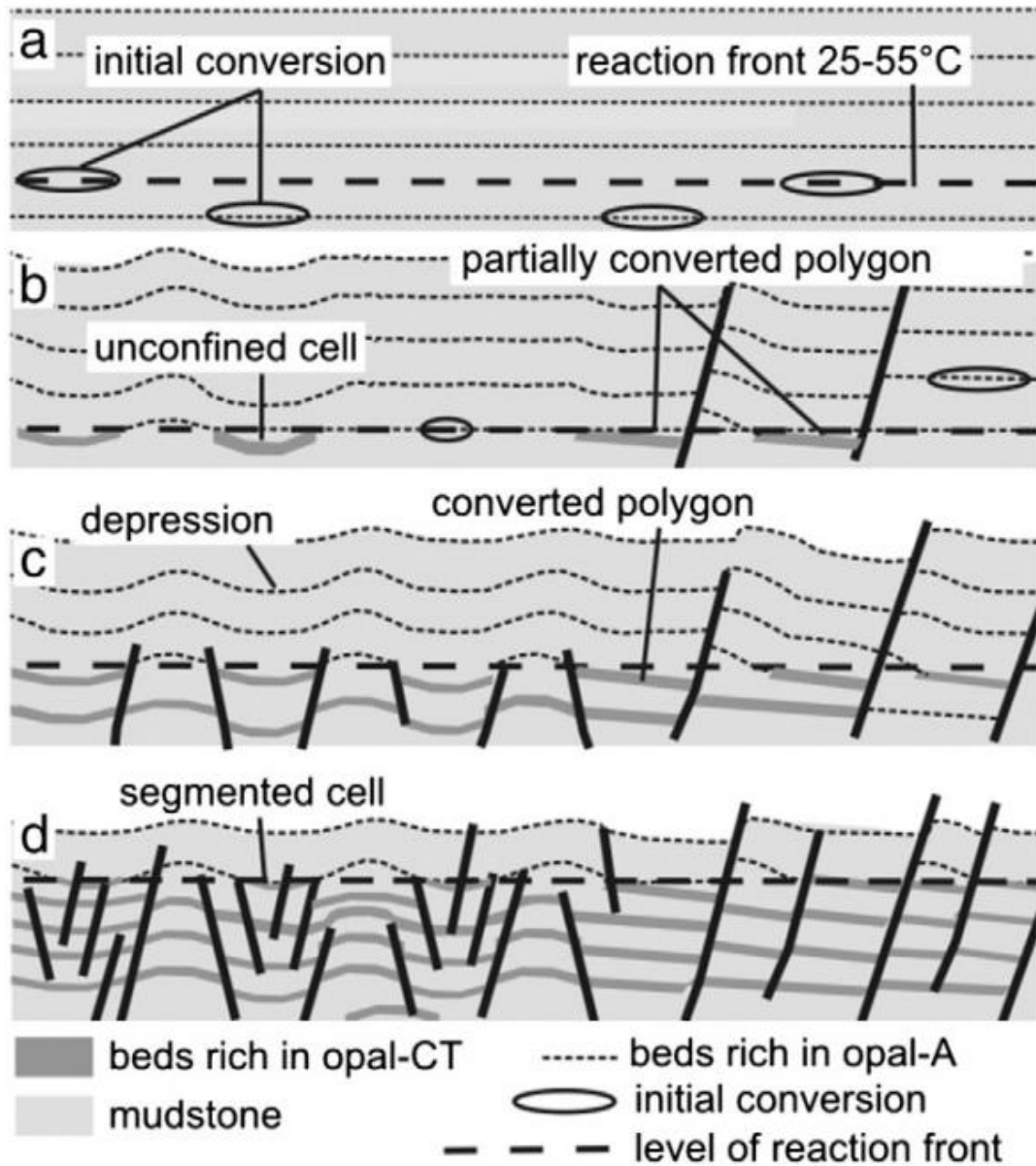


Figure 1.4: From Davies and Ireland, (2011), A schematic diagram summarising the mechanisms by which the conversion of Opal A to Opal CT can create polygonal faults. Offsets are maintained by differential compaction across the partially converted polygon. Unconfined cells create a series of digenetic lows the edges of which, act as sites for strain localisation and hence fault nucleation and growth.

is a pore fluid chemistry change from fresh to high salinity pore water. Goult (2008) also suggests that syneresis is geologically instantaneous, yet fault growth continues for millions of years during burial, a phenomenon which is not explained by syneresis. Goult (2008) also notes that a study by Pratt, (1998) infers that sub-areal cracks can be caused by dewatering during strong earthquakes and that the term syneresis itself refers to a geometry as opposed to a single process. Finally, Goult (2008) suggests that the results of previous work by Goult and Swarbrick (2005) indicate that the polygonal faults studied are still presently active with continued mechanical compaction. Goult (2008) concludes that low co-efficient of friction allow for continued fault growth and that syneresis and density inversion remain untested in laboratory conditions, nor has convincing evidence been provided from observational arguments.

Davies et al. (2009) used 3D seismic data from the Møre and Vørings basins, offshore Norway to describe the interaction between polygonal faults and an opal-A (biogenic silica) to opal-CT (tridymite and cristobalite) transition. Davies et al. (2009) observed a wavelength pattern comprised of quasi-circular folds termed cells. Davies et al. (2009) note that peaks in cells correspond to forced fold troughs in the overburden. Furthermore, the troughs are often flanked by polygonal faults. Davies et al. (2009) infer that mechanical compaction driven by porosity loss in the diagenetic zone drives fault growth (Fig. 1.4).

Shin et al., (2010) used numerical modelling to test end members of polygonal fault growth, deep blind faults, near surface faults and at surface faults. The models generated by Shin et al. (2010) were 2D, with a presumed shear plane and a laterally confined volume. The results suggest that for field data and the results to match, the effective stiffness of the sediment must be low. Mineral dissolution was proposed to account for low stiffness and to trigger polygonal fault growth. In addition, sediment stiffness decreases in time, with increased dissolution, so polygonal faults nucleate at different times within a single tier, with faults accumulating strains whilst others are only just nucleating.

1.2.1.3 Polygonal fault genesis: 2010 to present day

Davies and Ireland, (2011) use 3D seismic data from the Gjallar ridge, offshore Norway. Within the survey an Opal A/CT reaction front interacts with a polygonal

fault network. Two styles of interaction are described, the unconfined cells near the upper polygonal fault tips and the fault confined cells between the upper and lower fault tips. For both interaction styles Davies and Ireland (2011) propose a feedback loop whereby the reaction front interacts with silica rich beds, which are subsequently converted from opal-A to opal-CT. The opal A/CT reaction is accompanied by porosity loss, which drives subsidence and creates shear within the bed between the converted and unconverted cells on either side of the fault or fault tip. Fault propagation under this paradigm is thought to be preferentially upwards.

1.2.2 The evolution of polygonal fault tiers

1.2.2.1 Polygonal fault growth

Traditional models of fault growth have long been considered to be through radial propagation (see Barnett et al., 1987). However, polygonal fault arrays have been suggested to form early, during shallow burial (see 1.2.1.2) and as such, some studies have debated the mode of growth for polygonal fault arrays.

Cartwright (1994a) suggests that polygonal fault arrays have an early upward growth (see Cartwright (1994a), Figure 20 IV). Lonergan and Cartwright, (1999) suggest that the link between the present day configuration of a sand body within the area of study and the position of the polygonal fault array suggests that the polygonal faults helped to constrain the location of the sand body and hence were active near the seabed to influence depositional topography. Early growth was later inferred by Watterson et al. (2000) based on the skew of displacement maxima towards the base of the tier. Work by Stuevold et al. (2003) and Möller et al. (2004) from the Ormen Lange region of the Norwegian margin, paralleled observations made by Lonergan and Cartwright (1999). Stuevold et al. (2003) and Möller et al. (2004) showed that polygonal fault tiers initiated early, based on thickening packages in the polygonal fault hanging walls. A similar observation was made in work on the Sable Sub-basin, on the Canadian Atlantic margin by Hansen et al. (2004). Hansen et al. (2004) observed growth components within the Wyandot tier, a thin tier within Upper Cretaceous chalks that suggest early growth and interaction with the free surface (i.e. seabed).

Work by Nicol et al., (2003) examines the growth of polygonal faults from the Lake Hope region of Australia. Nicol et al. (2003) noted a predisposition for fault intersections with high intersection angles of greater than 60° . Fault linkage between abutting segments is permitted on faults that share a mutual footwall and hanging wall

faults are deactivated. This effect is caused by a thickening of a mobile overpressured unit within the footwall of the polygonal faults and a reciprocal thinning in the hanging wall.

modelling results from Shin et al., (2010) show that shallow faults have asymmetrical throw profiles under gravitational loading. The work of Shin et al., (2010) strongly indicate that the position of D_{max} does not necessarily equate to the position of polygonal fault growth under the established radial growth paradigm. This is due to an enhanced D_{max} position towards the upper half of the fault plane caused by differential sedimentation in the fault hanging wall.

Laurent et al., (2012) examined polygonal faults from the Gjallar ridge, Norwegian Margin, and suggest that polygonal faults propagate radially within specific mechanical units. The stacking of these mechanical units generates multiple tiers of faults that link via dip linkage. The work by Laurent et al., (2012) was based on a program that automatically picks all reflections within a specific volume. The throw data are then extracted from a coherency cube. In the coherency data the faults are represented as stepped discontinuities. From these Laurent et al. (2012) interpret a series of stepped relays to indicate dip linkage. However, as the fault geometry and throw values are extracted from coherency attribute, Laurent et al., (2012) do not consider the potential artefacts that arise from the generation of a coherency cube, notably the width of the pick window from which the coherency is calculated (Bahorich and Farmer, 1995). As no seismic data are clearly presented, nor is there a depth or TWT throw-depth plot presented, the throw data generated can equally be interpreted as artefacts from the generation of coherency cube.

1.2.2.2 Organisation of faults within tiers

Whilst there are numerous studies documenting polygonal fault geometry and lithological variability, there is a paucity of data on how polygonal faults are organised within a single tier. The early work of Cartwright, (1994b) noted that there were likely to be smaller ‘sub-tiers’ of polygonal faults contained within a single polygonal fault tier. This is based on the cross cutting relationships observed between polygonal faults at different stratigraphic levels. Lonergan et al. (1998) in their appraisal of polygonal fault geometry and intersections noted a space-filling effect with smaller polygonal faults abutting and truncating against larger polygonal faults within individual layers. Most recently Cartwright, (2011) described the term ‘master’ polygonal faults, which

describe the largest polygonal faults within a given tier and denote the upper and lower tier boundaries. Subsequently many studies have described an ordered system of polygonal fault height (Gay et al., 2004; Laurent et al., 2012; Ostanin et al., 2012; Seebeck et al., 2015). The origin and significance of changing fault size, whilst widely observed, has yet to be fully described or explained.

1.2.2.3 Mechanical stratigraphy and polygonal faults

Mechanical stratigraphy, as defined in a recent review by Laubach et al. (2009) is the sub-division of rock units according to mechanical properties or by the response of rock units to an applied force. This section specifically examines the impact of mechanical stratigraphy on faulting, the impact of mechanical stratigraphy on fracturing is beyond the purview of this study.

Mechanical stratigraphy has been shown to have significant implications for scaling (Gross et al., 1997; Wilkins and Gross, 2002), linkage geometry (Soliva and Benedicto, 2005), fault zone deformation (Ferrill and Morris, 2008) and distribution of faults within a particular rock unit (Morris et al., 2009). Moreover, the kinematics of fault propagation is also impacted by mechanical stratigraphy by blocking fault tips (Jackson et al., 2014; Rippon, 1984; Roche et al., 2012; Soliva and Benedicto, 2005; Wilkins and Gross, 2002). Mechanical stratigraphy is considered here to cover a wide range of conditions such as where there are bulk facies changes (e.g. shales to sands), or as a function of time where evolving diagenetic conditions alter the mechanical properties through cementation or through flux in geopressure (i.e. overpressure).

Mechanical stratigraphy as a function of changing lithology has been widely described around polygonal faults, in particular, in and around deep marine sand bodies. Lonergan and Cartwright (1999) first described the influence of polygonal faults on a deep-water sandstone reservoir in the UK sector of the northern North Sea (Fig. 1.5). This study showed that polygonal fault patterns can define and delineate the margins of a deep marine channel where polygonal fault densities decrease. Moreover, Lonergan and Cartwright (1999) also noted that few faults from the Eocene-Oligocene propagate through the sand body and that faults in a new tier above the channel aligned orthogonally to the margins of the channel. This indicated that the presence of a sand body precluded the presence of polygonal faults in the immediate vicinity. In contrast, work by Möller et al. (2004) and Stuevold et al. (2003) on the Ormen Lange dome showed that some polygonal faults were active during the deposition of the Palaeocene

Egga unit and were accommodating small growth packages in their hanging walls. This would suggest that the presence of sands is not a restricting feature on polygonal growth, provided polygonal faults reach the seabed.

Analogue modelling by Victor and Moretti, (2006) examined the controls of a sand body on a developing polygonal fault array. Victor and Moretti (2006) used a silicon based substrate over which a mixture of sand and corundum powder was placed. The channel was configured in both straight and meandering geometries and was filled with corundum powder. The entire array was then tilted between 0° and 5°. The results of this study showed that the presence of a channel does impact a developing polygonal fault array in that the contrast between channel and substrate is the locus for channel bounding faults. In addition the extension of the array due to gravity also created channel boudinage, formed by extensional channel-perpendicular faults that compartmentalise the channel geometry. Although the results obtained by Victor and Moretti (2006) widely matched the geometries described by Lonergan and Cartwright (1999), the method of the Victor and Moretti (2006) experiment did not represent polygonal fault genesis mechanisms. The experiment examined the effect of fault growth under gravitational instabilities and is more akin to salt roller deformation than 1D consolidation/dewatering of polygonal faults. Therefore the impact of the polygonal fault genesis mechanism where no or limited extension is implied (Cartwright and Lonergan, 1996) remains unquantified.

More recently a review by Cartwright (2011) re-examined the impact of sandstone bodies and showed an example of a polygonal fault array (Fig 14C in Cartwright, 2011), grading laterally into a channel, demarcated by a change in polygonal fault pattern. The study also showed how polygonal faults become decoupled in the presence of sands forming two sub-tiers where in the immediate vicinity of a sand body, and laterally re-coupled where the sand body was not present. The impact of mechanical stratigraphy arising from sand bodies was suggested to be controlled by the stratigraphic position and relative thickness of the sand body. These results were largely reiterated in a recent example by Jackson et al. (2014), which showed the decoupling of a polygonal fault tier from the Måløy slope, Norwegian Margin. Using well data, cores and two 3D seismic data cubes, Jackson et al. (2014) describe three fault families. The smallest is contained in reflections below the sand unit (Type 1), an intermediate fault family, present above the sand unit (Type 2) and the largest fault

family is present in the regions where the sand body pinches out (Type 3) (Fig. 1.5). From this, the study by Jackson et al. (2014) concludes with a summary of the utility of these sandstone/polygonal fault interactions in finding deep-water sand reservoirs.

These are specific examples where fault propagation and geometry are actively influenced by the presence of sands within otherwise fine-grained successions. One of the key observations that can be drawn from the work of Lonergan and Cartwright, (1999); Stuevold et al. (2003); Möller et al. (2004); Victor and Moretti, (2006); Cartwright, (2011) and Jackson et al., (2014) is that the impact of a sand body is dependent on the timing of fault propagation relative to the deposition of the sand body. In the examples described by Lonergan and Cartwright, (1999), Stuevold et al. (2003) and Möller et al. (2004), the timing of fault growth is suggested to precede or is synchronous with the deposition of the sand body, for at least some of the faults in the array, resulting in a re-organised polygonal fault geometry as outlined by the models of Victor and Moretti (2006) and observations by Cartwright (2011). However, in the examples from Jackson et al. (2014), polygonal fault growth is inferred to post-date deposition of the sands and results in a decoupling of the polygonal fault tier in the vicinity of the array. This highlights the importance firstly, of timing polygonal fault growth and secondly, demonstrates the potential for a temporal control on mechanical stratigraphy associated with bulk facies changes.

Another aspect of mechanical stratigraphy, as suggested by Laubach et al. (2009), is impact of changing diagenetic conditions through time. In the context of polygonal faults, this is perhaps best viewed in the context of the interaction between silica diagenesis and polygonal fault arrays. As previously described in section 1.2.1.2 and section 1.2.1.3, the silica diagenesis, particularly the conversion of opal-A (Biogenic silica) to opal-CT (cristobalite/tridymite) has been suggested as a causative mechanism for polygonal faulting by either differential compaction (Davies et al., 2009) or thermally triggered compaction of siliceous sediments (Davies and Ireland, 2011). In addition to these studies that focus on initiation, a

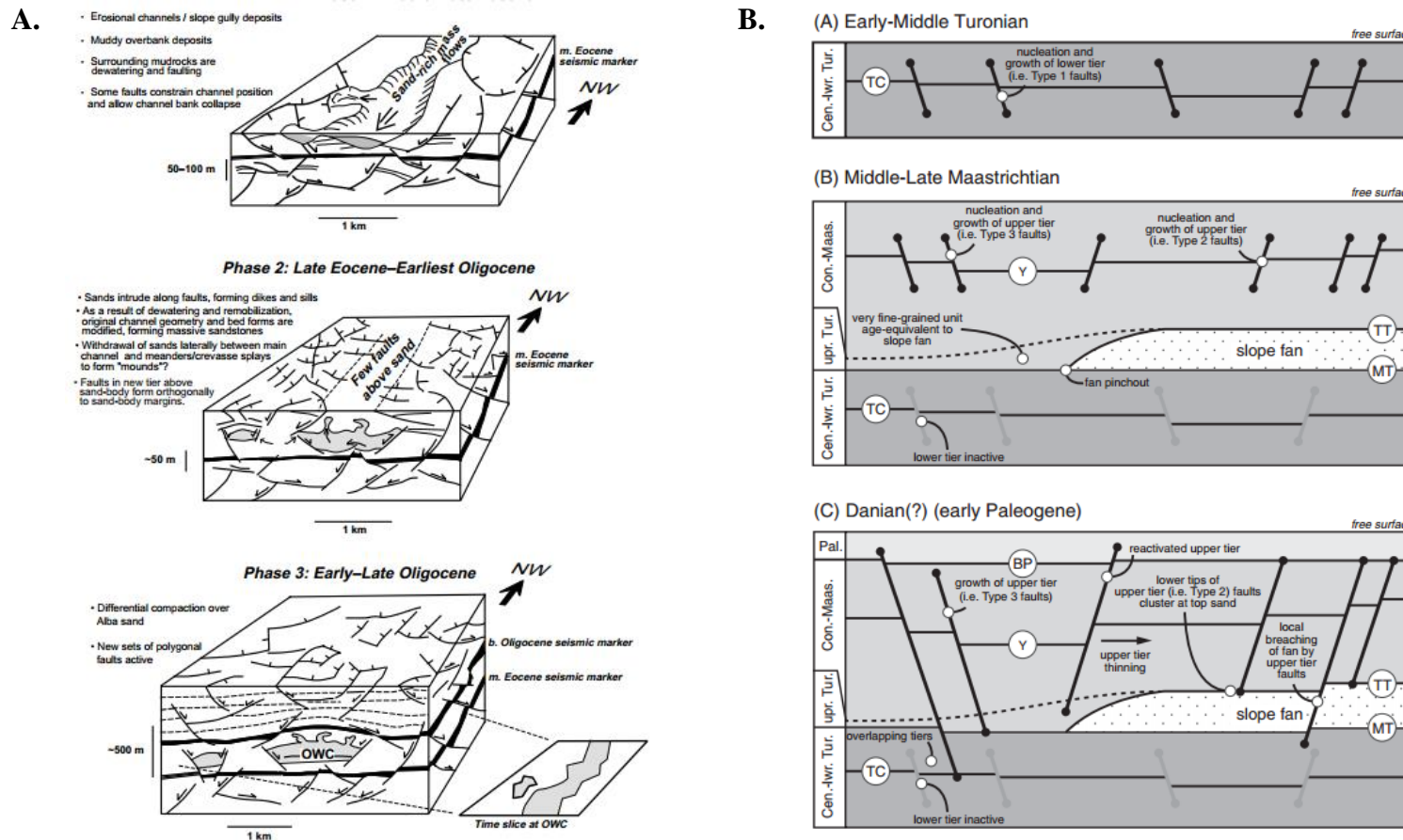


Figure 1.3: A (From Lonergan and Cartwright, 1999) A schematic evolutionary diagram illustrating the impact on polygonal fault geometry where sand deposition and polygonal fault growth are synchronous. (B) From Jackson et al., (2015) A schematic evolution detailing the impact of a sand body on polygonal fault growth during burial.

study by Neagu et al., (2010) measured the strains generated from diagenetic compaction. Neagu et al. (2010) studied the apparent flattening of polygonal fault planes below an Opal A/CT boundary on the Gjallar Ridge and Ormen Lange dome, on the Norwegian Margin. In addition to the reduction in dip at the Opal A/CT boundary, the study by Neagu et al. (2010) also discovered a systematic reduction in throw at the Opal A/CT boundary. An estimate of vertical compaction strain was calculated from the change in angle of the fault planes and compared with observed compaction from nearby well data. This study concluded that the fault planes have been compacted and flattened by the vertical compaction of siliceous sediments, precipitated by an Opal A/CT reaction front. This mechanism for fault plane compaction relies heavily on the fault planes being present prior to the development of an Opal A/CT reaction front. Whilst it is likely that the fault planes have been compacted below the Opal A/CT, the widely observed restriction in throw at the reaction front also indicates a mechanical behaviour. Data collected from an onshore example of an Opal A/CT boundary by Ishii et al. (2011), suggests that the Opal A/CT reaction front is stronger than both the Opal A and Opal CT rich intervals, due to the presence of both mineral phases within the reaction front. This increased strength could account for the restriction of throw at the reaction front observed by Neagu et al (2010). These examples summarise the effects of changing diagenetic conditions to create polygonal faults (Davies et al., 2009; Davies and Ireland, 2011) and to modify existing polygonal fault geometries and characteristics (Neagu et al., 2010, Ishii et al., 2011).

Another potentially important control on mechanical stratigraphy is the development of overpressure. Overpressure has been linked to polygonal fault genesis (see 1.2.1.2), however this interpretation has been the subject of some debate (James et al., 2000; Cartwright et al., 2003; Goult, 2008). A study by Bolton et al., (1998), highlighted the importance of timing overpressures and permeability evolution, particularly in sediments undergoing shear stress. Using physical testing of an artificial clay sample (80% Kaolinite and 20% fine sand, mixed with distilled water), the tests defined by Bolton et al. (1998) examined the evolution of porosity and permeability during uniaxial compression and overpressure. The testing revealed that the stress history of a sample plays a crucial role in not only governing the hydrological characteristics of a clay rich sediment but also on the style of deformation. In sediments that are initially

consolidated and then subject to increased fluid pressures form mode I fractures within brittle shear zones, whereas sediments that are under-consolidated deform through volume loss. The timing of polygonal fault growth and propagation relative to the generation of overpressure could be important to constraining not only genesis but also the process by which basal polygonal fault tips are retarded. A review of overpressure mechanisms by Osborne and Swarbrick, (1997) highlights many processes by which overpressure is generated, such as increasing compressive stress (through tectonics or disequilibrium compaction), increasing fluid volume change (Hydrocarbon generation, thermal expansion and diagenesis) and fluid movement (via processes such as buoyancy, osmosis and hydraulic head), are unlikely to apply ubiquitously in very shallow diagenetic settings at the regional scale ($10^4 - 10^6 \text{ km}^2$) that polygonal faults can cover. This study is important as it highlights that many of the mechanisms that have been proposed have a requirement for some burial and degree of influence from the local geothermal gradients. This highlights that there is a potential disconnect between the influence of overpressure (i.e. Nicol et al., 2003; Watterson et al., 2000) and shallow initiation polygonal fault initiation (e.g. Cartwright et al., 2004; Watrus et al., 2003).

In summary, mechanical stratigraphy in polygonal fault arrays has been primarily focussed towards the effects of bulk grain size changes from ultra-fine clays to sands. It is important to note that the lateral extent of a given polygonal fault array is often much larger than the coarse grained facies within a particular depositional system. Therefore, studies on the impact of bulk grain size changes are local effects when the entire tier is considered. What is lacking in the literature is a review into what, if any, mechanical controls exist within a clay rich polygonal fault tier, and in particular how diagenesis in fine grained rocks and sediments can influence the position of fault tips, the creation of sub-tiers and the dimensions of fault families within a polygonal fault array.

1.2.3 Interaction between polygonal faults and topographic features

In a recent review, Cartwright (2011) outlined how perturbation patterns in polygonal fault tiers could be used to constrain the nucleation position of polygonal faults. Cartwright (2011) proposed that in surveys where features such as turbidite channels occur near the base of the tier, then the presence/absence of a corresponding

perturbation pattern could indicate the nucleation position, either within a perturbed state of stress or away from a perturbed state of stress.

Perturbation patterns in joints and faults are characterised by deviations in orientation from a ‘background state’ to coincide with the stress field generated by a nearby structure or feature. This observation for joints has been widely documented, especially around faults (Dyer, 1988; Rawnsley et al, 1992; Rives et al, 1992). These perturbations are heavily dependent on the relative timing of joint formation and the fault activity (Peacock, 2001). Faults themselves can be regionally perturbed by crestal architecture of sub-surface features such as salt diapirs (Rowan et al, 1999; Davison et al, 2000; and Stewart 2006).

Perturbation of polygonal faults has also been described around a number of features including turbidite channels (Lonergan and Cartwright, 1999, see 1.2.2.3), tectonic faults (Hansen et al., 2004), hydrothermal mounds (Hansen et al., 2005 see Chapter 5), pockmarks (Imbert, 2009; Andresen and Huuse, 2011; Ho et al., 2013) and salt diapirs (Davison et al., 2000; Stewart, 2006; Carruthers et al., 2013). This section offers a short review of the key attributes of two previously used features that are associated with perturbed polygonal fault patterns, pockmarks and hydrothermal vents.

1.2.3.1 Pockmarks

A pockmark is defined as concave depression (King and MacLean, 1970). Pockmarks are sites of focussed fluid expulsion which create craters and depressions within the sea or lake bottom (Hovland et al., 2010, 2002). Fluid expulsion events are not confined to a single phase as pockmarks can reactivate rapidly even after lengthy periods of dormancy (Moss et al., 2012). Pockmarks have a variety of shapes and sizes as defined in Hovland et al (2002).

- Unit pockmarks: small scale 1-10m across and 0.5m deep
- ‘Normal’ pockmarks: 10m to 700m in diameter and 1m to 45m deep
- Elongate pockmarks: One axis is longer than its other axis, often found near slopes and offshore current influenced areas
- ‘Eyed’ pockmarks: A pock mark with a central high amplitude artefact caused by coarser grained material, biological activity/debris or carbonates
- Pockmark ‘strings:’ Small unit pockmarks arranged in a curvilinear array

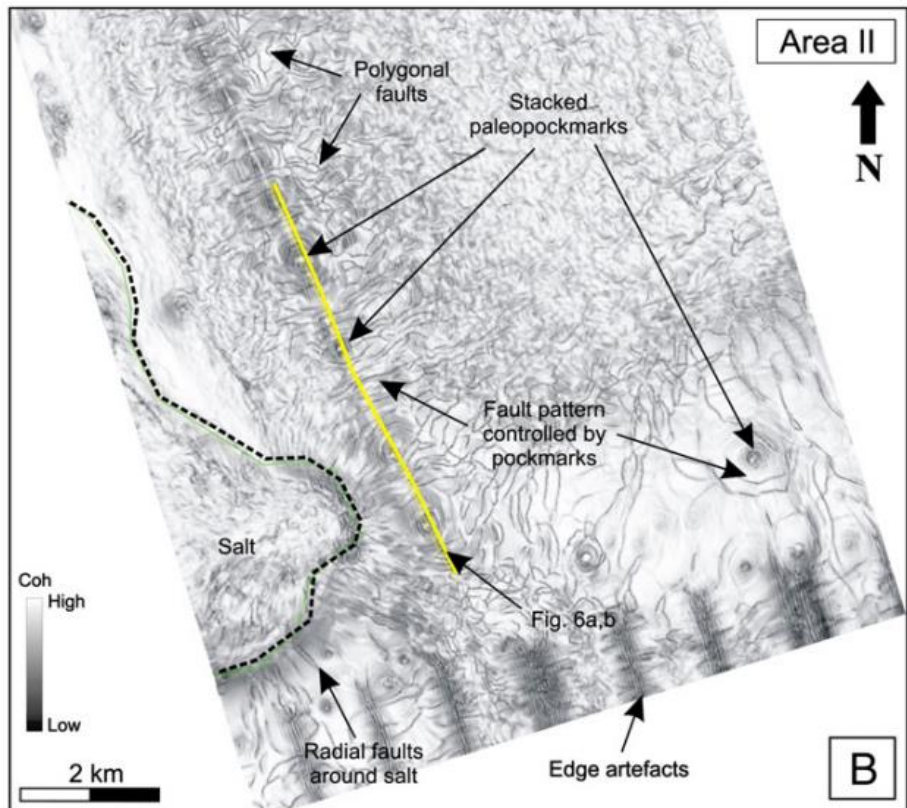
- Complex pockmarks: Amalgamation of several pockmarks or highly clustered normal pockmarks

Pockmarks have been widely described in a number of geological settings, have been found in association with gas seepage for hydrocarbon reservoirs (Cole et al., 2000; Judd et al., 1994; Rise et al., 1999) and can indicate a breaching of hydrocarbon sealing lithologies (Cartwright et al., 2007). Pockmarks have also been found in association with mixing of differing salinity water columns (Bussmann and Suess, 1998), earthquake seismicity (Hasiotis et al., 1996; Soter, 1999), fault lines (Gay et al., 2004) buried submarine channels (Gay et al., 2006a, 2006b) and sediment slumps (Pilcher and Argent, 2007). Pockmark dimensions are variable, internal dips are low between 6° - 18° (Fader, 1991) and pockmark widths can vary from a few metres to a few hundred metres across (Hovland et al., 2002). Pockmarks generally have a life span proportional with their size, unit pockmarks are thought to last a few decades before drifting sediments along the sea floor infill them, whereas normal pockmarks are thought to have a life span of a few thousand years (Hovland et al., 2010). In areas where sedimentation rates are much higher, pockmarks may be filled in much more rapidly (Çifci et al., 2003).

Perturbations of polygonal faults have been previously documented around pockmarks (Imbert, 2009; Andresen and Huuse, 2011) (Fig. 1.6). Imbert (2009) reviewed subsurface sediment remobilization structures and classified them based on how they interact with fluids expelled during compaction. Imbert (2009) describes the top of a polygonal fault tier. The observations are focussed near to a salt diapir, where pockmarks are partially enclosed by polygonal faults.

Andresen and Huuse, (2011) conducted a study in the Lower Congo basin and examined the relative timing of fluid expulsion. Analysis of coherency slices revealed a concentric pattern of faults around circular depressions. These depressions were found to be stacks of pockmarks in close association with polygonal faults systems (PFS) in the upper sections of their survey. The key observation made by Andresen and Huuse (2011) was that the stacked pockmarks are completely contained by polygonal fault cells. Andresen and Huuse (2011) conclude that the polygonal faults postdate the pockmarks. The concentric pattern of faults observed in

A.



B.

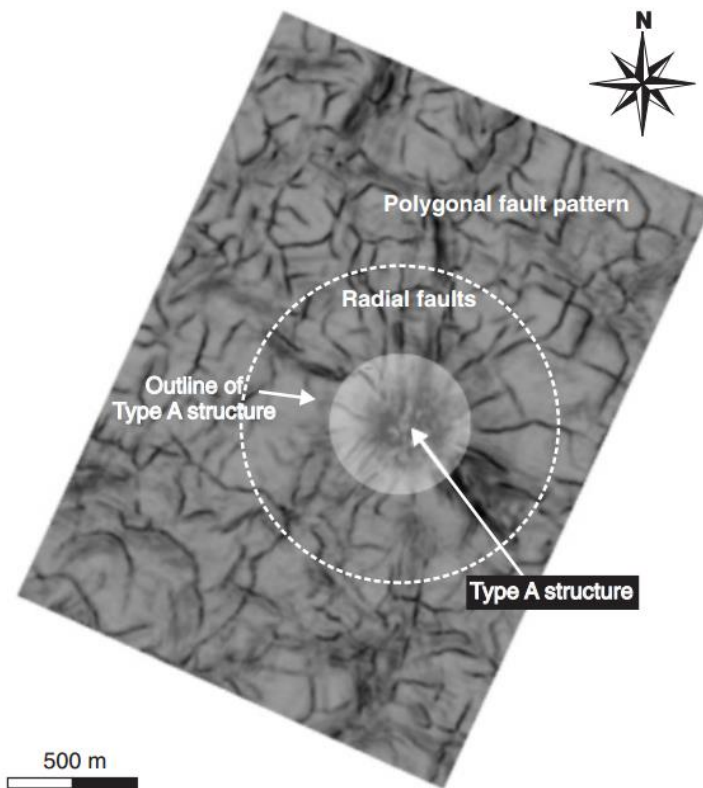


Figure 1.4: (A) From Andresen and Huuse, (2011). A coherence slice showing the perturbation of polygonal faults by palaeo- pockmarks and salt diapirs. (B) From Hansen et al. (2005) a coherency slice within the Oligocene from the Gjallar ridge showing the perturbation of polygonal faults around mud pillows.

coherency was attributed to differential compaction across the pockmark causing subtle stress perturbations that influenced the developing polygonal faults.

Both the work by Imbert (2009) and Andresen and Huuse (2011) demonstrate that polygonal faults and pockmarks are passively influenced by each other, in instances with pockmarks above (Imbert, 2009) and within a tier (Andresen and Huuse, 2011). The influence of pockmark at the base of tier has yet to be fully described and represents an ideal case study to examine the nucleation position in polygonal fault tiers.

1.2.3.2 Hydrothermal vents

A hydrothermal vent or hydrothermal mound is a dome or crater-like structure that is typically found in close association with a nearby sill or sill complex (Bell and Butcher, 2002; Jamtveit et al., 2004; Planke et al., 2005; Svensen et al., 2006). Mounds form in response to the high pressures generated by super-heated fluids from the contact aureole of a sill or dyke. The rapid venting of these fluids forms an initial crater and emplaces fluidized sediments from the conduit walls (Jamtveit et al., 2004). Hydrothermal vents have been widely recognized in seismic data (Bell and Butcher, 2002; Davies et al., 2002; Hansen et al., 2005; Planke et al., 2005; Hansen, 2006; Rollet et al., 2012; Grove, 2012; Zhao et al., 2014; Magee et al., 2014) and in field outcrops (Svensen et al., 2006; Moreau et al., 2012).

Hydrothermal vent dimensions are large, between 0.5 km and 3.5 km wide, up to 640 m high and have flank dips ranging from 5° to 26° (see Hansen, 2006 and references therein). Vent composition is also highly variable with some seismic studies, field studies and core data suggesting a largely sedimentary component of vent fill ranging from muds, sands, pelagic oozes and methanogenic carbonates (Svensen et al., 2003; Jamtveit et al., 2004; Hansen et al., 2005; Hansen, 2006; Svensen et al., 2006; Moreau et al., 2012). Other studies have postulated a volcanic/igneous source based on core and seismic data (Bell and Butcher, 2002; Davies et al., 2002; Grove, 2012; Rollet et al., 2012; Zhao et al., 2014).

Hydrothermal venting is thought to be a contributor to global changes in the Permian associated with the formation of the Siberian Traps and numerous breccia pipes, enabled greenhouse gases to escape (Svensen et al., 2009). Similar observations have been made to explain the Early Jurassic extinction events, associated with the

formation of the Karoo Large Igneous Province (Svensen et al., 2007) and the IETM (Initial Eocene Thermal Maximum) with igneous activity (including flood basalts and sill emplacement, see Chapter 6) during Late Palaeocene in the Vør ring and Møre basins (Svensen et al., 2004).

Hydrothermal vents have more recently been used to demonstrate the fluid migration pathways up normal fault planes by examining the spatial link between vent occurrences along a normal fault (Magee et al., 2015). In addition, hydrothermal vents have been used to help infer the timing between vents and polygonal faults based on the presence of perturbed (radial) polygonal fault patterns in the immediate vicinity of the vent (Hansen et al., 2005).

1.2.3.3 Further work on the perturbation of polygonal fault arrays by topographic features.

From the preceding review of perturbation patterns and two commonly used topographic features (pockmarks and hydrothermal vents), there is a *primie facie* case for using these structures to examine and define the nucleation position of polygonal faults within a tier, consistent with the methodology suggested by Cartwright (2011). Present research is limited to anecdotal observations (Hansen et al., 2005) or studies that are within the middle (Andresen and Huuse, 2011) or top of the tier (Imbert, 2009). A detailed review of topographic features at the base of tier and any associated perturbation patterns, could clarify where polygonal faults nucleated in the tier and potentially explicate when polygonal faults nucleate e.g., during shallow or deep burial?

1.3 Aims of the thesis

From the preceding review, polygonal fault geometry, sedimentology and initiation are widely documented from a variety of depositional and tectonic settings, however there is at present, very little constraint as to the timing of polygonal fault growth (during shallow or deep burial), spatial setting of polygonal fault initiation and growth, and how faults are organised within polygonal fault tiers.

There are three concepts that this study will address,

- Can the interaction between polygonal faults and bathymetric features at the base of a polygonal fault tier be an indicator for early initiation?

- How do polygonal fault arrays grow? Is growth radial or is growth asymmetrically skewed in a particular direction (i.e. upwards)?
- How are polygonal faults organised within a tier? Are all faults the same or does length height or throw vary? What controls the variation and when does the variation begin?

This study aims to examine, compare and contrast two polygonal fault arrays from passive margins. One survey is located in the Møre/Vøring Basin, Norwegian Margin and another is from the Lower Congo basin, offshore Angola. These two case study regions were selected as the tiers in the study area are both wedge shaped tiers, both have features at the base of the polygonal fault tier (pockmarks, Lower Congo Basin and hydrothermal vent complexes, Norwegian Margin). In addition, there are differences in the sediment thickness and ages of the polygonal fault hosting sequences. The Norwegian Margin tier is much thicker (up to 1km thick) and contains sediments of Eocene to Miocene age (see chapter 7), whereas the tier in the Lower Congo Basin is much thinner (up to 400m) and has sediments of Plio-Pleistocene age. These two tiers enable comparative analysis of both shallow (young) and deeply buried (mature) polygonal fault arrays.

1.4 Thesis structure

A brief overview of Chapters 2 to 8 is summarised here:

- Chapter 2: Methods

The methods section describes the processes of data acquisition, case study selection, horizon picking, fault interpretation and fault measurement.

Chapter 3: Regional Geology

This section introduces the basin scale tectonic and stratigraphic setting of each of the studied areas.

- Chapter 4: The controls on the development of Master polygonal faults within a single polygonal fault tier, Norwegian Margin.

This chapter examines the organisation of faults within a well-developed thick tier of polygonal faults and describes the temporal and spatial evolution of the Master polygonal faults.

- Chapter 5: Polygonal faults in a wedge shaped tier, Lower Congo Basin

This chapter describes the impact of evolving sedimentary load on the organisation of polygonal faults and how these observations relate to the temporal and spatial evolution of the polygonal fault array.

-

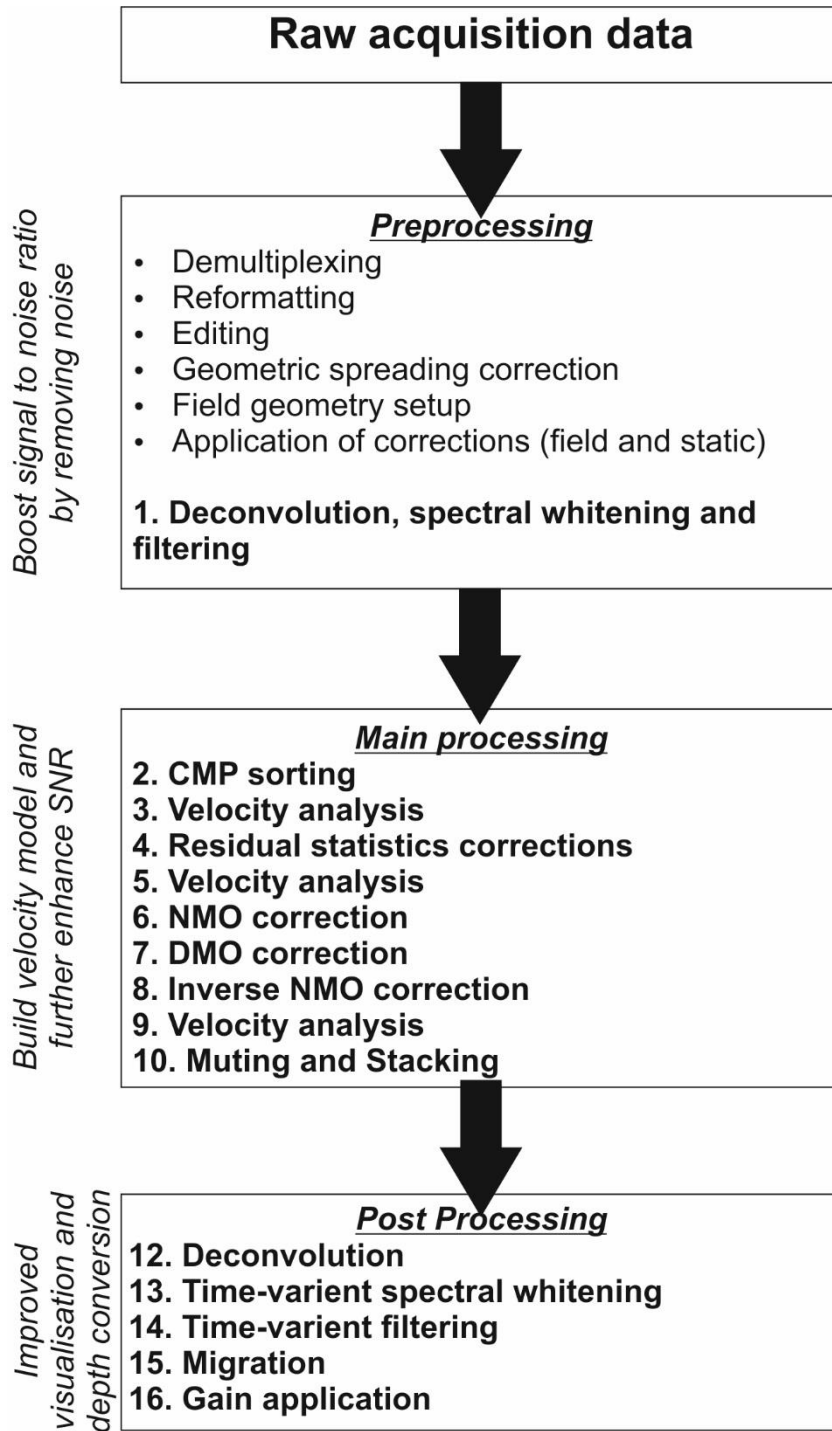


Figure 2.4: Modified from Yilmaz (2001). A schematic workflow for the processing of seismic data and the impact each stage has on the resultant seismic data.

Where RC is the ratio between the amplitude response of layer 1 (AI_0) and amplitude response of layer 2 (AI_1). The reflection coefficient is a numerical measure of the impact a rock interface has on reflection strength. Reflection coefficient values of ± 1 indicate that all the wave energy is reflected. Typical values for the reflection coefficients of rocks are generally ± 0.2 (Kearey et al., 2002). Therefore, a small amount of incident energy is reflected back to the surface and the majority of the energy transmitted into the rock.

During processing the amplitude response of the incident reflections is calibrated on a colour scheme. The colour convention used in seismic data is a crucial aspect of the data. The SEG colour convention is assigned during processing and defines how the increasing acoustic impedance in the data is expressed (Fig. 2.3). There are two colour conventions in use, the SEG Standard (also termed American polarity), which suggests an increase in acoustic impedance is displayed as a coloured peak, and the SEG reverse (so called, European polarity) convention which shows increasing impedance as a negative amplitude trough (Fig. 2.3). The phase of the wavelet is also an important consideration, and where the crest of the waveform lies in relation to a geologic boundary. A zero phase wavelet (for either the American or European convention), the wavelet is symmetrical and the crest of the peak or trough will lie in the interface of the interval with a different impedance contrast. Thus the zero phase dataset is the most useful for the interpretation of seismic stratigraphy. The colour convention of the seismic data used may be corroborated using the seismic response of the seabed. Normally the seabed represents the transition from water to sediment which is an increase in acoustic impedance contrast. Given that the colour conventions are calibrated to an increase in acoustic impedance, the amplitude response the seabed is the logical place to check the colour convention used (Fig. 2.3).

Another important consideration prior to beginning interpretation and fundamental to understanding and interrogating the raw seismic data set, are the resolution limits. Seismic resolution falls into vertical and lateral resolution. Vertical seismic resolution can be calculated from basic knowledge of the dominant frequency of the data. The wavelength of the data is given by;

$$\lambda = \frac{c}{f}$$

Equation 2.4

Where V is equal to the interval velocity and B is frequency of the seismic wave. Typically beds less than one quarter of the wavelength can be resolved seismically (Avseth et al., 2010; Brown, 2004). However it is also important to note that vertical resolution is impacted by changes in interval velocity as well as the frequency of the wavelet which attenuate with depth resulting in a decrease of vertical resolution with increasing depth. Nonetheless, it is possible to image beds that are a thirtieth of the dominant frequency, depending on the signal to noise ratio of the data as well as the density and velocity characteristics of the embedded units (Brown, 2004). Horizontal resolution in migrated 3D seismic data, as used in this thesis, is restricted by the lateral sampling of the data, which equates to the bin spacing between the CMP (common midpoint). This spacing can typically be found in the header files for the data cube or measured directly from the seismic data where the pixel width (in metres) on a map display corresponds to the bin spacing.

2.2.4 *Geophysics of studied datasets*

Both surveys used in this thesis use time migrated 3D seismic data. Due to the confidential nature of the datasets, many of the SEG-Y headers are blanked so detailed processing workflows are unavailable. It is however, likely that surveys used followed a very similar workflow that was presented in Fig. 2.4. Table 2.1 summarises the key geophysical characteristics of each survey area.

Table 2.1: A summary of key geophysical characteristics of each survey used in this study

	Modgunn Arch Survey	Angolan Margin Survey
<i>Trace sampling*</i>	4 ms	2 ms
<i>Interval velocity**</i>	1800 ms	1700 ms
<i>Frequency</i>	35 Hz	80 Hz
<i>Lateral resolution</i>	25 m	6.25 m
<i>Vertical resolution</i>	ca. 12 m	ca. 4 m
<i>Time Migrated</i>	Yes	Yes
<i>SEG polarity***</i>	Standard	Standard

* See Figure 2.10

** Interval velocity within the polygonal fault tiers studied

*** See Figure 2.4

2.3 Seismic mapping

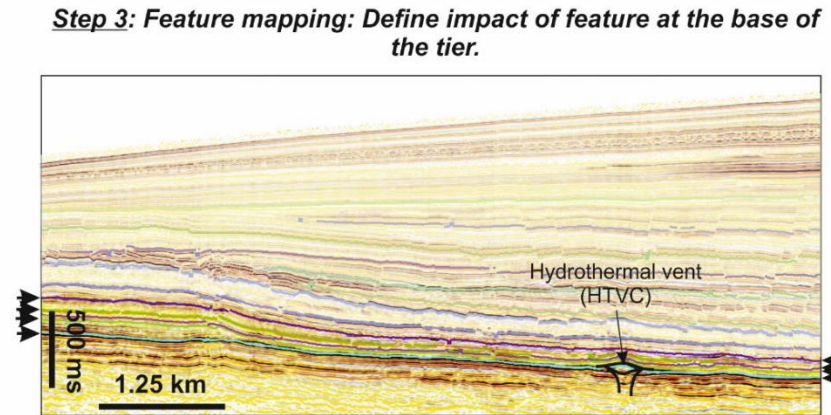
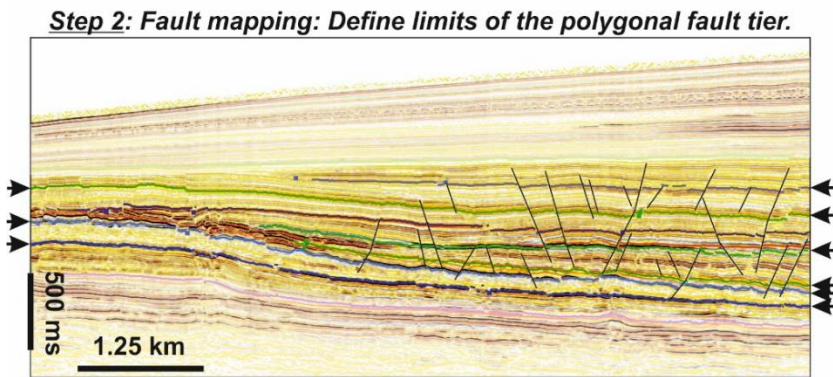
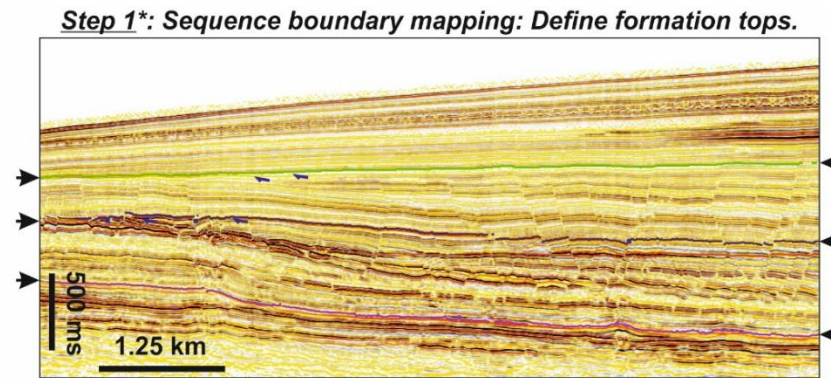
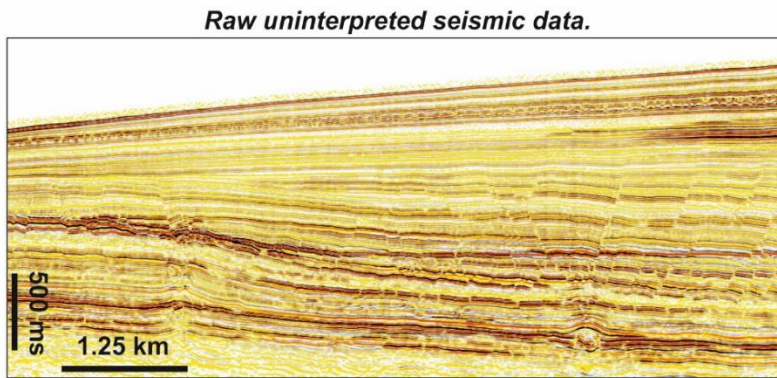
2.3.1 Horizon picking methodology

Prior to mapping any reflections, a detailed desk study was undertaken to understand the regional geology (see Chapter 3). The aim is to identify key reflections such as regional unconformities and previously mapped and defined formation tops. Any well data are then analysed and the formation tops in the well were related to the seismic reflection characteristics. Only one survey (Modgunn Arch) has well control. As the raw data files were unavailable, no synthetic seismic data could be generated. Instead, the data was matched to the seismic using the two formation boundaries, the Mid-Miocene unconformity which defines the junction between the Brygge and Kai formations and the Plio-Pleistocene unconformity which defines junction between the Kai and Naust formations. Once these data were matched to the seismic, the mapping of reflections could proceed.

The selection of which reflections to map and the extent to which they are mapped was defined on the basis of the structural and stratigraphic context. Stratigraphic reflections such as unconformities were regionally mapped across the entire survey (where possible) and were the first reflections to be mapped (Fig. 2.5). The unconformities are picked as negative (soft) reflections. The West African survey had very little information to guide the mapping process. Instead of using key stratigraphic markers, initial mapping was focussed on the top, middle and base of the polygonal fault tier, selecting the most prominent reflections. The horizons selected must also cover the whole extent of the survey. The next stage was to pick and define a number of horizons from within the polygonal fault tier (Fig. 2.5). The final step of horizon mapping was to locate and generate a series of smaller localised maps around isolated topographic features at the base of the tier such as pockmarks, channels and tectonic faults.

2.3.2 ASAP picking technique

The maps were created from an initial coarse seed grid with a line spacing of 40 lines x 40 lines. This initial seed grid was then used as the basis for an ASAP (Automatic Seismic Area Picker) algorithm to interpolate between the grid lines. The ASAP algorithm tracks



* Step 1 can be calibrated from well data where available

Figure 2.5: Schematic diagram detailing how seismic horizons are selected and mapped throughout the survey. In this example from the Modgunn Arch Survey (Chapters 4 and 6), the first step maps seismic horizons that form the formation boundaries, in this case defined by regional unconformities. The second step creates horizons through the polygonal fault tier to examine pattern change. The final step (step 3) examines the impact of topographic features at the base of the polygonal fault tier.

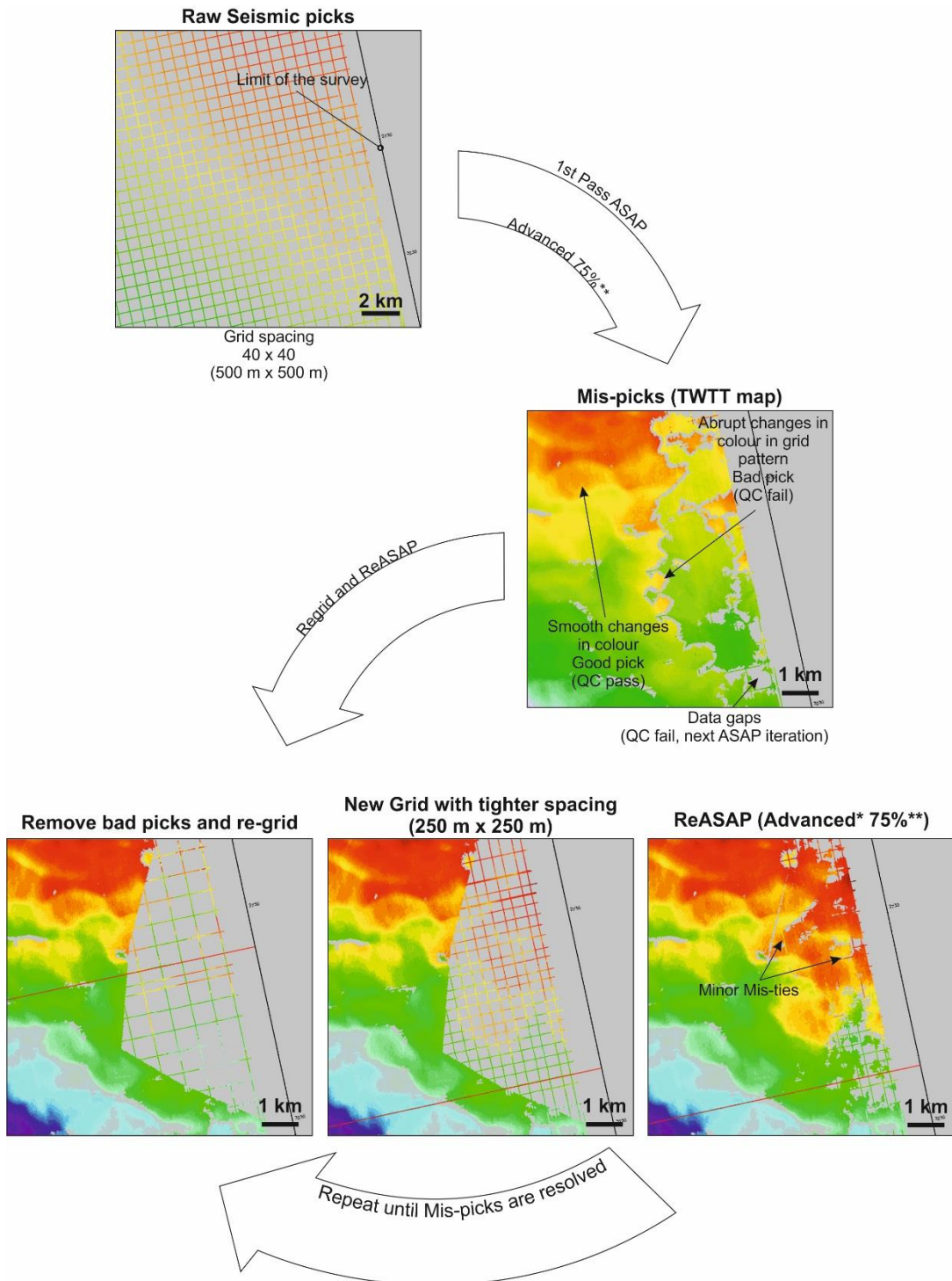


Figure 2.6: A diagram showing the picking methodology used for creating the seismic TWTT map of the Plio-Pleistocene Unconformity from the Modgunn Arch (see Chapter 6).

*Refers to the ASAP picking algorithm ** Refers to the quality attribute, see text for details

similar events within the seismic data from seed points (the raw seismic grid) to create parent points (the interpolated data between the grid). There are three tracking techniques that have varying degrees of constraint. Simple tracking has no consistency checks and traces are followed from point to point (Schlumberger, 1999). Extended and Advanced use a 3x3 and 5x5 grid respectively to cross check both the child point attributes (phase, amplitude, dip etc.) against seed points, as well as against other seed points in the same grid (Schlumberger, 1999). The quality level parameter in the ASAP also adjusts the criteria the algorithm uses when comparing seed points to child points and ultimately defines whether a child point is selected and mapped. Higher quality values require a better the match between parent and seed points in terms of dip (expressed as gradient, s/m) and amplitude.

This survey used an iterative ASAP methodology where the algorithm was repeatedly applied to same area, with the gird and ASAP output acting as a seed point for the next iteration. The first ASAP pass was set to an advanced (5x5 search algorithm) and a quality setting of 75% as it is the most rigorous. Each subsequent ASAP pass has the quality attribute decreased by 20% until, the final quality parameter reached 15%, where the search algorithm changed from advanced to extended and to simple. The results from each previous pass were used as the basis for next. The algorithms with little or no constraint or lower quality attributes are interpolating between smaller and smaller spaces. If the earlier passes are of sufficient quality and generate a good quality surface, subsequent passes with extended and simple algorithms may be skipped. In instances where only a few small ‘holes’ remain that are only a few pixels (equivalent to seismic bins) across, then the Simple attribute may be substituted into the work flow at an earlier stage. These maps were quality checked using time, time dip and amplitude attribute maps to look for mis-picks (Fig. 2.6). Mis-ties, areas of interest, and low quality signal areas were re-mapped using a smaller seed grids with a line spacing of 20 x 20 to 10 x 10 (Fig. 2.6). Each horizon is subsequently checked for mis-picks before a final attribute map is computed and used as the basis for structural analysis (see Section 2.5)

2.4 Analytical techniques

2.4.1 The polygonal fault problem

Polygonal fault arrays, as discussed in Chapter 1, can have an extremely large spatial extent (up to $2 \times 10^6 \text{ km}^2$) and can be easily mapped using a variety of attribute maps.

The primary methods for fault detection used in this study are amplitude maps and time-dip maps. Amplitude maps record the amplitude response of the mapped peak or trough. Where the picked reflection crosses a fault, an anomalous low (or no) amplitude is recorded. In time, dip maps use an algorithm to calculate gradients within the seismic data, expressed as a two way travel time per metre (s/m).

These attributes maps have been selected over others, such as coherency and ant tracking as they are easily reproduced directly from mapping reflections and not the data volume. This gives greater quality control on the map produced whilst still allowing clear imaging of faults. Coherency volumes are highly susceptible to producing artefacts as coherency does not image steeply dipping features in section well and produces artefacts that are prone to misinterpretation. These artefacts have been interpreted has evidence for dip linkage and evidence for high numbers of tiers (see Laurent et al., 2012; Seebeck et al., 2015).

Whilst polygonal faults can be detected regionally with relative ease, the next problem faced is related to the large areal extent polygonal fault arrays occupy. Polygonal fault arrays have extremely high numbers of faults within them. For example Block 17 has upwards of 60,000 faults spread over 400 km². The polygonal fault problem is thus that with huge numbers of faults, spread over a very large area; how can case study regions be defined?

More traditional statistical analyses such as selecting faults from random number generation or by measurement of 1% of all faults present will leave large gaps in measurement coverage and ‘hide’ meaning-full data trends within clouds of data. The primary problem with polygonal fault arrays is their sensitivity to nearby structures which locally alter fault characteristics. Equally, comparison and representation of some fault attributes such as orientation in rose plots, do not consider the spatial context, over which, the data is collected. In datasets with large fault numbers (and by extension, are spread over a large area), non-related trends can become mixed together generating false data trends, or real data trends become lost altogether in a data ‘cloud’.

In this study, the approach taken was to pick areas that represent a particular behaviour or response from the polygonal fault array. The aim was to compare and contrast fault attributes with areas where the fault behaviour no longer exists. Alternatively, small case study areas were used to generate a ‘snapshot’ of fault attributes at a particular

interval. The selection criteria for the case study areas is in part defined by the number of faults present. The minimum requirement when selecting a case study area would be to have a statistically significant number of faults present throughout the tier, with 15 being the minimum number used throughout the results chapters. The case study areas are then sized to capture the minimum number of faults. The dimensions of the case study areas must match within a single survey for a comparable result. The dimensions of the case study areas are related to the seismic resolution of the survey, which in turn defines how many faults are imaged. For example, the minimum case study sample area in the Modgunn Arch survey area, where vertical resolution is 8 m and lateral resolution is 12.5 m, the case study area is 64 km². In contrast, the Offshore Angolan survey, which has lateral resolution of 6.25 m and vertical resolution of 3 m, has a minimum case study size of 1.5 km².

In addition to the dimensions of the case study areas, another important consideration is how the case study areas are distributed across a survey area. The distribution of the case study areas is suggested to be governed, in part, by the objectives of the study. For example, Chapter 5 uses the wedge shaped geometry of the Offshore Angolan tier to examine the effects of shallow burial on an incipient polygonal fault array. As such the case study areas are distributed accordingly to capture fault characteristics at particular depth intervals of every 50 m burial, facilitated by four case study areas distributed in a line across the wedge. Alternatively, in Chapter 4, which examines changes in fault organisation and diagenesis, two case study areas are used to elucidate the impact of diagenesis on a single fault tier.

2.4.1.1 Fault displacement

Fault separation is divided into three components, a vertical component (throw) and a horizontal component (heave). Dip displacement is the measurement of

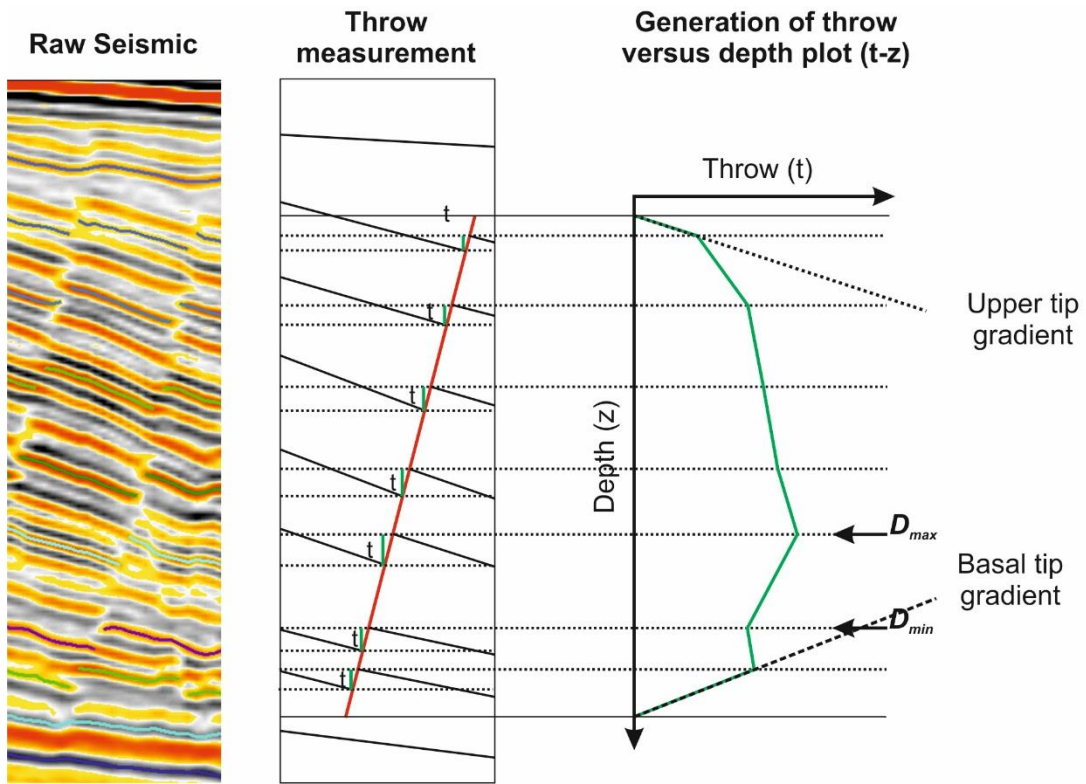


Figure 2.7: A schematic diagram showing how displacement measurements from seismic data are used to create throw depth (t - z) plots. T - z plots are also the basis for displacement-height plots and plots of tip gradients (upper and basal)

displacement along the fault plane. One of the major components of fault displacement considered through the thesis is throw mapping. Throw mapping can be done in one of two ways, using a throw-depth profile (t-z plot) measured perpendicular to the fault plane or an along strike throw profile. Both throw profiles and t-z plots are used to examine throw distribution within polygonal fault networks.

These profiles can be used to examine kinematic behaviours such as blind propagation (Baudon and Cartwright, 2008a, 2008c; Childs et al., 2003) where faults radially propagate from an initial nucleation point. Throw-depth plots have also been used to identify areas of dip linkage where two blind fault tips propagate together in the subsurface (Cartwright et al., 1995; Mansfield and Cartwright, 2001, 1996; Nicol et al., 1996; Stuevold et al., 2003; Walsh et al., 2003). Additionally, t-z plots can be used to infer the kinematics of fault reactivation (Baudon and Cartwright, 2008b). In all these cases, the key identifying feature is the location and position of displacement maxima (D_{max}) and minima (D_{min}) (Fig. 2.7). Blind fault propagation assumes that the geologic media is homogenous. Heterogeneities such as lithology changes as described in Chapter 1 can impede displacement accumulation by restricting fault tips (Rippon, 1984).

Faults used in this study were detected using amplitude and time dip attribute maps. For the analysis of faults both t-z plots and throw profiles are used in this study. The measurement of t-z plots is done by taking a line of section at 90° to the fault trace. Throw values were measured in TWT direct from the seismic data and were obtained by measuring the vertical distance from the footwall to hanging wall cut-offs (Fig. 2.8). The throw values were depth converted using the interval velocities for that dataset (Table 2.1). For t-z plots this was done at the displacement maxima (D_{max}) position. For the construction of throw profiles multiple t-z profiles are measured across a fault trace and then contoured using the Surfer 14 program using the built-in kriging correlation algorithm.

The accuracy of throw measurement is equal to the trace sampling interval of the data (Baudon and Cartwright, 2008a). The trace sampling limit may be measured directly from the seismic data at a high level zoom and measuring the distance between sample points, defined by changes in the gradient of the wavelet trace (Fig. 2.9)

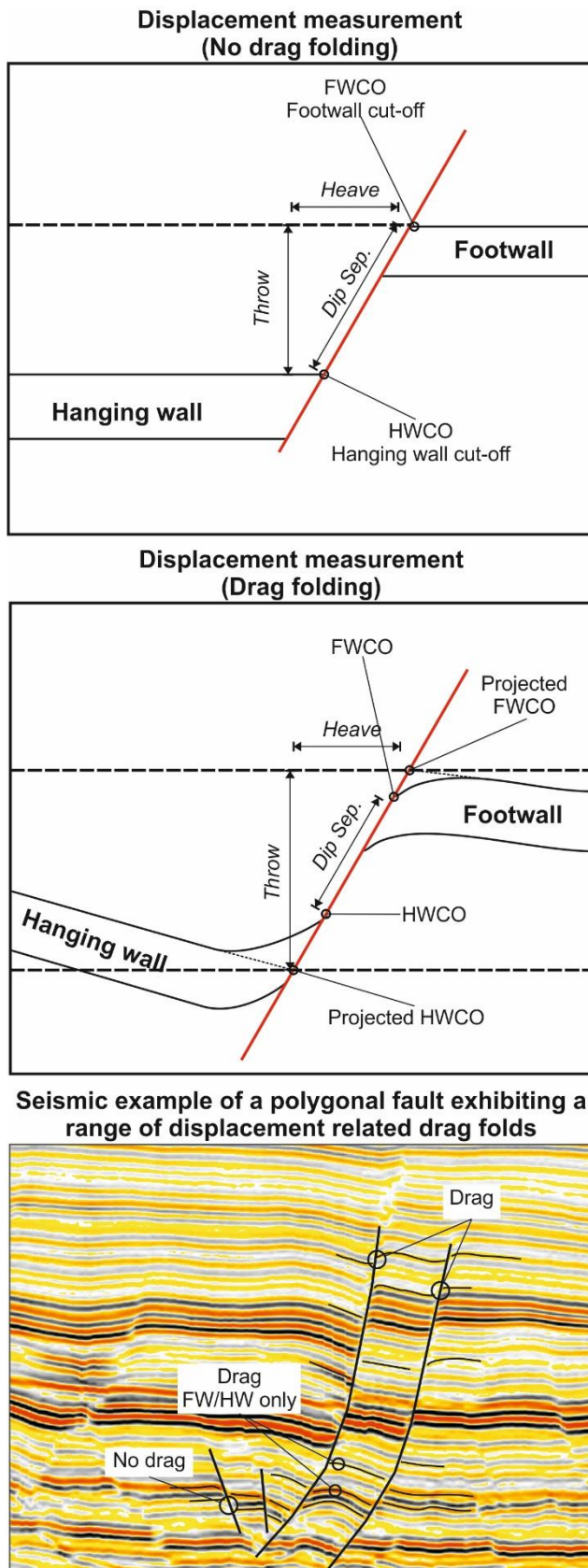


Figure 2.8: A schematic diagram of different aspects of displacement measurement for faults with and without drag folding and a seismic example showing the variability of displacement styles that can be exhibited by a single polygonal fault.

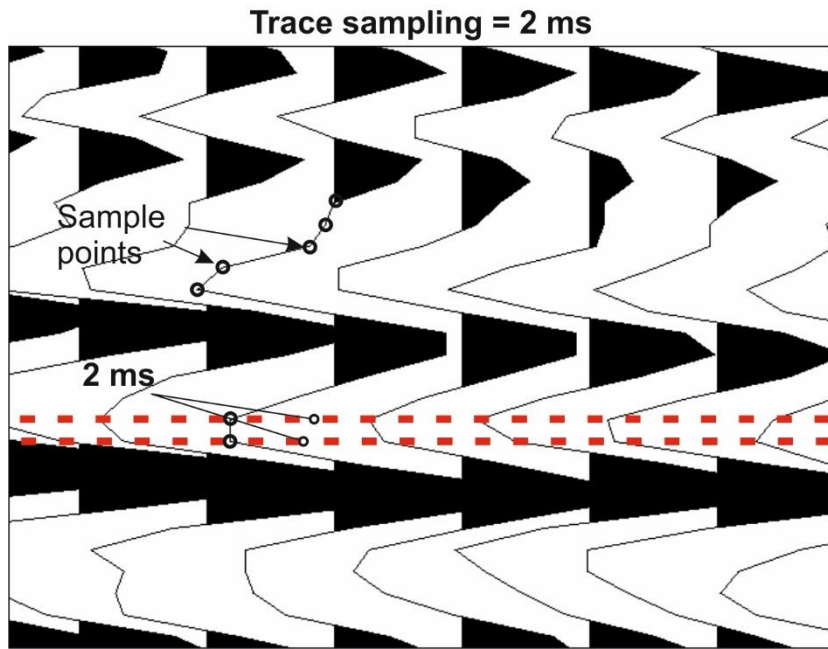


Figure 2.9: A high level zoom view of the seismic data from the Angolan Margin survey showing how trace sampling limit can be measured from seismic data. The trace sampling can be measured by firstly identifying the sample points, evidenced by changing gradients in the wavelet trace. Measuring between the sample points of the wavelet trace gives the sample limit in TWT. The trace sampling limit defines the lower limit of offset that can be measured from the seismic data.

The trace sampling limit also defines the minimum throw values that can be recorded for the data. Trace sampling limits and interval velocities are recorded in Table 2.1. Further sources of error arise from the presence of drag fold and differential compaction across the fault (Walsh and Watterson, 1988; Mansfield and Cartwright, 1996; Cartwright et al., 1998). Differential compaction and drag folding are unlikely to be a source of error for t-z plots from the Angolan Margin as throws are very low (<20 ms, 18 ms). However, the throws recorded from the Norwegian Margin are much higher (up to 80 ms, 72 m) and drag folding can clearly be seen along some faults. Where there is significant drag folding, the estimated position of the hanging wall cut-off is projected onto the fault plane to omit the drag folding (Fig. 2.8).

2.4.1.2 *Fault tips and Fault tip gradients*

Fault tips are regions of a fault that are highly susceptible to mechanical restriction (McGrath and Davison, 1995; Wilkins and Gross, 2002; Soliva and Benedicto, 2005; Morris et al., 2009; Roche et al., 2012) and interaction with other faults (Peacock and Sanderson, 1991; Cartwright et al., 1995; Dawers and Anders, 1995; Mansfield and Cartwright, 1996; Kristensen et al., 2008; Stuevold et al., 2003; Soliva and Benedicto, 2004; Fossen et al., 2010), in the case of lateral tips. In this study, fault tips, particularly basal and upper fault tip gradients are used to infer changes in mechanical stratigraphy that could explain how tier boundaries form. This method builds on the work of Baudon and Cartwright, (2008b), Wilkins and Gross, (2012) and Roche et al. (2012) to infer both the mode of tip propagation (blind or syn-sedimentary) and the presence or absence of mechanical boundaries that could restrict fault growth.

Detection of fault tips in this study was conducted using a calibrated time-dip map, where the steepest values of time-dip have a particular colour attributed to them. This allows for the differentiation between gently folded sections of the fault tip (fault propagation folding) and the fault plane, which shows a seismically resolvable offset.

Colour coded time tip maps can be used to quickly assess regions of a fault with and without offset. This is a powerful tool which helped define the seismic response of a fault plane and fault propagation folding. These colour coded time dip maps were used to differentiate between fault tip monoclines and fault planes. This is a crucial aspect of defining polygonal fault geometry as ascertaining where the limit polygonal fault propagation, of both upper and lower tips is located, defines the hallmark, layer-bound

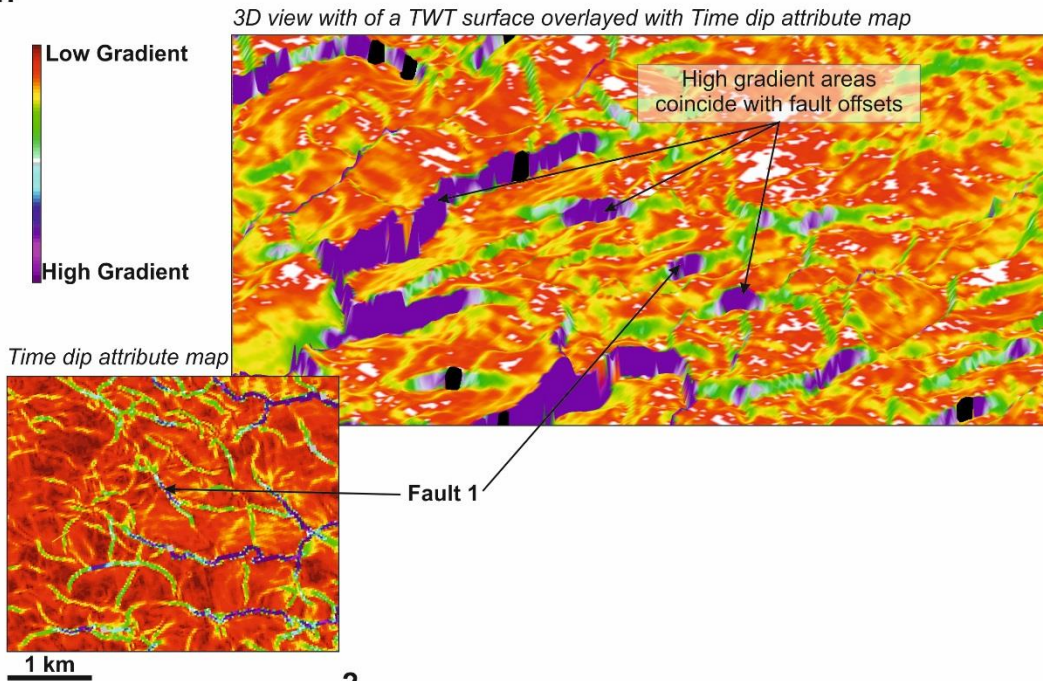
geometry of polygonal faults. In addition to colour coded time dip maps, fault tip folds are defined by their geometry in seismic data, A full review of tip-line folds is beyond the scope of this study, however for a review of physical, natural and seismic examples of tip-line folds see Jackson et al. (2006). Fault tip folds were defined as gentle changes in gradient overlying fault tips. In seismic these are manifested as folding that operates over four traces or more. In contrast fault offsets usually occur over two traces. Moreover, as polygonal faults have a quasi-elliptical geometry, any fault propagation folding moves up sequence with the fault tip. These three criteria are used to differentiate between fault offset and fault propagation folding.

Fault tip gradients are measured from the last seismically resolvable offset (see 2.5.1.1) to the last point at which the fault tip can be imaged. The gradient is therefore the ratio between the last throw value and the distance to end of the fault. Fault tip gradients are taken in large numbers (>50) and the presence or absence of a mechanical boundary is inferred, not only from the values, but also from the distribution of those values. Where values are widely distributed then fault tips are likely to be un-restricted or seismically attenuated. Alternatively, where tip gradients fall in a narrow distribution, then tip gradients can be used to infer a single mechanical unit or mechanical restriction, depending on tip position.

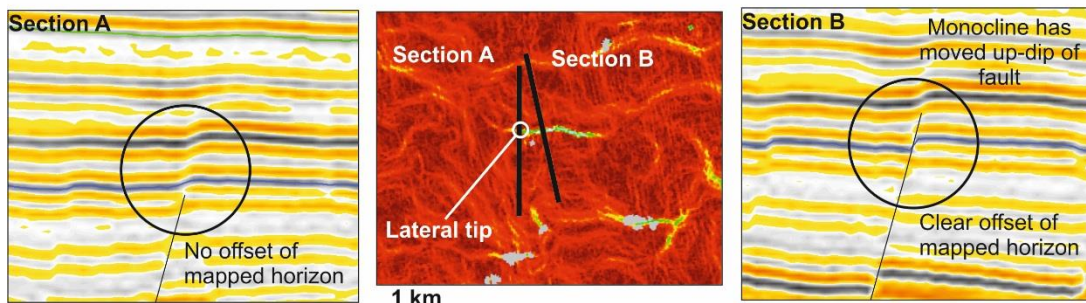
2.4.1.3 Fault orientation and length

Fault orientation was analysed using amplitude and time dip seismic attribute maps. The maps were generated from locally mapped intervals (see 2.3.1) and the horizons were analysed by hand. The measurement of rose diagrams was done by hand for two reasons, firstly, due to the data loading and server set-up within the 3D Seismic lab at Cardiff the datasets were loaded into a Schlumberger Geoframe 4.042 which does not have a fault analysis package and at the time these studies were undertaken, there were very few Petrel machines available in the lab. Secondly, after testing on a small trial volume in Petrel 2013, it was apparent that the data would require full fault modelling to generate the plots. Given that a small case study area in the Offshore Angolan survey had upwards of 200+ faults within an area of 4 km^2 it was.

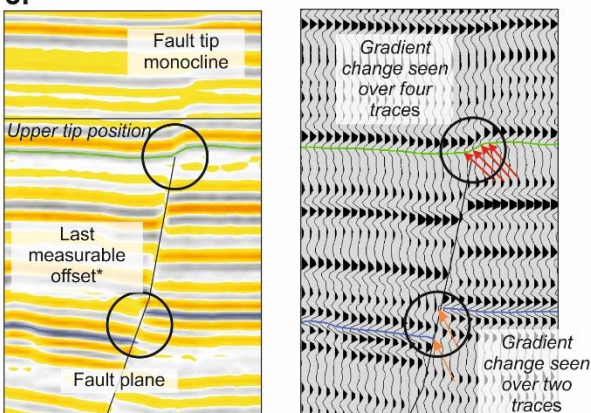
1.



2.



3.



Fault tip checklist

1. Does the tip position correspond with high gradient values on a colour calibrated time dip chart?
2. Does the fault propagation fold migrate up-sequence?
3. Does the change in gradient associated with fault propagation fold operate over four or more traces?

Figure 2.10: Summary of the three criteria for used to identify and differentiate between fault propagation folding and true fault offset. 1. Colour coded time dip maps where high seismic gradients are assigned a distinct colour value. Generally the steepest section refer to fault offsets whereas lower gradients can indicate tip-line folds. 2. Imaging the changing position of fault propagation folds .3. Differentiating between offset and propagation folding by examining the number of traces that have been deformed. Fault propagation folds are usually imaged over four or more reflections, whereas offsets are imaged over two.

decided that due to time constraints and the complexity of branchline linkage, the hand method would be faster and less prone to follow mis-picks and data errors. Fault orientation was measured using the British right hand rule, with fault length measured at the same time, using the built in planimeter tool within Geoframe. Where faults curved the faults were analysed in section to elucidate whether the curve was the result of linkage or a natural curve in the data. Where the curve was the product of a single fault orientation was measured from tip to tip. Similarly care was taken to ensure that co-linear faults were not mis-interpreted as a single fault. These data were formatted into a data file and plotted using GEOrient structural analysis software. The rose diagrams are set with a petal size presenting 5° and the petal size representing the frequency of data that fits within that bin. Rose diagrams have been suggested to be a problematic and an imperfect way of representing orientation data owing to the arbitrary way in which bins are assigned. Alternative methods for displaying rose diagrams such as MARD (moving average rose diagrams) as suggested by Munro and Blenkinsop, (2012) may give a better representation of the data by evaluating the frequency of each bin and those either side of the bin. Whilst these results may be useful for data with a single strike, the multi-azimuthal striking nature of polygonal faults would give a false weighting of the data and hence impart bias into the resultant output.

2.4.1.4 *Fault spacing*

Polygonal fault spacing was analysed using fault frequency as a proxy for spacing. Fault frequency is derived from selecting an area and counting all faults wholly contained within that specific region. This method is derived from the methodology for measuring fault density from Lonergan et al., (1998), whereby fault density is inferred from the total fault length per km^2 . The area in which the counting is done must be carefully selected to encapsulate statistically significant data for all measure horizons, with a minimum of 15 fault traces. The horizons used must also be able to be regionally correlated within the tier and ideally, capture changes around important stratigraphy boundaries, such as unconformities, diagenetic boundaries, sand intervals etc.

The resultant counts are presented in a method akin to the plotting of t-z values whereby the t (throw) is replaced by the number of faults. This generates an indication of the number of faults at a given depth. Fault frequency and has been used to aid in

the definition of the polygonal fault tiers (Carruthers et al., 2013) and is applied in this study at a higher resolution to elucidate the presence of sub-tiers (Cartwright, 1994).

Fault frequency is independent of pattern changes and is a crude proxy to the intensity of faulting in a particular area. There are a number of caveats to this method. The counting method may under represent some polygonal fault numbers where there are large numbers of faults on the periphery of the study area or where fault lengths exceed the dimensions of case study area. It can also be influenced by fault linkage where unlinked tips may link higher or lower in the stratigraphy, reducing fault numbers and giving an over estimation of fault numbers. Additionally, this measurement does not have a spatial component which may indicate that the study area must achieve a balance between capturing statistically significant data whilst ensuring that the area doesn't cover too large an area where changes in intensity are lost in the background.

2.4.2 Statistical analysis

Statistical analyses are used in Chapter 6 to distinguish differing populations of features or faults. The statistical tests applied were initially to examine the normality of the data distribution using an Anderson-Darling test where

$$\#_a^6 L F J F \frac{S}{J} \overset{\alpha}{\rightarrow} : t F F s; \geq Z' Q_{\alpha}, E Z' \% F Q_a ? \geq 5; ; ?$$

Equation 2.5

The normality of the data was then used to inform the statistical correlation tests that were undertaken. The preferred statistical test used in this study was the Spearman's rank (or Spearman's rho) test.

$$LL s F \frac{x \tilde{A} \phi}{J: J^6 F s};$$

Equation 2.6

Where d is the change in ranking between each sample and n is the total number of samples. This test is a non-parametric test that examines the change in rank between data sets. Spearman's rho can be used for normal and non-normal data and is selected here as it is less sensitive to outliers in the data set. The p and r values give an indication of the closeness of the correlation and the degree of confidence respectively. The degree of confidence was correlated using a table of r .

3 Regional Geology

3.1 Offshore Angola

The Lower Congo basin is a large salt basin located on the West African margin that extends from offshore Cameroon to Namibia (Brownfield and Charpentier, 2006). The study area in Chapters 4 and 5 are located on the mid-slope position at water depths of between 1000 m and 1500 m.

3.1.1 Basin Evolution

The Lower Congo Basin is one of several sub-basins found along the West African Margin, that in recent years, have been the focus of much study for hydrocarbon prospectivity (see Brownfield and Charpentier, 2006 and Liu et al., 2008). These basins formed during the break up of Gondwana during the late Jurassic and early Cretaceous (Fig. 3.1).

The pre-rift stratigraphy is dominated by alluvial/aeolian quartz rich sandstones of the Lucala Formation, deposited over Precambrian basement made of sheared and folded metamorphic rocks and intrusive igneous rocks (Burwood, 1999; Brownfield and Charpentier, 2006).

Initially broad dates for rifting were suggested for the opening of the rift between South America and Africa. The rifting and final break-up of South America and Africa began in the South Atlantic and moved progressively northwards during the Early Cretaceous (Mascle and Phillips, 1972; Larson and Ladd, 1973; Guiraud and Maurin, 1992; Uchupi, 1989; Binks and Fairhead, 1992) and was dated to the Neocomian (144-127 My). Three distinct rift phases have been identified by Karner et al. (1997) and Karner and Driscoll (1999). The earliest rifting phase occurred during the Berriasian to Hautervian epoch, the second occurred during Hautervain to late Barremian and the latest rifting stage occurred during the late Barremian to late Aptian (Fig. 3.1). Each rifting phase is demarcated by a regional hinge zone with the earliest rifting bound by the Eastern Hinge zone and the later extension delimited by the Atlantic hinge zone (Karner et al., 1997; Karner and Driscoll, 1999). The hinge zones record the shifting of extension along the rift flanks. With the end of rifting coinciding the emplacement of oceanic crust (Karner et al., 1997). Each rifting phase is represented by a regional unconformity representing break-up and uplift along the rift hinge. Seismic expression of these units included divergent and rotated reflections within asymmetrical half grabens (Karner et al. 1997). The rifting events created a

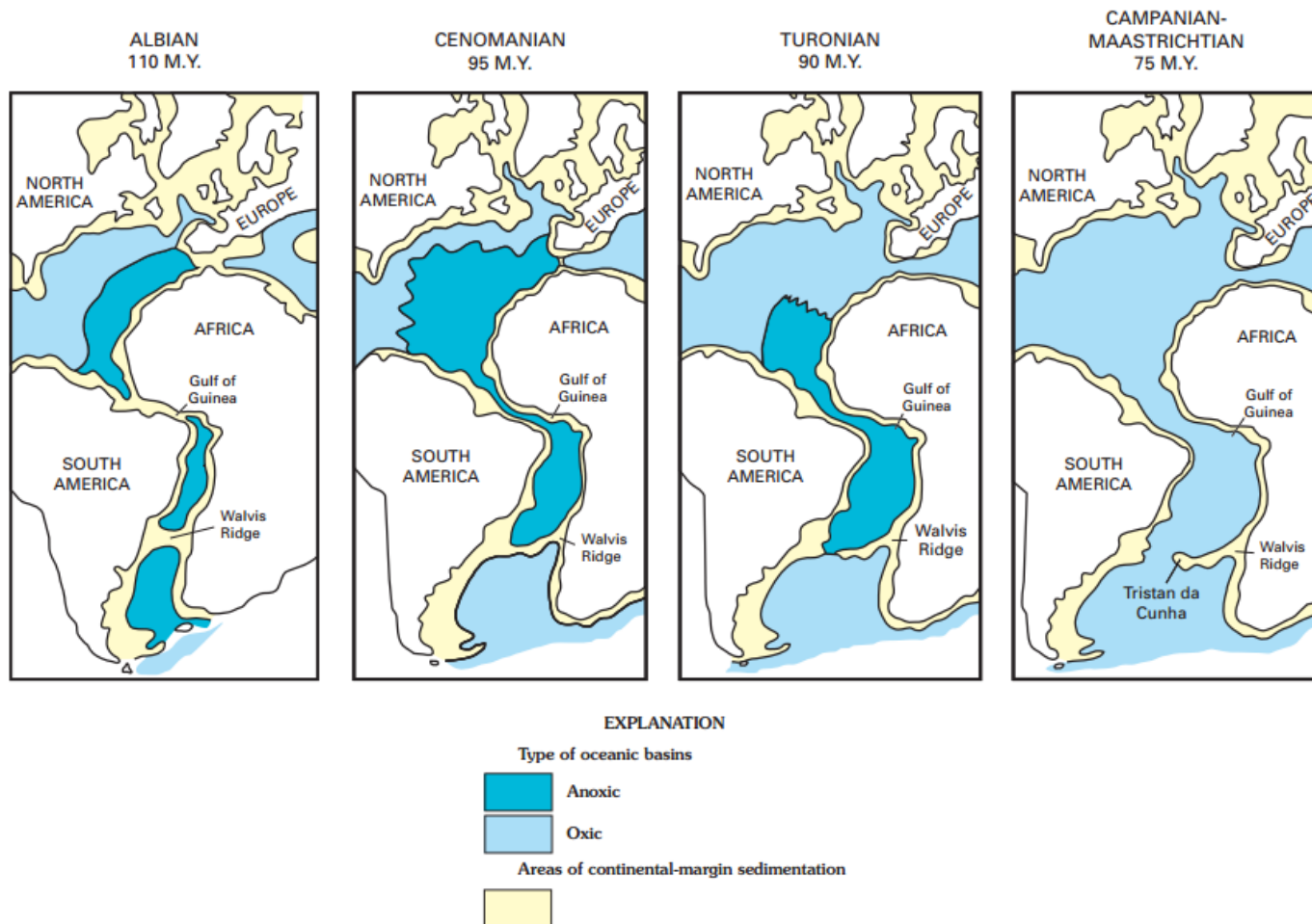


Figure 3.1: (From Brownfield and Charpentier, 2006) A palaeogeographic reconstruction of evolving plate tectonic configurations during the break-up of the South Atlantic

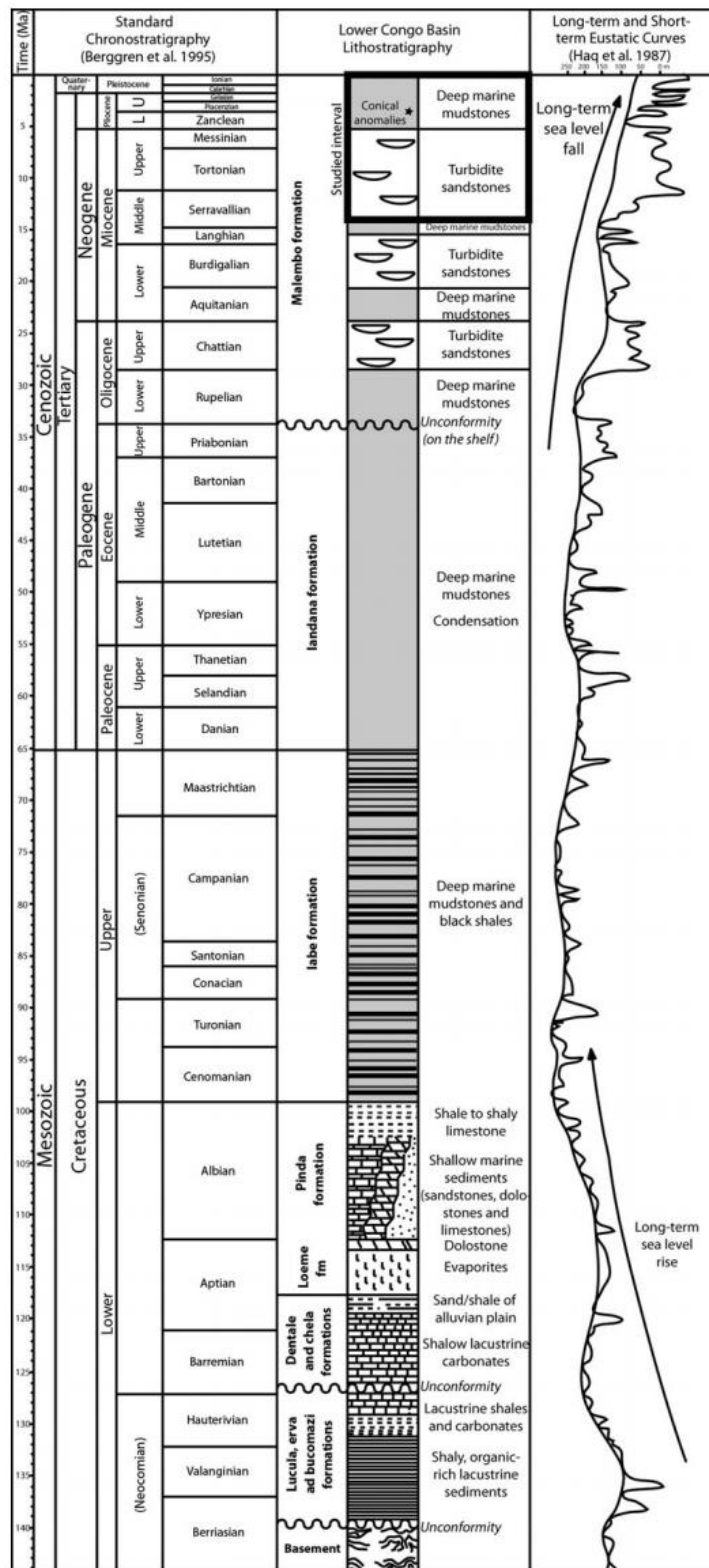


Figure. 3.2 (From Monnier et al., 2014) A regional stratigraphic column of the Lower Congo Basin

series of deep anoxic lacustrine basins dominated by shales siltstones and marls up to 1 km thick (Karner et al., 1997; Burwood, 1999; Brownfield and Charpentier, 2006) (Fig.. 3.2). Many studies ascribe the tectonic setting of Loeme formation evaporites to post rift thermal subsidence (Hudec and Jackson, 2002; Calassou and Moretti, 2003; Tari et al., 2003; Brownfield and Charpentier, 2006). The syn-rift sequence is interpreted by Karner et al. (2003), Karner and Gamboa (2007) as well as by Hudec and Jackson (2004) to also include the salt. Karner et al. (2003) and Karner and Gamboa, (2007) purport that hinges at the margins of the rift accommodate brittle upper crust and ductile lower crust extension. At the centre of the rift, there is a gradual transition from brittle to ductile deformation and accommodation of lithospheric stretching without the requirement for pervasive normal faulting. This in turn locally exposed the pre-salt margins and helped form a widespread, shallow restricted basin, in which up to 1 km of evaporites were deposited (Karner et al. 2003). Hudec and Jackson (2004) also infer that the salt was bound by a structurally controlled distal ramp, consistent with the syn-rift late hypothesis. The evaporites were not deposited as a single massive salt body but were segregated into several smaller sub-basins by the Mid Ocean Ridge and cite the evidence from magnetic anomalies, map reconstruction, regional stratigraphy and hydrothermally altered potash deposits within the salt (Hudec and Jackson, 2004).

The post rift thermal subsidence coupled with sea level rise established shallow marine conditions during the Mid-Cretaceous across the West African Margin from Nigeria to Angola (Eichenseer et al., 1999). These shallow marine conditions are typified by an oolitic siliciclastic barrier system between 600 m and 1200 m in thickness (Brownfield and Charpentier, 2006; Eichenseer et al., 1999) (Fig.. 3.2). Continued thermal subsidence and sea-level rise during the Mid to Late Cretaceous and Paleogene deposited thick accumulations of organic rich shales (Burwood, 1999; Coward et al., 1999; Holbourn et al., 1999; Valle et al., 2001; Broucke et al., 2004; Brownfield and Charpentier, 2006). The Eocene-Oligocene transition is demarcated by a major erosional event that records a global drop in sea-level (McGinnis et al., 1993; Seranne, 1999). During the Oligo-Miocene there is a westwards progradation of a deltaic system, punctuated by sea level changes (1 – 3 My). These changes forced deep incision and erosion of the Zaire River, which was subsequently deposited in the marine domain as a large turbiditic submarine fan (Droz et al., 1996; Lavier et al.,

2001; Broucke et al., 2004; Gay et al., 2006) (Fig.. 3.2) These turbidites flowed into a deep water basin, predominately comprised of deep marine shales (up to 3000 m thick) and deposited stacked sequences of turbidite channels and debris flows up to 25m thick (Anderson et al., 2000; Valle et al., 2001; Babonneau et al., 2004; Broucke et al., 2004; Séranne and Anka, 2005; Brownfield and Charpentier, 2006; Anka et al., 2009; Savoye et al., 2009). The position of the Miocene turbidite channels are strongly controlled by either tectonic structures such as faulted rafts (Anderson et al., 2000; Broucke et al., 2004) or inherent sedimentary architecture such as levees (Broucke et al., 2004) and canyons (Babonneau et al., 2004). Pliocene to recent submarine deposits are delivered to the abyssal plain the only sediment deposited is presently hemipelagic muds (Monnier et al., 2014).

3.1.2 The structural evolution of the Lower Congo Basin

The Aptian age salt of the Lower Congo basin is the primary control on structures and stratigraphy within the basin. There are four structural domains in the lower Congo Basin as summarised in Calassou and Moretti, (2003) and by Fig. 3.3 and Fig. 3.4;

1. A 100 km wide extensional domain dominated by salt rollers and large normal faults.
2. A transitional domain with vertical diapirs between 0 – 50 km wide.
3. A compressional domain with thrusts, reverse faults and extensive folding up to 200 km wide.
4. An external domain with no evidence of faulting overlying oceanic crust and has Miocene to Recent age accumulations of sediment, up to 4 km thick.

These salt structures have been the subject of much study with Angolan margin forming the type locality for raft tectonics (Duval et al., 1992; Lundin, 1992; Spathopoulos, 1996; Cramez and Jackson, 2000). Using cross-section restorations, Hudec and Jackson, (2004) were able to identify three distinct phases of basin evolution and basement deformation. The earliest phase occurred in the Aptian and Albian and is characterised by a differential seaward tilting of the basin that enabled the early seaward extension. The seaward extension established growth structures in both the extensional and compressional domains. This uplift was very short lived and ceased in the late Albian due to thinning of the salt. The second phase

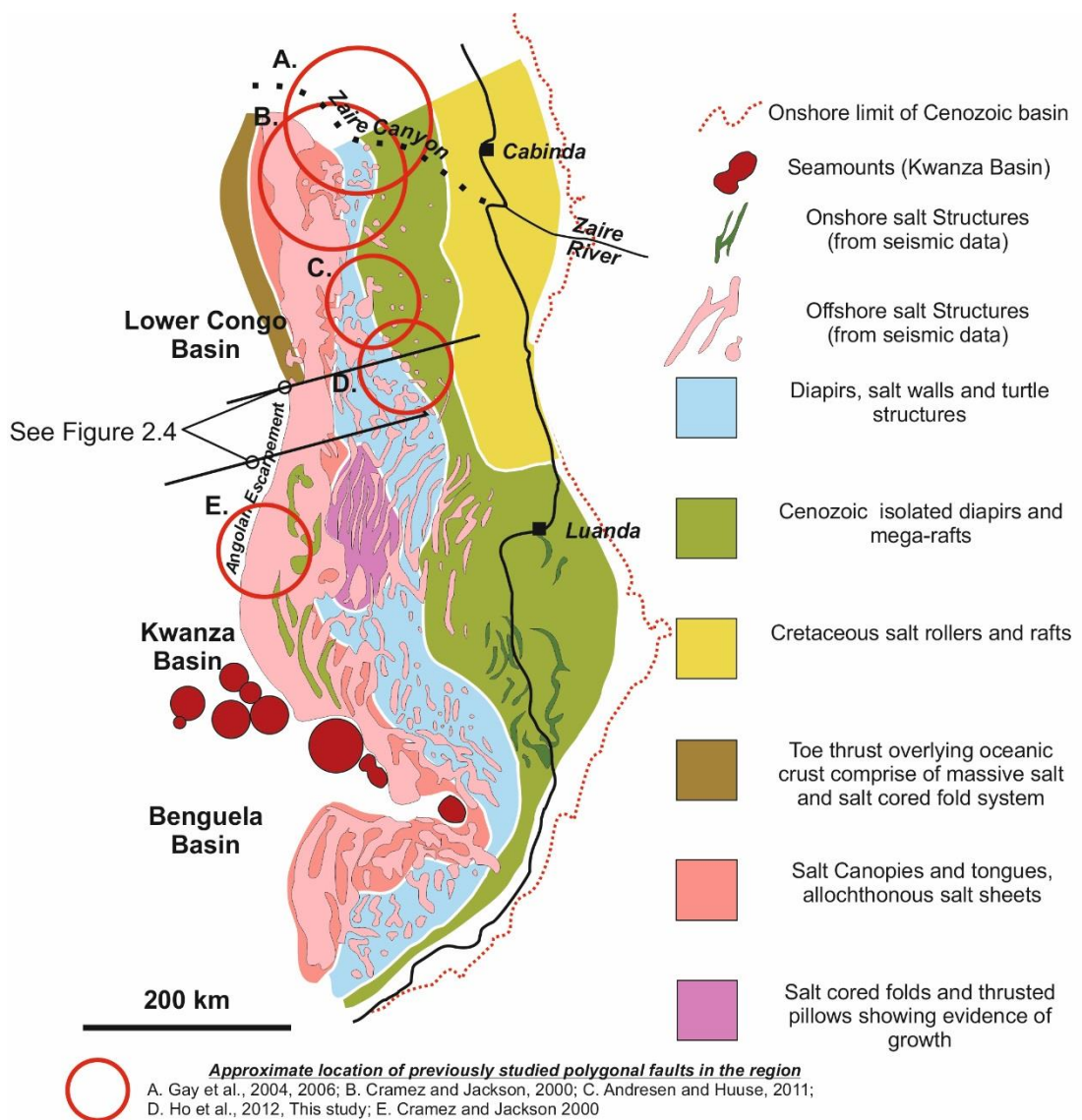


Figure 3.3: Redrawn from Tari et al., 2003, A structural geology map of the Southern section of the West African margin summarising the salt tectonic regimes in the Lower Congo, Kwanza and Benguela basins

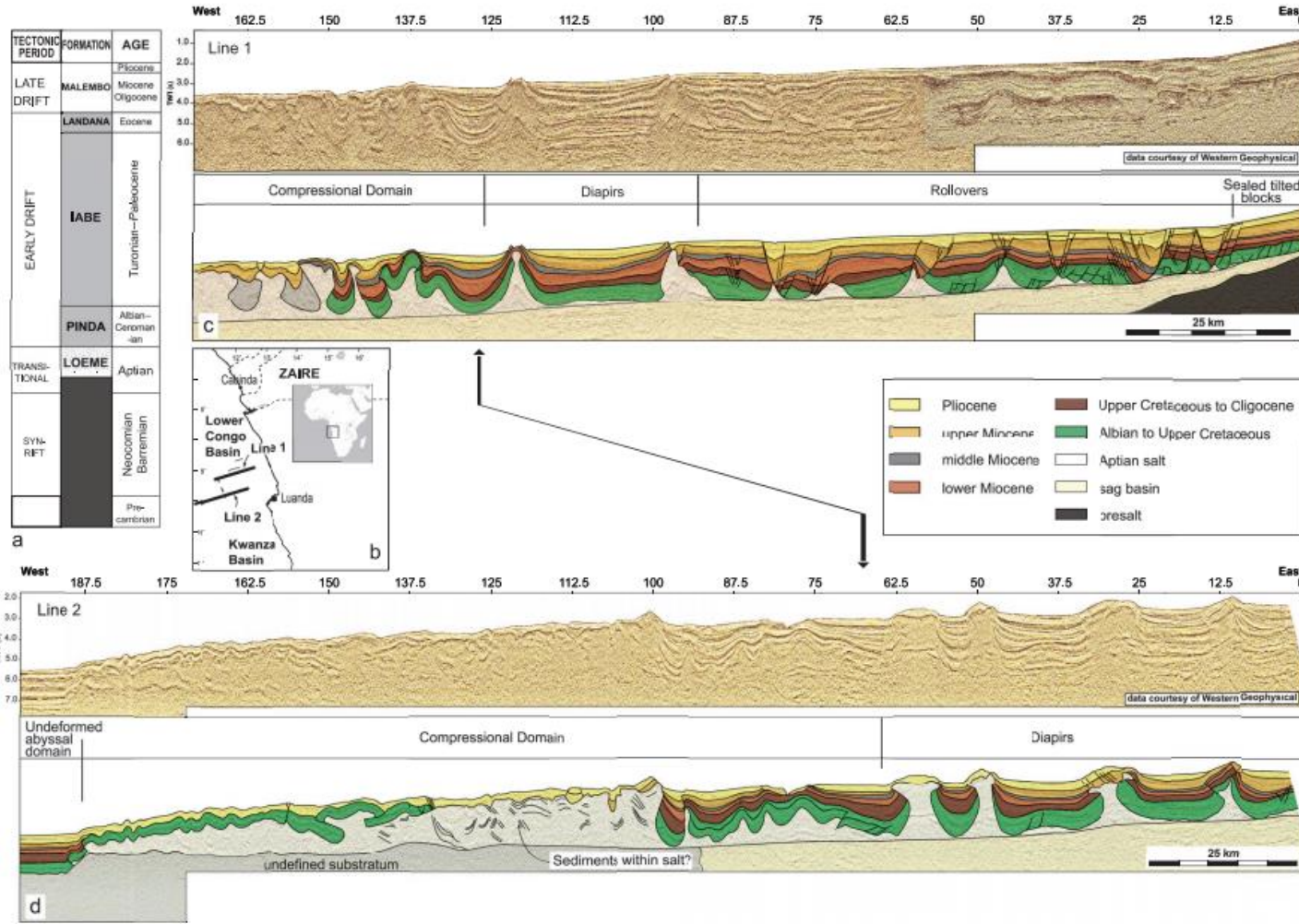


Figure 3.4: (From Fort et al 2004) Regional cross sections of the structural domains within the salt basin

occurred in the late Cretaceous to Oligocene and uplifted the deep marine basin by reactivating basement structures (Karner et al., 2003; Hudec and Jackson, 2004) as well as creating the large monocline province (Cramez and Jackson, 2000). The final phase of basin evolution is Miocene to recent uplift and seaward tilt of the basin. This uplift began in the Mid Miocene and persists to the present day (Lundin, 1992; Hudec and Jackson, 2004), with evidence of sea-floor folding around some contractional structures (Brun and Fort, 2004). Early interpretations of the cause of Miocene uplift have been attributed to the formation of a large plateau region, onshore Kwanza basin (Lundin, 1992). Additional data from apatite fission track and analysis of regional biostratigraphy shows a number of hiatus' associated with the uplift of the onshore Precambrian craton (Jackson et al., 2005). Indeed, the uplift was shown to strongly affect the landward rim of the basin and thus only affected the Inner Kwanza Basin and onshore regions.(Hudec and Jackson, 2004; Jackson et al., 2005). Moreover the estimates of uplift vary spatially. Jackson et al. (2005) suggest uplifts of up to 150 m in the north and more than 1000 m to the south of basin.

However more recently it has been suggested that renewed down dip migration and contraction of the salt (Duval et al., 1992; Hudec and Jackson, 2004; Jackson et al., 2005). The contraction of the salt was translated landward and initially forced the migration and thrusting of the Angolan salt nappe and later vertical welding of some diapirs in the region due to buttressing of Miocene and Recent sediments at the toe of the nappe (Hudec and Jackson, 2004). The downslope motion of the salt is widely attributed to gravity sliding/spreading (Duval et al., 1992; Lundin, 1992; Anderson et al., 2000; Hudec and Jackson, 2002; Valle et al., 2001; Tari et al., 2003; Hudec and Jackson, 2004)

3.1.3 Occurrences of polygonal faults on the West African margin

Polygonal faults have been previously reported in several studies on the West African margin (Cartwright and Dewhurst, 1998; Cramez and Jackson, 2000; Gay et al., 2004, 2006; Andresen and Huuse, 2011; Ho et al., 2012; Monnier et al., 2014) (Fig. 3.3). All of the studies noted polygonal faults in the Tertiary of the Namibian and Orange basin (Cartwright and Dewhurst, 1998). Further north, polygonal faults have been found in the Neogene of the Lower Congo and Gabon basins (Cramez and Jackson, 2000), Upper Miocene to Lower Quaternary of the Lower Congo Basin, North of the Zaire Canyon (Gay et al., 2004, 2006) and the Plio-Pliestocene of the Lower Congo Basin,

south of Zaire Canyon (Andresen and Huuse, 2011; Ho et al., 2012; Monnier et al., 2014). All polygonal faults previously described in the literature are found in formations that are clay rich sequences and have upper tips in close proximity to the seabed.

3.2 Norwegian Margin

This section examines the geological history of the Norwegian Margin. The Norwegian Margin is located between 62°N and 69°N offshore of northwestern Norway (Fig. 3.5), in water depths of up to 1800 m. There are two major basins on the Norwegian Margin, the Vøring Basin, located between the Bivrost fracture zone to the northeast and the Jan Mayen fracture zone to the southwest (Lundin and Doré, 1997). The second basin is the Møre basin bound to the northwest by the Jan Mayen fracture zone and has the southeastern boundary demarcated by the Shetland-Fareo Escarpment (Lundin and Doré, 1997). The survey used in this study is located on southern tip of the Modgunn Arch, a Cenozoic inversion structure, located between both the Vøring and Møre basins, over the Jan Mayen Fracture zone (Blystad et al., 1995)

3.2.1 Structural evolution of the Vøring and Møre basins

3.2.1.1 *Pre-rift Architecture: Caledonian Orogeny*

The Caledonian Orogeny spanned from Late Cambrian to Silurian, during the consolidation of several smaller plates (Baltica, Avalonia and Laurentia) to form Laurussia (Euramerica) (Ziegler, 1988; Roberts, 2003) More recently four distinct tectonic events within the Caledonian Orogeny have been recognised and summarised in Roberts (2003). The oldest tectonic event, The Finnmarkian Event, involved the accretion of Baltica and an unnamed magmatic island arc. The next Caledonian event, the Trondheim event, involved the obduction of a micro-continent against the Baltica continent. Subsequent tectonic events (Taconian and Scandian events respectively) initially involved the remote expression of thermotectonic events, in the form of island-arc accretion along the Laurentian Margin and later involved the subduction of the Baltic Margin beneath the Laurentia plate. The final and latest phase is the Solundian phase which is the Mid to Late Devonian post-orogenic collapse which created a change in tectonic regimes from compressional to extensional tectonics. The extensional tectonic domain is evidenced with the development of basal shear zones and half grabens infilled by continental alluvial sedimentation (Ziegler, 1988; Andersen and Jamveit, 1990; Andersen et al., 1994; Folkestad and Steel, 2001)

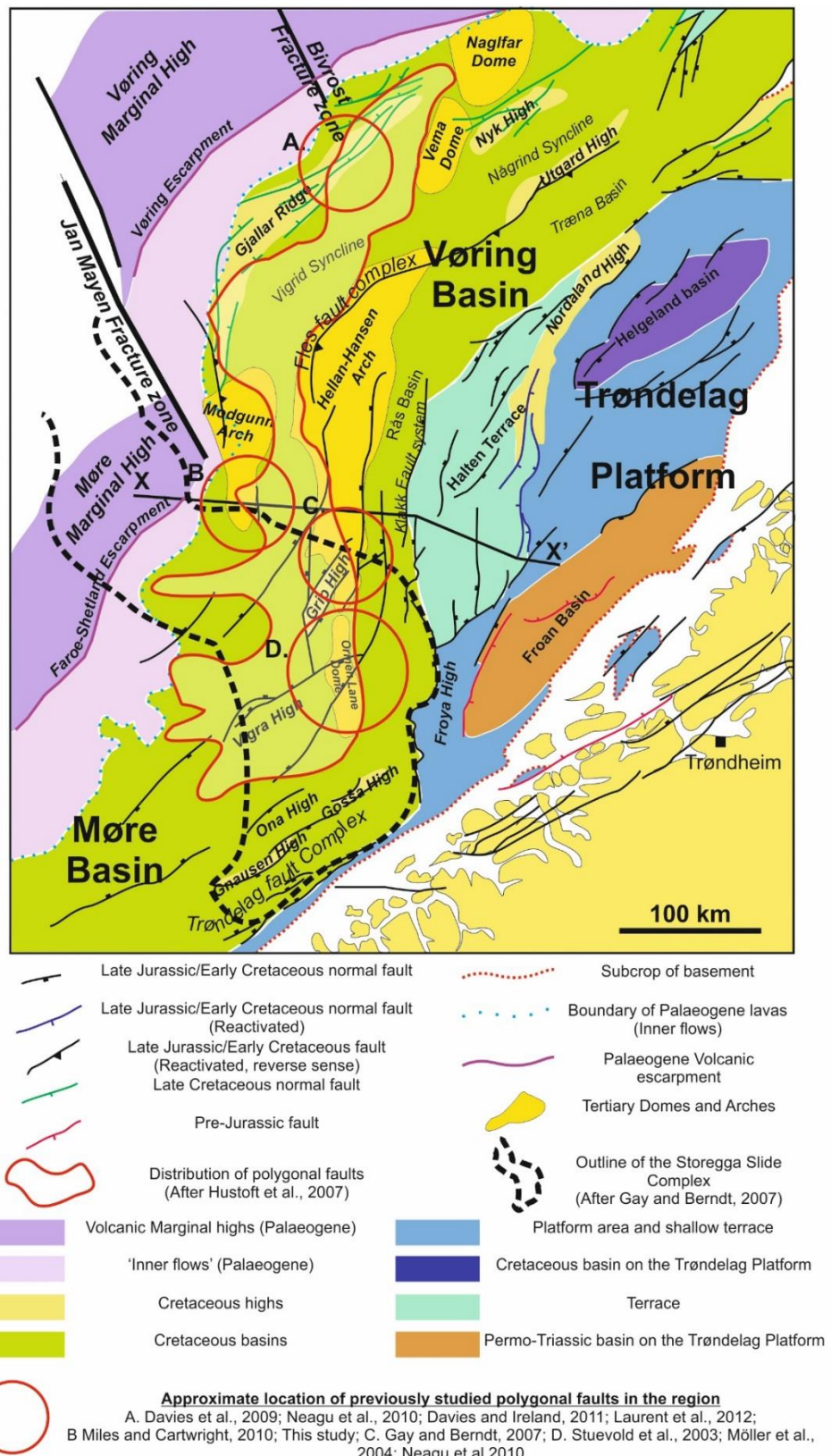


Figure 3.5: Tectonic map of the Vøring and Møre basins on the Norwegian Margin summarising the location of major structures as well as the distribution of polygonal faults in the region. For line of section see Fig. 3.7

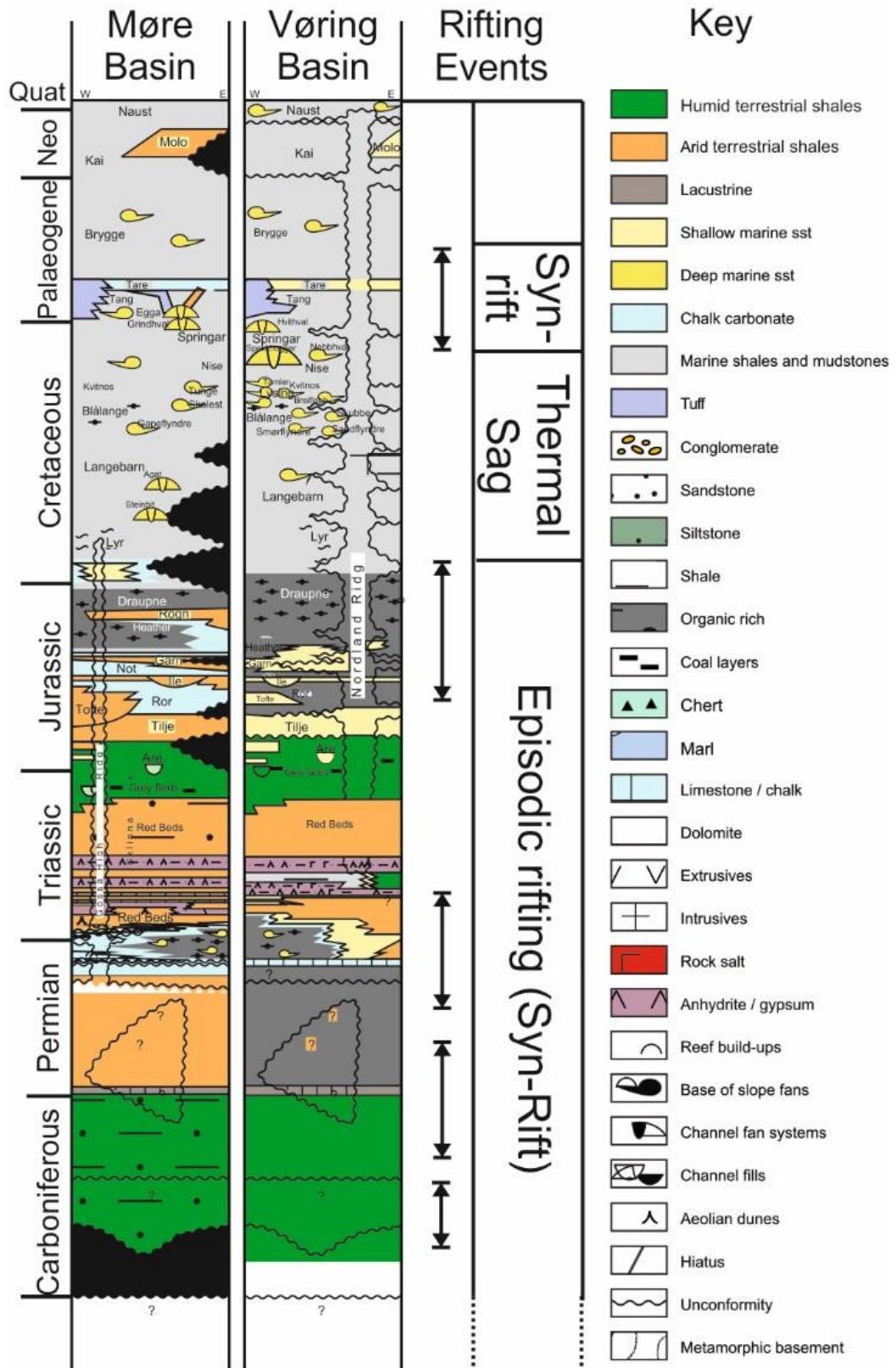


Figure 3.6: Tectono-stratigraphic column of the Møre and Vøring basin modified from the Norwegian Lexicon stratigraphic wall chart (Naturhistorisk Museum, 2015)

3.2.1.2 *Syn-rift basins*

Three distinct phases of early, pre-break-up rifting have been recognised on the Norwegian Margin during the Mid Carboniferous, Carboniferous-Permian and Permo-Triassic (Ziegler, 1988; Brekke et al., 2001). The structure of the rift was dominated by N-S and NE-SW trending normal faults with NW-SE transfer faults (Lundin and Doré, 1997; Doré et al., 1999; Brekke, 2000). The overall Carboniferous stratigraphic succession on the Norwegian Margin records the evolution of a rift dominated sedimentary system with alluvial and fluvio-deltaic systems, draining into two palaeoseaways to the southwest and northeast of the Norwegian Margin (Brekke et al., 2001 and references therein).

The Early Permian on the Norwegian Margin is a continuation of the terrestrial sedimentation seen in the Carboniferous. Carboniferous-Permian rifting initiated due to the onset of an E-W transtension/extension that reactivated NW-SE basement structures (Brekke et al., 2001) (Fig. 3.5)

The Permo-Triassic rifting and crustal extension was driven by thermal subsidence of the margin and almost exclusively accommodated along a series of boundary faults orientated NNE to NNW. Thermal subsidence is also coupled with uplift along the Norwegian mainland. The sedimentation is predominately terrestrial alluvio-fluvial deposits with minor marine incursions (Brekke, 2001). Many of the Palaeozoic and early Mesozoic syn rift deposits and structures are preserved on the Trøndelag Platform (Blystad et al., 1995; Brekke, 2000; Brekke et al., 2001; Sommaruga and Bøe, 2002) (Fig. 3.5, Fig. 3.6)

3.2.1.3 *Formation of Vørting and Møre Basins: Rift to Drift*

The Vørting and Møre basins are large basins which comprise grabens, deep basins and structural highs that formed during the Mid/Late Jurassic to Early Cretaceous crustal stretching and thinning (Blystad et al., 1995). The development of the Vørting and Møre basins show strong contrasts. The Vørting Basin developed over several phases of faulting, the earliest of which occurred in the Late-Mid Jurassic to Early Cretaceous (Brekke, 2000; Gómez et al., 2004; Skogseid et al., 2000) (Fig. 3.8). The earliest faulting along the Fles fault complex created a number of smaller sub-basins and structures. These include the Rås and Træna basins to the East and the Vigrid and Någrind syclines to the west (Blystad et al., 1995; Brekke, 2000). During the mid-

Cretaceous these sub-basins were overprinted by thermal subsidence and were thus incorporated into the larger Vøring basin (Fig. 3.7). Late-Jurassic to Early Cretaceous rifting is the main phase of deformation in the Møre basin. The early rifting phase comprise of landward dipping fault blocks, many of which had very high throws of 2.5 km or more (Brekke, 2000). Many of these tilted fault blocks formed incipient highs within the basin (Fig. 3.7).

The Mid to late Cretaceous of the Vøring and Møre basins formed large basins as the result of crustal downwarping as very little evidence for faulting can be seen in the basin (Blystad et al., 1995; Brekke, 2000). This is coupled with the rise of the margins of both the Vøring and Møre basins, evidenced by thinning and onlapping Cretaceous sediment (Brekke, 2000) (Fig. 3.7). This regime of passive subsidence continued in the Møre basin until the early Palaeogene. In contrast the Vøring Margin underwent significant folding and uplift during the late Cretaceous due to tectonic inversion (Doré et al., 1999; Brekke, 2000; Skogseid et al., 2000). The primary locus for folding in the Vøring basin was the Fles fault system that was reactivated and forms the core of a faulted antiform (Fig. 3.7). In the northern sector of the Vøring basin, the Nyk and Utgard highs define three large synclinal folds (Brekke, 2000). These folding events formed in the latest Cretaceous as the folding of the Upper cretaceous units becomes progressively more open in the North of the Basin and the northern most anticlines of the Utgard and Nyk highs show no onlaps with Cretaceous strata. The flexure of the crust in the Vøring Basin and passive subsidence of Møre basins created deep marine basins into which thick shales up to 8km thick accumulated and have been the subject of much exploration for their potential to generate hydrocarbons (Brekke et al., 1999; Brekke, 2000; Skogseid et al., 2000; Brekke et al., 2001). In addition there are localised occurrences of thick (up to 1 km) of sandy turbidites sourced from the emergent platform areas and transported along NW-SE lineaments (Brekke et al., 2001) (Fig. 3.8).

The Palaeogene of both the Vøring and Møre basin records the continued uplift of the Cretaceous basins and is punctuated by a flat to weakly folded unconformity at the base of the Palaeogene (Brekke, 2000). The early Palaeogene in both the Møre and Vøring basins is significant as it marks the rifting and significant igneous activity arising from a mantle plumes under the thinned lithosphere (Eldholm et al., 1989; Doré et al., 1999; Brekke, 2000; Planke et al., 2000; Berndt et al., 2001; Planke et al., 2005)

(Fig. 3.5, Fig. 3.7). In the Vør ring and Møre basins, there is evidence of sub-aerial lava flows on the Vør ring escarpment as well as the Fareo-Shetland escarpment at the edges of the Vør ring and Møre basins respectively. Within the basins themselves the igneous activity and synchronous with the extrusive volcanics on the northwestern basin margins, there is widespread emplacement of sills into the Cretaceous basin fill on the northwestern side of both basins. In the Møre Basin, sill emplacement was constrained by the Møre-Trøndelag fault system with deepest sills being found to the east of the basin and become shallower, stepping through stratigraphy (Brekke, 2000). Faulting and deformation associated with the continental break-up of Greenland and Norway was focused on the margins of the basins, in particular the Gjallar Ridge (Brekke, 2000; Gernigon et al., 2003, 2004). Palaeocene sedimentation was deposited during a period of rifting and uplift of the Fennoscandian shield, creating a shallow basin with a stratified water column (Brekke et al., 2001; Brunstad et al., 2008) which deposited marine clays with minor sandstones and siltstones (Dalland et al., 1995; Brekke et al., 2001) (Fig. 3.8). The break-up of Norway from Greenland deposited thick flood basalts along the Vør ring Escarpment and Gjallar ridge areas. In the south, magmatism and igneous activity is expressed in deposits of tuffaceous clays (Dalland et al., 1995; Brekke, 2000; Brunstad et al., 2008) formed from the deposition of volcanic ash in the restricted, deep basins (Fig. 3.8).

3.2.2 Post rift sedimentation and tectonic inversion

Post rift, the Norwegian margin was subjected to inversion, caused by a change in the plate motion (Lundin and Doré, 2002). This change in plate motion created large domes and elongated antiforms such as the Hellan Hansen and Modgunn Arch (Fig. 3.7). The inversion related domes helped to constrain the position of contourite deposits within the shelf environment (Bryn et al., 2005; Eidvin et al., 2007; Hjelstuen et al., 2004).

The Brygge formation was deposited from Early Eocene to Early Miocene (c. 55-18Ma)(Chand et al., 2011; Eidvin et al., 2007). The Brygge formation represents one of the major tectono-stratigraphic elements of the Norwegian margin. The oldest sediments of the Brygge formation are terrigenous in origin and are continental shelf deposits that were deposited prior to the opening of the Greenland - Norway and

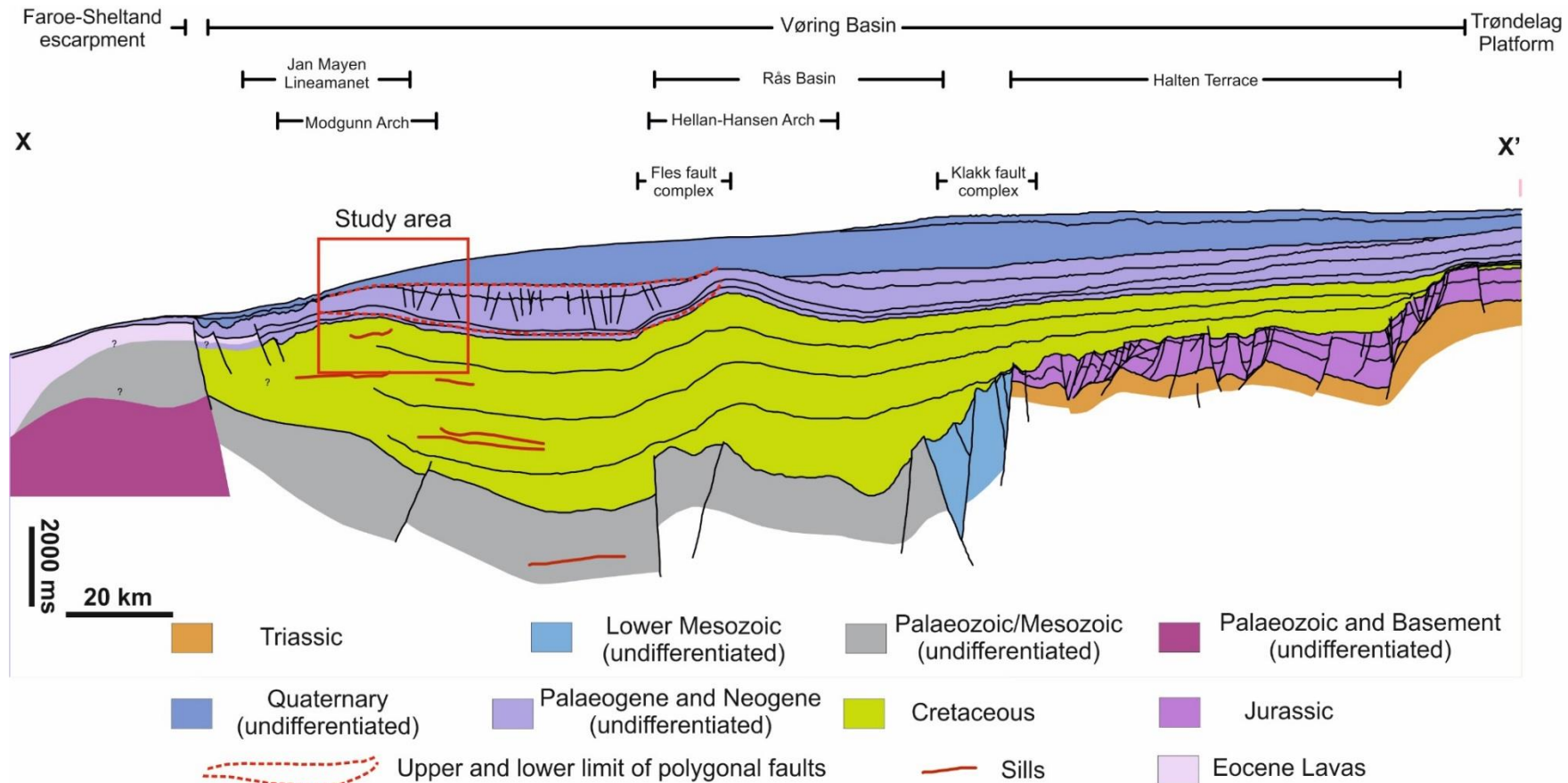


Figure 3.7: Modified from Blystad et al 1995 summarising the structural and stratigraphic context of the Hellan Hansen and Modgunn arches. For line of section see Fig. 3.5.

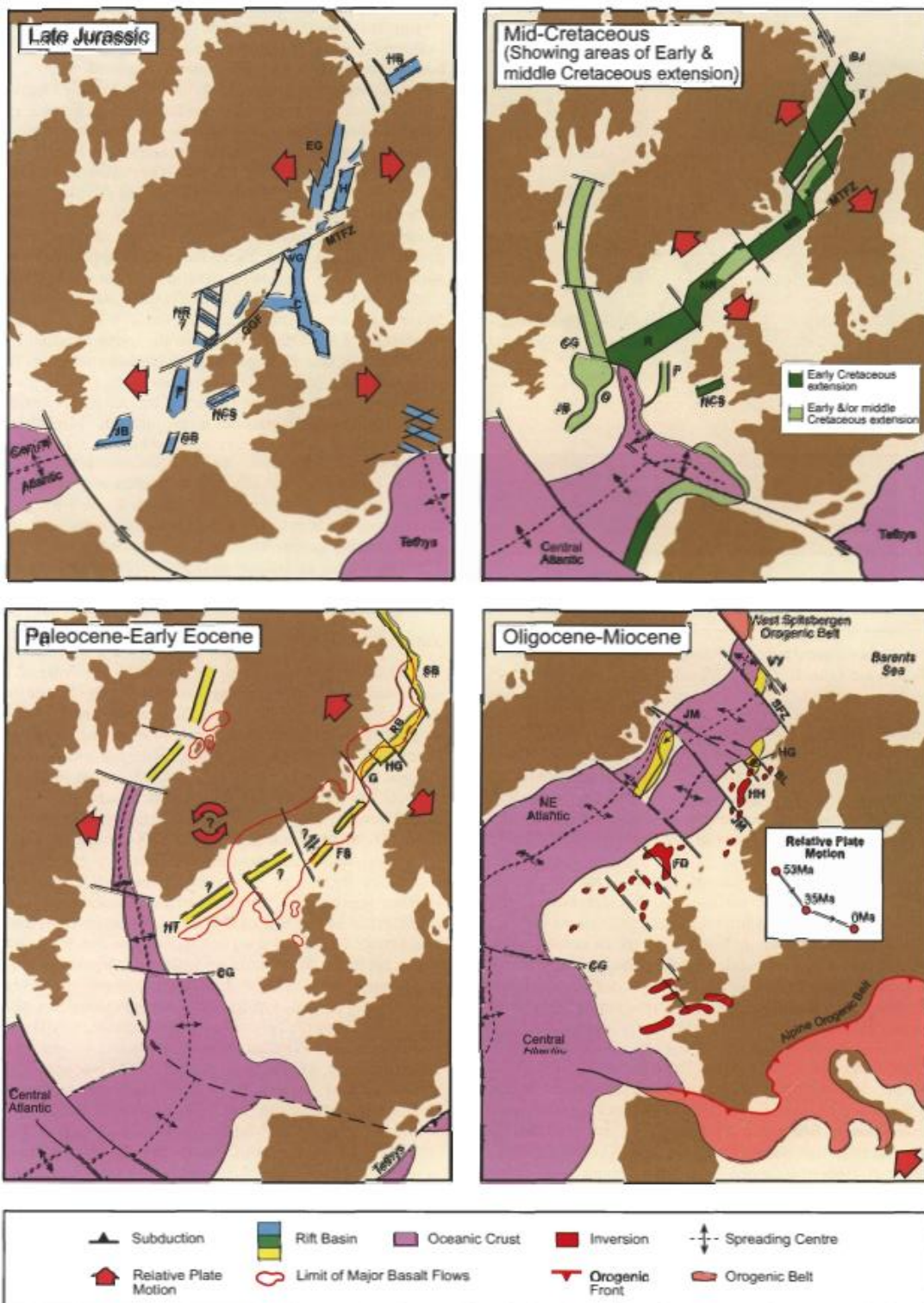


Figure 3.8: (From Lundin and Doré, 1997) Palaeogeographic reconstruction of the NE Atlantic from Late Jurassic to Miocene age

Greenland - Scotland seaways (Chand et al., 2011; Eldholm et al., 1989; Thiede and Myhre, 1996). The opening of these seaways coupled with subsidence and flooding deposited a succession of hemipelagic oozes composed of biosiliceous clays and muds (Fig. 3.6). This unconformity coincides with the reactivation and growth of the Modgunn and Hellan Hansen arches (Brekke, 2000). The timing of activation and cessation of uplift is not clearly defined as doming has been observed to affect Late Miocene age sediments (Løseth and Henriksen, 2005). The Kai formation is Early Miocene to Late Pliocene in age and is primarily composed of hemipelagic calcareous and siliceous oozes that form large contourite drifts (Bryn et al., 2005; Eidvin et al., 2007; Hjelstuen et al., 2004) (Fig. 3.6). The contourite drifts form around incipient highs and reflect the establishment of oceanic currents within the developing sea way between Norway and Greenland.

The upper most formation in the region is the Naust formation. The Naust formation is a late Pliocene early Pleistocene succession of glacio-marine sediments (muds, ice rafted debris and debris flows), deposited in a wedge geometry (Swiecicki et al., 1998). The Naust formation is influenced by contour currents as well as glaciogenic debris flows resulting in an interlayering of the two deposits within the basin (Bünz et al., 2003). The survey area studied is located on the northern side wall of the Storegga slide, a large submarine landslide that transported 3400 km³ of sediment up to 800 km NW of Norway into the abyssal plain, and occurred 8.2k.y.a (Bünz et al., 2003; Haflidason et al., 2004; Kvalstad et al., 2005). The Storegga slide affected an area of 95,000 km² and is made of up to multiple slide lobe events (Haflidason et al., 2004; Solheim et al., 2005) (Fig. 3.5). The main unit of failure was the Brygge formation (Bryn et al., 2005) which was exposed in the sidewalls, headwalls and in the glide plane. The cause of the slope failure has been ascribed to a variety of factors including the inherent mechanical weakness of the lithology which consists of thick accumulations of oozes and clays, fault reactivation as a function of isostatic loading due to ice flux and the presence of erosional troughs formed by ice streams that further compounded intrinsic sediment instabilities by differentially loading the mechanically weak, gently sloping sediments.

3.2.3 Distribution of polygonal faults on the Norwegian Margin

The polygonal faults have been widely reported on the Norwegian Margin (Fig. 3.5). Polygonal faults were first reported on the Norwegian Margin by Hjelstuen et al.,

(1997) who noted arrays of small offset polygonal faults around the Vema Dome. Later studies by Berndt et al. (2003) and Stuevold et al. (2003) describe more polygonal faults on the Møre and Vørting basins. Stuevold et al. (2003) describe polygonal faults in the Upper Cretaceous and Palaeocene sequence around the Ormen Lange dome and examines their impact on fluid flow in area. Berndt et al. (2003) describe a wide spread polygonal fault network in the Miocene (Kai formation) that is present in the Møre and Vørting basins.

4 The controls on the development of Master polygonal faults within a single polygonal fault tier

Abstract

Polygonal fault systems are complex features within the subsurface, not least, because of the diversity of patterns that have been described from tiers in a wide variety of depositional settings and basins globally. One of the key features of polygonal fault systems is the tier, which aptly describes the tendency of polygonal faults to form within specific packages or formations with a fine-grain size. Within a single polygonal fault tier, fault dimensions vary significantly with the largest polygonal faults being termed Master polygonal faults (Cartwright, 2011). The controls on the development of Master polygonal faults and polygonal fault organisation is at present, poorly understood.

This study examines a tier from the Modgunn Arch, Norwegian Margin. This tier shows a small number of very large polygonal faults with trace lengths of >900 m and fault heights of > 600 m. These faults are the largest in the tier and are defined, in this study, as Master polygonal faults. This study presents two case studies of Master polygonal faults from a single polygonal fault tier; one case study focusses on an area where fault traces show a high degree of connectivity, whereas a second case study examines an area where fault traces show a low degree of connectivity. This chapter suggests that faults in the two study areas show subtle differences in throw character and tier organisation. This study suggests that Master polygonal faulting is a product of the number branchline intersections, preferred orientation and fault dimensions. In areas of a tier where the polygonal fault array has a high degree of connectivity, Master polygonal faults can develop through preferential alignment to regional stresses. In areas where polygonal fault connectivity is low, Master polygonal faults develop from the largest polygonal faults which preferentially accrue the greatest strain. This study demonstrates that there are multiple pathways in which polygonal faults can continue propagating and outpace surrounding faults in a single network.

4.1 Introduction

Polygonal fault tiers are partitioned into a package of offset reflections with a clear upper and lower boundary. Several tiers may be present within a fine grained sequence and are usually confined within discrete stratigraphic intervals, usually at or between formation tops (Cartwright, 2011; Cartwright and Lonergan, 1996; Gay et al., 2004; Hansen et al., 2004; Lonergan and Cartwright, 1999; Watterson et al., 2000). Beyond the individual tier boundaries, seismic reflections are un-deformed (Carruthers et al., 2013; Cartwright, 2011; Cartwright and Lonergan, 1996; Dewhurst et al., 1999). Changes in fault frequency and orientation within polygonal fault tiers, both vertically and laterally, have been attributed to the presence of sand rich channels (Cartwright, 2011; Lonergan and Cartwright, 1999), clay to limestone transitional changes (Ostanin et al., 2012) and changes in clay mineralogy (Cartwright and Dewhurst, 1998; Dewhurst et al., 1999).

Description of upper and lower tier boundary zones, and in particular, their controls, have been largely overlooked in previous studies of polygonal faults. Lithological variation has been suggested to be a major control on tier boundaries, Jackson et al., (2014) and Cartwright (2011) demonstrated that polygonal fault sets can become decoupled in the presence of sands within the polygonal fault tier, with Cartwright (2011) describing each decoupled fault set as a sub tier. However, other studies have shown that polygonal faults are able to propagate through sand rich intervals (Möller et al., 2004), where polygonal fault activity is synchronous with channel deposition, polygonal faults can help constrain the position of the sand body (Lonergan and Cartwright, 1999; Möller et al., 2004). This would suggest that where sands are unconsolidated and diagenetically immature, polygonal faults are able to propagate through sandy lithologies. In contrast, where sands have undergone some burial, as seen in the schematic diagrams presented in Jackson et al. (2014), polygonal fault growth is terminated. Therefore, the efficiency of lithology based tier boundaries is strongly influenced by the timing relationship between polygonal fault formation and the sandstone body. Furthermore, due to the potentially vast areal extent of polygonal fault arrays (up to 10^6 km² in areal coverage (Cartwright, 2011), any sand body is likely to represent a very localised barrier to polygonal fault growth, when such barriers are considered in the context of the whole tier. In cases where there are no sandstone bodies, fault tips have been shown to be constrained by a change in the

rheological state of muds and clays. In an example from onshore Australia, the basal tips of a polygonal fault tier are constrained by a low velocity, low amplitude zone, attributed to an under-compacted mudstone (Nicol et al., 2003; Watterson et al., 2000). These tier boundaries represent localised barriers to fault growth, and as such, these mechanisms cannot fully account for the formation of Master polygonal faults within a single tier, especially where such features are absent.

Whilst there are many descriptions of polygonal fault arrays and the interaction between polygonal faults and changing lithologies, there are some fundamental questions regarding the internal organisation of faults within a polygonal fault tier, in particular, how and why these organisational changes occur in predominantly fine-grained tiers. Many studies have described a loose hierarchy of 1st, 2nd and 3rd order of faulting (Gay et al., 2004; Laurent et al., 2012; Ostanin et al., 2012; Seebeck et al., 2015) whilst others have given more formal terms for fault organisation by defining the largest faults in the tier as Master faults (Cartwright, 2011). Other studies have anecdotally suggested the presence of sub-tiers (Cartwright, 1994b) and the presence of ‘space-filling’ geometries of smaller polygonal faults, constrained by larger polygonal faults.(Lonergan et al., 1998). Whilst many studies define polygonal fault arrays and note a loose ‘hierarchy’ of faulting present within a tier, no study attempts to reconcile the impact that the organisation hierarchies have on the evolution of polygonal fault tiers.

This study uses a large, well-imaged survey on the eastern flank of the Modgunn Arch and associated well data. This survey was chosen as it shows a clearly imaged Opal A/CT boundary across the area, indicating the presence of a fine-grained siliceous ooze (Neagu et al., 2010a, 2010b). This study uses two 64 km² case study areas within a single polygonal fault tier on the eastern flank of the Modgunn Arch. The overall research objective is to understand how Master polygonal faults are organised within a tier, and define the controls on Master polygonal fault propagation. This study undertakes simple but high resolution analysis on fault throw, orientation, and fault frequency within each case study area at different stratigraphic intervals. By comparing the results of two case study areas, it is postulated that any differences in the organisation of polygonal faults within a single tier should become apparent.

4.2 **Regional seismic stratigraphy**

Well 6403 6/1 intersects the survey on the southern tip of the Modgunn Arch and details a number of formations that allow lithological calibration of the seismic data. The analysis of the well is focussed on formations that host the polygonal fault array. Formations that are untouched by the polygonal fault tier studied here are not described.

4.2.1 *Rogaland Group (H10-H9)*

The Rogaland Group has a low gamma response, which gradually increases in the upper third of the formation where it is capped by a peak in the gamma log. The changes in gamma are reciprocated in the density and sonic velocity in this interval, which also decrease in the upper third of the formation. This unit is interpreted to be a mix of mafic derived tuffs which have a low gamma response (Rider, 2002) with increasing shale content up sequence.

The Rogaland Group has variable thickness, in the south-east, the upper reflection package of the Rogaland Group is up to 175 ms (ca.160 m) thick and thickens over the crest of the Modgunn Arch (Fig. 4.1). To the North of the survey, the Rogaland Group reflection package thins to 50 ms (ca. 45 m). The top of the Rogaland Group package consists of three, medium frequency and low to medium amplitude, continuous reflections. These reflections gradually become less frequent and thin to the east and south east of the survey area (Fig. 4.1).

4.2.2 *Brygge Fm. (H9-H4)*

The base of the package is defined by a prominent high amplitude reflection of H9. This reflection package is a large lens of sediment that thins to the west, south and north of the survey area over the Modgunn Arch (Fig. 4.1). The unit is characterised by medium to high amplitude, continuous, coherent reflections up to 700 ms (630 m) in thickness to the east. Petrophysical analysis of this interval shows a low density, low gamma interval with no appreciable drop in sonic velocity. A thin peak in the gamma ray response at 1920 m MD is suggestive of an unconformity (Rider, 2002). Above the unconformity, there is an increase in the gamma response. This is interpreted as the position for the Mid Miocene unconformity (MMU) (H4) and the junction between the Kai and Brygge Formations. The peak in both sonic and density (Fig. 4.1) around 1960 m MD is caused by an Opal A/CT transition boundary (Neagu et al., 2010a). Opal A/CT boundaries have been widely reported from the Norwegian

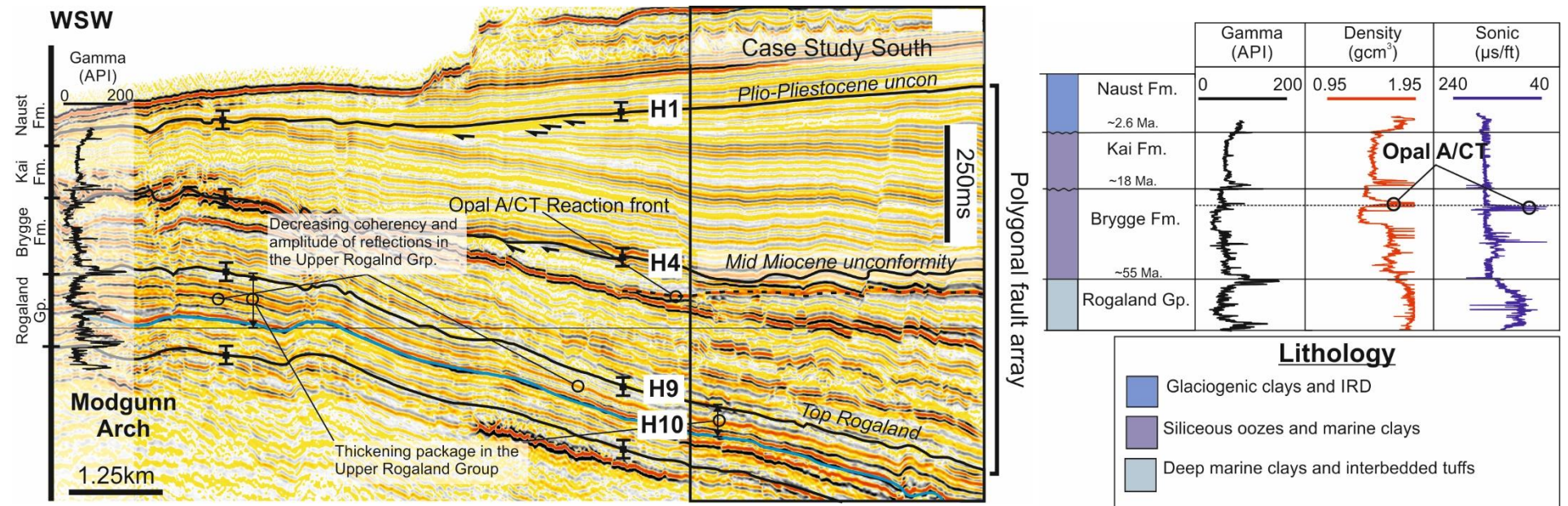


Figure 4.1: (Left) Seismic cross section with the well tie and key stratigraphic horizons, (Right) A diagram summarising the wireline log responses of each formation

margin as well as the Faroe-Shetland Channels (Davies and Cartwright, 2007, 2002; Davies et al., 2009a; Ireland et al., 2011, 2010; Neagu et al., 2010a, 2010b). Opal A/CT reactions are transient features within the sedimentary record, controlled primarily by temperature and time (as a proxy for burial), but also by pH and clay content (Davies and Cartwright, 2002; Meadows and Davies, 2007; Neagu et al., 2010a). The Opal A/CT boundary is a discordant high amplitude reflection characterised as a peak (see Chapter 2) and is indicative of an increase in impedance contrast. The Opal A/CT reflection is evidenced at a regional scale as a convex reflection that cuts discordantly across reflections at the survey edges, and is concordant with seismic reflections near the centre of the survey (see Fig. 4.1).

4.2.3 Kai Formation (H4-H1)

The Kai Formation developed over the entire survey area and is of variable thickness ranging from ca. 200 m over the Modgunn Arch to up to 600 m in the east of the survey area. The base and top of the package are defined by unconformities, with the Mid Miocene unconformity at the base (H4) and the Plio-Pleistocene unconformity (PPU) at the top (H1) which truncates reflections to the east of the Modgunn Arch. The reflection package contains a mixture of high to medium amplitude continuous reflections (Fig. 4.1, Fig. 4.2). The well response of the Kai Formation shows a broadly homogenous gamma, density and sonic response. The gamma response is higher than the Brygge Formation suggesting that the Kai Formation has a greater proportion of clay.

4.3 Fault populations of the Modgunn Arch region

The polygonal fault tier is contained within the Brygge and Kai Formations to the east of the Modgunn Arch. The tier is broadly wedge shaped and thickens to c. 1 km in the east of the survey. To the west of the survey area, the polygonal fault array laterally dies out. Near the crest of the Modgunn Arch, the polygonal fault array is replaced by a new set of faults that lie above the crest of the Modgunn Arch (Fig. 4.3). The faults over the crest of the Modgunn Arch are aligned NW-SE, parallel to the crest and segregated from the polygonal fault array by a c. 3 km wide transition zone and are termed crestal faults. This study focusses on the polygonal fault array present to the east of the Modgunn Arch.

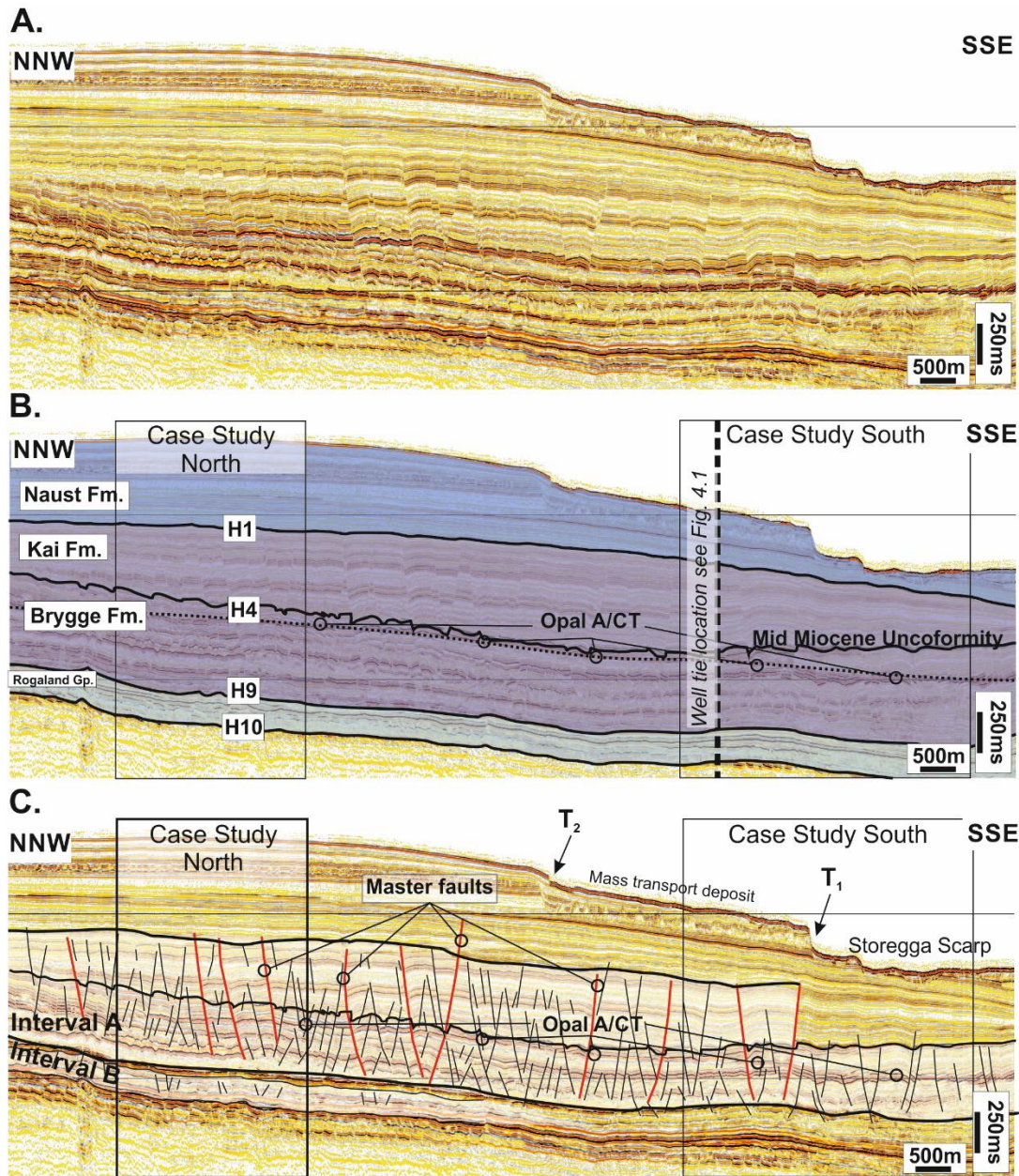


Figure 4.2: Seismic cross section detailing the lateral continuity of seismic units and key seismic horizons. (A) uninterpreted seismic data(B) Lithology overlay to show lateral continuity of lithology between case study areas. (H1) Plio-Pleistocene Unconformity, (H4) Mid-Miocene Unconformity (H9) Top Rogaland Group, (H10) Intra Rogaland. T₂ and T₁ refer to terraces from the northern head wall of the Storegga Slide. (C) The vertical distribution of faulted intervals within the lithological formations and showing the fault families of Master faults (Red)

The fault traces exhibited by polygonal faults on the Modgunn Arch are curvilinear and anastomosing fault traces of variable length ranging from a few hundred metres to a few kilometres (Fig. 4.3).

In section, polygonal faults show exclusively normal offsets with no preferred orientation for dipping up or down slope (Fig. 4.2). The fault profile is broadly listric in shape with a bimodal dip across the Opal A/CT boundary, with dips below the Opal A/CT ca. 35° dip. Above the Opal A/CT boundary, dips are on the order of ca. 42°. This dip change occurs on all the polygonal faults that cross the Opal A/CT boundary across the survey, and has been observed and explained in other nearby polygonal fault tiers on the Ormen Lange domes and Gjallar Dome (Neagu et al., 2010b). Polygonal faults are not all the same size in this tier, The upper tip position of polygonal faults in the tier varies, some polygonal faults tip out below the MMU whereas others tip out at the PPU. Generally, basal tips across the polygonal fault tier tip out towards the base of the Brygge Formation. The polygonal faults that tip out at the PPU are generally the largest faults in terms of height (>600 m) and trace length (>900 m) and are termed Master polygonal faults (*sensu* Cartwright, 2011).

Master polygonal faults are seen throughout the polygonal fault tier (Fig. 4.2), however Master polygonal faults in the north of the polygonal fault tier show a greater number of intersections with smaller fault traces than those in the south of the tier. Therefore two areas of study were chosen, Case Study North (CSN) examined Master polygonal faults in a highly connected array and Case Study South (CSS) examined Master faults in an array with low connectivity. Both case study areas covered a similar areal extent (64 km²) and contained similar numbers of Master polygonal faults (Fig. 4.3)

4.3.1 Displacement Distributions

The displacement distributions of Master polygonal faults differ within the case studies. In CSN, there are comparatively fewer faults displaying an apparent reduction in displacement near the Opal A/CT reaction front (Fig. 4.4). These isolated examples are seen across all faults sizes. No polygonal faults in either CSS or CSN show any reduction in throw near the MMU that could suggest dip linkage and/or reactivation (Baudon and Cartwright, 2008a; Cartwright et al., 1995).

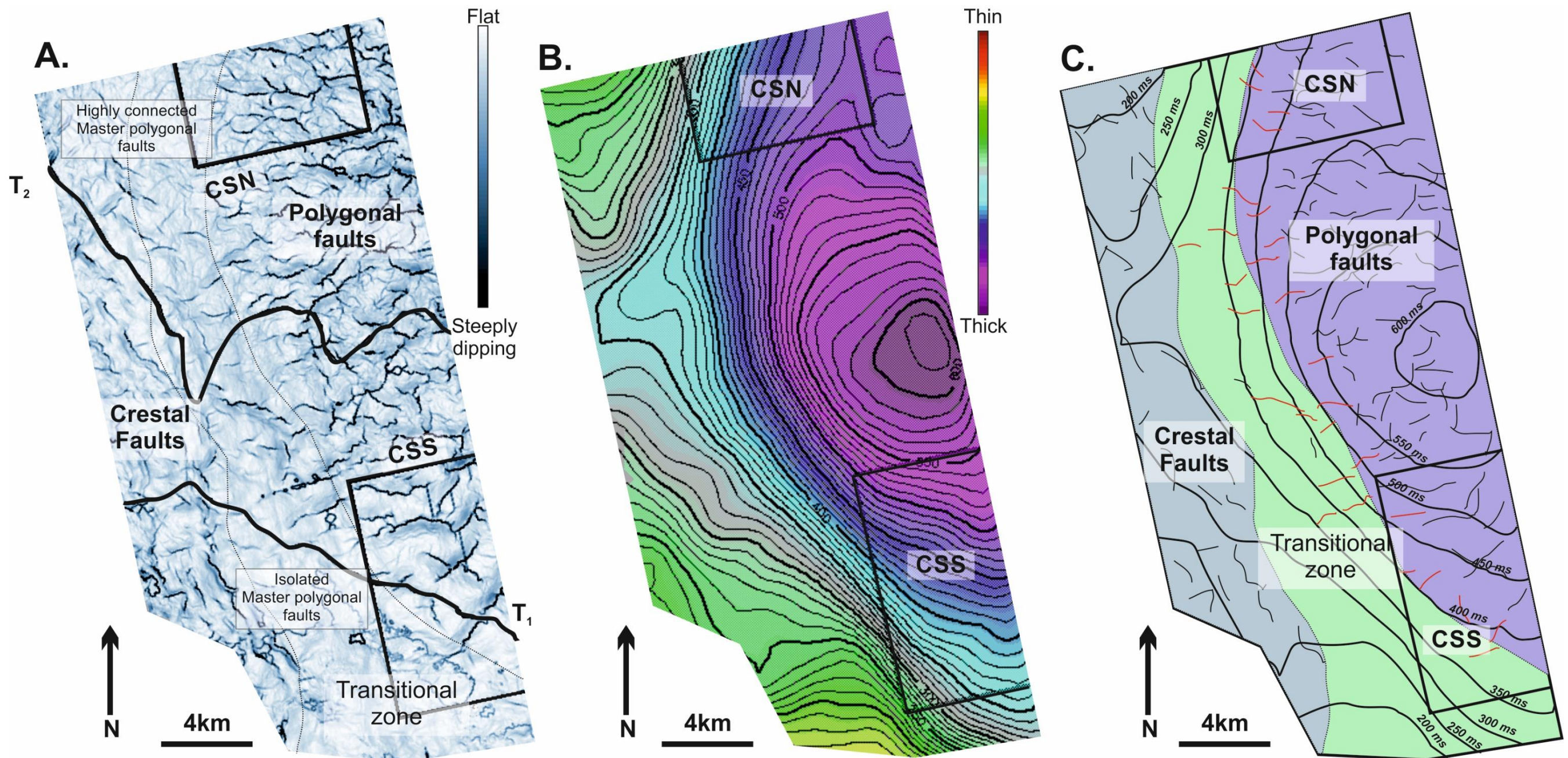


Figure 4.3: (A) Time dip attribute map of horizon H2 detailing the lateral boundary between polygonal faults and crestal faults (B) TWTT Isochron map of the Kai formation showing thickness changes across the upper half of the tier. (C) Composite fault map of H2 summarising both the time dip (A) and the isochron map (B). The composite map shows the relationship between overburden thickness in the Kai formation and the directionality of the polygonal faults at the margins of the tier (seen in red). Note that the polygonal faults at the margins all strike perpendicular to the isochron contours

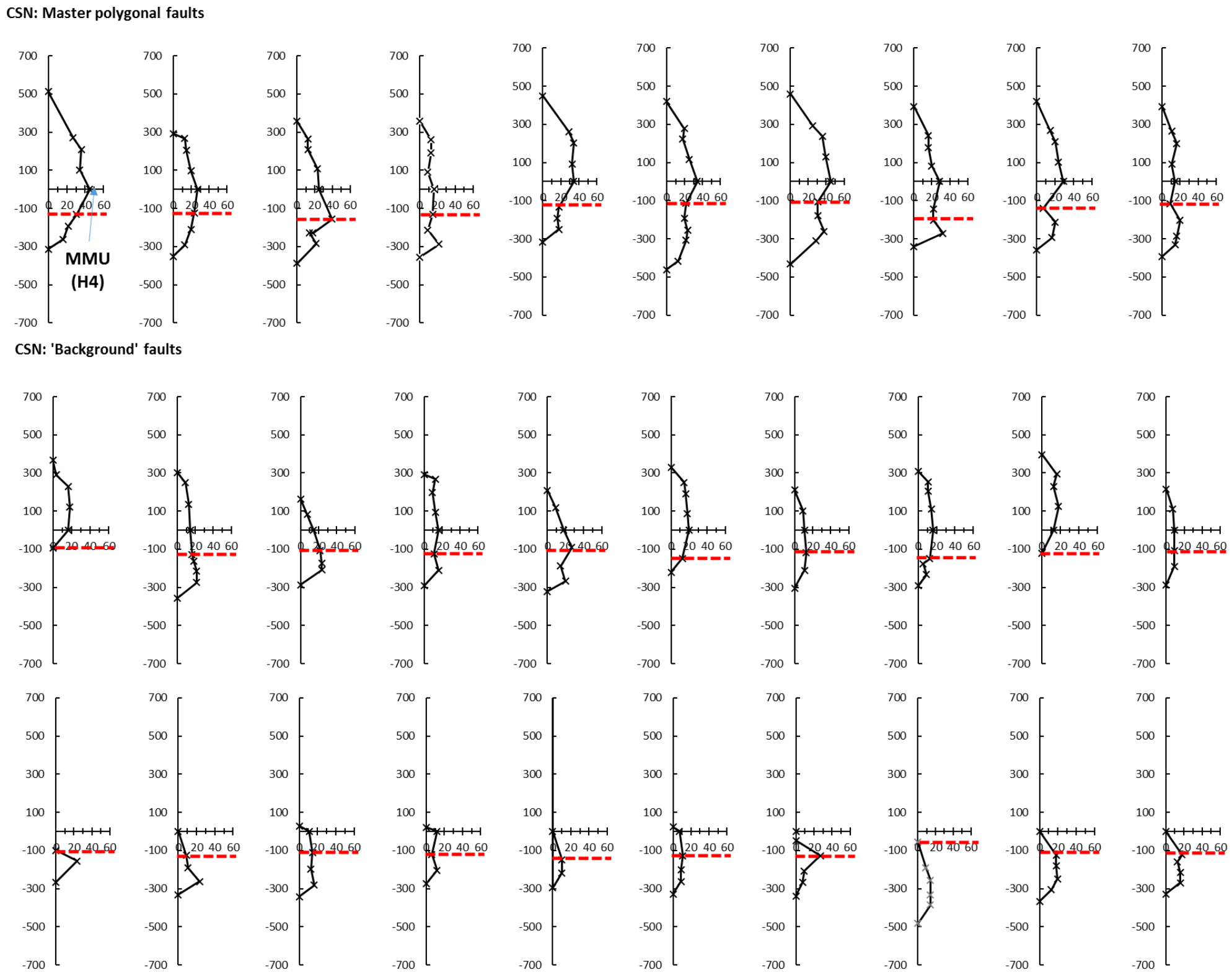


Figure 4.4: T-z plots of faults of CSN. The x axis is depth in metres relative to the Mid Miocene Unconformity (H4) and the y axis is displacement. The red dashed line marks the position of the Opal A/CT boundary, note the absence of any restriction of throw (throw minima) at the Opal A/CT boundary in the tier and master polygonal fault families

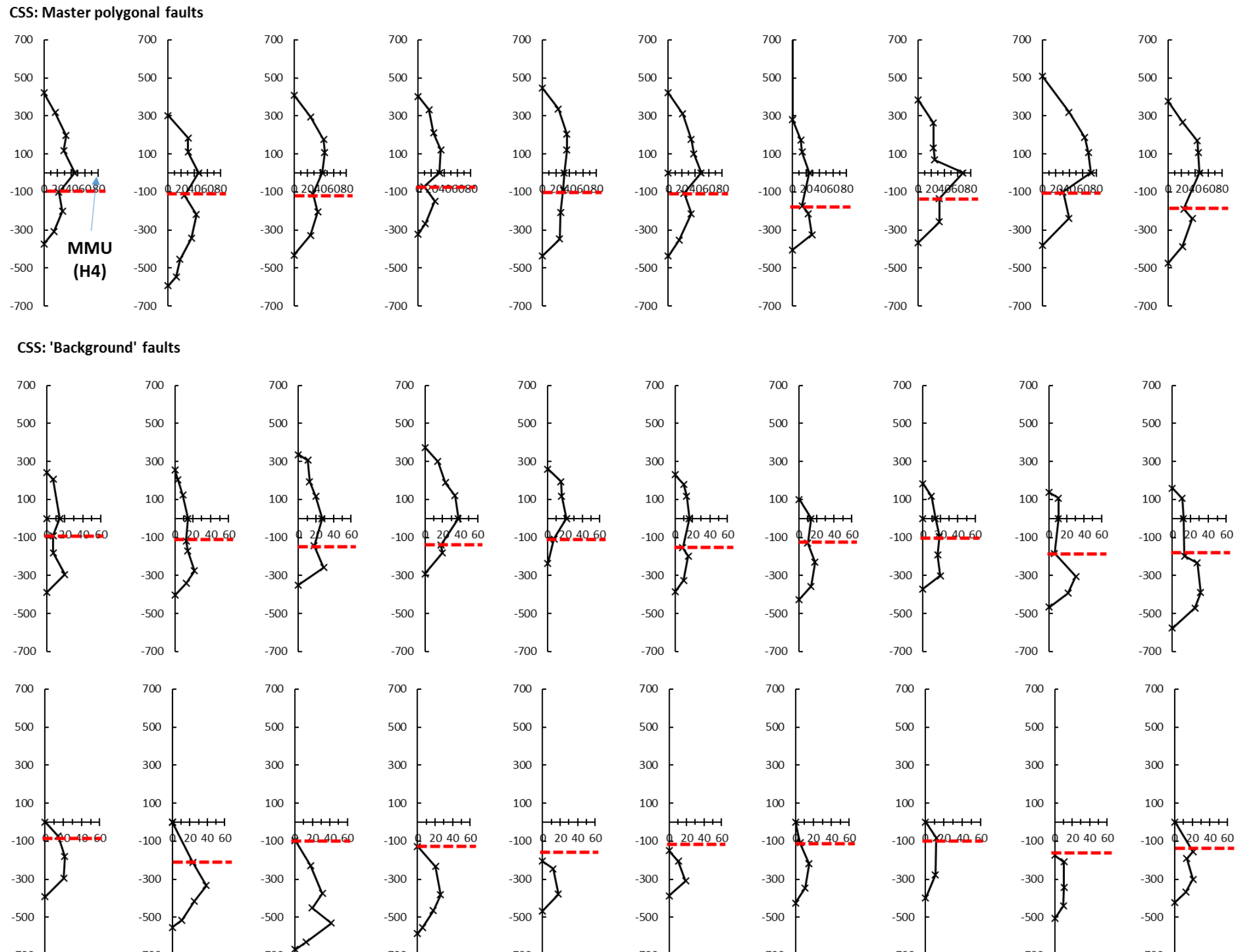


Figure 4.5: T-z plots for faults across CSS. The x axis is depth in metres relative to the Mid Miocene Unconformity (H4) and the y axis is displacement. The red dashed line marks the position of the Opal A/CT boundary, note the restriction of throw (throw minima) at the Opal A/CT boundary in the tier and master polygonal fault families

In CSS, there is an apparent reduction in throw values in the vicinity of the Opal A/CT reaction front, as described from the Ormen Lange Dome and the Gjallar ridge by Neagu et al (2010a). This gives the displacement profiles across Master polygonal faults a broadly ‘M’-shaped distribution, similar to those described by Muraoka and Kamata, (1983) (Fig. 4.5). Indeed, many of the smaller ‘background’ polygonal faults also show a similar reduction in displacement across the Opal A/CT reaction front or have upper tips that appear to tip out above the Opal A/CT reaction front.

4.3.2 Fault populations

Wider analysis of faults in both CSN and CSS show that Master polygonal faults form groups within displacement-height plots. These clusters suggest that the background faults of both CSS and CSN have similar displacement-height characteristics. The smallest faults in both CSN and CSS also have a D_{max}/H ratio of between 0.13 and 0.25. With increasing fault size, the clusters between faults in CSS and CSN become more discrete. Master polygonal faults in CSN have D_{max}/H ratio of between 0.25 and 0.55, whereas faults in CSS have a ratio between 0.13 and 0.25. Displacement-length plots (Fig. 4.6) show very little diagnostic difference between CSN and CSS. Faults within CSS are the longest faults measured between the two case study areas.

The primary difference between the clustering and scaling of faulting in CSN and CSS is the number of free tips and fault frequency. In CSS, there are far fewer faults than in CSN at equivalent horizons. Moreover, the decreasing numbers of faults is reciprocated with an increasing number of free tips. The majority of Master and background faults in CSS have at least one free tip, whereas in CSN, the percentage of faults with free tips is low (<5%).

Fault frequency differs between the two case study areas. In CSN there are three discrete peaks in the frequency of faults observed within a given horizon, whereas in CSS only one is observed (Fig. 4.7). These peaks correspond to the position of the smallest background faults. In CSN, the peaks in fault frequency are localised to horizons H4, H6 and H8a, in CSS the fault frequency peaks at H6 (Fig. 4.7). Horizon H4N corresponds to the Mid Miocene unconformity, the underlying peak in fault frequency for H6 correspond to peaks within the middle of the Brygge Formation.

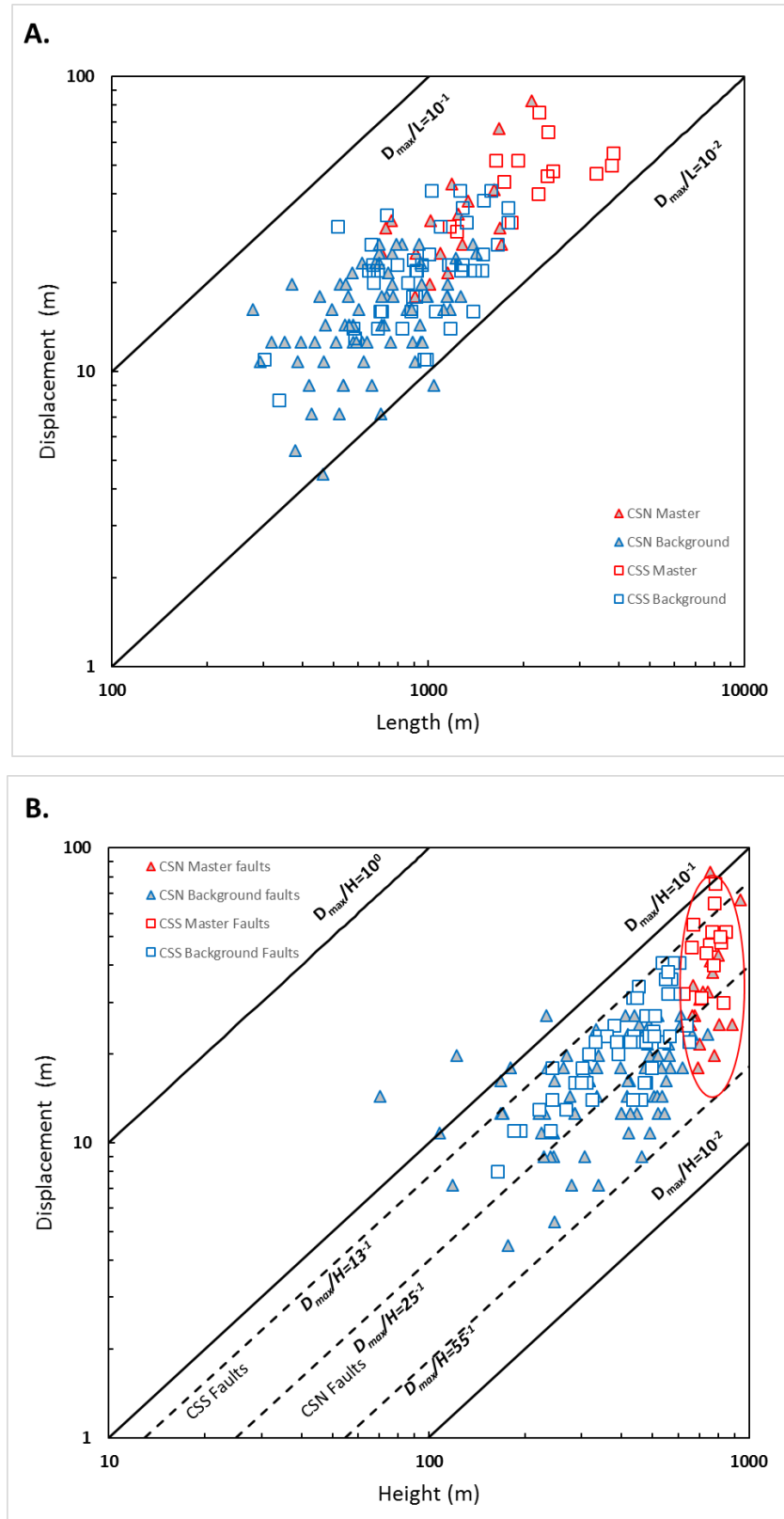


Figure 4.6: (A) Displacement-length plot, segregated by Master faults (blue), and background faults (red) (B) Displacement height plot segregated by fault population showing the clustering of Master faults at the upper end of the scale. Note the different scaling relationships between CSN and CSS.

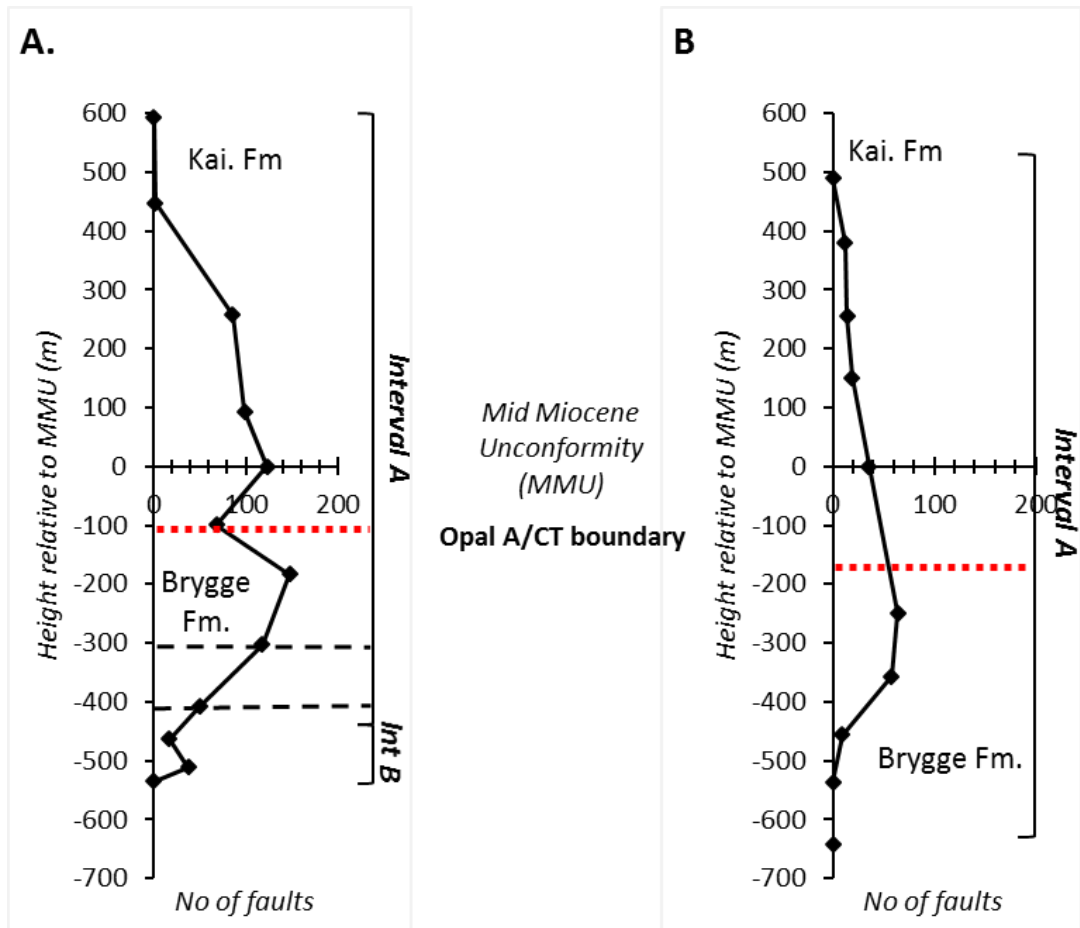


Figure 4.7: (A) Fault frequency graph for CSN, (B) fault frequency graph for CSS. The red dashed line indicates the position of the Opal A/CT boundary and the black dashed lines indicate the position of the low amplitude zone. Note the significantly higher numbers of polygonal faults in CSN compared with CSS and the impact of the Opal A/CT boundary on CSN. Note the change in position of the Opal A-CT boundary is due to the parabolic reflection geometry of the Opal A/CT reaction front

There are on average three times more faults present per horizon in CSN (62 faults per horizon) than CSS (21 faults per horizon).

4.3.3 Preferred orientation of polygonal faults

In addition to the differences in displacement-height scaling seen between the two case study areas, there are significant differences in the preferred orientation of polygonal faults in each case study area.

The strike of the polygonal fault pattern at the base of the polygonal fault tier shows a polymodal distribution with faults linking primarily through perpendicular branchlines. However, towards the middle and top of the polygonal fault tier, the linkage is primarily through oblique intersections ($<60^\circ$ between fault traces). In both case study areas the Master faults occur in relatively small numbers (<20 faults per case study area) and the orientation of these faults is different in each case study area. In CSN, the faults are preferentially orientated E-W whereas in CSS, the faults are preferentially orientated NE-SW (Fig. 4.8).

In CSN, there are three clear trends within the case study area, each corresponding to the stratigraphic position relative to the Opal A/CT boundary. Beneath the Opal A/CT boundary, the primary preferred orientation is orientated NNE-SSW, with a secondary orthogonal trend oriented WNW-ESE. This orientation develops at the base of the tier H8, (see Fig. 4.8) and continues to the Opal A/CT reaction front. The primary trend lies parallel and the secondary trend is perpendicular to the strike of the eastern flank of the Modgunn Arch. At the Opal A/CT reaction front (H5, Fig. 4.8), the orientation changes to the WNW-ESE trend, which continues until the tier dies out beneath H1 in the Kai Formation. The change in orientation is concomitant with a gradual decrease in the number of faults. Additionally, there are changes in the geometry of the polygonal fault traces above and below the Opal A/CT boundary. Beneath the Opal A/CT boundary polygonal fault traces are short, curvilinear traces with oblique and orthogonal intersections. Above the Opal A/CT boundary, polygonal fault traces change to curvilinear and anastomosing trace geometries with oblique intersections between different fault branchlines.

By contrast, the preferred orientations in CSS are more chaotic, and change from horizon to horizon. CSS horizons H2, H3, H4 and H6 show a preferred alignment NE-SW, parallel to the strike of regional slope whereas H5 and H7 show a

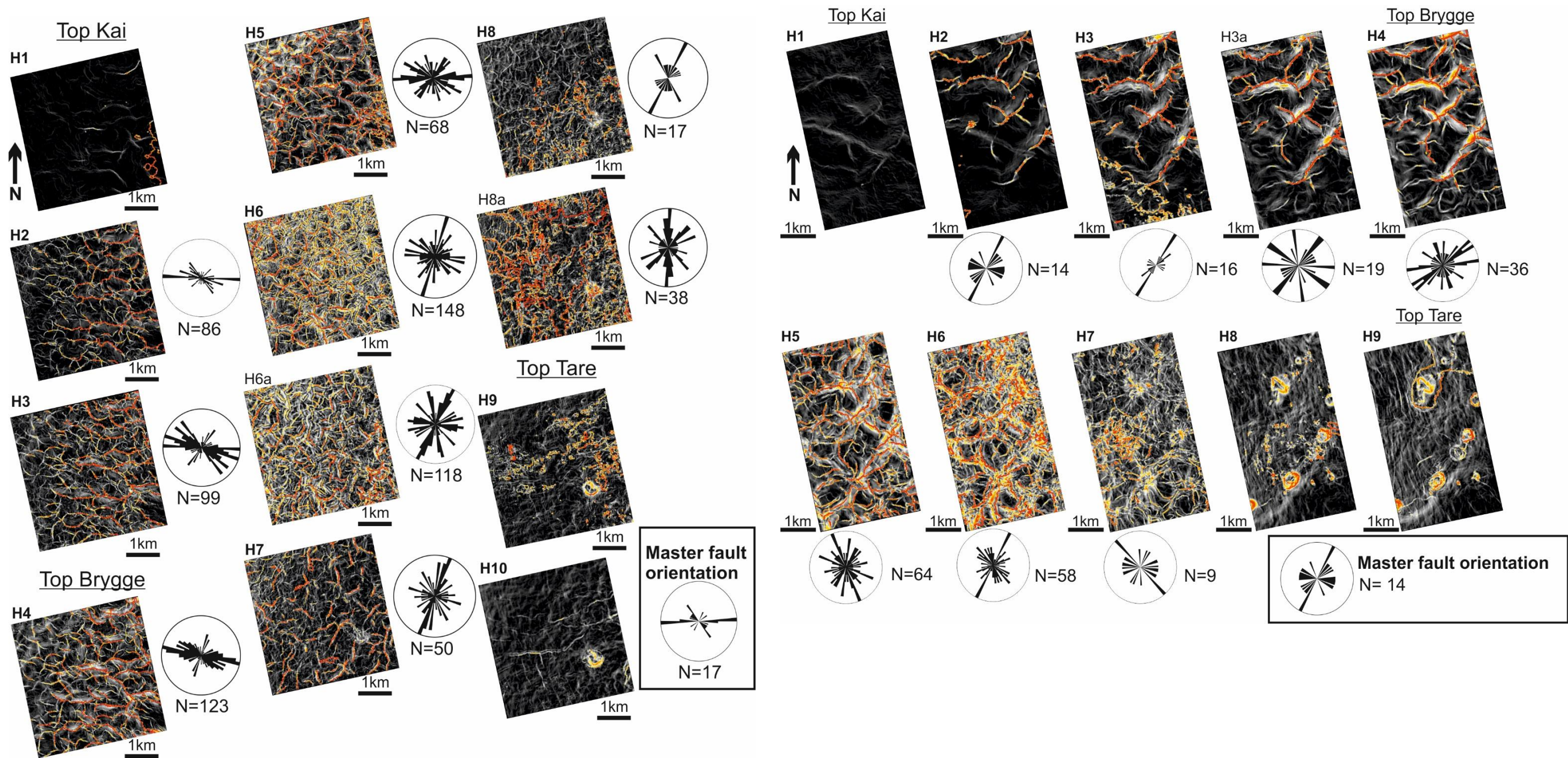


Figure 4.8: (A) Time dip attribute maps for horizons in CSN showing preferred orientations of polygonal faults. Polygonal faults below the Opal A/CT boundary (H5) are aligned parallel to slope contours (See Fig. 6.1), above the A/CT boundary (H5) faults are aligned east to west. Faults above H5 have curvilinear traces whereas faults below H5 display broadly linear traces. (B) Time dip attribute maps for showing random preferred orientations from layer to layer.

preferentially oblique alignment NW-SE and H3a shows no clear preferential alignment (Fig. 4.8). The fault trace geometry is curvilinear, irrespective of the stratigraphic position of the horizon relative to the Opal A/CT boundary. The fault array in CSS shows limited connectivity between fault branchlines with the greatest degree of connectivity found between Master faults and a small number of connecting faults. These Master faults and the associated branchlines occur in relative isolation throughout much of the tier, except towards the middle of the tier, where fault numbers are greatest (up to 64 faults).

4.4 Discussion

The preceding data shows that whilst Master polygonal faults in both CSS and CSN are part of a single tier, the changes in orientation and frequency of polygonal faults between two closely spaced case study areas is strongly indicative that the Master fault populations in CSS and CSN are responding differently to changing states of regional stress.

4.4.1 Timing polygonal fault growth

The alignment of faults seen in CSN and CSS, would suggest the Modgunn Arch was developing at the time of polygonal fault formation. The growth of the Modgunn Arch has been suggested to have occurred in the Mid Miocene, c.a. 16 Ma based on the presence of a basin wide regional unconformity in the Miocene sediments, expressed in this survey as the MMU (Brekke, 2000; Lundin and Doré, 2002). Furthermore, an absence of growth packages in the lower third of the polygonal fault array is also more suggestive of blind fault growth with no clear evidence for interaction between upper fault tips and palaeo-seabed (Baudon and Cartwright, 2008b; Shin et al., 2010). The present day stress field on the Vøring Plateau region was established in the Pliocene during the onset of landward uplift and westward basin tilt (Brekke, 2000), alignments to the modern day stress field seen in CSN (Fig. 4.9) could suggest recent polygonal fault activity within the last 5 Ma.

The maturity of a given array has been suggested to be where the greatest degree of fault connectivity is observed (Cartwright, 2011). In both CSS and CSN, the greatest degree of connectivity is found in the Brygge Formation. Polygonal fault growth is interpreted to have initiated in the Brygge formation and grows preferentially upward with faults competing for space. This forces upper tips to terminate and abut larger, faster/earlier growing faults. It is unclear whether fault growth is via segment linkage

as dip linkages are not observed in the seismic data, but maybe present below resolution limit. In addition, the throw-depth plots show no obvious or consistent displacement maxima or minima to indicate where separate faults are linking vertically (Baudon and Cartwright, 2008a; Laurent et al., 2012; Stuevold et al., 2003). Some of the observed displacement minimas that are present can be attributed to the Opal A/CT reaction front. Growth of the polygonal fault array is suggested to be similar to that proposed by Cowie and Shipton, (1998) where fault growth undergoes periods of preferential lengthening and periods of displacement accumulation. Applying the same observation to both case study areas as a whole, CSN has the fewest free tips per horizon and is suggested to be an older part of the array relative to CSS.

An additional complexity of polygonal faults in the Modgunn Arch, is the presence of a fossilised Opal A/CT boundary. Both polygonal fault growth and opal diagenesis have been suggested to occur concurrently, with opal diagenesis often cited as one of the causative mechanisms for polygonal fault genesis (Davies et al., 2009b; Davies and Ireland, 2011). The Opal A/CT reaction front is not a static feature, and the reaction front migrates upwards through time (Davies and Cartwright, 2002; Meadows and Davies, 2007; Davies et al., 2009a; Neagu et al., 2010a; Ireland et al., 2010; Davies and Ireland, 2011). The migration and subsequent fossilisation of the silica diagenetic reaction front could be taken as a significant event during the formation of this tier. The evolving mechanical properties as a result of this diagenetic reaction are of particular importance to an evolving polygonal fault system.

Neagu et al. (2010a), examined polygonal faults in a similar depositional setting on the Norwegian Margin from the Gjallar ridge. Neagu et al., (2010a) noted a number of changes in the displacement, dip and seismic character of polygonal faults and used these observations as a proxy for inferring diagenesis-related compaction. Neagu et al., (2010a) noted that the offset of the Opal A/CT reaction front is a measure of post-fossilisation displacement. Neagu et al. (2010a) suggested a mechanical model post-fossilisation was possible due to a number of factors including; a reduced friction angle in Opal CT rich sediments, lubrication of the fault planes by expelled pore fluids or elevated fluid pressures.

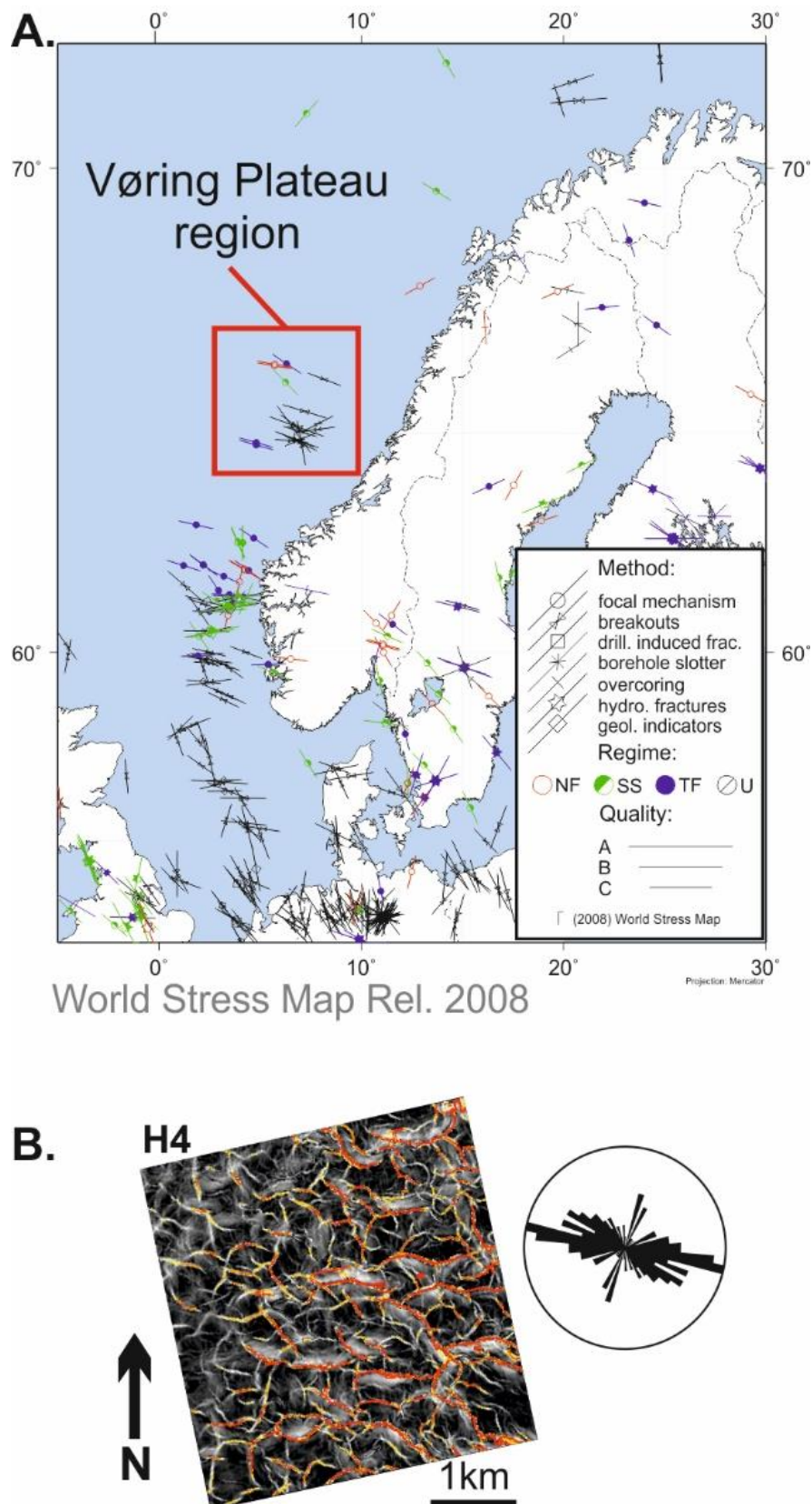


Figure 4.9: (A) World stress map (from Heidbach et al. 2008) of the Norwegian margin showing the orientation of maximum horizontal stress (SH) in the Vøring plateau region compared with (B) the orientation of the faults from interval A

Neagu et al (2010b) also examined the broad region timing of the fossilisation of the Opal A/CT reaction front and inferred an approximate age of Late Miocene to Early Pliocene across the region, based on the concordance between a regional reflection and the reaction front. However, the study notes that given the variation in controlling factors of Opal A/CT diagenesis, and the uncertainty in timing key surfaces, it is probable that there are some margin-wide variations in Opal A/CT fossilisation. In the context of the Modgunn Arch survey presented here, there are no major shifts in position of the Opal A/CT reaction front and it lies beneath the Mid-Miocene Unconformity (MMU) across the survey area. It seems probable that in the context of this localised section of a polygonal fault tier that the fossilisation of the reaction front is likely to be broadly synchronous across the area.

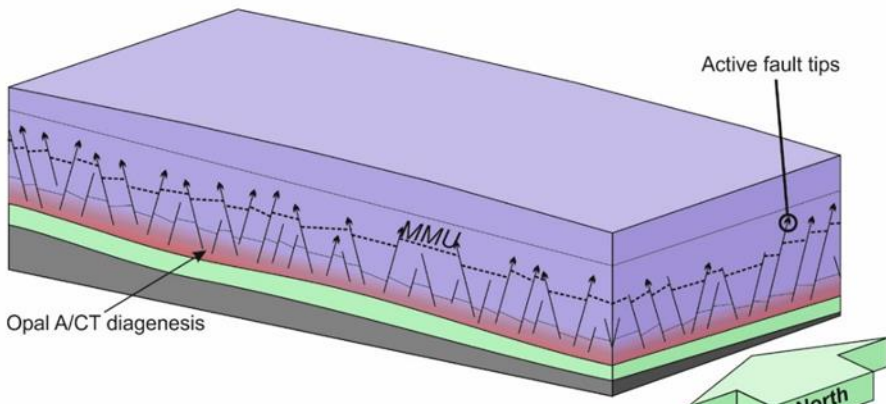
In this study, very few of the largest faults in CSN show any offset of the Opal A/CT reaction front, whereas in CSS the polygonal faults do offset the reaction front, evidenced by an apparent reduction in throw in the Opal A/CT boundary. This would indicate that post-fossilisation polygonal fault propagation was most prevalent in the south of the tier (Fig. 4.10). Polygonal fault tier formation is inferred to have started in and around the vicinity of CSN and gradually spread south. This would appear to indicate that propagation of Master polygonal faults is not synchronous, even within a single tier. Furthermore, it would suggest that polygonal faults of the Modgunn Arch area underwent blind propagation as recently as 5 Ma, based on the orientation to modern stress fields and post fossilisation offset of the Opal A/CT reaction front (Fig. 4.9).

4.4.2 Evolution of Master polygonal faults

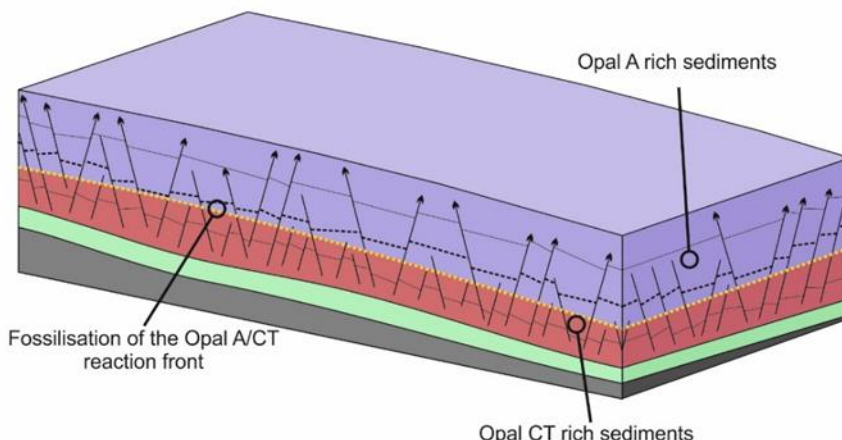
The upper tip and basal tip positions of polygonal faults coupled with displacement-height and displacement-length scaling would indicate that both CSS and CSN are part of a single polygonal fault tier. Moreover, displacement-height data presented in Fig. 4.6 shows progressive segregation of Master fault populations in CSN and CSS, whereas the smaller ‘background’ faults in both CSS and CSN are contained within a single group.

This is suggested here to be indicative of polygonal fault growth, whereby Master faults form in two pathways. Unlinked fault tips preferentially accrue displacement as strain localises on isolated faults (Fig. 4.10), resulting in comparatively higher displacements. In contrast, where lateral fault tips are pinned by linking or abutting

A: Synchronous polygonal fault growth and Opal A/CT diagenesis



B: Fossilisation of the Opal A/CT reaction front



C: Differential fault growth within the polygonal fault tier

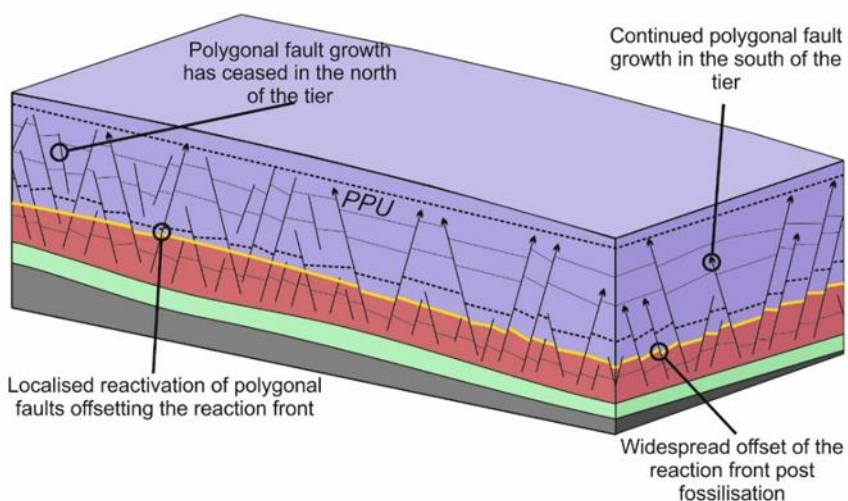


Figure 4.10: An evolutionary diagram summarising the development of the Modgunn Arch polygonal fault tier. (A) Polygonal fault growth is synchronous with Opal A/CT diagenesis. (B) Opal A/CT diagenesis arrests and begins to fossilise. Smaller polygonal faults contained below the Opal A/CT boundary are also fossilised and prevented from becoming reactivated. (C) Polygonal fault growth has ceased in the north of the tier but continues to the south of the survey area, offsetting the now fossilised reaction front.

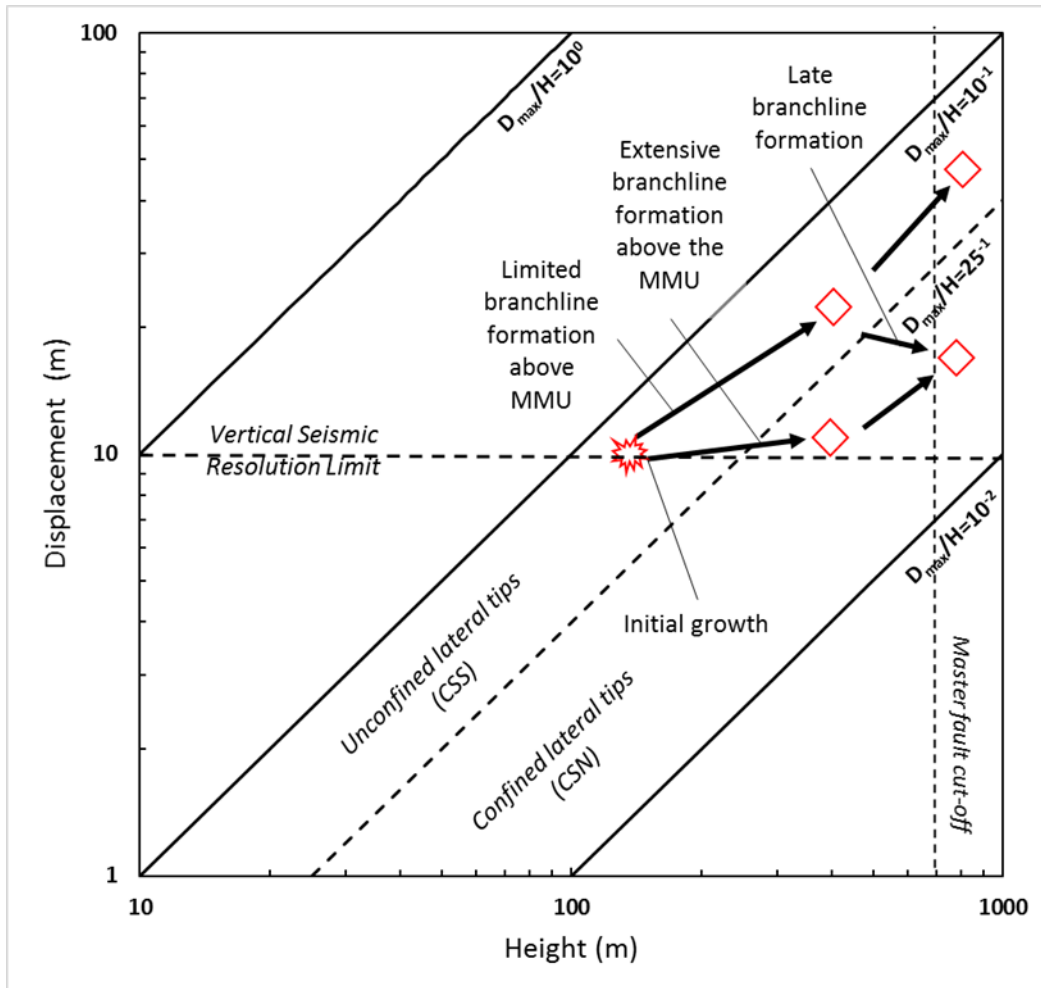


Figure 4.11: A schematic log-log displacement-height plot displaying growth trajectories for polygonal faults with confined and unconfined tips

faults early in the tier history, polygonal fault growth is via preferential vertical growth with displacement shared and transferred along hard linked branchlines (Maerten et al., 1999; Nicol et al., 2003, 1996; Willemse et al., 1996). The differences in the number of linkages between CSS and CSN may account for some of the variation in displacement height ratios presented in Fig. 4.6.

The change in orientation observed in both CSN and CSS is indicative of regional stress conditions at the time of array formation. Polygonal faults are sensitive to changing local and regional stress conditions, primarily observed through forced alignments. Forced alignments between polygonal faults and large tectonic/intrusive features have been widely observed around intrusive mud structures (Hansen et al., 2005), salt diapirs (Carruthers et al., 2013; Cartwright, 2011; Davison et al., 2000; Stewart, 2006), tectonic faults (Hansen et al., 2004), and to regional remote stress (Ostanin et al., 2012). The changing orientation of the master faults in CSN and CSS indicates two ways in which master faults may develop in a single polygonal fault tier. It is inferred here that the polygonal faults in CSN propagated under the influence of a NE-SW striking regional slope on the flank of the Modgunn Arch. This slope created a perturbation in stress which forced the NE-SW preferred fault alignment. The change in the preferential orientation of both Master polygonal faults and the polygonal fault array as a whole, above the Opal A/CT boundary, coincides with the modern day orientation of tectonic stress (Heidbach et al., 2008) (Fig. 4.9). This could suggest that the creation of master polygonal faults in CSN occurred preferentially on polygonal faults that were sympathetically aligned to an E-W horizontal stress direction. Given the saturation of the polygonal fault array, with a high degree of connectivity, it is suggested that the growth of master polygonal faults in CSN arose as a function of the additional strain imparted by sympathetic alignment to regional stresses.

In contrast, CSS Master faults are aligned parallel to the strike of the eastern flank of the Modgunn arch. The Master faults here occur in arrays with fewer faults and in comparative isolation, with only a few branchline intersections. A study by Tuckwell et al., (2003) demonstrated that longer fractures, if developed early, can grow to dominate the directionality of strikes within an array by modifying the local stress field. It is inferred here that the master faults of CSS are early forming relative to the local array and form a pre-existing structural grain. This pre-existing network overprints the regional stress field and forces polygonal fault growth to conform to

local stress in the fault framework. This is possible as polygonal fault arrays are considered to form in low or virtually isotropic states of horizontal stress (Cartwright and Lonergan, 1996; Goult, 2001). The presence of pre-existing faults in low strain regions has also been shown to generate anti-clusters of normal faults in response to stress reduction shadows (Ackermann and Schlische, 1997) or to force the re-orientation of incipient faults to a local stress field, imposed by pre-existing faults (Maerten et al., 2002). The change in preferred orientation for faults at different levels in CSS is suggested to be an artefact of smaller subordinate faults growing within a pre-established framework of larger Master polygonal faults.

The implications for this mechanism would be that within a polygonal fault tier, the distribution of far field stresses would appear to influence the early dimensions of polygonal faults. In this study, the location of CSN is proximal to the crest of the Modgunn Arch and has smaller, more numerous fault arrays strongly aligned parallel to the strike of a regional slope. In contrast, CSS is distal to the crest and nearer the down plunging tip of the arch and the polygonal fault orientations are under limited influence from the nearby Modgunn Arch. This distal position to far-field stress from a large structure, allows early forming polygonal faults in CSS to grow large enough to overprint any later changes in regional stress.

Fault dimensions are significant as larger faults have been found to accommodate up to 70% of the extensional deformation in plaster models (Fossen and Gabrielsen, 1996), suggesting that larger faults accrue and accommodate more strain (and hence deformation) than smaller faults in the tier. This would suggest that faults that dominate the array in their early history continue to do so throughout the tier evolution. This interplay between far field stresses and fault dimensions will later define the distribution of strain through the history of the polygonal fault tier.

4.5 Conclusions

Master polygonal faults are the largest faults within a polygonal fault tier. This study demonstrates that within a single polygonal fault tier, master faults can develop from a number of pathways and these pathways are in part controlled by the number of linkages within the local array.

Where a polygonal faults array is highly connected, Master polygonal faults develop due to sympathetic alignment to regional far-field stress. This imparts additional strain

onto the fault plane and permits slip. In areas where polygonal fault arrays contain fewer branchlines, lateral tips are free to propagate, allowing some polygonal faults to locally dominate the local array. Once established, these large polygonal faults dominate the array throughout the tier history and overprint the any regional far-field stress.

The polygonal fault tier described here also offers the opportunity to review relative timing for fault propagation. The fossilisation of the Opal A/CT boundary is thought to represent a temporal marker and that offset of the Opal A/CT occurs post fossilisation. Very few of the Master polygonal faults in CSN show any offset of the Opal A/CT boundary, whereas offset of the Opal A/CT is more common in CSS. This could indicate that polygonal fault propagation continued in CSS whereas CSN the continued polygonal fault propagation is more isolated. Given the number of faults present in CSN, it is likely that this part of the tier represents the mature section of the tier.

5 The thin end of the wedge: determining early polygonal fault growth and tier evolution from shallowly buried polygonal faults

Abstract

The propagation of polygonal fault arrays has traditionally been an elusive topic of study given the resolution limitations inherent to 3D seismic data and the paucity of accessible field outcrop. However, as computing power and processing knowledge increase, polygonal faults can be increasingly well imaged in very thin accumulations of sediment. This study examines one such example of shallowly hosted polygonal faults contained within a wedge shaped tier, using a high-resolution 3D seismic cube. From this, thin tier changes in the polygonal fault array are documented as the wedge thickness increases from 100 m to 350 m. Results from this study suggests that polygonal fault linkages are fixed very early in the tier history and with continued accumulation of sediment, polygonal faults begin to demonstrate organisational hierarchies. Furthermore, it is proposed that polygonal fault array exhibits spatial variation in nucleation timings, with the oldest faults being found in the thickest parts of the wedge. These conclusions have important economic implications for hydrocarbon exploration, particularly for constraining seal integrity and timing the openness of fluid migration pathways.

5.1 Introduction

Polygonal fault nucleation and growth has been the subject of considerable debate, often compounded by a paucity of information in two key areas. Firstly, there is limited information as to the minimum depth at which polygonal faults can be hosted, more specifically, defining if nucleation occurs at shallow depths, near the seabed (termed ‘early growth’) or if nucleation occurs after burial. Secondly, constraining the minimum sediment thickness required to host polygonal faults would aid in informing how nucleation is initiated, the polygonal fault ‘genesis mechanism’.

Early polygonal fault growth has been suggested by Cartwright, (1994a, 1994b) who noted polygonal faults in thin accumulations of sediment near the margins of polygonal fault tiers. Others have noted kinematic evidence for shallowly hosted polygonal faults and noted growth packages in the hanging walls of some polygonal faults (Cartwright, 1994b; Lonergan et al., 1998; Stuevold et al., 2003; Hansen et al., 2004), whilst other studies have provided anecdotal evidence for early growth in the North Sea (Goult and Swarbrick, 2005) but this supposition is contested by James et al. (2006). Gay et al. (2004) also argued for a shallow burial depth based on a tenuous link to ‘dewatering’ furrows which developed at the seabed above polygonal faults, from offshore Angola. Shallowly hosted polygonal faults have been observed on the bed of Lake Superior in pinger data with centimetre scale displacements. The Lake Superior study concluded that nucleation of polygonal faults can occur rapidly soon after deposition given their shallow depth and small displacements (Wattrus et al., 2003; Cartwright et al., 2004). Additionally, the nucleation position of polygonal faults has been proposed to be elucidated from kinematic relationships of conjugate polygonal faults, whereby each fault in the conjugate pair typically roots on a single horizon, inferred to be the nucleation position (Imbert, 2009).

With the exception of the potential polygonal fault array discovered in Lake Superior by Wattrus et al, (2003) and Cartwright et al. (2004), there is a discrete lack of descriptions of shallowly hosted polygonal faults. The previously described examples of shallowly hosted polygonal faults examine the differing styles of perturbed polygonal fault patterns around salt diapirs and pockmarks (Ho et al., 2013) or examine the differing styles of fluid venting structures (Ho et al., 2012a, 2012b). To date no study has specifically examined the evolution of a shallow polygonal fault tier. Moreover, there is very little known about some of the fundamental features of

Polygonal faults. At present there is no study that indicates when the distinctive polygonal patterns, a hallmark trait of polygonal faults, becomes established. In addition, whilst many studies have described an ordered hierarchy of polygonal faults (Gay et al., 2004; Gay and Berndt, 2007; Cartwright, 2011; Laurent et al., 2012; Ostanin et al., 2012; Seebeck et al., 2015). No study has yet to describe when these ordered hierarchies develop within the tier. These relationships could offer important insight into the propagation history of a polygonal fault tier.

This chapter uses a high-resolution seismic dataset from the West African margin with faults hosted in a single wedge-shaped package of sediments with sediment thicknesses ranging from 150 m to 400 m. This study uses qualitative and quantitative methods to examine both shallow and buried polygonal faults within a single tier. This chapter looks to examine the earliest parts of the tier history focussing on four key questions, 1) when do polygonal faults become linked? 2) Do all polygonal faults form at the same time? 3) When do polygonal fault tiers begin to form organisational hierarchies (i.e. master faults, Cartwright 2011)? 4) What are the controls on fault organisation?

Whilst the genetic mechanism of polygonal faults and the timing of their nucleation has been widely debated, what is required is an understanding of how a polygonal fault system evolves and grows both spatially and temporally. To date, no study examines the transition from shallow burial to deep burial. The increasing tier thickness in a wedge shaped tier configuration, records the impact of progressive burial on polygonal faults. This could shed light on important clues as to the initiation, branchline evolution and organisational changes that occur within a polygonal fault tier through time. The temporal and spatial evolution of a polygonal fault array is an important consideration, as is the prevailing diagenetic and sedimentary environments during polygonal fault growth. Understanding when polygonal faults form organisational hierarchies and complex networks has significant implications for the prediction of sealing and fluid flow characteristics for fine-grained successions. Moreover, understanding the spatial evolution of polygonal fault arrays is important to timing fluid flow and reservoir compartmentalisation.

5.2 Seismic stratigraphy

The seismic stratigraphy from the previous chapter is re-used here and focuses explicitly on Unit 1. Horizons with Unit 1 have been renumbered to include additional horizons from the thicker sections of the wedge-shaped polygonal fault tier.

5.2.1 *Reflection units*

There are two units of reflections described in this study, Unit 1A and Unit 1B. Reflections in Unit 1A are parallel medium to low amplitude positive reflections that are regionally traced across the entire survey. The base of the unit is defined as H10 and the top is defined as H6. The base of Unit 1B is Horizon H6. The H6 reflection is a high amplitude, coherent, continuous reflection that is present throughout the survey area. The H6 reflection has a high acoustic impedance, as reflections up to 15 ms below H6 are dimmed and muted (Fig. 5.1). The high amplitude reflection could be an indicator of bulk facies change generating a ‘hard’ reflection response due to increasing acoustic impedance contrast (Avseth et al., 2010). In addition, horizon H5 is significant as it contains the first mapped occurrence of linear enhanced amplitudes (LEAs) as well as showing significant thickening of the wedge. The LEA’s characterise Unit 1B and are locally enhanced reflections contained entirely within the H6 reflection (Fig. 5.2). The enhanced amplitudes are linear, aligned WNW-ESE and are up to 4km in length to the north and progressively shorten to c.a. 500 m to the south with an average spacing of c.a. 600 m. Many LEAs are found in close within elongate furrows of similar dimensions to the LEAs. LEAs are not laterally contiguous across the region, to the south-west and southeast of the survey area, the LEA’s disappear and are replaced by a large scale, feature-less enhanced reflection (Fig. 5.2D). To the north the LEAs appear to be constrained by the hanging walls of the most shallowly hosted polygonal faults. The LEAs are vertically persistent and are found on reflections above H5 including the Seabed reflection, the latter of which defines the top of the seismic unit.

5.2.2 *Sedimentation rates*

Very limited chronostratigraphic data are available for the survey area, with no chronostratigraphic dates available for reflections within the tier. However, there are published dates in Ho et al. (2012a) for the positive reflection immediately below the

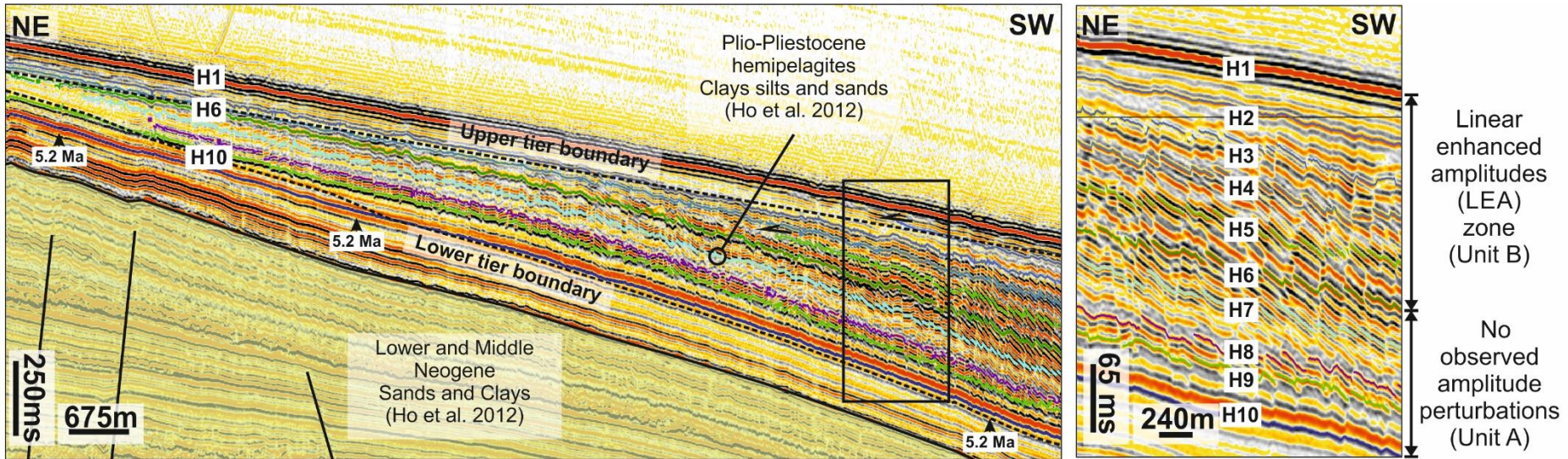


Figure 5.1: Regional seismic section detailing the wedge shaped tier configuration and regional stratigraphy. The chronostratigraphic ages are taken from Ho et al., (2012a). (Right) Zoomed seismic section showing all mapped horizons in the tier.

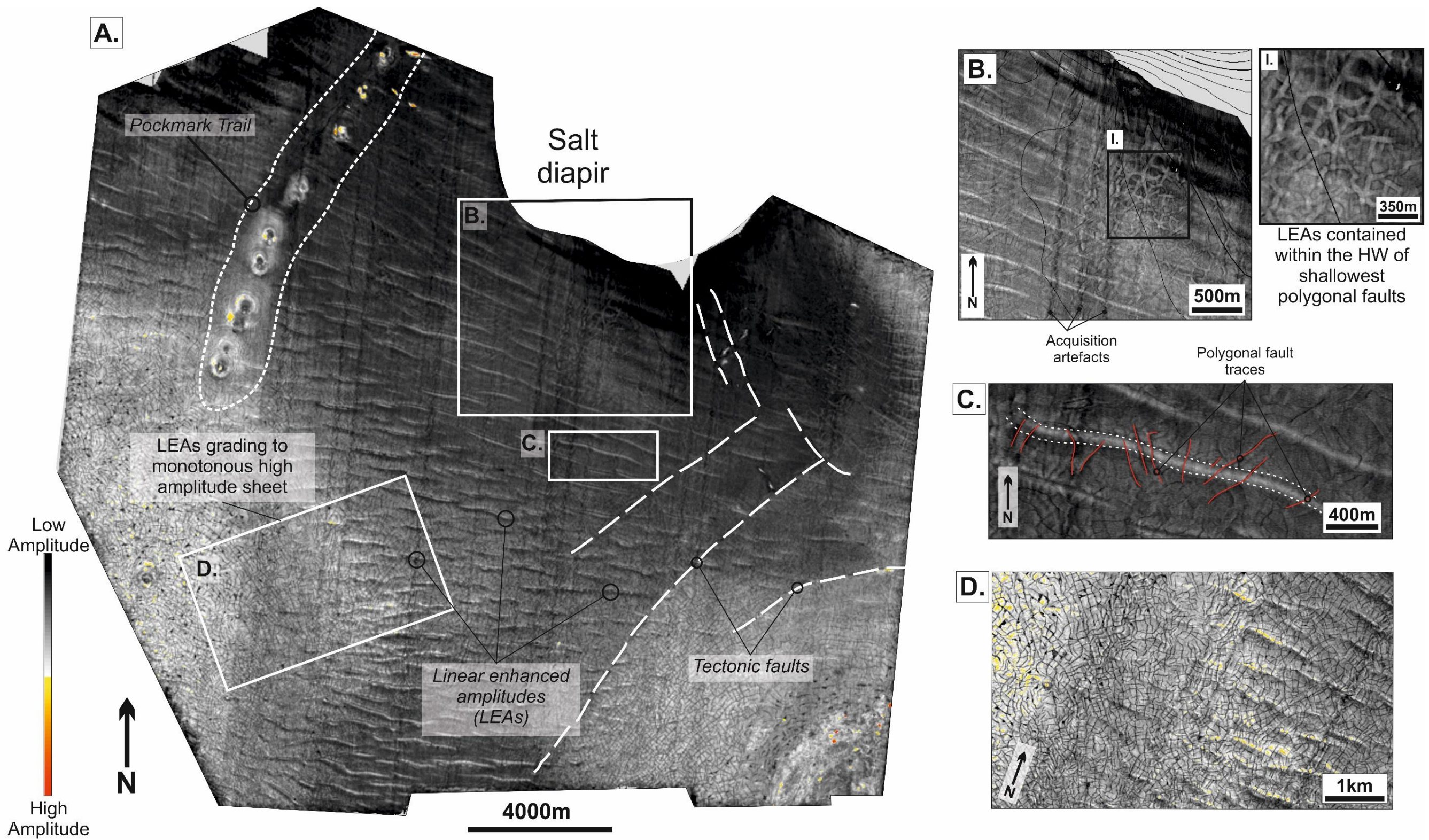


Figure 5.2: (A) Acoustic amplitude map of the H6 reflection showing the LEA's as linear to sinuous enhanced amplitudes, denoted by the light grey colour. Note the homogenous high amplitude responses within the thickest portions of the tier (see). (B) Zoomed section showing the LEAs contained within the polygonal fault hanging wall (C) Zoomed section showing the morphology of a single LEA. Note that the LEA is not related to the polygonal fault array (in red). (D) Zoomed section showing the loss of the LEA shape within a homogeneous high amplitude response.

H10 reflection (Fig. 5.1) which would suggest that the H10 reflection dated at less than 5.2 Ma. Due to the absence of well control, backstripping, which is necessary to account for burial compaction (see Allen and Allen, 2005) is unable to be carried out. However, using the available data, an estimated average sedimentation rate for the polygonal fault tier can be calculated for the maximum and minimum tier thickness. This gives a sedimentation rate of between 15 m/Mya and 51m/Mya for the thinnest and thickest ends of the wedge respectively.

5.3 PFS in a wedge shape geometry

The geometry of the tier is broadly wedge-shaped, with the thickest portions of the wedge found in the southwest and southeast of the survey (Fig. 5.3). Polygonal faults are present across the majority of the wedge and are found in sediment. The base of the wedge has a dip of ca. 1° and the dips are locally perturbed by the presence of pockmarks (see Chapter 7), upper tip folds from tectonic faults and the uplifted flanks around the salt diapir. The top of the wedge is defined by the modern day seabed and has a dip of <1° to the south and southeast.

5.3.1 The geometry and evolution of polygonal fault hosting body

The accumulation of the wedge is influenced by two processes, uplift of the region immediately surrounding the salt diapir, evidenced by the upturning and flexure of the Neogene sediments in the southwest (Fig. 5.4) and also by tectonic faults that attenuate the thickness of the wedge by down-throwing the base of the wedge to the southeast. These two structural domains for creating the wedge are segregated by a local high that is weakly folded and faulted, the root of which, is unknown due to the cut-off within seismic data (Fig. 5.3). These components result in a reflection package that is broadly wedge shaped, with variable thicknesses.

On the southern flank of the salt diapir the wedge body thins to 115 ms (107 m) and is thickest to the southeast where the sediment package is 521 ms (470 m) thick. As described in section 5.2.1, there are two principal reflection units (Units 1 and 2), with Unit 1 further subdivided into Unit 1A and Unit 1B. Examination of the isochron intervals between the horizons H10 and H9 within Unit 1B (Fig. 5.5) show broadly consistent thicknesses across the survey area, with the exception of two small packages of thickening where the unfaulted hemipelagites (Unit 2 in Chapter 7) onlaps the underlying reflections that have been exhumed by salt motion (Fig. 5.3). The upper half of Unit 1B, between H2 and H7, shows increasing wedge

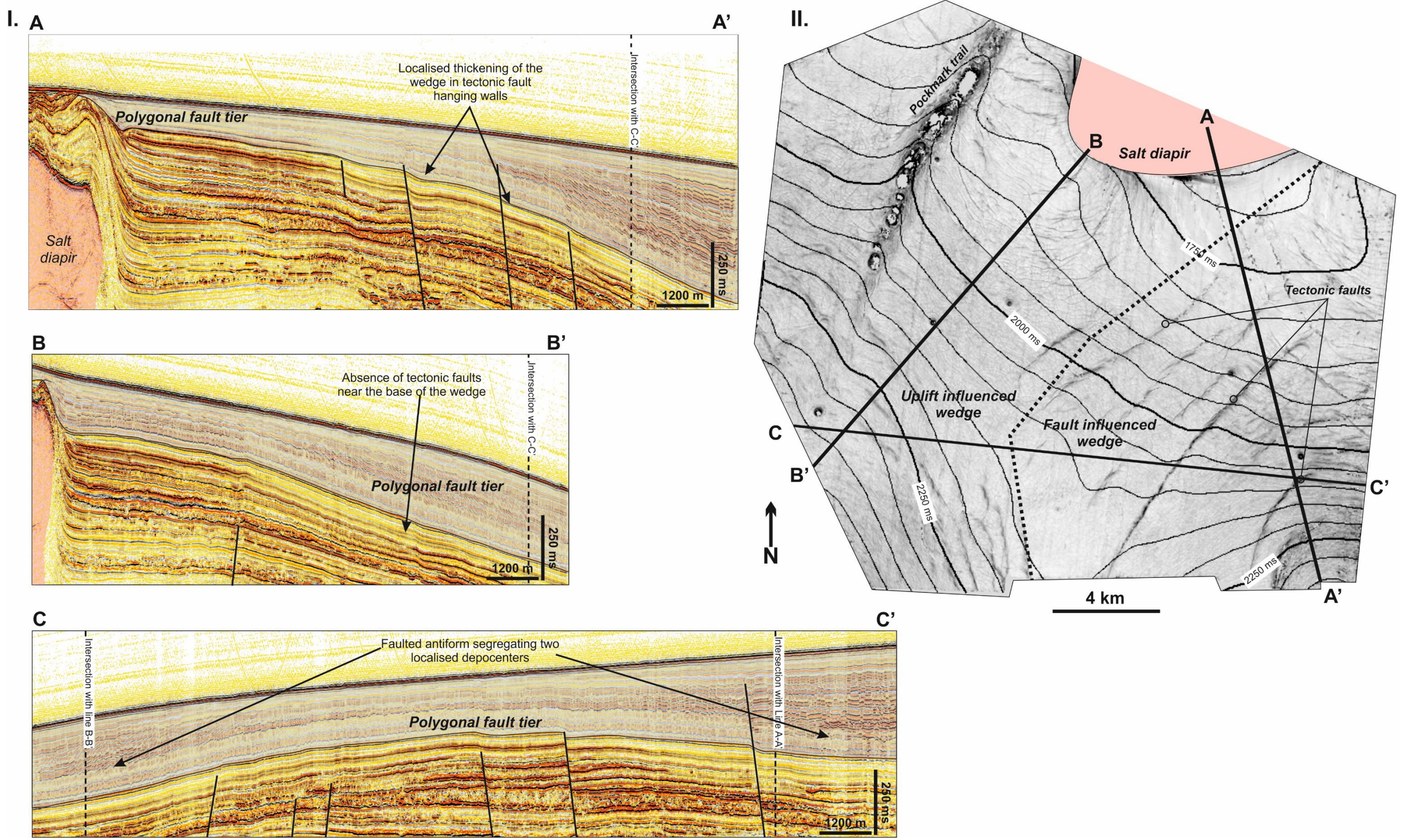


Figure 5.3: A series of seismic cross sections detailing the wedge shaped body of the polygonal fault tier and the strucutral elements influencing the geometry of the sediment package

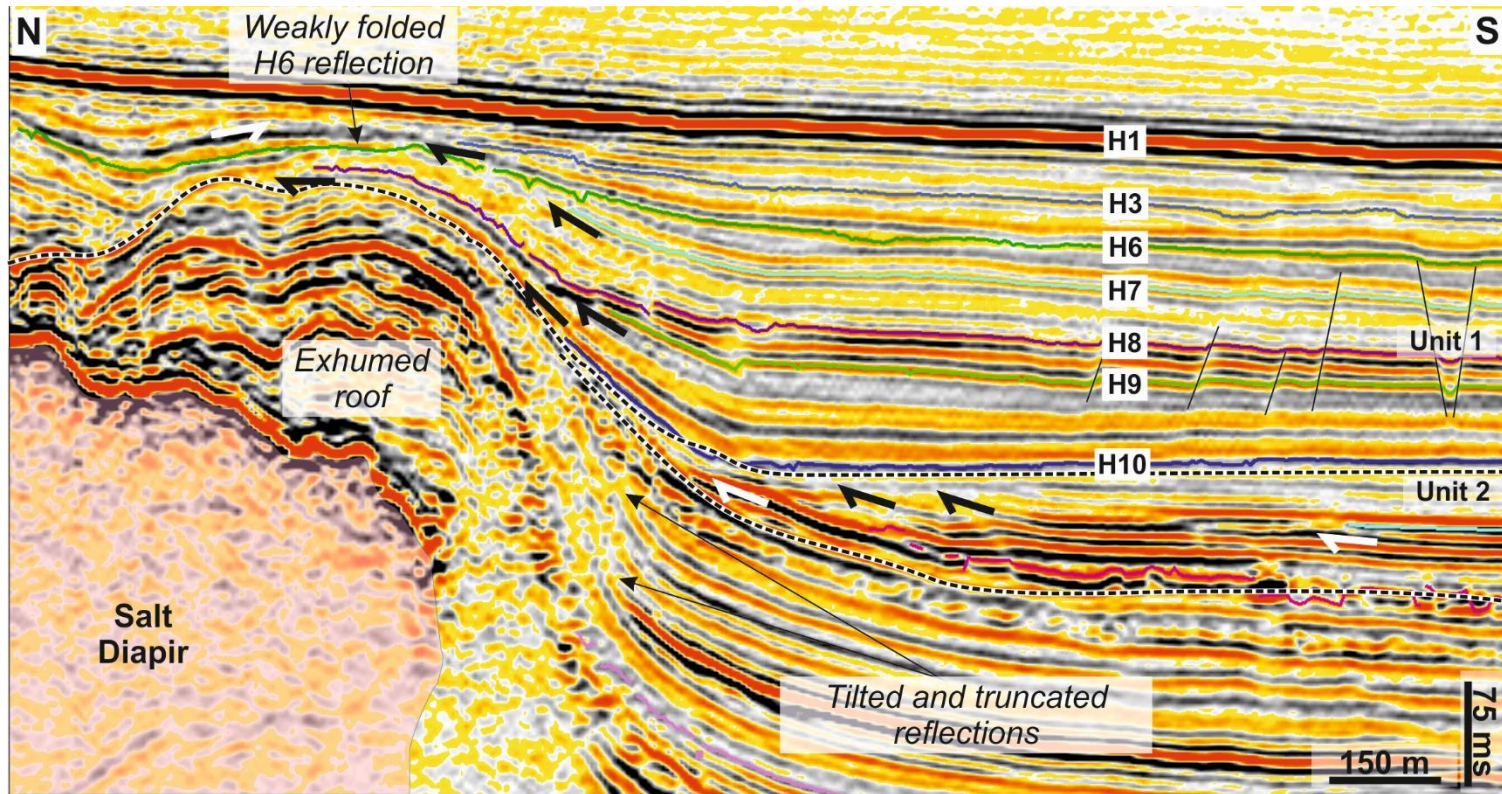


Figure 5.4: Zoomed seismic section across the salt diapir displaying thinning of the polygonal fault tier (Unit 1) at the salt diapir

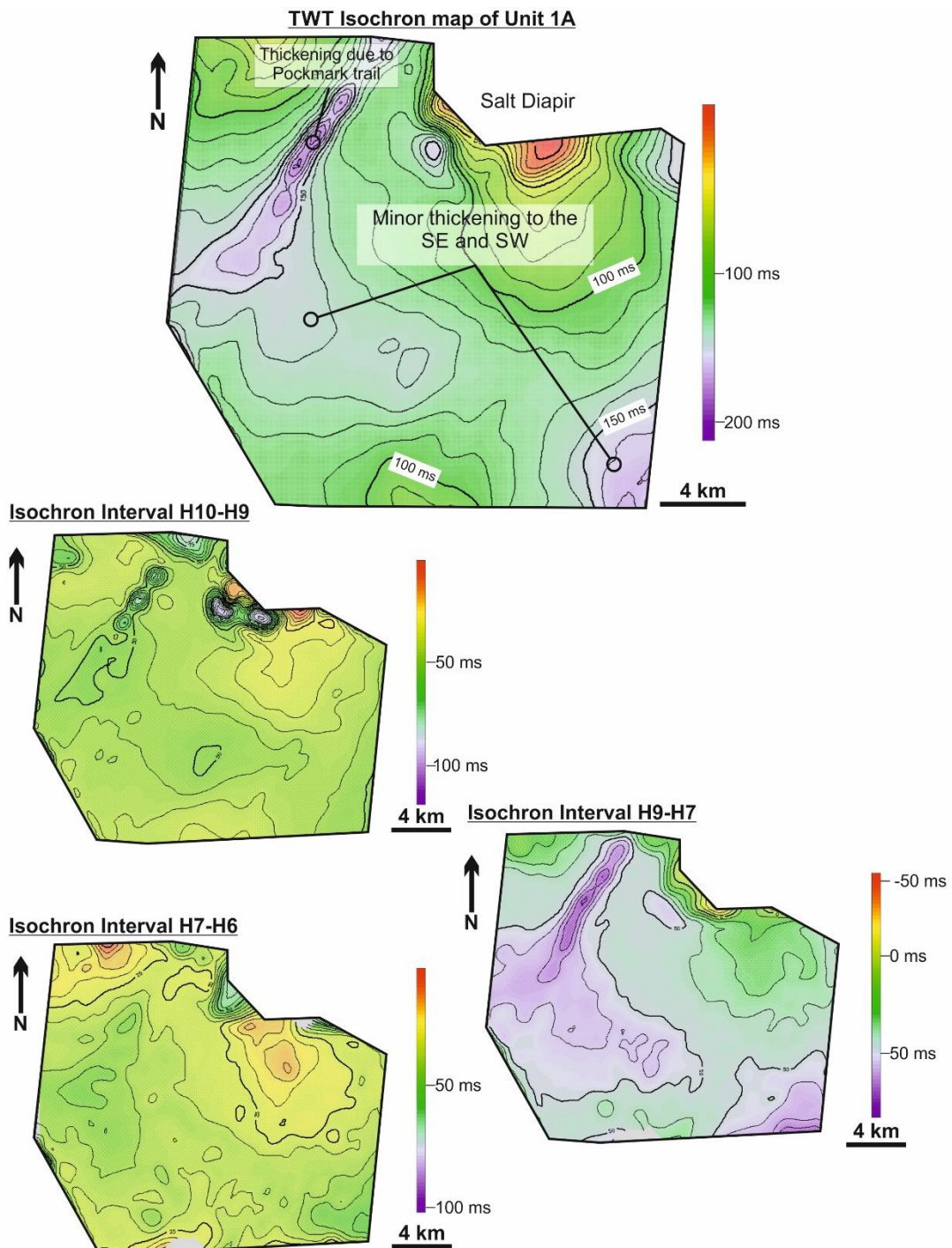


Figure 5.5: Isochron maps across horizons in Unit 1A showing the evolution of the wedge

thickness to the west and southeast (Fig. 5.5). The thickening to the west is due to the reflections being disturbed by the presence of an advancing pockmark trail (Ho et al., 2012b) whereas thickening to southeast is caused by localised thickening across the upper tip of a tectonic fault (Fig. 5.5). The interval between H7 and H6, has an average sediment thickness of 25 ms (22 m) thick. There is localised thinning of the package against the uplifted roof complex on the southern side of the diapir where the H7 reflection is truncated by the H6 reflection (Fig. 5.5). Unit 1A, in contrast, shows pronounced thickening to the south east of the study area and pronounced thinning around the flanks of the salt diapir, indicating a potential condensed sequence with minimal sedimentation. Within the Unit 1A, the interval between H5 and H8 shows significant thickening (from ca. 50 ms to 100 ms) in the middle of the slope, within two localised depocenters to the southeast and southwest (Fig. 5.6).

The stratal termination position gradually steps northeast for stratigraphically younger reflections. The mid-slope thickening package is the locus for onlaps such as those seen around the H6 reflection. The isochron interval between H3 and H1 shows that the localised depocenters to the southeast and southwest have largely been infilled and a southwesterly dipping slope is now established (Fig. 5.6).

Based on the parallel to sub-parallel reflections (Mitchum et al., 1977), the distance from the Zaire canyon, (located approximately 200 – 300 km to the north of the position of this survey) and the low sedimentation rates, the polygonal fault hosting sediments is interpreted as fine-grained hemipelagites. The northward migration of the stratal terminations of some of the reflections described here are consistent with pelagic sedimentation in fault and flexure controlled lows that arise a result of Late Pliocene salt motion and margin uplift. The uplift and motion of the salt and local tectonic faults during the Pliocene, created localised thickening across tectonic fault hanging walls as well as thinning of the sediment around the salt diapir.

5.3.2 The geometry of the polygonal fault tier.

Polygonal faults in the thinnest section of the tier are between 50 m and 95 m tall in sediment thickness as low as 150 m. The basal tip position is on or above the H9 reflection with upper tips between H7 and H6. As the wedge thickness increases the basal tip position gradually breaks through the H9 reflection and lies above a prominent bright red ‘hard’ reflection (Avseth et al., 2010) above the H10 at >250 m

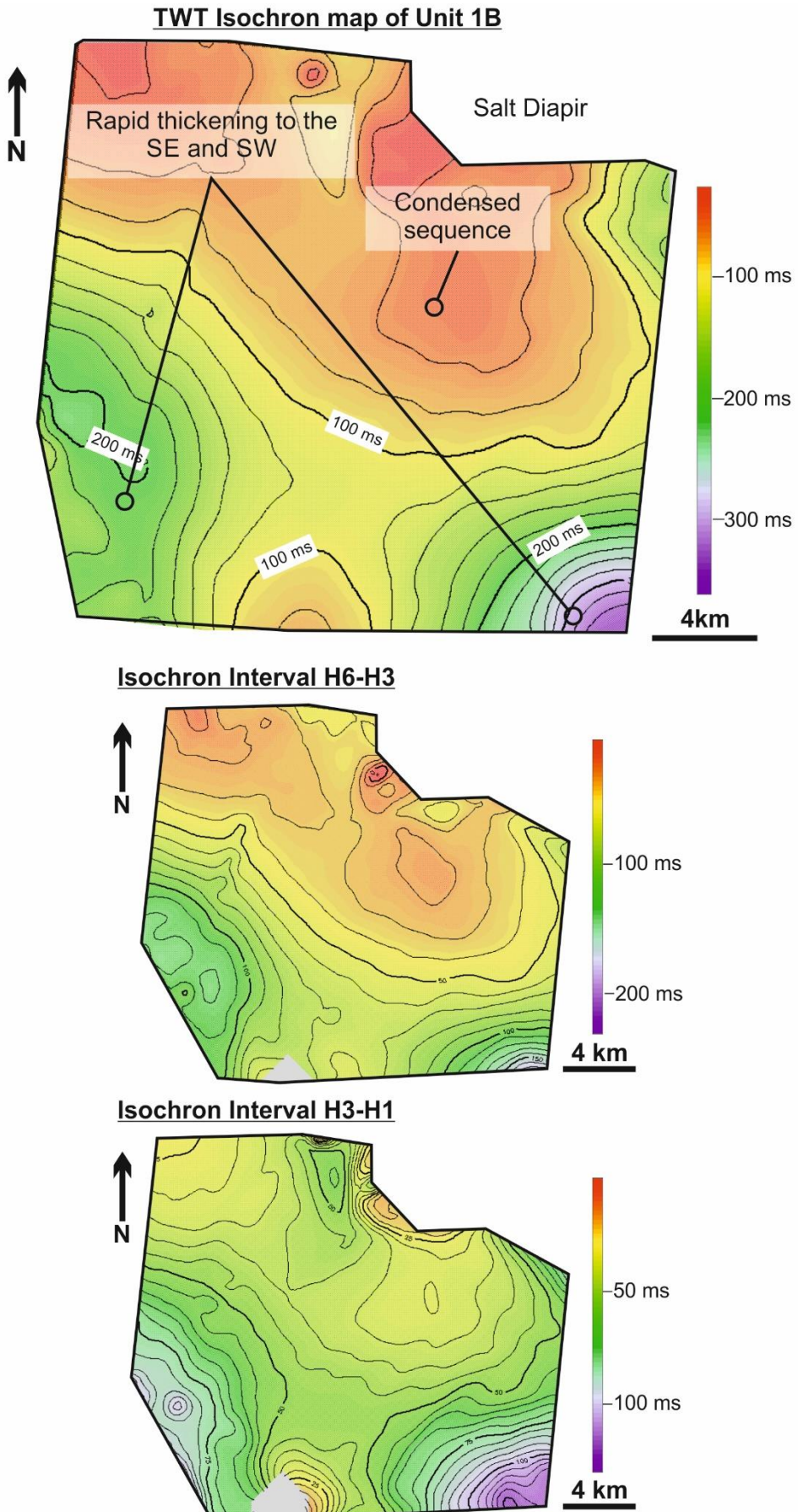


Figure 5.6: Isochron maps across horizons in Unit 1B showing the evolution of the wedge

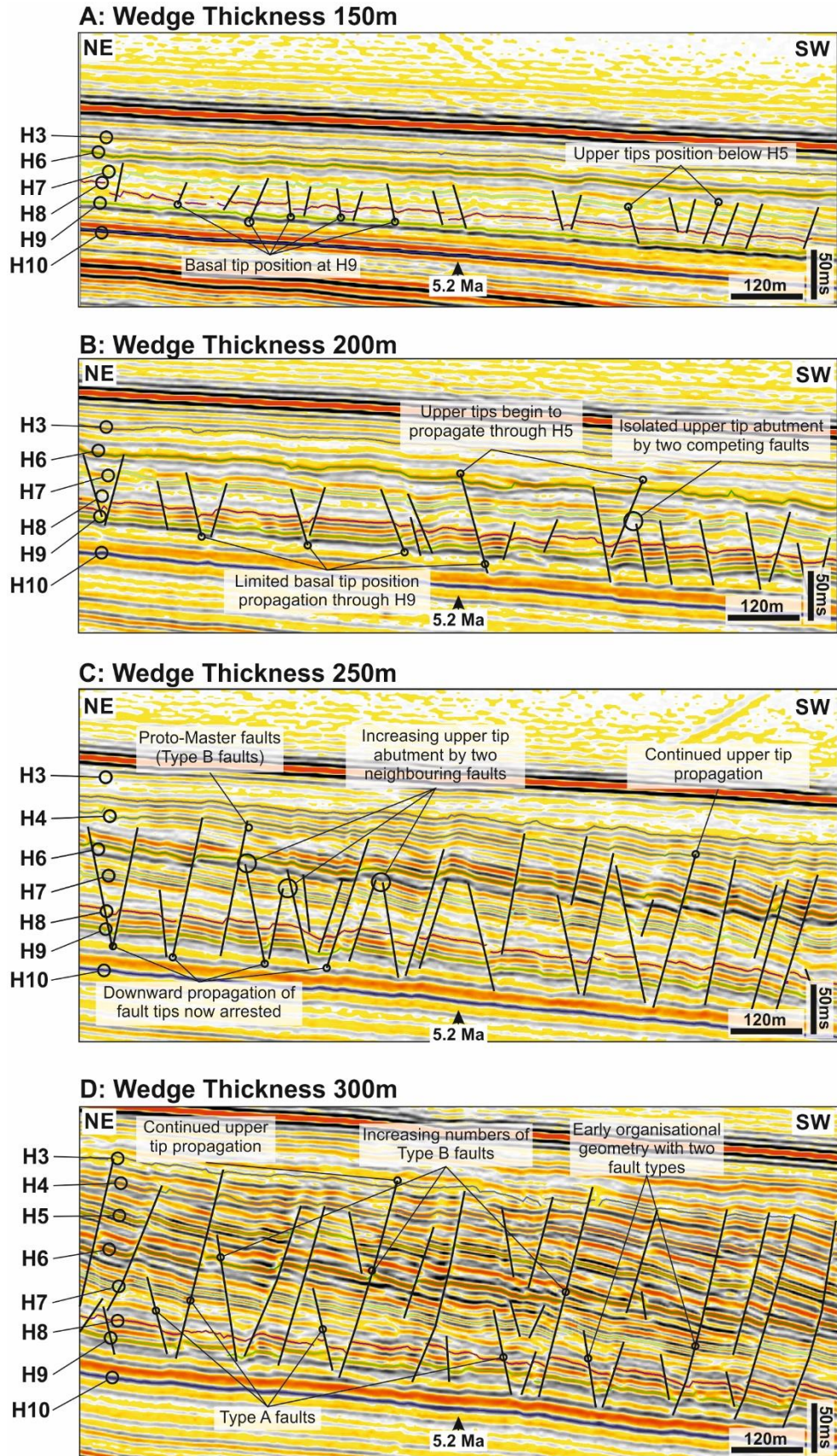


Figure 5.7: A series of seismic cross-sections showing changing internal polygonal fault organisation and tip positions with increasing wedge thickness.

of sediment thickness (Fig. 5.7). Equally, the upper tip position also migrates upwards through stratigraphy. At 150 m wedge thickness the upper tip lies at the H6 reflection whereas as the wedge thickens to 300 m the upper tip position is near the H8 reflection. (Fig. 5.7). The movement of the upper tip position through stratigraphy, creates polygonal faults with heights that crudely scale with wedge thickness. Statistical analysis of the polygonal faults across the wedge show increasing variability in fault height (Fig. 5.8). Polygonal fault height at the thinnest end of the wedge shows broadly consistent fault heights and limited variation. As the wedge thickens, this variation increases with some faults scaling to the full thickness of the wedge and others abutting against other taller faults between H7, H6 and H5 (Fig. 5.7, Fig. 5.8). The upper tip boundary, defined by position of multiple polygonal fault the upper tips lies between 30 m and 60 m below the seabed and occur discordantly across several reflection cycles. Broadly, polygonal fault tips are consistent but there are isolated examples of polygonal fault tips that extend beyond the tip position and offset reflections either close to the seabed or beneath deeper into the stratigraphy (Fig. 5.9). Both upper and lower tip terminate rapidly in seismic data and terminate in weak folding of seismic reflections under or overlying the fault tips.

The upper tip gradients within the array show variation between 0.05 and 0.4 for faults of all depths (Fig. 5.10B). The basal tips of the polygonal fault array are found across several reflections between H10 and H9 (Fig. 5.10A). Basal tip gradients are much more variable than the upper tips with tip gradients ranging from 0.1 to 0.7 (A). The base of the polygonal fault tier locally appears to step up stratigraphy to terminate between H2 and H3 in the region immediately south of the salt diapir.

Polygonal fault planform geometry is complex across the wedge (Fig. 5.11). Lateral tips of polygonal faults in the shallow section abut and form a network of non-colinear horsts and grabens (Fig. 5.11) ranging from 70 m to 800 m in length. Shallow and deep polygonal faults exhibit some subtle variations in fault pattern. The shallowest (<150 m burial) faults in the north of the survey have basal tips between H9 and H8 and have upper tips located at H6. Polygonal fault patterns in the shallow sections of the tier have curvilinear fault traces with a high degree of connectivity between fault traces (Fig. 5.11 feature y).

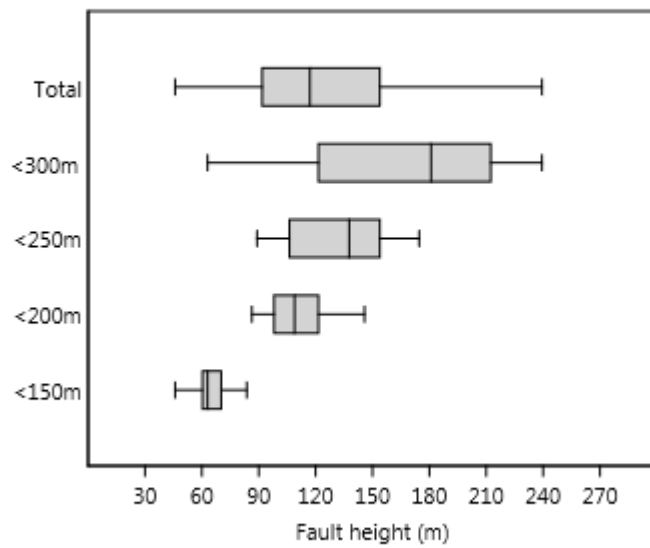


Figure 5.8: Box plot showing the increasing variability in fault height with increasing wedge thickness (y-axis).

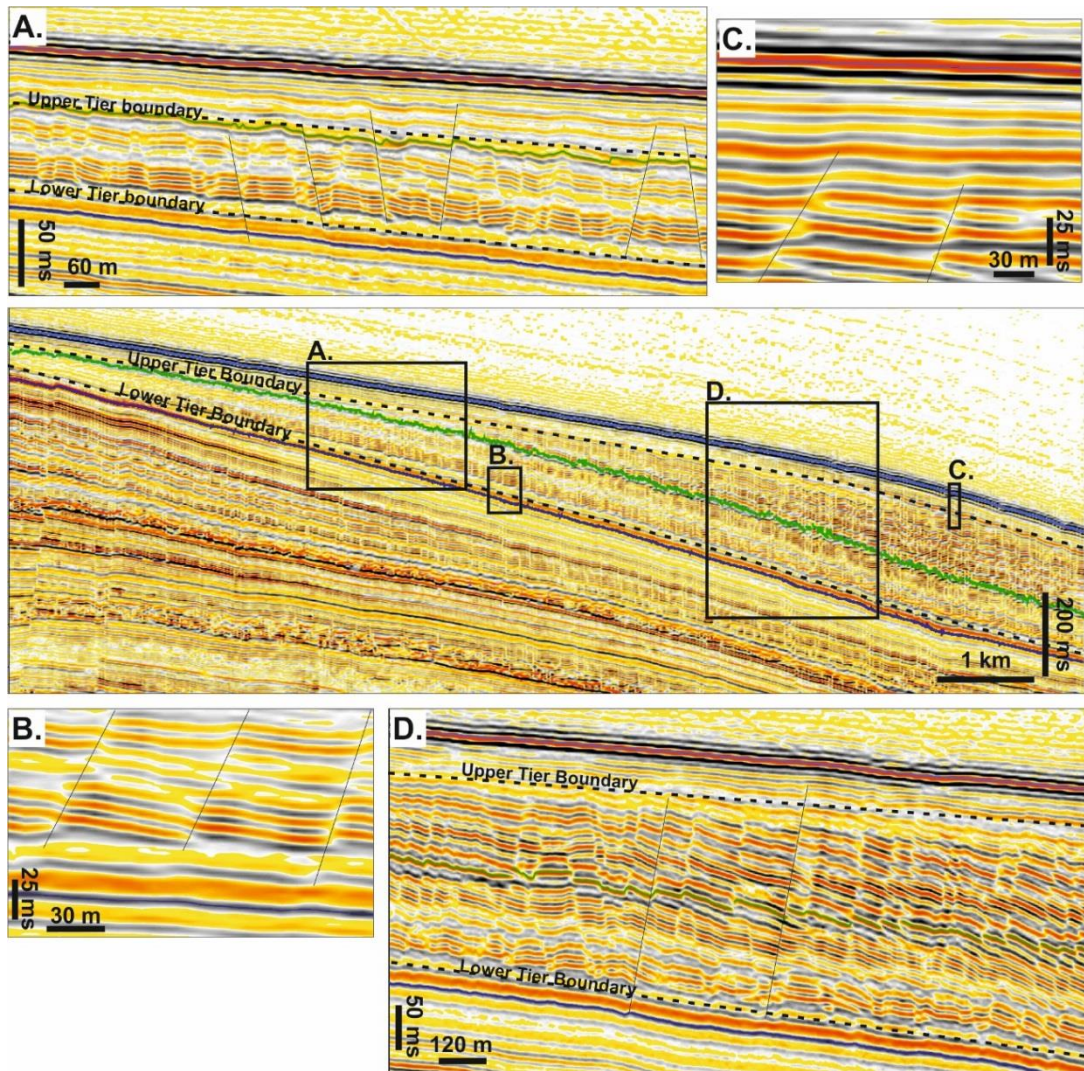


Figure 5.9: Seismic cross-section with zoomed sections showing the (A) upper and lower tip geometry in the shallow section of the tier (B) zoomed section of basal tip geometry (C) Zoomed section of upper tip geometry (D) zoomed section showing upper and lower tip geometries in the thicker section of the tier

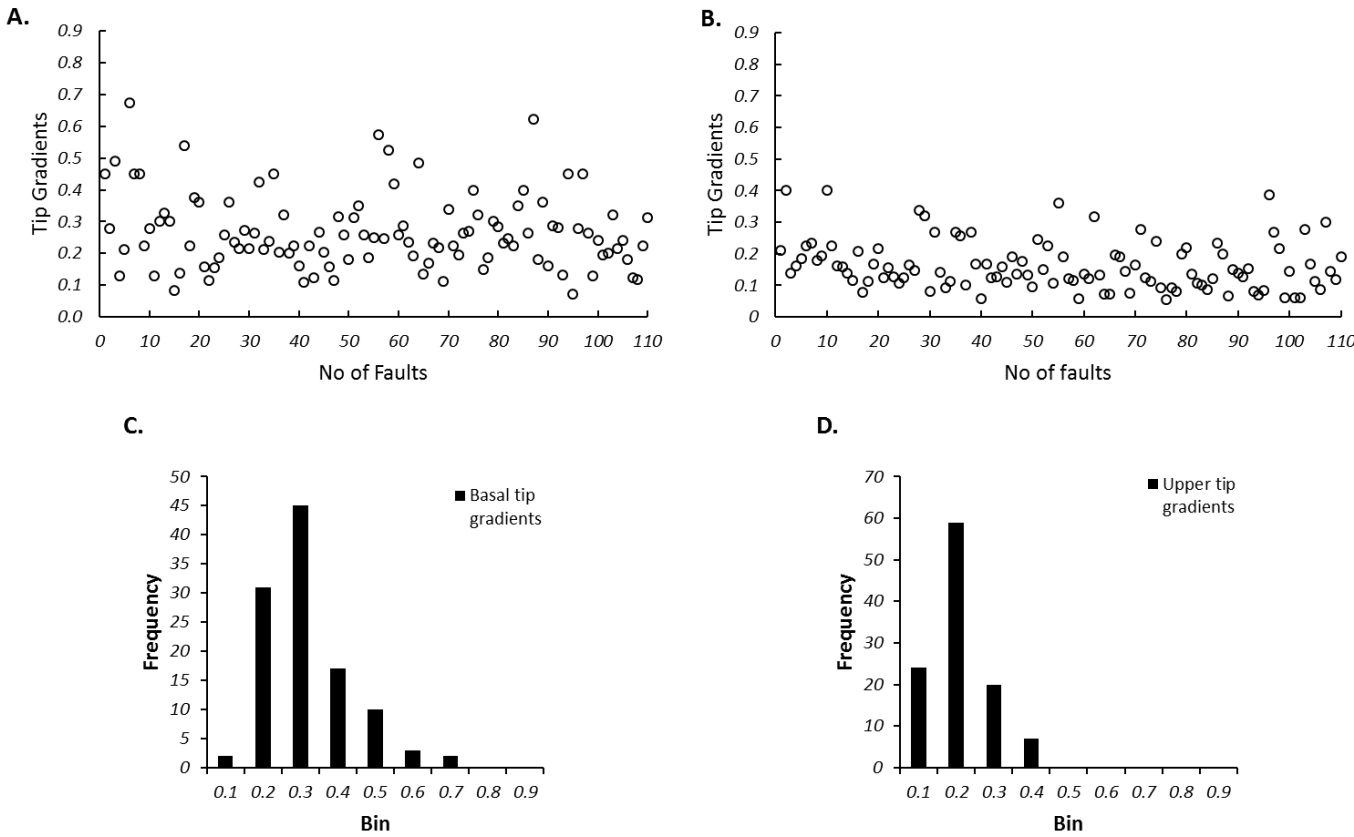


Figure 5.10: (A) Basal tip gradients for a 110 faults within the wedge (B) Upper tip gradients of 110 faults within the wedge, (C) Histogram displaying the distribution of displacement gradient, (D) Histogram displaying the distribution of upper tip gradients

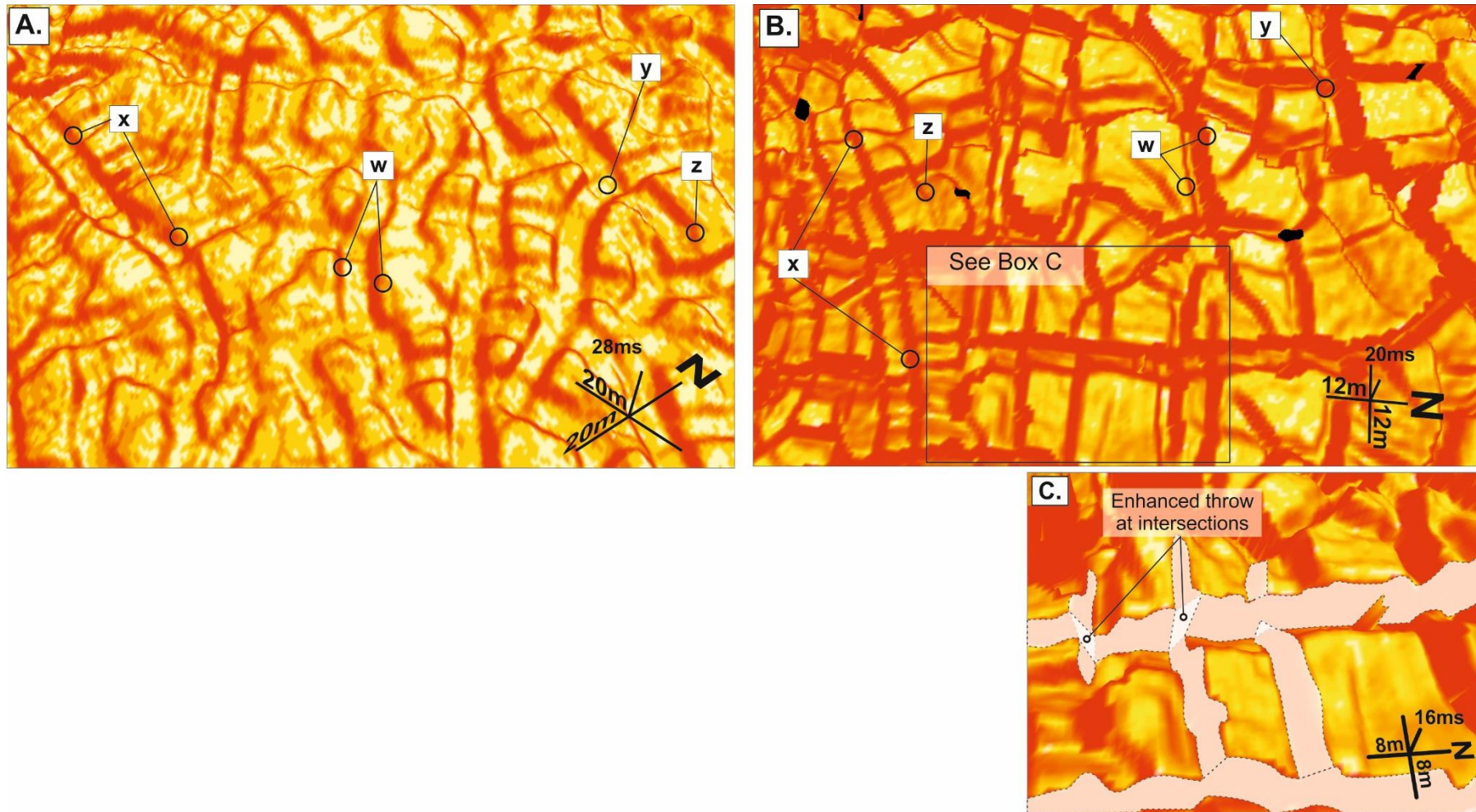


Figure 5.11: 3D view of horizon H5 showing the geometry of fault linkage in the shallowest faults in the tier (A) and the deeply buried faults (B). (C) Zoomed 3D view showing complex intersections where cross cutting faults combine throws at the intersections

The three dimensional geometry of the hanging wall blocks is complex. Many polygonal faults, both in the shallow and deeper sections of the tier show a high intersection angle (60° - 100°) between individual fault intersections. The array has a very high degree of connectivity with very few free tips in the array. The three-dimensional geometry of the fault intersections shows a complex cross cutting relationships and abutments where fault hanging walls from non-colinear faults intersect and cross-cut one another (Fig. 5.11). This results in high throws at intersections where displacement from two linked fault branchlines combine in a common hanging wall (Dickinson, 1954; Nicol et al., 2003; Stuevold et al., 2003; Nelson, 2007). These cross-cutting relationships are observed in both shallow and deep sections of the wedge, however in the deeper sections of the wedge this effect is much more pronounced (Fig. 5.11).

Polygonal faults show a degree of pattern evolution within the fault array. Polygonal fault numbers decreasing between H2 and H5, as well as preferred orientation shifting ENE-WSW to NW-SE. Orientations of polygonal fault strike show a multi-azimuthal strike although shallower horizons (H6 and above) show a distinctive preferred orientation of NW-SW, parallel to the strike of slope at the base of the polygonal fault tier (Fig. 5.12). Polygonal fault planform patterns in horizons H9, H8 and H7 show highly connected, curvilinear traces akin to those observed in the shallower sections of the array (Fig. 5.12). Horizons H6 to H3 show rectilinear fault traces. The faults patterns at this stratigraphic level show an ordered fault hierarchy of fault traces (sensu Ho et al., 2013) up to 2 km in length (1st order) intersected at 90° by a network of 150 m to 300 m long fault traces (2nd order) (Fig. 5.11 , feature z).

5.3.3 *Polygonal fault displacement*

Polygonal fault displacement characteristics are described in the following section at a variety of scales from broad scale for the whole tier to throw distributions across individual faults

5.3.3.1 *Displacement distributions through the wedge*

Polygonal fault displacement distributions fall into two broad categories, c-type and m-type displacement distributions. C-type displacement distributions are characterised by a single displacement maximum, towards the centre of the middle

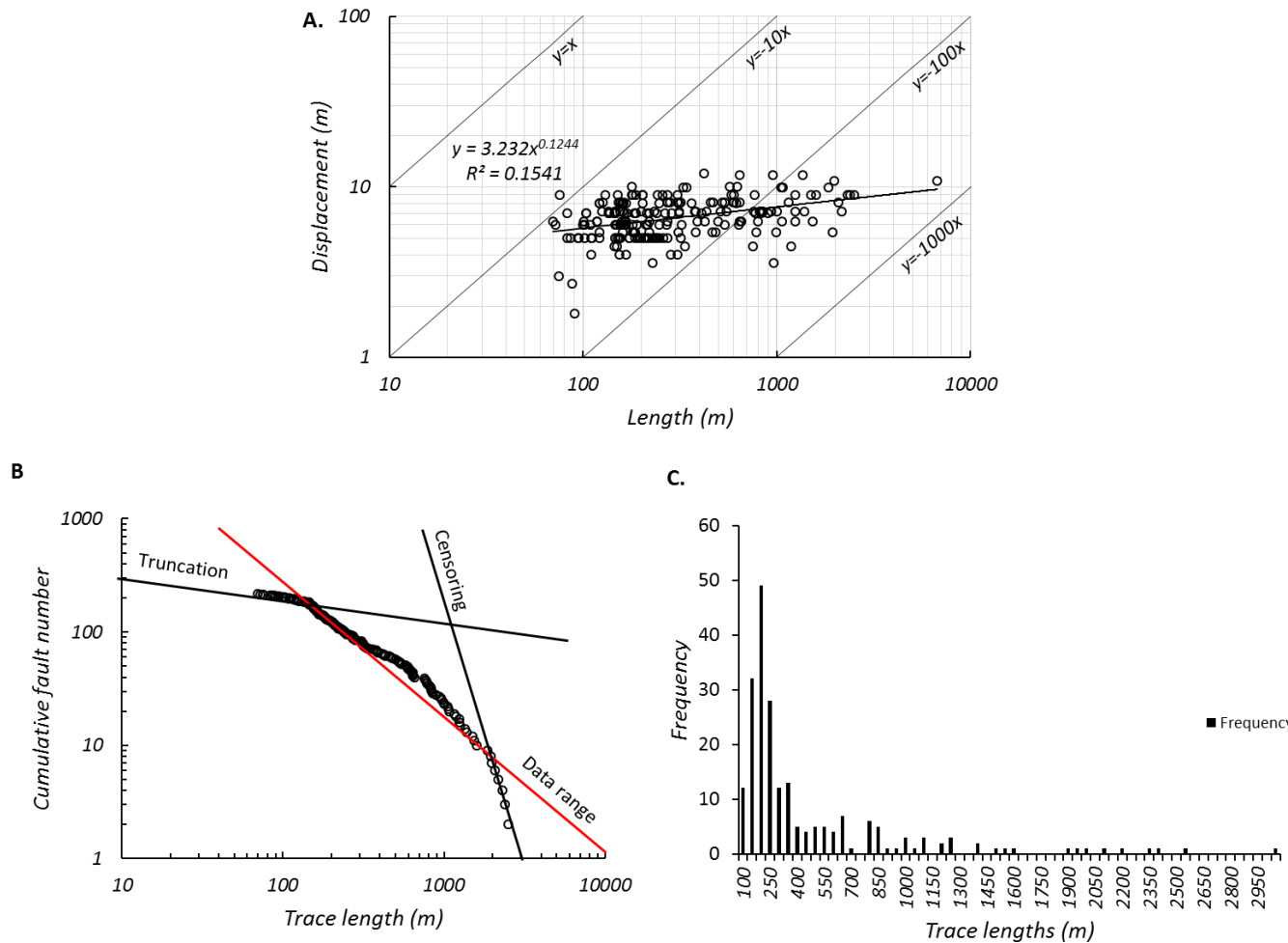


Figure 5.14: (A) A log-log plot of displacement versus length, (B) A plot of cumulative fault number detailing the data range and the effects of under-sampling in the dataset, (C) Frequency plot of fault lengths showing the distribution of measured fault lengths

of the fault. M-type distributions contain two displacement maxima skewed towards the tips of the faults. The displacement distributions appear to be linked to a particular seismic unit, with c-type faults more common in 1A faults (informally described as Type A) of the tier than faults located at the thicker end of the wedge. Polygonal faults hosted in both Unit 1A and Unit 1B (Type B faults) are dominated by m-type displacement distributions (Fig. 5.15)

Polygonal faults hosted in Unit A are the shortest faults present within a survey and are on average <120 m in height, Lengths of polygonal faults in Unit A are variable and can range from 90 m to 800 m in length, with no clear preferred orientation (Fig. 5.15). The upper and basal tip positions for Type A faults is diffuse and spread across several reflection cycles as opposed to being constrained by a single reflection. Moreover, for faults that are hosted where the wedge thickness is >200 m, the upper tip position is more likely to breach the H5 reflection, in regions where the wedge less than 200 m the H5 reflection tends to define the upper tip position. The upper tips of Type A faults are interpreted to occur on reflections between the H6 and H5 reflections. The basal tips are interpreted to occur on reflections between H10 and H9. The distribution of displacement on Unit A hosted faults is typically c-shaped (Muraoka and Kamata, 1983) with displacement maxima located between H8 and H7. There are isolated examples where there is a displacement minima located at H8 and these are seen infrequently and attributed to artefacts generated by nearby fault linkage (Fig. 5.15). Polygonal faults within 1B or Type B faults cut both Unit 1A and have upper tips within the upper third of Unit 1B. These faults are only present where the wedge thickness exceeds 250 m. Polygonal fault lengths for Type B faults are also variable and have a similar range to the Type A faults ranging from 120 m to 900 m. Polygonal fault height varies from 150 m to 250 m. Upper tip positions of Type B faults are also variable and are located on reflections between Seabed and H9. Similarly, basal tips are spread over the same range of reflections as Type A faults with basal tips located between the H10 and H9 reflections. Upper tips are also spread across a range of reflections ranging from the H3 and H1. The distribution of throw in type B faults is variable with two end member throw distributions; a c-type and an m-type distribution (Fig. 5.15).

The c-type distributions are found in a variety of lengths, heights and orientations. The c-type faults are characterised by a single displacement maxima located in 1A,

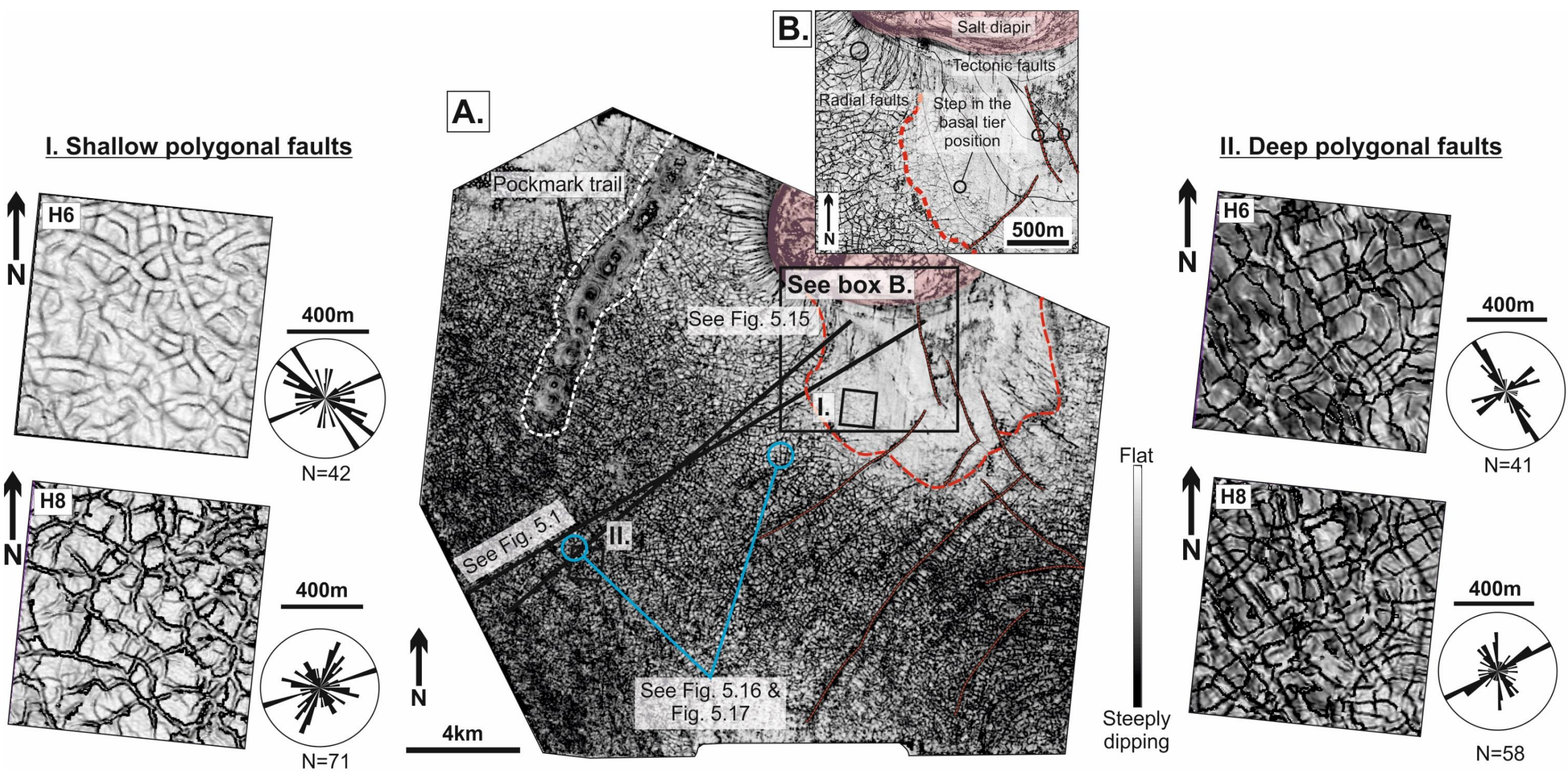


Figure 5.12: (A) Time-dip attribute map of Horizon H9 showing the step in the basal tip position. (B) Zoomed section showing the lateral dissipation of polygonal fault (I and II) Time-dip maps of H7 and H6 showing the local orientation of polygonal fault strikes.

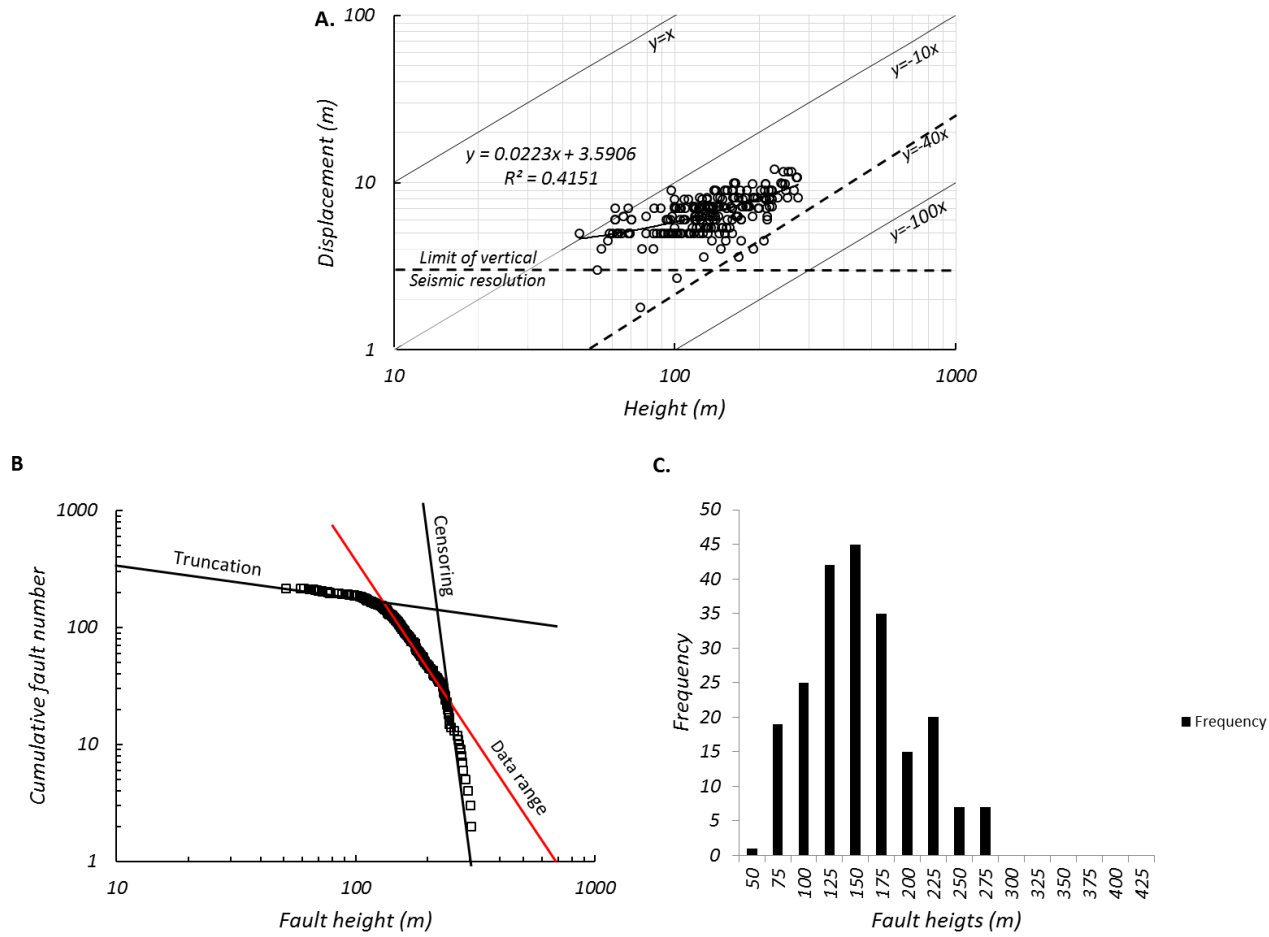


Figure 5.13: (A) A log-log plot of displacement versus height, (B) A plot of cumulative fault number detailing the data range and the effects of under-sampling in the dataset, (C) Frequency plot of fault lengths showing the distribution of measured fault lengths

between H7 and H6. The m-type throw distribution is characterised by displacement minima located between H6 and H4 reflections (Fig. 5.15). There are also two displacement maxima, one located in Unit 1A between the H7 and H6 reflection and another in Unit 1B at the H5 reflection (Fig. 5.15).

5.3.3.2 Polygonal fault displacement length and displacement – height characteristics

Polygonal fault displacement is low, consistently less than 12m and average displacement maxima is 7m. Displacement-height plots show that fault displacement and height show a linear scaling relationship (Fig. 5.13A). Cumulative fault frequency for displacement shows that there is a narrow range of faulting before the dataset is truncated and censored by sampling bias and seismic resolution limitations (Fig. 5.13B). The range of fault heights documented is also narrow and shows an average fault height of 150 m (Fig. 5.13C)

Polygonal fault lengths however, are much more variable, typically ranging from 70 m to 6.7 km with a mean trace length of 450 m. Displacement-length plots show that polygonal faults can reach lengths of several kilometres and yet displacement maxima remain at 12 m or less throughout the tier (Fig. 5.14). Displacement-length ratios vary by at least two orders of magnitude ranging from 8:1 to 600:1 and show a power law scaling (see Chapter 4). Cumulative fault plot shows a wide range of fault lengths with limited censoring and truncation (Fig. 5.14B). Trace length frequency data shows a predisposition for polygonal faults to form short traces (250 m or less). This indicates that the shorter 2nd order faults in a given fault pattern are the most common faults in the array, whilst the longer first order faults are comparatively rare with only isolated examples of faults exceeding 1.5 km in length (Fig. 5.14C).

5.3.3.3 Throw distributions along strike

Throw distributions were also examined along strike. These plots look at first order faults and their linkage with 2nd order fault sets. These plots specifically consider the impact of isolated branchlines, paired branchlines that are made of two colinear faults and the distribution of throw within a polygonal cell, which is a compartment bound on all sides by a fault. Each of these styles of interaction were considered for deep (300 m mean wedge thickness) and shallow (200 m mean wedge thickness). Generally, the polygonal faults show basal tips with low plunge and upper tips with.

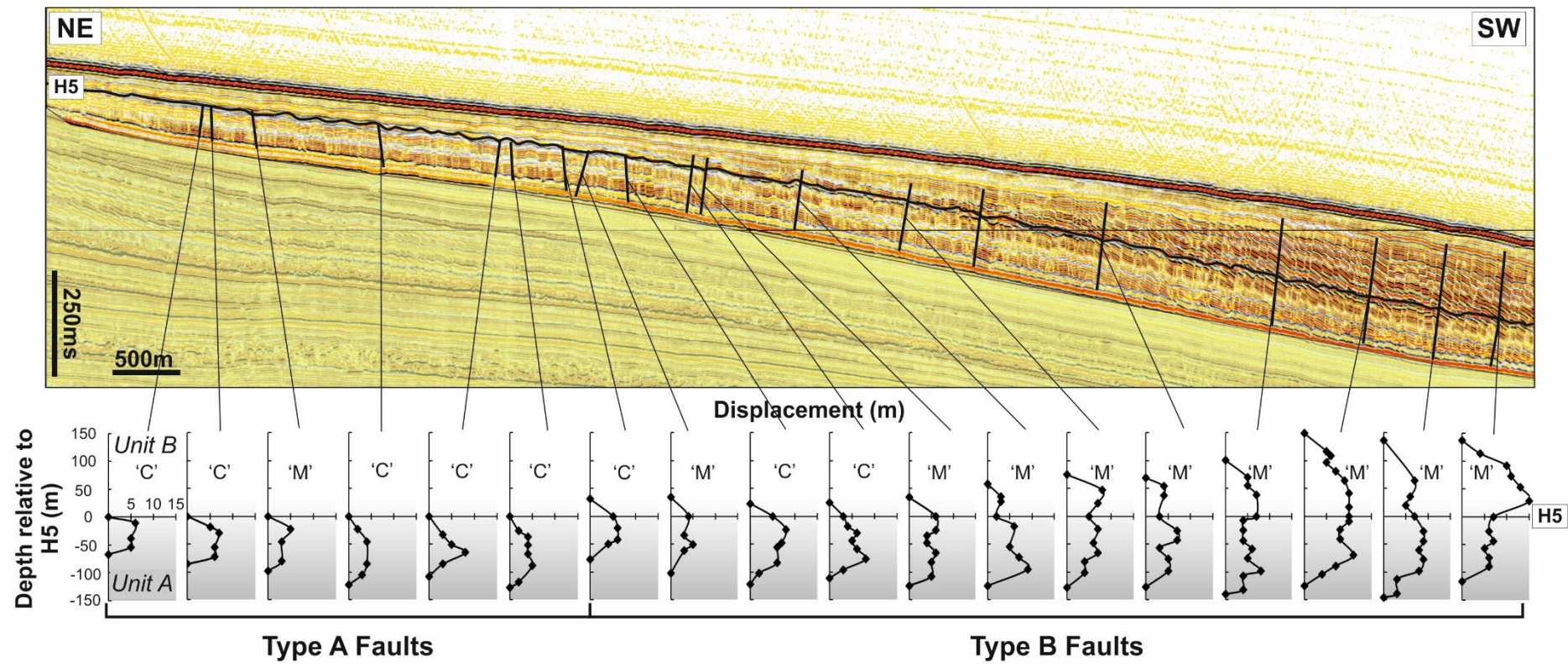


Figure 5.15: Seismic cross section showing the variability in fault throw relative to a single seismic horizon H5. The faults show a gradual transition from c-shaped to m-shaped faults within the tier, due in part to increased fault linkages

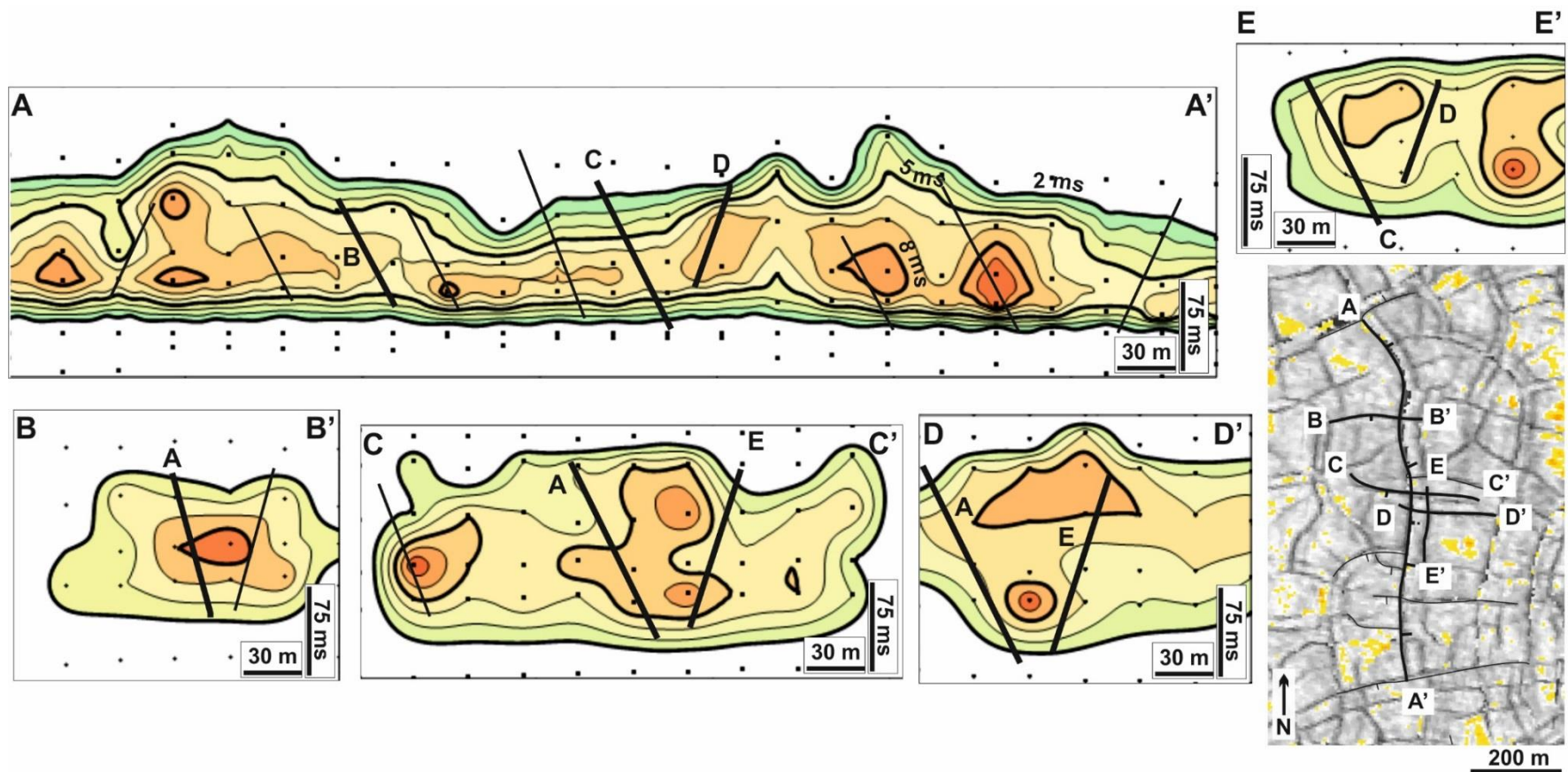


Figure 5.16: Along strike plots of fault displacement for five polygonal faults at 200 m wedge thickness, including a 1st order fault (A), an isolated (B), paired (C and D) and colinear(E) 2nd order faults

variable plunge along the fault length with some sections of faults showing steep and low plunge sections.

The distribution of the shallow wedge shows that all the faults have undulating upper tip positions when viewed along strike with some faults breaching the H5 reflection. The throw distribution along the first order fault (A) shows both ‘c’ and ‘m’ distribution types with localised maxima of between 6 and 8 ms occurring in close proximity to branchlines (Fig. 5.16A). These maxima are the largest observed along its four branchlines. The isolated branchline shows a single displacement maximum axio-symmetrically aligned to the centre of the tier, within the hanging wall of fault A and an unnamed fault. The colinear fault sets (C and D, see Fig. 5.16) in contrast show a double displacement maxima of (6 – 7 ms) in the hanging wall, localised towards the upper and lower limits of the polygonal fault plane. The 1st order fault (A) and its smaller colinear fault (E) show localised maxima towards the centre of the tier.

The deeper fault set shows differing geometry. Here, the 1st order fault (A) shows a broadly consistent tip geometry located between H3 and H2 whereas the basal tip shows minor variation in the basal tip position with small undulations that penetrate deeper into Unit 2 (Fig. 5.17A). As seen in its shallowly buried contemporary, the displacement distributions fluctuate between archetypal ‘c’ and ‘m’ distributions, especially near branchlines, with displacement maxima values varying between 8 and 11 ms along the length of the fault (Fig. 5.17). The isolated branchline (B) shows a double displacement maximum near the intersection with A and an unnamed colinear branchline. The upper tip of branchline B shows a varied tip position

The colinear branchline C has its displacement located away from the intersections with the main fault (A) and its colinear fault (E). Branchline E is much shorter than its counterparts and is 100 ms (97 m) tall, with its upper tip restricted vertically by another nearby fault plane.

5.4 Discussion

5.4.1 Polygonal fault nucleation

This survey offers clear evidence for polygonal fault nucleation in sediment thicknesses of 100 m. It is therefore necessary to attempt to account for the presence of polygonal faults at such shallow depths. In addition to the six nucleation

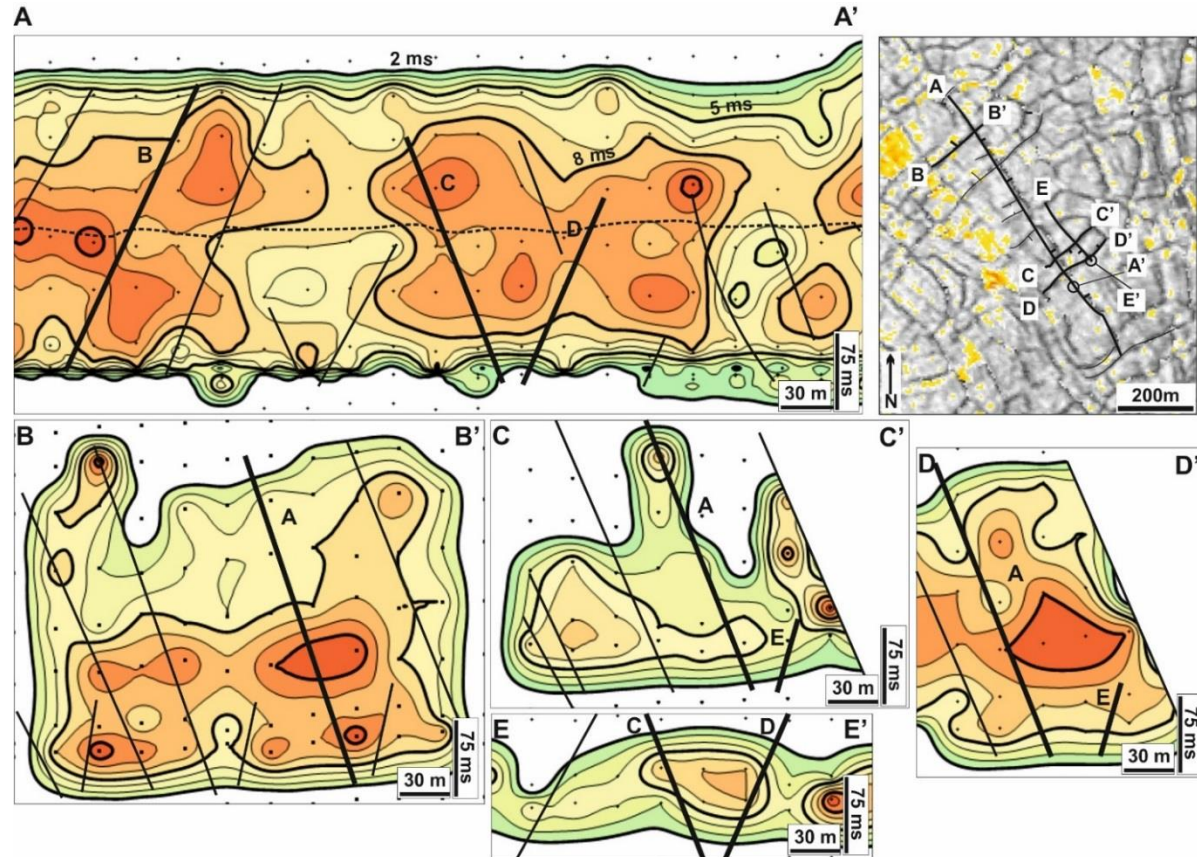


Figure 5.17: Along strike plots of fault displacement for five polygonal faults at 300 m wedge thickness, including a 1st order fault (A), an isolated (B), paired (C and D) and colinear(E) 2nd order faults

mechanisms described in 5.1 (see Cartwright et al., 2003; Goult, 2008; Cartwright, 2011 for reviews), some recent studies on polygonal faults have begun to consider soil mechanics, particularly the Cam-Clay model, as a potential cause of polygonal faulting (Dehandschutter et al., 2005; Laurent et al., 2012; Roberts, 2014). The Cam-Clay model explicitly examines the role of low rate of increasing strain on saturated clays and soils under triaxial loading (Smith and Smith, 1998). A study by Dehandschutter et al. (2005), proposed an early mechanism for faults observed in the Boom clay, Belgium. Dehandschutter et al. (2005) suggests that at burial depths less than 200 m, a feedback mechanism operates whereby a combination of compaction, minor tilting and gravitational forces all operate to form shear bands. The shear banding undergoes layer parallel shortening and volume loss, draining the sediment and ultimately leading to brittle failure as the compaction pathway crosses the critical state line. Laurent et al. (2012) infer that isochoric (same-volume) shear in clays is driven by ‘strain hardening’, horizontal contraction of clays during burial, low coefficients of friction and sufficient burial to breach the yield cap which delimits the transition from elastic to plastic behaviours and allows strain localisation. The models proposed by Dehandschutter et al. (2005) and Laurent et al. (2012) do not consider the impact of the evolving diagenesis, particularly the impact of cement precipitation on their models or consider how this impacts the proposed deviation from K_0 .

A recent a study by Roberts (2014) examined and numerically modelled the Cam-Clay mechanism within two end member models of orthotropic diagenetic volume strain (i.e. 1D consolidation) and isotropic diagenetic volume strain (isotropic compaction/contraction). These models were used to test chemical driven volume reduction in diatomaceous (siliceous) mudstones. Roberts (2014) showed that when chemical volume change was expressed in all three axes and equalled 20%, the modified stress path permitted shear failure along similar lines to that proposed by Laurent et al. (2012).

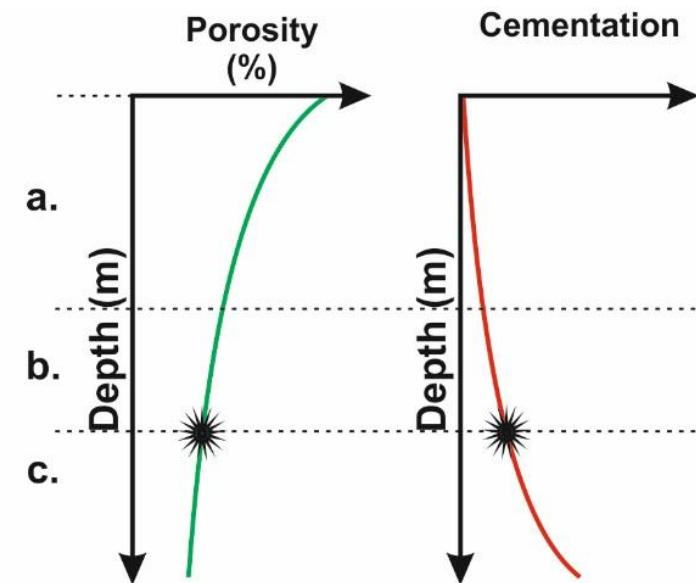
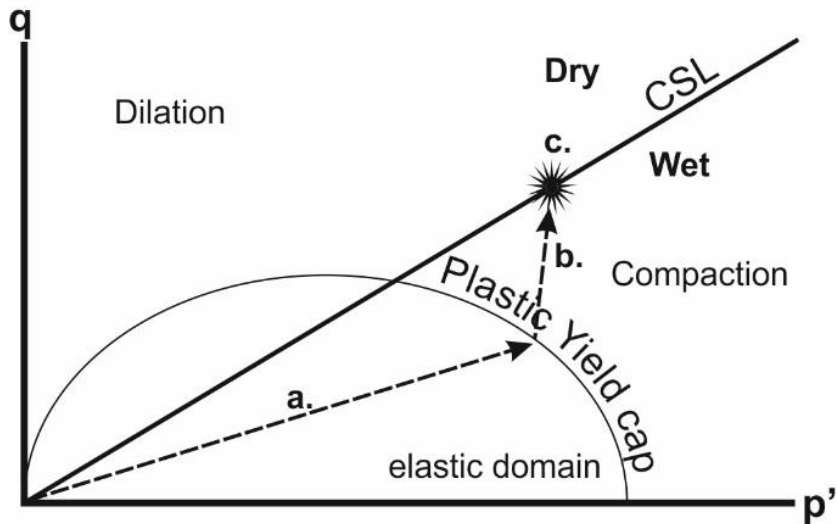
Following the work of Dehandschutter et al. (2005), Laurent et al. (2012) and Roberts (2014), and given the shallowly buried nature of some of the polygonal faults in the wedge, it is proposed here that the shallow polygonal faults seen in this survey formed due to the consolidation of clays along similar lines to the proposed the Cam-Clay model of Roberts (2014) and Laurent et al. (2012). The sediment hosting polygonal faults was, initially compacted along the K_0 line. Subsequent porosity collapse, the

oxidation of organic material and precipitation of early diagenetic cements perturbs the sediment stress pathway from K_0 towards the critical state line (CSL) (Fig. 5.18). The CSL defines a threshold where shearing can continue without changes in either stress or volume (Smith and Smith, 1998). Crucially, in the conceptual diagrams of Dehandschutter et al. (2005), Laurent et al. (2012) and Roberts (2014), show the intersection of the CSL by the suggested polygonal fault strain pathway occurs on the ‘wet’ side of the plot. The ‘wet’ side refers to the wettability of clay grains and the propensity for clays to retain small amounts of water around the clay grain. As pore throats collapse under normal consolidation, the volume (and hence water content) is reduced, with more water retained on the clay particles than in pore space and is hence, ‘wetter’ (Smith and Smith, 1998). The intersection of the CSL on the ‘wet’ side of the plot in deviatoric-mean stress space is important as the rheology of the clays promotes work hardening of the sediment and therefore increasingly brittle behaviour in the shear zone (Dehandschutter et al., 2005), (Fig. 5.18).

The discussion on shallow fault nucleation processes also highlights another important consideration for very young polygonal fault arrays with a geometric configuration, in that, with differential sedimentation across the study region, there is also a differential state of compaction between thick and thin ends of the tier.

This would result in fault trigger conditions at the thick end of the tier, where sedimentation rates are higher, evolving much more rapidly, by changing pore fluid pressure, pore structure and differential mass transfer compared with the thin end of the wedge where the sedimentation rates are low.

This could indicate that polygonal fault genesis could be triggered preferentially where sedimentation rate is greatest, and conditions necessary for polygonal fault growth are reached first. From the present day configuration, the trigger conditions necessary for polygonal fault formation are reached early within the first hundred metres of burial. However with a simple wedge shaped geometry some parts of the tier would reach these conditions earlier than others resulting in polygonal faults nucleating in thicker sections of the tier and progressively migrating (and younging) up-dip as different regions of a single reach the ‘trigger’ parameter (Goult, 2001).



*Isotropic volume reduction from Roberts (2014)

Figure 5.18: A schematic diagram of the Cam Clay model in deviatoric (q)-mean effective stress (p'), space, redrawn from Dehanschutter et al. (2005). The diagram summarises the stress pathway for polygonal fault (a) loading of sediments along the K_0 pathway, (b) loading towards the critical stress line (CSL) after the plastic limit is reached during the compaction and pore collapse of the sediment, (c) nucleation of polygonal faults.

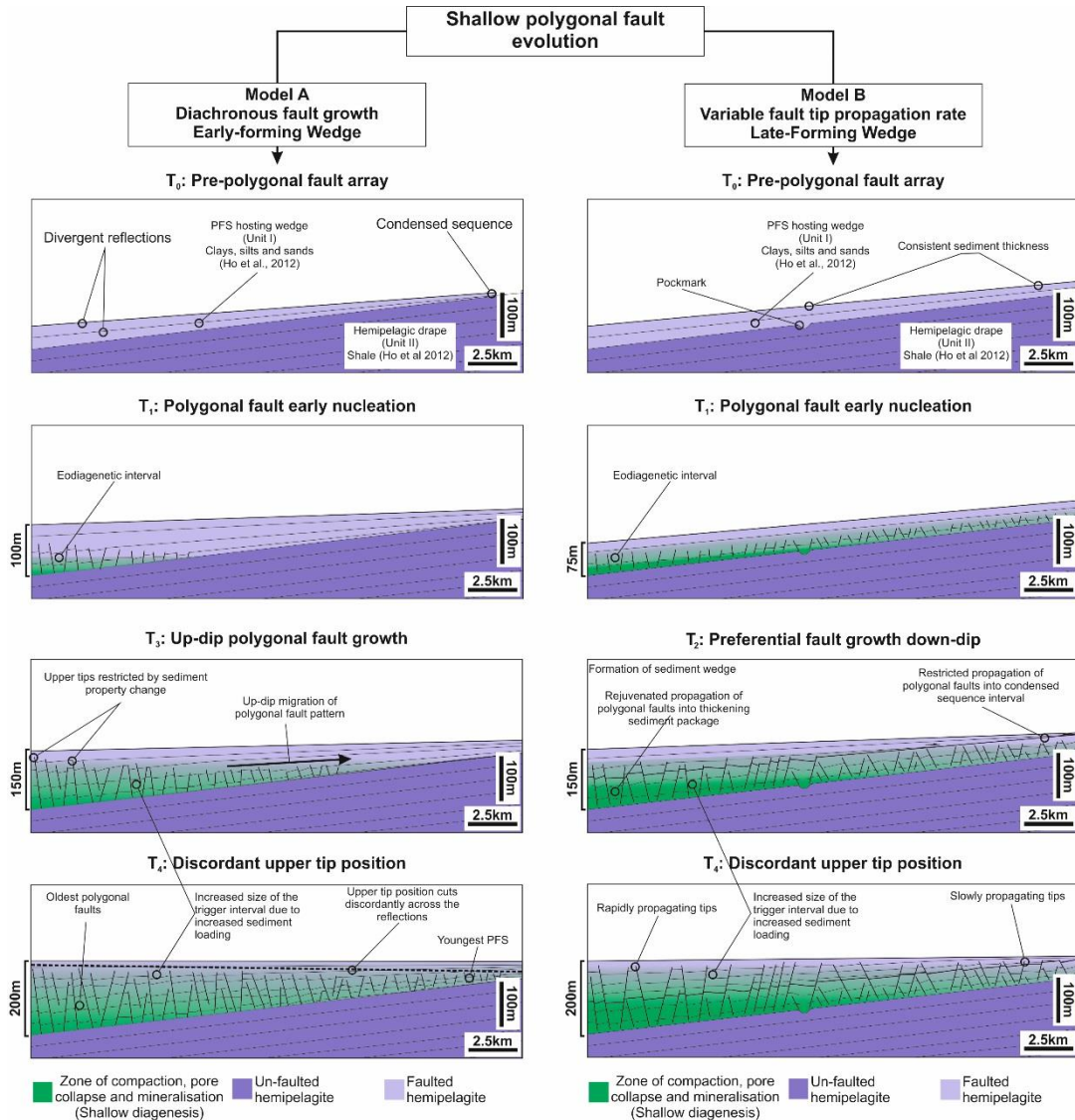


Figure 5.19: Schematic diagram showing two end member models of how differential sedimentation across a polygonal fault tier can influence polygonal fault tier evolution. **Model A:** Polygonal fault nucleation occurs first in the deepest sections of polygonal fault tier and gradually youngs up-dip as more of the tier reaches the 'trigger' parameter. **Model B:** Polygonal fault nucleation is synchronous across the area and later wedge formation creates differential loading across the area, allowing polygonal faults in the thickest sections of the tier to propagate and restricting polygonal fault tip propagation in condensed sequences

(Fig. 5.19, Model A). Alternatively, all faults in the tier could have nucleated at a similar time within a single sheet of sediment. A gradual shift in the sedimentary fill from sheet to wedge forces a shift in the locus of fault tip propagation towards the thickest sedimentary package (Fig. 5.19, Model B). Both Model A and Model B show the discordant upper tip position and the gradual increase in fault height through the tier, and achieve this through either different relative timings of fault nucleation or different rates of propagation. These two models are therefore considered to be end member models for creating polygonal faults in a wedge shaped geometry. Evidence for Model A may be seen on amplitude maps of the H5 reflection where there are LEAs locally constrained by polygonal fault hanging walls and by the stepping up of the basal tips immediately south of the salt diapir. The presence of LEA within the polygonal fault hanging walls would suggest that the faults were interacting with the seabed (Fig. 5.20). Similar sediment/polygonal fault interactions have been suggested where polygonal faults have constrained the margins of deep marine channels (Lonergan and Cartwright, 1999; Möller et al., 2004). It is not inconceivable that the area has active sedimentary processes (erosion, transport, deposition etc.) could be focussed in fault controlled/influenced lows. This would also suggest that polygonal faults within majority of the tier were not at the surface, whereas those immediately south of the salt diapir were (Fig. 5.20).

A case can also be made for wedge development through Model B, whereby the isochron maps for Unit 1A show a broadly sheet-like deposit in the interval between H1 and H2 and H4 to H5. Localised thickening in Interval 1A is attributed to a large fan (H2 to H4, see Fig. 5.5). As has been suggested in Chapter 4, polygonal fault growth was suggested to have initiated within the first 50m of burial, it seems probable that if polygonal faults can nucleate around the flanks of a pockmark in such shallow burial conditions, that other polygonal faults may also have nucleated and grown at the same time. This would indicate that sedimentary loading drives the variation in height and throw across the wedge. Where sedimentation rates are higher, polygonal faults can propagate more rapidly. This rapid propagation is driven by a combination of sediment loading and enhanced diagenesis, driven by increased burial. This drives tip propagation with fault branchlines competing for space to propagate. This results in localisation of stain onto specific faults, or sections of

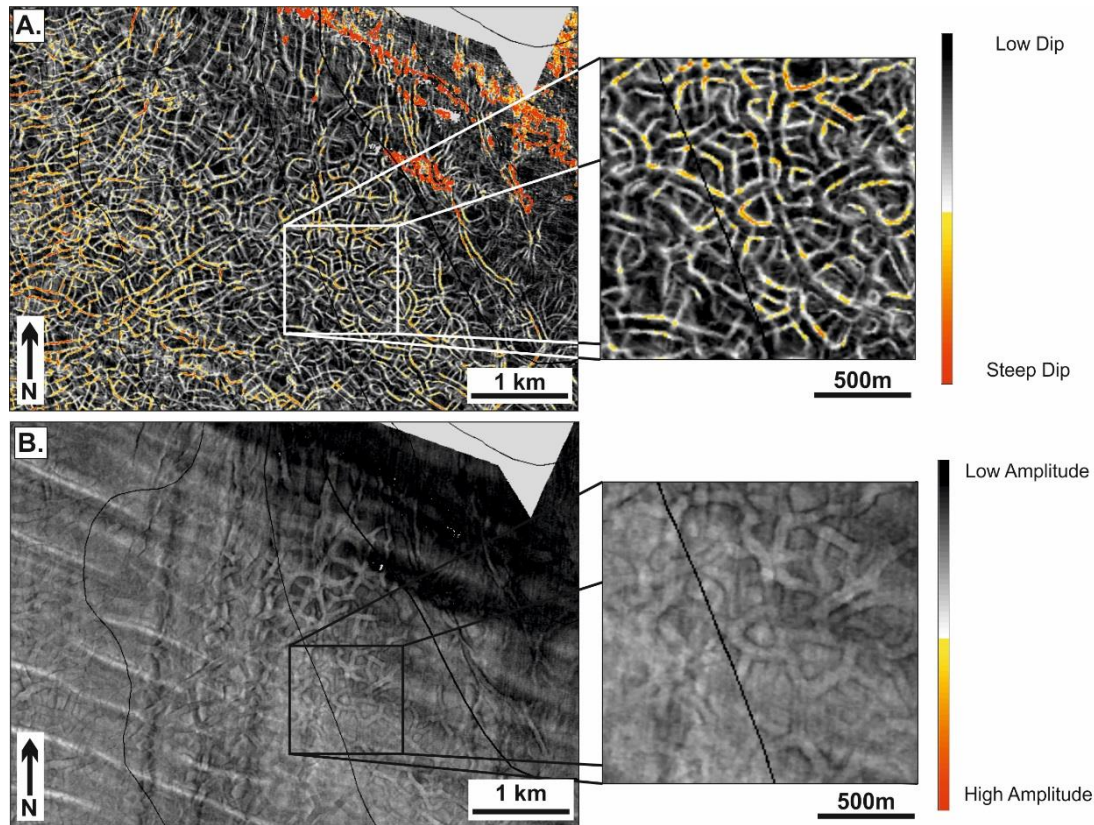


Figure 5.20: (A) Time dip map of the area immediately south of the salt diapir showing small-scale polygonal faults; (B) Amplitude attribute map of the same area showing LEAs. Note the precise match between the time dip fault trace map and the amplitude maps in the inset zoomed areas, interpreted here as evidence for localised syn-sedimentary fault growth in the region of the tier where sedimentation rates are extremely low

faults and creates the m-shaped t-z profiles, common in thicker ends of the wedge (Fig. 5.15, Fig. 5.16, Fig. 5.17).

5.4.2 Blind or syn-sedimentary growth in polygonal fault tiers?

Polygonal faults are classically seen as being excellent examples of blind faults, nucleating at depth, and then propagating radially from the nucleation site (Lonergan et al., 1998; Stuevold et al., 2003). Based on criterion set out in Baudon and Cartwright, (2008b), the steep plunge of upper tips, the presence of an upper tip propagation fold and the absence of syn-sedimentary faulting can be used to assess whether polygonal fault growth is blind or syn-sedimentary in this survey. Whilst the data presented here shows clear evidence for fault tip propagation folds (Fig. 5.9), the absence of syn-sedimentary faulting is more difficult to refute. The sedimentation rate in this survey is very low and so any fault that reaches the seabed would create a fault scarp into which sediment accumulates. The healing of this fault scarp is very dependent on sedimentation rate and sedimentation type where depositional systems can either drape or fill topographic lows (Castelltort et al., 2004a). Additionally, given that the sedimentation rate is very low, it is likely that any syn-sedimentary packages will be below the vertical resolution limit where different beds can be differentiated seismically as discrete reflections. Therefore, in the context of polygonal faults, a polygonal fault may show evidence of syn-sedimentary activity, but depending on the depositional setting and seismic resolution may never express the hanging wall thickening associated with growth strata. Possible evidence for blind growth may be evidenced by the LEAs, the majority of which, show no interaction with the underlying polygonal faults. However it should be noted that some polygonal faults in the shallowest section of the tier show evidence for syn-sedimentary behaviour. The LEAs demonstrate evidence of seismic facies change in the hanging wall, evidenced by increased amplitude responses.

Another difficulty in supporting syn-sedimentary growth for polygonal faults is the upper tip plunge. Whilst some faults show steeply plunging upper tips (Fig. 5.16A, Fig. 5.17B, C) akin to blind growth, others show very gently plunging upper tips (Fig. 5.16B, C, D, E, Fig. 5.17A, E), suggesting syn-sedimentary growth. It is interpreted here that the gently plunging upper tips are more likely to represent the effects of a mechanical boundary (*sensu* Rippon, 1984) just below the seabed, whereby the shear strength of the sediment is insufficient to sustain a shear offset.

As described in the previous chapter, polygonal fault nucleation is proposed to occur within the lower third of the fault tier based on the spatial relationship between residual topography from a buried pockmark and a perturbed polygonal fault pattern. Based on the presence of polygonal faults in shallow accumulations and the impact of differential compaction around pockmarks, there is evidence to suggest polygonal fault growth can be ‘early’, i.e. within 100 m or less of burial, in the context of this polygonal fault tier. Overall, the polygonal faults of this survey are proposed to be blind with no clear evidence for any faults reaching the seabed. The upper tip gradients in Fig. 5.10B are commonly <0.3 , a suggested cut-off for syn-sedimentary faulting (Baudon and Cartwright, 2008b; Stuevold et al., 2003). However, the narrow range of values, could also support the interpretation of mechanical restriction of upper tip propagation.

5.4.3 Kinematic evidence for polygonal fault propagation

Another aspect of polygonal fault growth would be how displacements accumulate on fault planes, in particular, whether throw and tip propagation occurs either radially (Barnett et al., 1987) from a fixed point, or asymmetrically, biased in one direction (Wilkins and Gross, 2002). In the previous chapter, polygonal fault tip propagation was suggested to be preferentially upwards, based on the spatial relationship between the presence of perturbed polygonal fault patterns and residual pockmark topography (see Chapter 4). This study offers additional evidence for an asymmetrical radial growth model. Fig. 5.7 shows polygonal faults at different wedge thicknesses and shows a progressive migration of upper tips as wedge thickness increases and gives clear kinematic indicators for the preferential upward propagation mechanism of polygonal faults. Additionally, this observation also demonstrates that polygonal fault nucleation position occurs in the lower third to lower quarter of this polygonal fault array.

There are salient differences between the polygonal faults in the thin and thick end of the wedge (see Fig. 5.15). The throw-depth ($t-z$) plots presented in Fig. 5.15, when placed together are proposed here to be an estimation of how displacement accumulated. Based on the data collected here polygonal fault growth is suggested to be initially radial with both upper and lower tips propagating (Fig. 5.21). As the basal tips encounter mechanical stratigraphy and become increasingly restricted, the locus of propagation shifts and becomes more asymmetrical with preferential upper tip

propagation. This may also be kinematically expressed in the upper tip geometries of the polygonal faults when viewed along strike. The upper tip geometry is not confined to a single horizon, nor are they the typically ellipses of Barnett et al. (1987). The upper tip geometry of individual polygonal faults shows sections where polygonal fault tips vary from gently to steeply plunging along its length. These effects are particularly pronounced at the thicker ends of the wedge where seemingly isolated sections of fault propagate upwards and form isolated displacement maxima with steeply plunging tips. This would indicate that fault tip propagation is not homogenous across the length of a polygonal fault and may be localised to sections of fault where there are a high number of branchline intersections that act as loci for preferential strain accumulation.

The distribution of throw maxima and minima in this survey are dependent on a combination of branchline linkage (Bürgmann et al., 1994; Willemse et al., 1996; Maerten et al., 1999; Gupta and Scholz, 2000) and sedimentation rate (Castelltort et al., 2004b). Where the sedimentation rate is exceptionally low, the interaction between throw accumulation and sedimentation rate becomes crucial. As indicated in Fig. 5.21, growth where sedimentation rates are lower result in more ‘c’ shaped plots as both upper and lower tips are restricted by the mechanical free surface and a basal unit respectively. In contrast where sedimentation rates are higher and the wedge is thicker, ‘m’ plots are more prevalent due to isolated sections of polygonal fault propagating to shallower depth. In this survey, the displacement maxima on a ‘c’ shaped displacement maxima on a branchline can force an ‘m’ shaped throw profile on a nearby branchline as displacement (and strain) is focused elsewhere with a block.

5.4.4 Polygonal fault organisation

Polygonal faults hosted within this wedge show some key early behaviours. From the displacement-length plots and 3D seismic attribute maps it is clear that polygonal fault linkage forms exceedingly early in the tier history, where polygonal faults show a high connectivity within the first 150 m of burial and the longest faults in the array share common hanging walls with intersecting branchlines, all of which can be observed in the first 150 m of burial. This would indicate that some polygonal fault lengths are fixed from a very early stage in their formation and that the network formation must occur soon after burial. It is also important to note that whilst polygonal fault heights crudely scale with tier thickness, variability in fault height also increases with depth

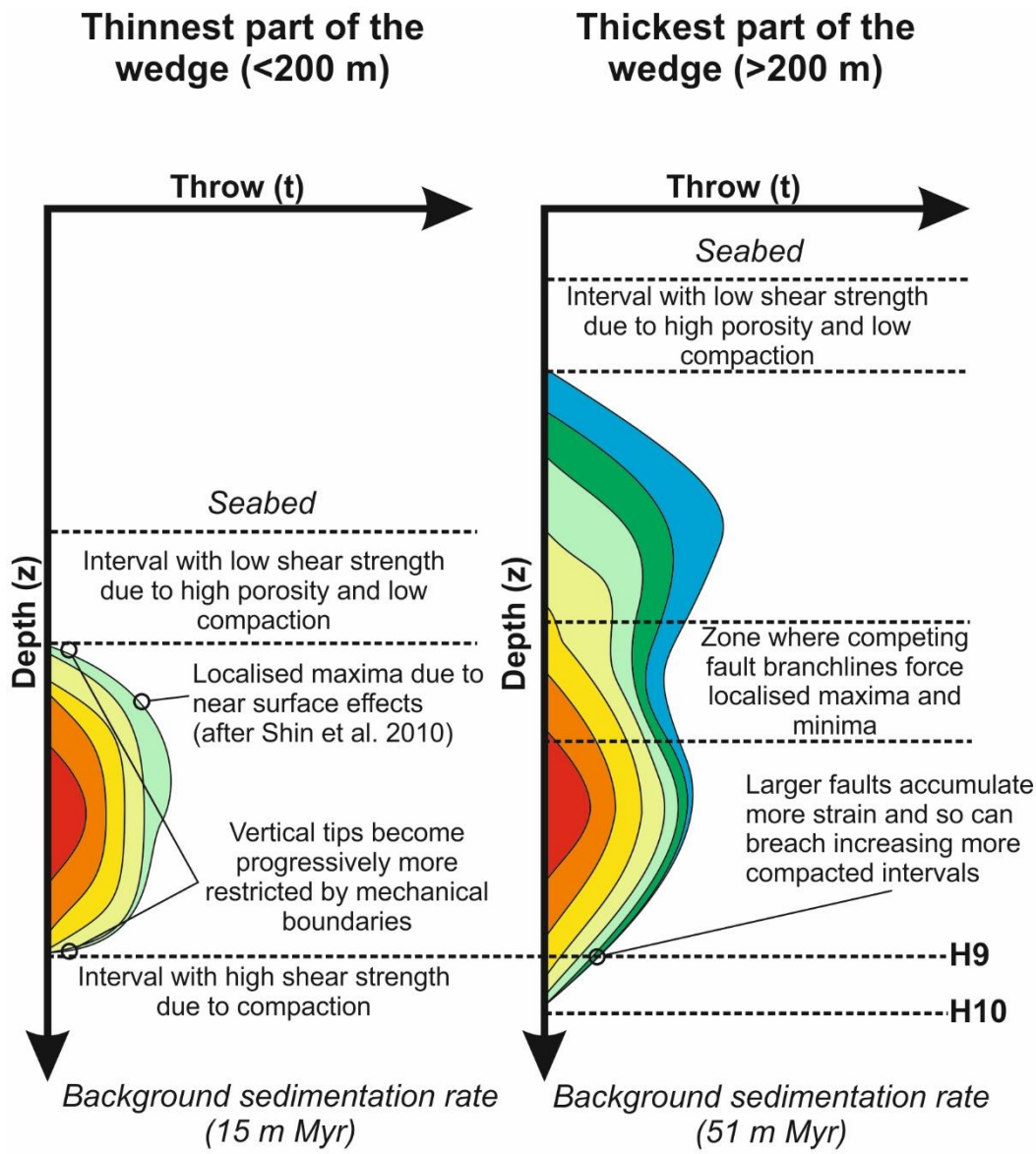


Figure 5.21: Schematic diagrams reconstructing the evolution of displacement on polygonal faults at thin and thick ends of the tier

(Fig. 5.8). This is attributed to polygonal fault organisation within the wedge. The range of polygonal fault heights found in the thicker (200–300 m) end of the wedge is attributed to early polygonal fault organisation where some faults have their upper tips restricted by larger and more dominant neighbouring faults. Many studies to date have observed faults of different scales within polygonal fault tiers (Cartwright, 2011; Laurent et al., 2012; Ostanin et al., 2012; Seebeck et al., 2015). Master faults, as described by Cartwright (2011) are the largest faults within a polygonal fault tier and define the upper and lower limits of a polygonal fault tier. The taller faults force abutment and upper tip restriction of smaller subordinate polygonal faults is inferred to be the early stages of fault organisation within the faulted interval. The tallest and longest faults within the thicker portions of the wedge are interpreted to be early master faults termed here as proto-master faults. Additionally, the larger fault that forces the abutment, the ‘blocking’ fault, and restricted fault do not come into contact, suggesting a soft linkage between the restricted fault tips and blocking fault hanging wall. Soft-linkage is proposed to be the result of a propagating fault tip interacting with a contractional stress field in the footwall of the blocking fault (Shin et al., 2010) that arrests growth.

5.4.5 Tier boundaries

The basal tip gradients for polygonal faults throughout the wedge are variable, ranging from 0.1 to 0.7 and average 0.28. The cause of these steep gradients could be due to mechanical restriction due to the presence of a ductile detachment at the base of the tier or an artefact of seismic resolution (Fig. 5.22).

Vertical polarity of ‘domino’ fault arrays has been previously suggested to be a proxy for the presence/absence of basal layer detachments (Stewart and Argent, 2000). The polygonal fault array studied here would indicate that there is a detachment as the majority of the largest faults dip landward, giving a synthetic sense of shear, relative to regional slope. However the nature of the detachment is much more difficult to elucidate. The polygonal fault dips are on average 50° with less than 1° perturbation in dip from top to base, resulting in straight to very gently curving faults in section (Fig. 5.9). Many studies on faults where there is flow at the basal tips, particularly in salt (Bally, 1988; Rowan et al., 1999) and shale sequences (Cohen and McClay, 1996; Morley, 2003; Sapin et al., 2012) show listric and low angle (25° to 35° dip) normal faults. The difference in fault geometry between other detachment style faults and the

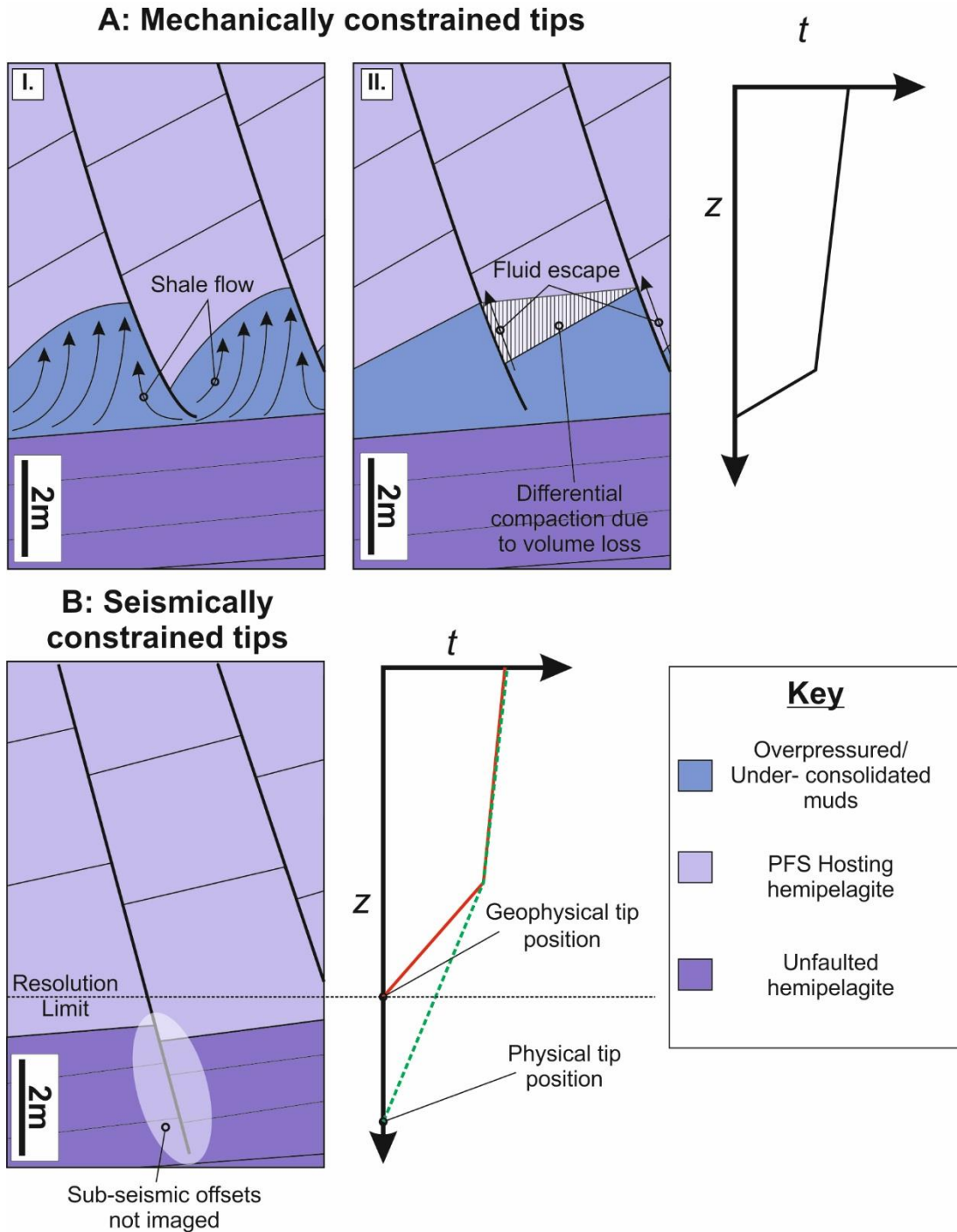


Figure 5.22: Schematic diagrams detailing the potential controls on basal tip configuration. (A) steep basal tip gradients are attributed to shale flow or fluid pumping (after Sibson, 2000) of overpressured horizons that would constitute mechanically constrained tips. (B) Alternatively basal tip gradients are steepened as a product of the resolution limit giving a false impression of a mechanical constrain on basal tip position.

Polygonal faults, coupled with the high resolution of the data must therefore suggest it is unlikely that there is ductile flow (*sensu stricto* salt and shale rollers) within a detachment at the base of this polygonal fault tier. Alternatively, volume loss could accommodate the rapid decrease in throw through differential compaction in the hanging wall of polygonal faults. A recent field study by Tewksbury et al., (2014) on polygonal faults in chalk, suggested an intimate link between fluid flow and polygonal faulting relating to overpressure. Tewksbury et al. (2014) report steeply dipping (80°) veins of calcite, with slickensides that are the expression of normal faults. Tewksbury et al. (2014) infer that Mohr Coulomb failure could not reproduce the dip angles expressed in the calcite veins. However the presence of veins would suggest fluid conduit and, isotopic data supports a synchronous timing between vein and fault formation. This leads the conclusion that the polygonal faults exposed in Egypt are influenced by high fluid pressures during burial.

Normal faults have been suggested to form dynamic fluid flow features (Sibson, 2000). Faults have been proposed to aid in the modulation of overpressures whereby fluid pressures increase shear stress on a fault plane. Where fluid pressures overcome regional states of stress and fault plane friction, can permit slip, releasing fluids (Sibson, 2000). Fluid flow along polygonal fault planes has been widely suggested from numerous studies. Overpressure has been attributed to three broad categories, increase in compressive stress, fluid volume change through diagenesis or hydrocarbon generation and fluid movement (Osborne and Swarbrick, 1997). In shallow (<500 m) burial conditions overpressure is unlikely to be caused by thermogenic expansion, diagenesis or hydrocarbon generation/cracking. Moreover, increasing compressive stress through disequilibrium compaction is more common in rapidly subsiding, thick shale sequences (Osborne and Swarbrick, 1997) and unlikely to apply to the tier studied here. An additional complexity to the basal tiers is the seismic resolution limit, despite the high resolution of the data (3 m vertical resolution and 6.25 m lateral resolution) it is conceivable that the true basal tip position extends beyond its current geophysical position and has a very different geometric configuration, resulting in a different basal tip gradient (Fig. 5.22).

The basal tier boundary represents the lowest limit of seismically resolvable offsets within the tier and is notable for having a variable stratigraphic position. In the north the basal boundary is at the H9 reflection whereas to the south of the survey the basal

tier boundary lies below H10. Moreover, the basal tips within the polygonal faults are spread across several reflection cycles between H10 and H9 and the spread of basal tip gradients indicate that there is no single mechanical unit that restricts basal tip propagation. It is suggested here that the basal tips gradually die out downwards and into the un-faulted hemipelagic unit. This is likely to be aided in part by the bright medium to high amplitude reflection between H9 and H10 that is interpreted here as a potential indicator of changing mechanical properties such as compaction within the un-faulted hemipelagite. Therefore, the basal tip gradients whilst they indicate a bulk mechanical change, by a changing gradient, they are also likely to be skewed (steepened) by the seismic resolution cut-off.

The cumulative throw values for both c and m-type throw distributions show linear to smooth curves with no steps in throw plots that could indicate evidence for reactivation of faults at the H5 reflection (Fig. 5.16, Fig. 5.17) (Childs et al., 2003; Omosanya and Alves, 2014). Therefore the m-type distributions are not the product of reactivation (*sensu* Baudon and Cartwright, 2008a) but are likely to be the product of throw perturbation from nearby branchline intersection (Bürgmann et al., 1994; Gupta and Scholz, 2000; Maerten et al., 1999; Willemse et al., 1996). The propagation of polygonal faults in the thicker sections of the tier are undergoing constant blind growth with no interruptions or breaks in fault activity. As with basal tips, it is necessary to consider that the true upper tip position is not fully imaged and may extend several metres to tens of metres closer to modern day seabed than is currently imaged.

5.5 Conclusions

This study provides a unique opportunity to examine polygonal fault growth and early fault organisation as faults undergo increasing degrees of burial.

Polygonal faults in the thinnest sections of the tier show high degrees of connectivity and indicating that polygonal faults rapidly form complex and highly connected arrays. Moreover as the polygonal fault array becomes buried, polygonal faults begin to organise and form early stage organisational hierarchies. These organisational hierarchies arise as propagating fault tips interact and abut. Some faults are able to grow to the full height of the tier and are termed proto-master faults

This study also suggests that the spatial evolution of polygonal faults could be strongly influenced by the geometric configuration of the sediment package in which the

Polygonal faults are hosted. In this instance, within the wedge shaped tier, the oldest polygonal faults are found in the thickest sections of the tier and progressively young up-dip.

In summary, constraining when and where polygonal fault evolution occurs is potentially of vital importance to hydrocarbon exploration in examining the timing of fluid pathways, seal integrity and reservoir compartmentalisation. Although understanding the mechanism that forms the array still remains elusive, understanding the evolutionary process within the first 300 m of burial gives important clues to the elusive and controversial matter of polygonal fault genesis.

6 The origin of radial polygonal faults around hydrothermal vent complexes

Abstract:

Hydrothermal vent complexes (HTVC) are mounded structures that occur on the modern and palaeo-seabed in several basins across the globe. Previously studied interactions between HTVCs and polygonal faults have noted radial fault patterns in the immediate vicinity of the HTVC. These perturbed patterns have been attributed to a synchronous timing between the formation of both mounds and fault array. This chapter examines well-imaged, 3D seismic data from the Norwegian Margin to investigate and define the controls on the formation of radial faults, as seen around HTVCs associated with a single sill. This survey uses qualitative and quantitative analyses to assess the interaction and relationship between the dimensions of HTVCs and the dimensions of radially aligned faults. The results of this study reveal that the radial fault patterns in this survey form in response to differential compaction of the vent fill. This raises an alternative view on the implications of these features in using the perturbed nature of the radial faults to constrain timing of a polygonal fault array. This study suggests that the formation of a perturbed pattern could form much later due to compaction after (>200 m) burial as opposed to an indicator of early/synchronous timing between venting and fault formation.

6.1 Introduction

Hydrothermal vent complexes (HTVC's) are mounds that form in close association with an underlying igneous body, typically a sill or sill complex (Jamtveit et al., 2004; Magee et al., 2014; Planke et al., 2005; Svensen et al., 2006). The composition of hydrothermal mounds have been described in a number of field examples and in seismic datasets. In both field and seismic studies there are well documented examples of magmatic (Davies et al., 2002; Grove, 2012; Hansen, 2006) and amagmatic (Hansen et al., 2005; Rollet et al., 2012) material present in the mounded structures. From a seismic perspective the difficulties in constraining the internal fill of the vents is further compounded by the difficulty in imaging these mounds. Seismic imaging often proves problematic and requires mounds to be at a shallow depth with sufficient acoustic contrast present between mound and surrounding lithology to generate a reflection (Jackson, 2012). This often means that the internal geometry of the mounds is obscured or poorly imaged.

In contrast radial faults are almost ubiquitous where an intrusion of material causes a doming of its overburden, with radial patterns observed around salt diapirs (Carruthers et al., 2013; Davison et al., 2000; Rowan et al., 1999; Stewart, 2006), igneous intrusions (Hansen and Cartwright, 2006; Ode, 1957; Squyres et al., 1992) as well as around HTVCs (Hansen et al., 2005). Hansen et al. (2005) suggested a possible interpretation whereby the radial patterns around the vents imaged on the Gjallar ridge formed in response to a synchronous timing between vent formation and fault nucleation. In addition a review by Cartwright, (2011) suggested that features at the base of the tier, as proposed by Hansen et al. (2005) could be used to reconcile the nucleation position of a polygonal fault tier and hence, reconstruct the nucleation position. This would suggest that the original interpretation of Hansen et al. (2005) is important to assessing polygonal fault growth for the Gjallar ridge, as described in Chapter 1 of this thesis. In more general terms of understanding horizontal stress anisotropy, radial patterns around intrusive features such as salt domes have been the subject of much discussion and explanation, the mechanism that forms radially aligned faults around HTVCs has yet to be fully discussed or explained and neither have the implications for radial fault formation been explored.

This chapter aims to examine the formation of radially aligned faults above HTVC's add new insights into the internal reflection characteristics of HTVC's, using well

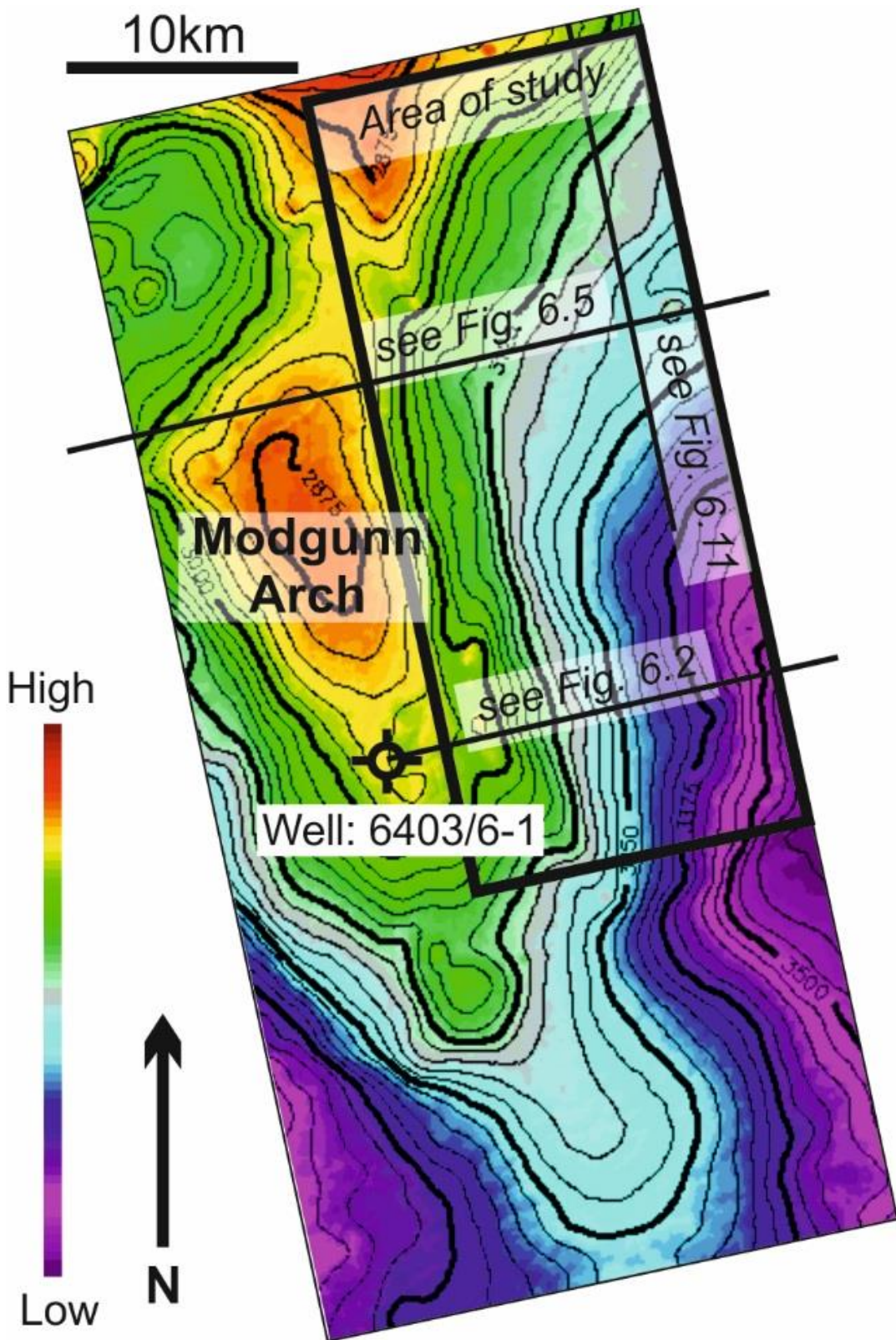


Figure 6.1: Shaded Contour TWTT relief map of Tier base horizon (TBH, see Fig. 6.5) detailing the Modgunn arch and the area of study discussed in this chapter

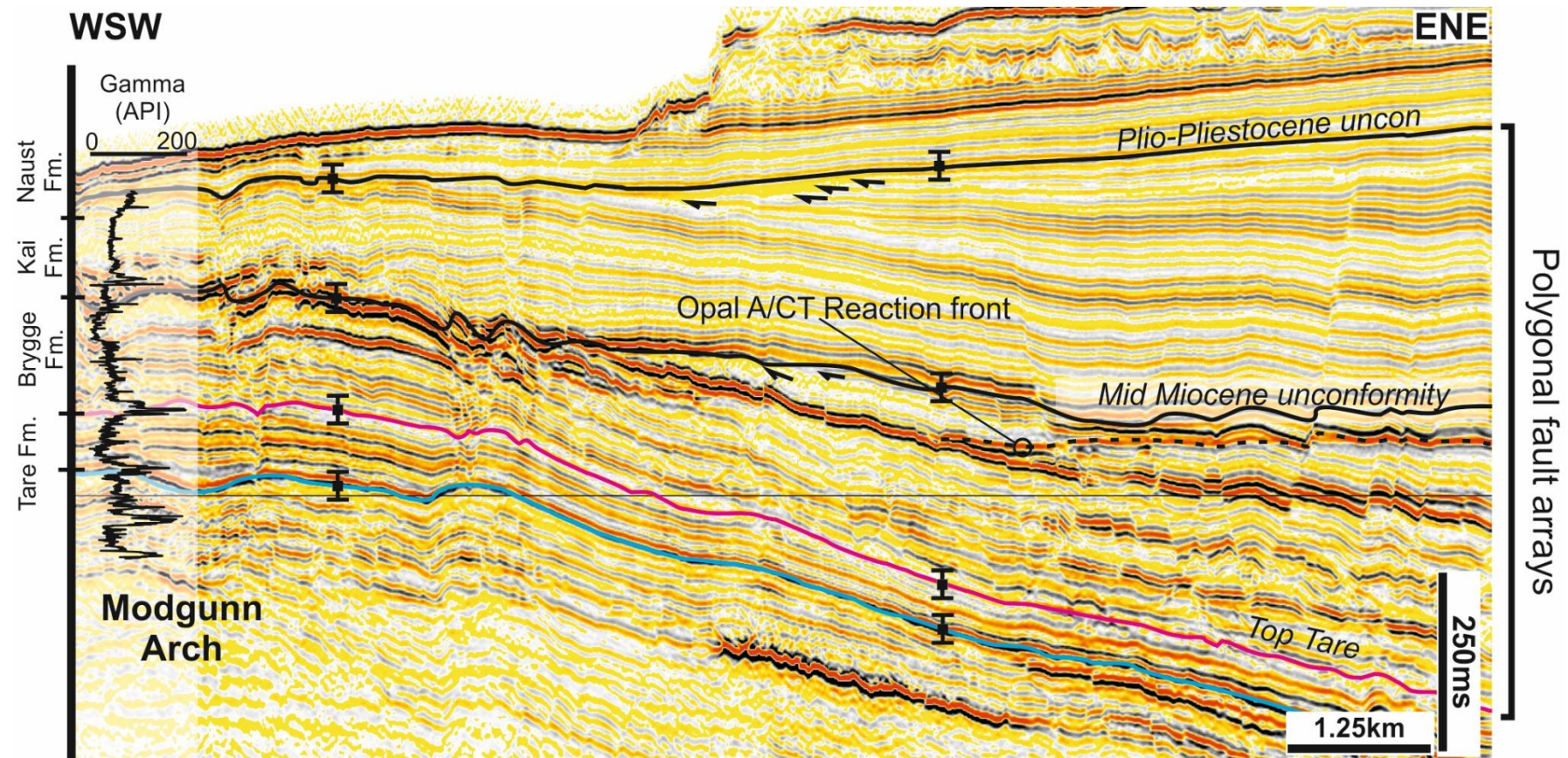


Figure 6.2: Calibrated seismic line with well tie showing the major formations and key horizons discussed in the chapter. For more information on lithology see Chapter 7

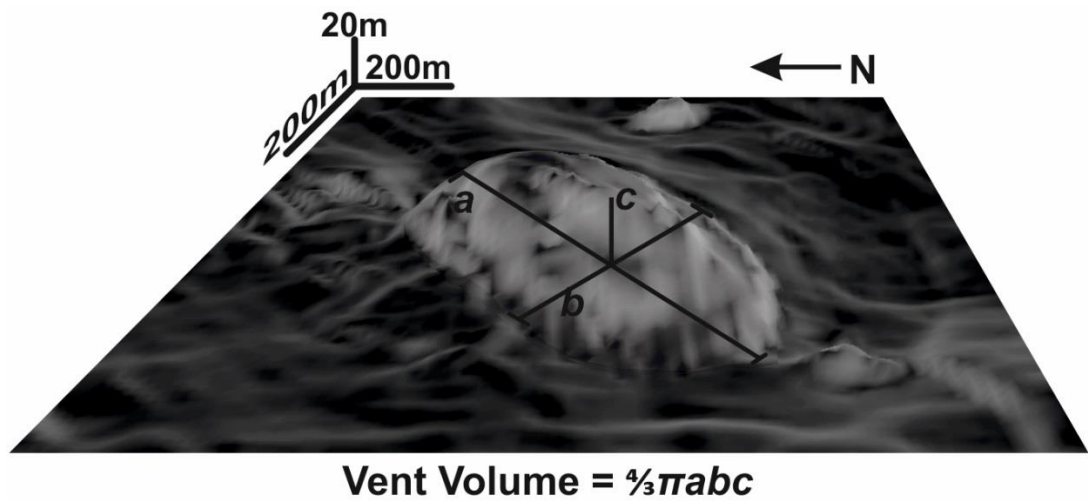


Figure 6.3: A 3D view of Vent 6 (see Fig. 6.6 for vent location) defining the principle axis used to measure vent volume

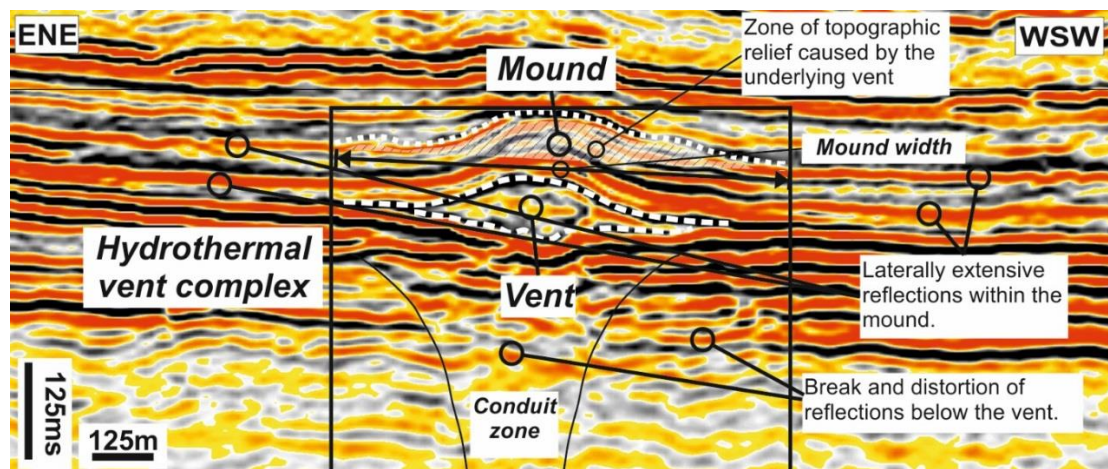


Figure 6.4: Seismic cross section across a HTVC (Line of section same as Fig. 6.10a) defining the key features and position of mound, vent and hydrothermal complex

processed 3D seismic data from the Modgunn Arch on the Norwegian margin. The study focusses on 19 HTVC's that underlie an Eocene - Pliocene age polygonal fault system. The HTVCs with their associated radial fault array are located at the base of a polygonal fault tier, thus enabling the interrogation of interpretation supplied by Hansen et al. (2005), whilst being able to examine the implications for constraining polygonal fault growth.

6.2 Results: Radial faults around HTVC's

The Upper Cretaceous package contains a number of bright locally enhanced reflections that mute and dim underlying reflections. Whilst high amplitude, positive reflections are common throughout the Upper Cretaceous, one is the most laterally extensive (Bright reflection 1, BR1) underlies the polygonal fault tier 1 on the eastern side of the Modgunn Arch, covering an area of ca. 630 Km². The geometry of this large enhanced reflection is variable, the eastern edge of the survey shows the enhanced reflection to lie broadly concordant with the surrounding horizontal reflection. However on the western and southern edges, the reflection turns upward dipping approximately 45° to lie discordant to surrounding horizontal reflections (Fig. 6.5, Fig. 6.7 & Fig. 6.6). This gives BR1 a convex down profile. In addition to the locally enhanced reflection, at the base of the polygonal fault tier 1, a number of structures are associated with the upturned tips of BR1. There are 27 mounded structures that are distributed over the area underlain by BR1. A gentle fold can also be seen across the region that coincides with the upturned tips of BR1.

6.2.1 Interpretation of BR1

The large convex down reflection displays some key and diagnostic features. The dimming of reflections beneath the reflection suggests a strong acoustic contrast between BR1 and the surrounding rock type. The strong acoustic contrast, the convex down geometry and association with mounded structures on the margins of BR1, all suggest that the lithology of BR1 is intrusive and is likely to be igneous in origin. (Fig. 6.7, Fig. 6.6 & Fig. 6.9). The geometry of BR1 is similar to widely reported saucer-shaped sills from field and seismic data (Polteau et al., 2008). Furthermore saucer-shaped sills have been widely reported from the NE Atlantic margin from Rockall trough (Hansen, 2006; Magee et al., 2014), Faeroe-Shetland platform (Hansen et al., 2004; White et al., 2003), Møre Basin (Hansen and Cartwright, 2006; Planke et al., 2005, Miles and Cartwright, 2010) and indeed, across the Vøring Basin

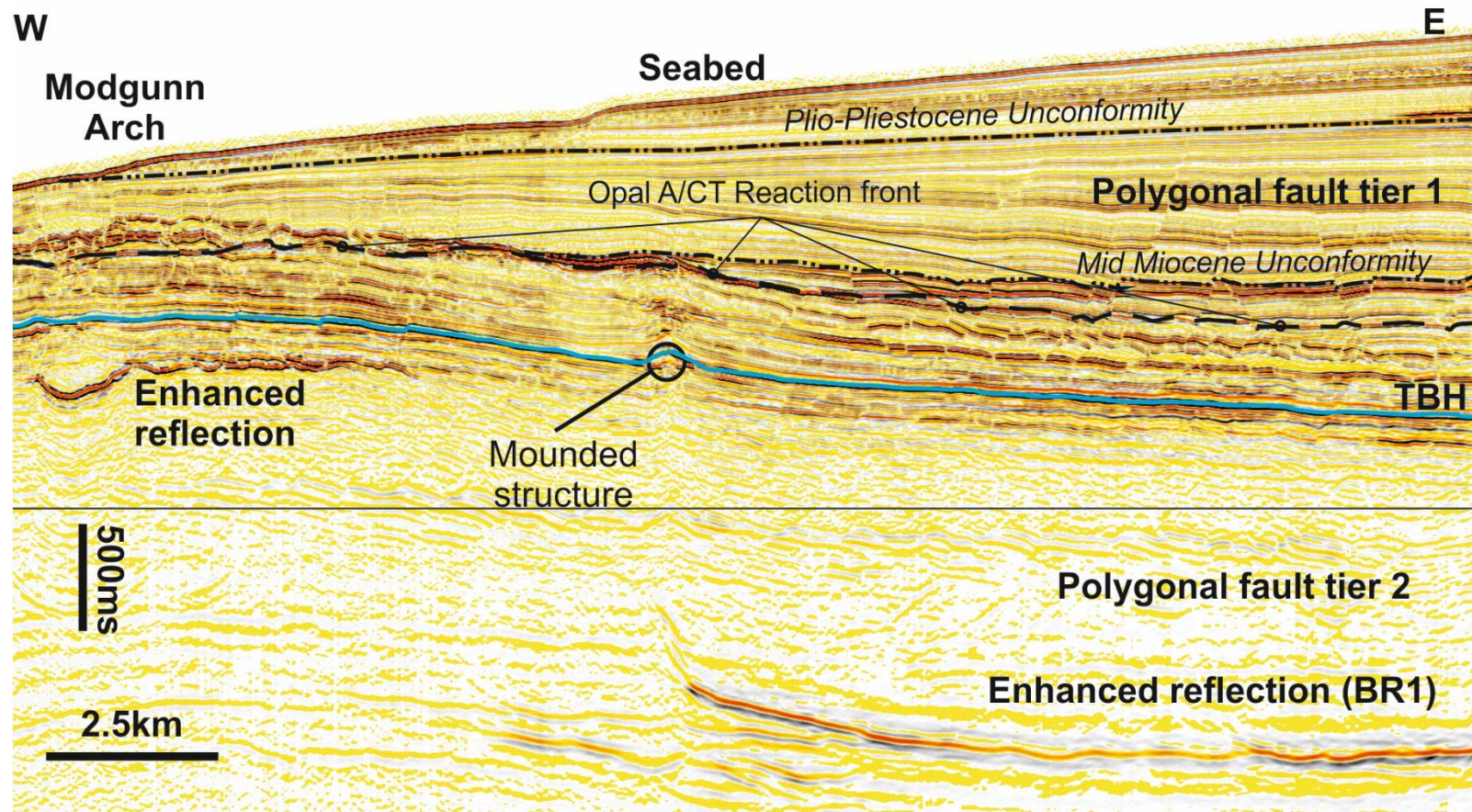


Figure 6.5: Regional cross section showing key features of the survey area

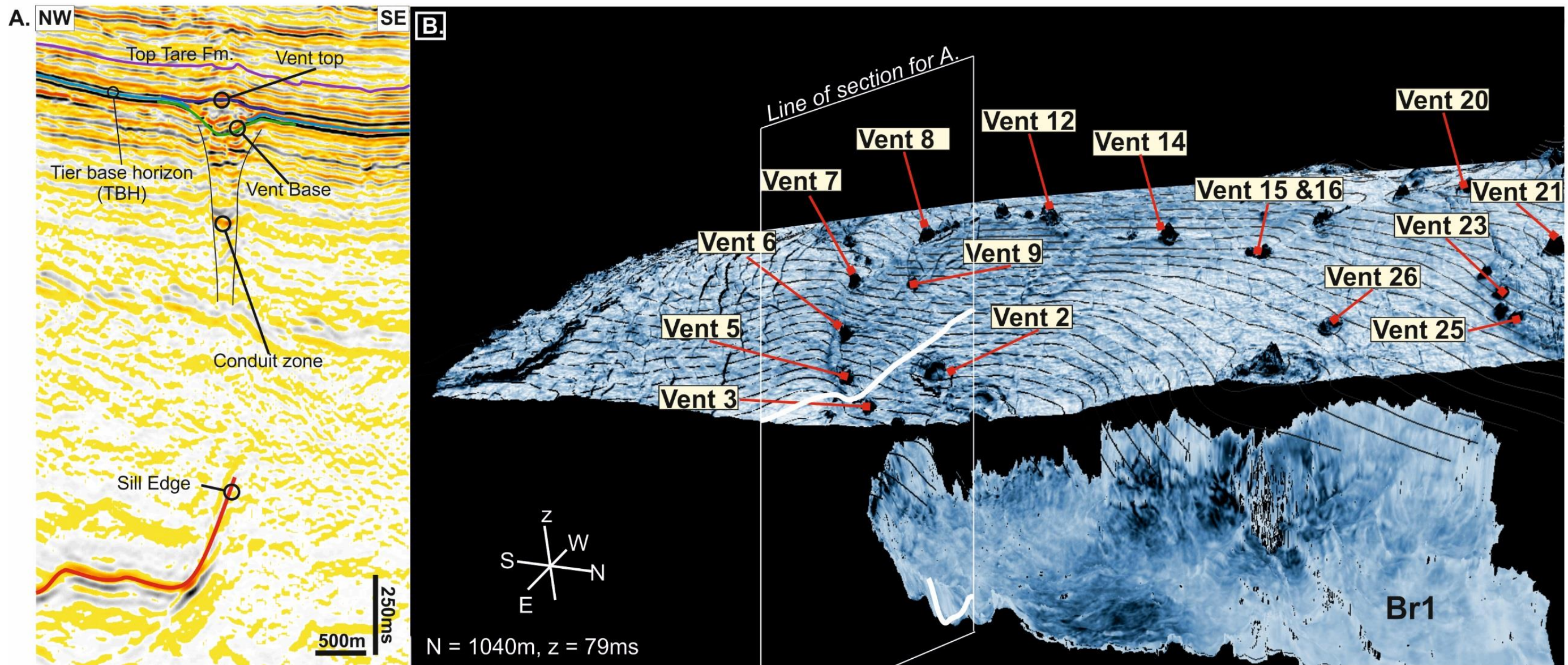


Figure 6.6: (A) Seismic cross section showing key features of the hydrothermal vent complexes including key seismic horizons and the association between sill and vents (B) 3D amplitude map showing the vents and the underlying sill (Br1).

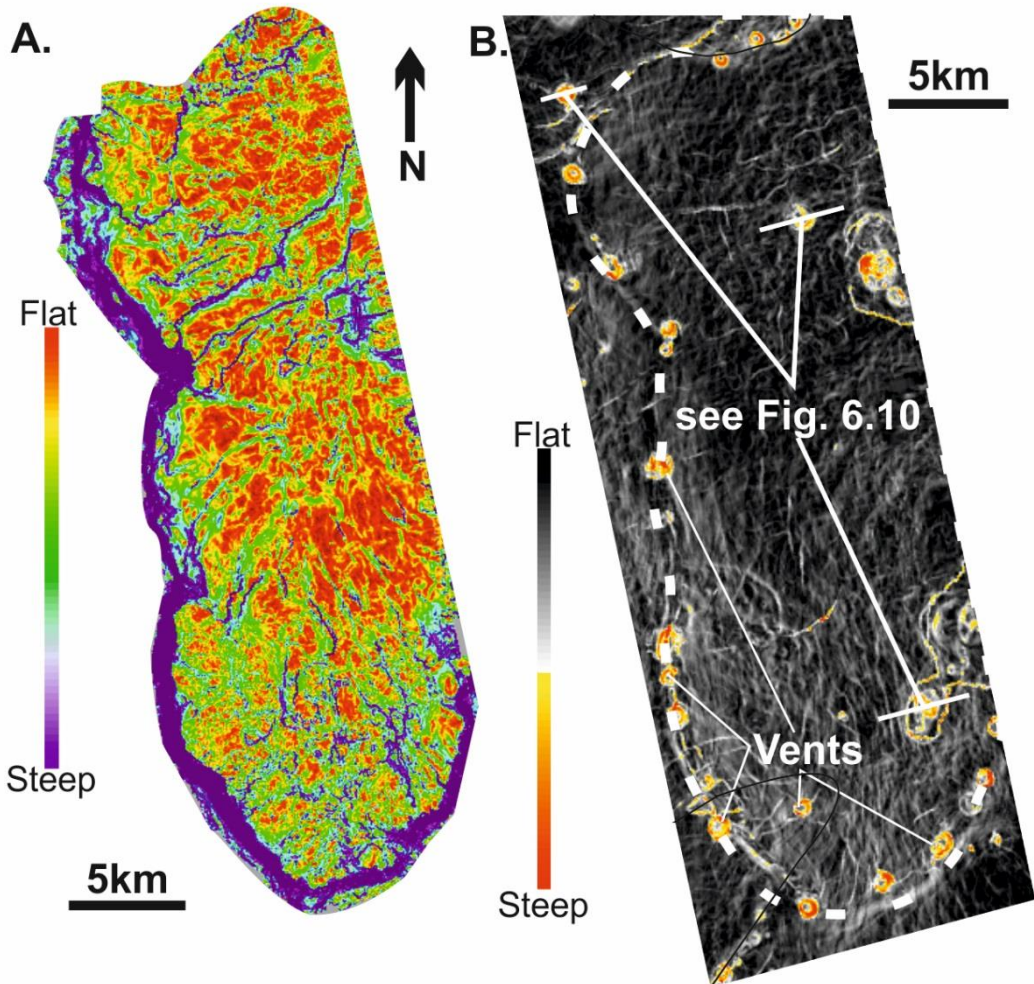


Figure 6.7: A) Time dip map of reflection BRI showing the geometry and upturn edges (in purple), (B) Time dip map of TBH (Tier base horizon) showing circular to quasi circular dip anomalies, interpreted as hydrothermal mounds (see text)

(Brekke, 2000; Brekke et al., 1999). Gentle folding described where the upper tips of BR1 lie are reminiscent of the forced folds widely described where sills are observed (Hansen and Cartwright, 2006; Magee et al., 2014; Smallwood and Maresh, 2002; Trude et al., 2003) and suggest that BR1 has forced a volume change, resulting in intrusion related uplift. In some instances, onlap of this uplifted surface can be observed and enables the dating of sills (Trude et al., 2003). Although there are other intrusive features, such as sandstone sills and injectites (Cartwright et al., 2007), that could generate similar acoustic responses and forced folding, the large lateral extent of BR1 and the presence of mounds would favour an igneous intrusion.

6.2.2 Morphology of the mounded structures on the tier base horizon

The mounded structures observed along Tier base horizon (TBH) display a wide range of geometries in section and in plan view. The mounds are seen in close association with the underlying saucer shaped sill and are interpreted here to be hydrothermal vent complexes (HTVC). HTVC's are widely observed across the globe in close association with sills, including nearby examples from the Norwegian Margin (Dumke et al., 2014; Planke et al., 2005; Svensen et al., 2003), Faeroe – Shetland basin (Davies et al 2002, Hansen, 2006, Grove, 2013), NE Rockall trough (Hansen, 2006, Magee et al 2014) as well as examples from offshore China (Zhao et al., 2014), Offshore Australia (Jackson, 2012; Rollet et al., 2012) and onshore in the Karoo Basin, South Africa (Svensen et al., 2006).

6.2.2.1 HTVC geometry

In plan-view, the HTVCs and associated mounds are quasi circular to elongated ellipses in shape and are of varying sizes ranging from 258 m to 1400 m in width and between 33 m and 138 m relief (Fig. 6.8). The vent spacing is variable with some HTVCs occurring in relative isolation and others occurring in localised pairs or trios (Fig. 6.9). In section, the mounded structures are shallowly dipping convex up highs. The HTVCs vent base is a high amplitude, negative reflection that can be consistently mapped across the base of the mound. The geometries of this reflection are variable and can be smooth or have topography. They can also show evidence for erosional truncation in the reflections underlying the mound base, or concordance with surrounding reflections. Mound top is the first negative reflection that shows evidence for onlap or erosional truncation of an underlying reflection. The HTVCs have a two-

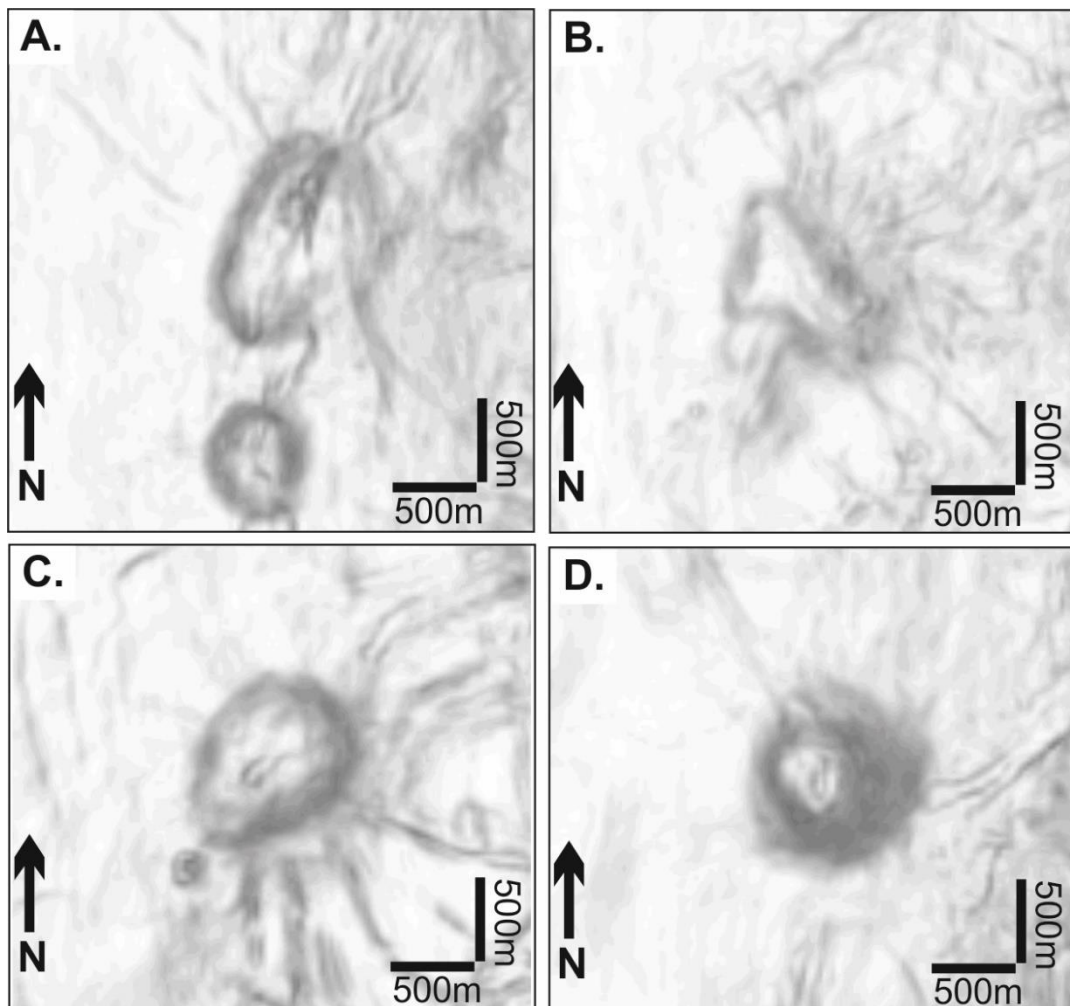


Figure 6.8: Coherence slices through a selection of vents showing the range of observed morphologies for the vents including; (A) Elongate, (B) Irregular, (C) Ellipsoid, (D) Circular.

layer stratigraphy consisting of the mound formed by reflections draping the vent from the Tare Formation and the vent fill which lies between vent top and vent base.

Relative timings between individual HTVCs are deduced from the position of the vent top horizon relative to a reference horizon. In this instance, the reference horizon is the TBH horizon (Tier Base horizon), generally the vent top horizon is one or two reflection cycles above or below TBH suggesting a broadly synchronous timing for vent emplacement. This observation is true for isolated and clustered HTVCs around the circumference of BR1.

The vent tops are hosted within the Tare Formation, and the vent base locally truncates the base Tare (which corresponds to the Tier base horizon). The Tare Formation shows evidence for thinning over the HTVCs. Drape geometries are common in the Tare Formation and are found immediately above the vent top horizon and cover one to two reflection cycles. Onlaps and the healing of mound topography occurs in the Brygge Formation, with onlapping reflections observed either terminating on the top Tare Formation reflection or within the first 3 reflection cycles above the top Tare horizon. Typically, onlaps for all 28 HTVCs are found within the first five reflection cycles within above or below the Top Tare horizon (Fig. 6.9).

6.2.2.2 *Reflection types*

Internal characteristics are described as seismically expressed features that are found between vent top and vent base (Fig. 6.10). Within the survey, three distinct internal reflection geometries were identified, strongly layered, weakly layered and transparent. Strongly layered vents (see Fig. 6.10a) display convex up, coherent, parallel reflections that downlap against mound base. These HTVCs are found exclusively on the margins of BR1. Strongly layered internal reflections are also relatively common, with half of the HTVCs (9 of 19) displaying internal layering. Weakly layered vents display laterally discontinuous reflections typically covering 5 or more traces. Transparent vents are very low amplitude, negative reflections that appear in seismic to be ‘transparent’ (i.e. no obvious internal reflections). These HTVCs are the largest seen in the survey and are typically found in the centre of the large enhanced reflection. Transparent HTVCs show no seismically resolvable radial patterns in either seismic attribute maps or flattened coherence slices. Transparent

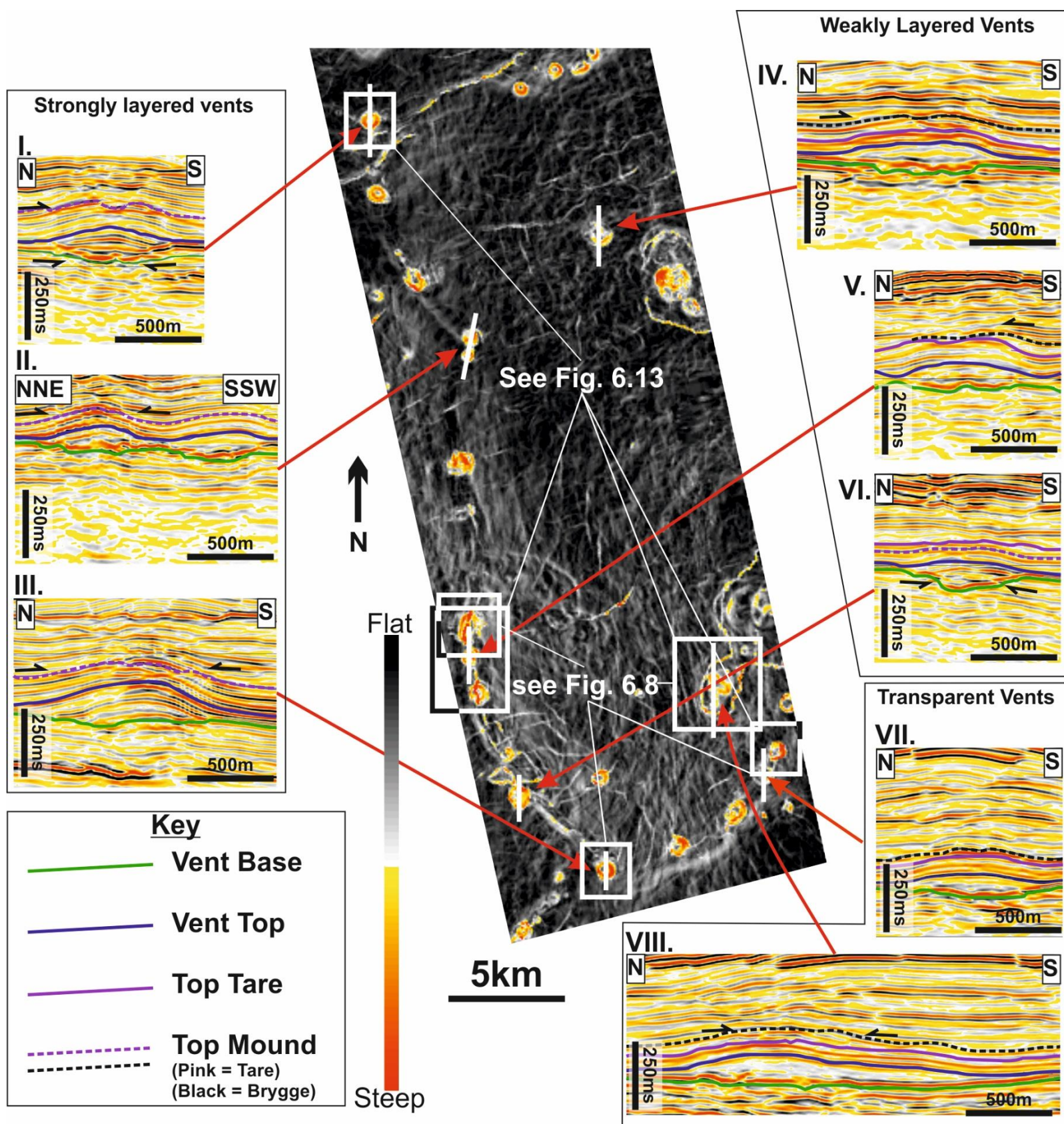


Figure 6.9: Close up of the time dip map of TBH with seismic cross sections across a number of vents showing the variation in HTVC geometries. Vent base horizon can be concordant (III, VIII) or show erosional truncation (I, IV & VI). The position of mound top is variable and can onlap within the Brygge Fm. (IV, V, VII & VIII.) or within the Tare Fm. (I, II, VI). Some mounds show no clear evidence for onlap at all (VI & VII).

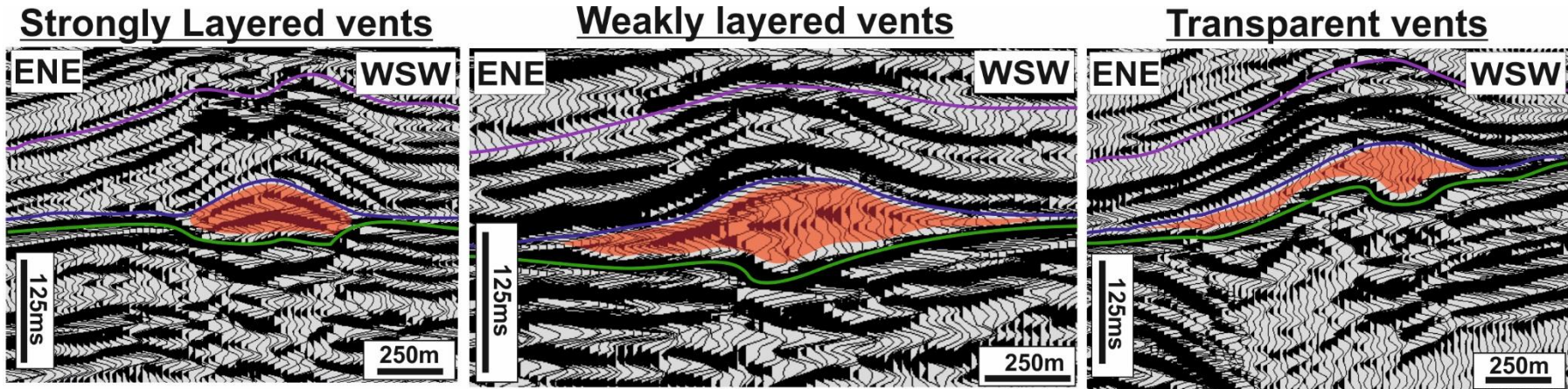


Figure 6.10: Seismic sections with enhanced gain displaying the three types of vent internal reflection. Mound top (Purple), Vent top (Blue), Vent base (Green)

vents are the least frequently observed with only 3 of the 19 mounds displaying internal ‘transparency’.

6.2.3 Impact of the HTVCs on nearby faults

In addition to the network of sills and hydrothermal vents, the Modgunn Arch hosts two polygonal fault arrays, one array within the Cretaceous (Polygonal fault tier 2, PFS2) and another in the Oligo-Miocene (Polygonal fault tier 1, PFS1). The HTVCs are found within the base of PFS1 and the interaction between HTVCs and faults within PFS1 are described further.

6.2.3.1 Polygonal faults and HTVCs

PFS1 is a single polygonal fault tier and is divided into two faulted intervals. A thin interval ca. 100m thick at the very base of tier (Interval B), is contained within the base of the Brygge Formation (Fig. 6.11). Another thicker interval up to 1km thick (Interval A), is found in both the Brygge and Kai Formations. Both intervals show fault sets with distinct upper tip positions at different stratigraphic levels, whilst remaining relatively interconnected, with many faults from interval A breaching both intervals (see x, Fig. 6.11). This would indicate that there are individual subsets of faults within a single polygonal fault tier. Average displacement/height ratio for interval B is 0.15, whereas interval A the displacement/height ratio is a third of an order of magnitude smaller at 0.05 (Fig. 6.12). The displacement-length ratios for faults in both interval A and B show that both populations have a similar scaling range. Polygonal faults in interval B show linear to curvilinear traces up to 1km in length and high displacements of 20 m. Intersections are common and varied, ranging from relay style tip overlaps to orthogonal intersections between fault branchlines. Despite the high numbers of faults present, the majority of faults in this interval have offsets that are at the seismic resolution limit of imaging (4 ms).

Each mound has a distinct fault pattern associated with it. These patterns occur at the base of the Brygge Formation fault patterns in the immediate vicinity (within 2km or less) show a sympathetic alignment to the flanks of the mounds with a zone of faulting striking downslope (Fig. 6.11, Fig. 6.13). This alignment of the faults gives a radial planform pattern. The width of radial patterns varies significantly with some radial fault lengths asymmetrically distributed (See Fig. 6.13B) whilst others are

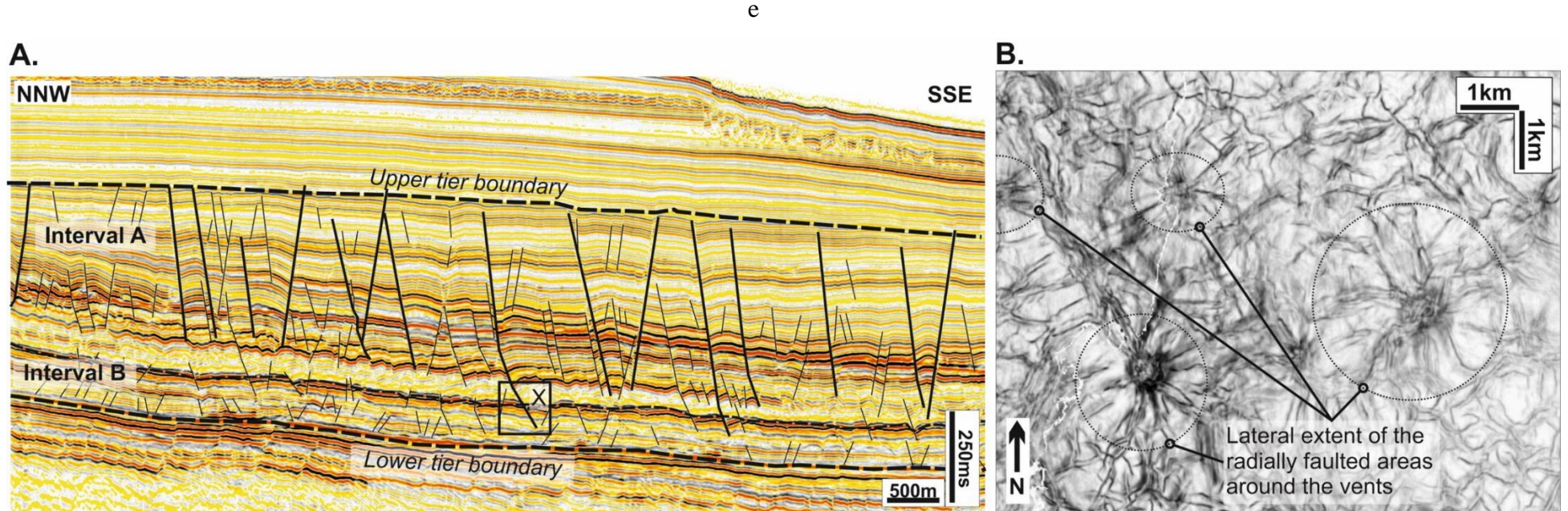


Figure 6.11: (A) Seismic cross-section detailing the fault architecture of Tier 1. Tier 1 is divided into two intervals (Interval A and B) based on the change in scaling between the two intervals in displacement-height space (see Figure 6.12). Faults in bold are the Master faults (*sensu* Cartwright, 2011) and are the largest faults in terms of height, length and displacement. The Lower tier boundary is defined by the Top Tara reflection and the upper tier boundary is near the Plio-Pleistocene unconformity. Note that the boundaries are not strict as some master faults have lower tips that tip out in Interval B (see X) (B) A flattened coherence slice, 100ms above the top Tara reflection that displays the strongly polarised (radial) fault orientations in the vicinity of the mounds and the 'background' polygonal fault pattern.

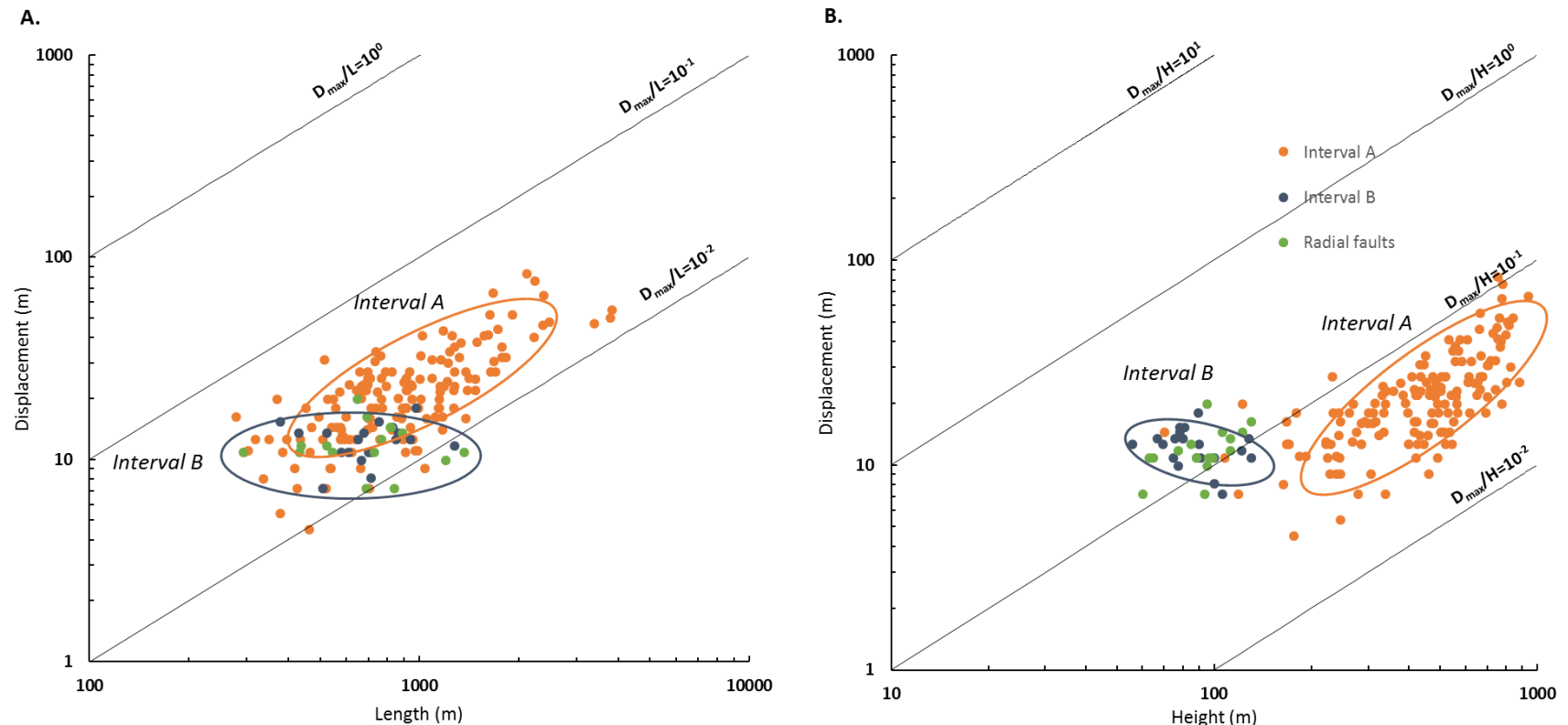


Figure 6.12: (A) Log-Log plot of Displacement length for faults in Interval A, B and radial faults (B) Log-Log plot of displacement height for faults in interval A, B and radial faults. Note the change in displacement height relationship between the radial faults and faults in interval B and the faults in interval A. Note the low numbers of faults measured in Interval B is due many faults having displacement at or below resolution limit

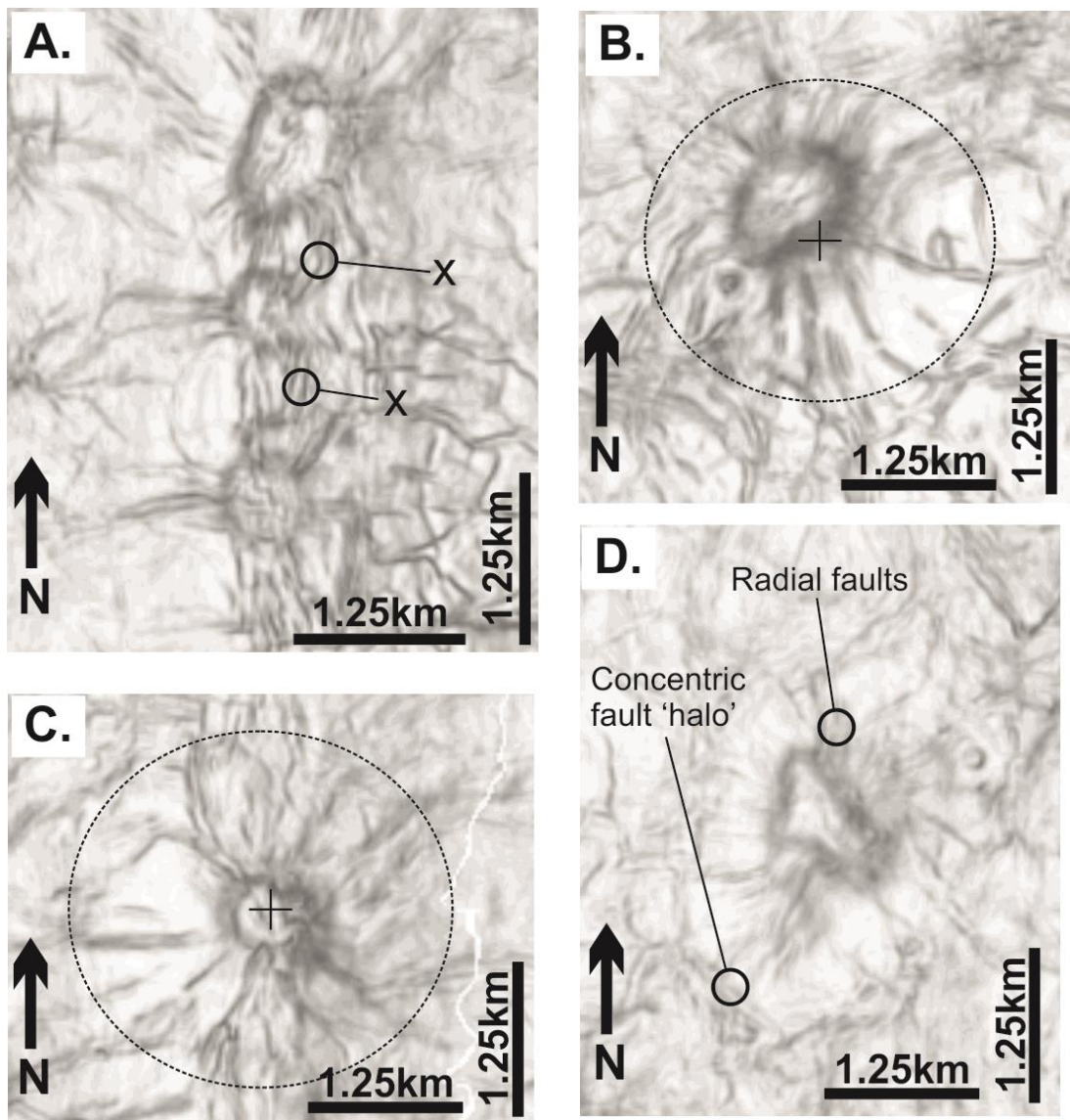


Figure 6.13: Coherence slices across selected vents detailing the variability in radial fault zones. (A) Shared radial faults, (B) Asymmetrical radial faults as the vent is offset from the centre of the radial faults, denoted by the cross. (C) Symmetrical radial faults. (D) Radial and concentric faults

,

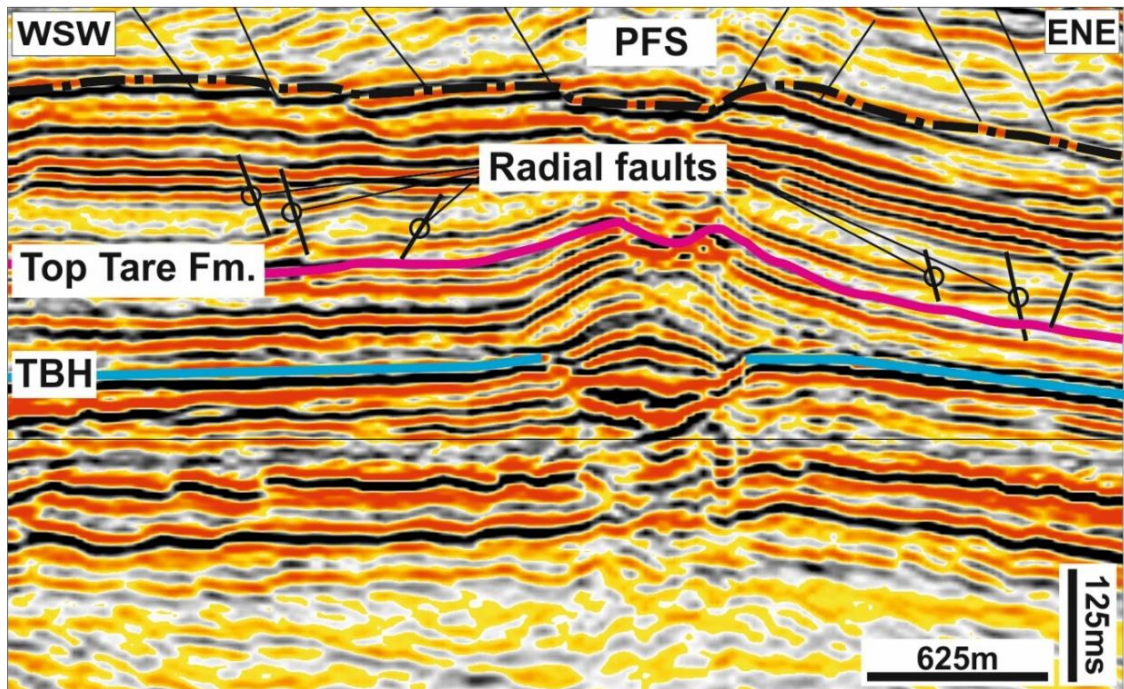


Figure 6.14: Seismic cross section with enhanced gain showing the decoupling between the radial faults and the overlying polygonal fault tier.

symmetrically aligned (Fig. 6.13C). Radial patterns in surrounding closely spaced HTVCs seemingly link to form curved fault traces (see x, Fig. 6.13A). displacement length and displacement height profiles suggest that these radial faults have similar displacement characteristics to the polygonal faults in interval B. Throw values on the radial faults are very low (<20m) and many are close to trace sample limit of the seismic data (4ms). Radial faults here are not vertically persistent with radial patterns disappearing by the Lower Brygge horizon particularly to the north where they are constrained by a low amplitude reflection package (Fig. 6.11, Fig. 6.14). It is also important to note that the radial faults are the only faults associated with the mounds and there is no faulting observed at the crest of the mound. One of the largest mounds within the case study shows a radial fault pattern, ringed by a concentric fault ‘halo’ (Fig. 6.13D). The halo is best observed around the southeast of the vent where it coincides with the edge of the vent. The vertical extent of the radial faults is generally confined to Interval B of PFS1. In the north of the survey, the radial faults have an upper tip position 100 milliseconds above the top Tare reflection. The only instance where a radial fault can be traced into higher stratigraphic levels is associated with Vent 5, where a single radial fault transects the majority of the tier. The interaction between polygonal faults and radial faults is complex. There is no evidence for polygonal faults cross cutting radial faults. The radial faults have broadly linear traces except where two radial faults meet (see Fig. 6.13a). Curvilinear fault traces are found within the polygonal fault array fault tips curving to meet radial faults, suggesting that the radial faults are linked

6.2.3.2 Analysis of the relationship between radial faults and HTVCs

A total of 27 HTVCs are shown in (Fig. 6.7, Fig. 6.6, Fig. 6.9), many of which overlie multiple sills. To analyse the interaction between radial faults and HTVCs, only HTVCs associated with a single igneous intrusion, BR1, are analysed here to circumvent potential uncertainties with regard to potential re-activation of the HTVCs by multiple sill intrusion phases that may influence the radial fault array. Of the 27 HTVCs a subset of 19 mounded structures are described further and had their associated radial patterns analysed.

As the radial fault patterns are hosted above the mounds, only mound attributes are examined further. The average radial area for all 19 vents is 2.34 km^2 . The average mound volume is 0.03 km^3 and there is an average dip on the flanks of the mound of

2°. The attributes examined in Fig. 6.15 are the spatial attributes of the mound plotted against the radial faulted area. General trends within the cross plots show a positive correlation between the spatial attributes of the mounds such as mound area, volume, relief and radius. The cross-plot of mound dip against radially faulted area shows no clear correlation. Statistical analysis of these trends was conducted to assess the statistical significance of the correlation seen between some of the mound attributes and the width of the radial fault zone. The null hypothesis of this test was that there is no correlation between mound attributes and the dimensions of the radially faulted area.

Of the 19 HTVC's analysed, only the mound volume, mound radius and dip are normally distributed using the Anderson-Darling test. Based on the mix of normal and non-normal distributions and scatter of the data, Spearman's Rank was used to assess the correlation between the dimensions of the radial faulted area and various mound attributes. The mound dip attribute shows no significant correlation to the width of the radially faulted area based on the high p-values and very low significance levels. Mound relief attribute shows a weak correlation based on a p-value of 0.81 and has a low 90% significance. The mound attributes that suggest a strong positive correlation (p-values of 0.0009, 0.017 and 0.0015) between the spatial attributes of the mounds (mound width, mound volume and mound area respectively) also have a high significance level of 95%. These trends are also true when data was also analysed omitting the mounds that show no radial pattern (Table 6-2)

The data were also segregated by internal reflection type and re-analysed. Generally, the cross plots show that vents with similar internal reflection types, form groups (Fig. 6.15). This suggests that the vent types have similar attributes and suggest that the vent types are distinct. There is a correlation between vent width and the width of the radial faults (A. Fig. 6.15) in mounds associated with strongly layered vents. The largest radial faults are typically associated with strongly layered vents are on average 2.8 times the width of vent. Weakly layered vents show a weak correlation between vent thickness and the width of the radial faults.

6.3 Discussion

To understand the process involved in creating the radial fault patterns described here, there are two possibilities for timing the radial faults. 1) An early timing model,

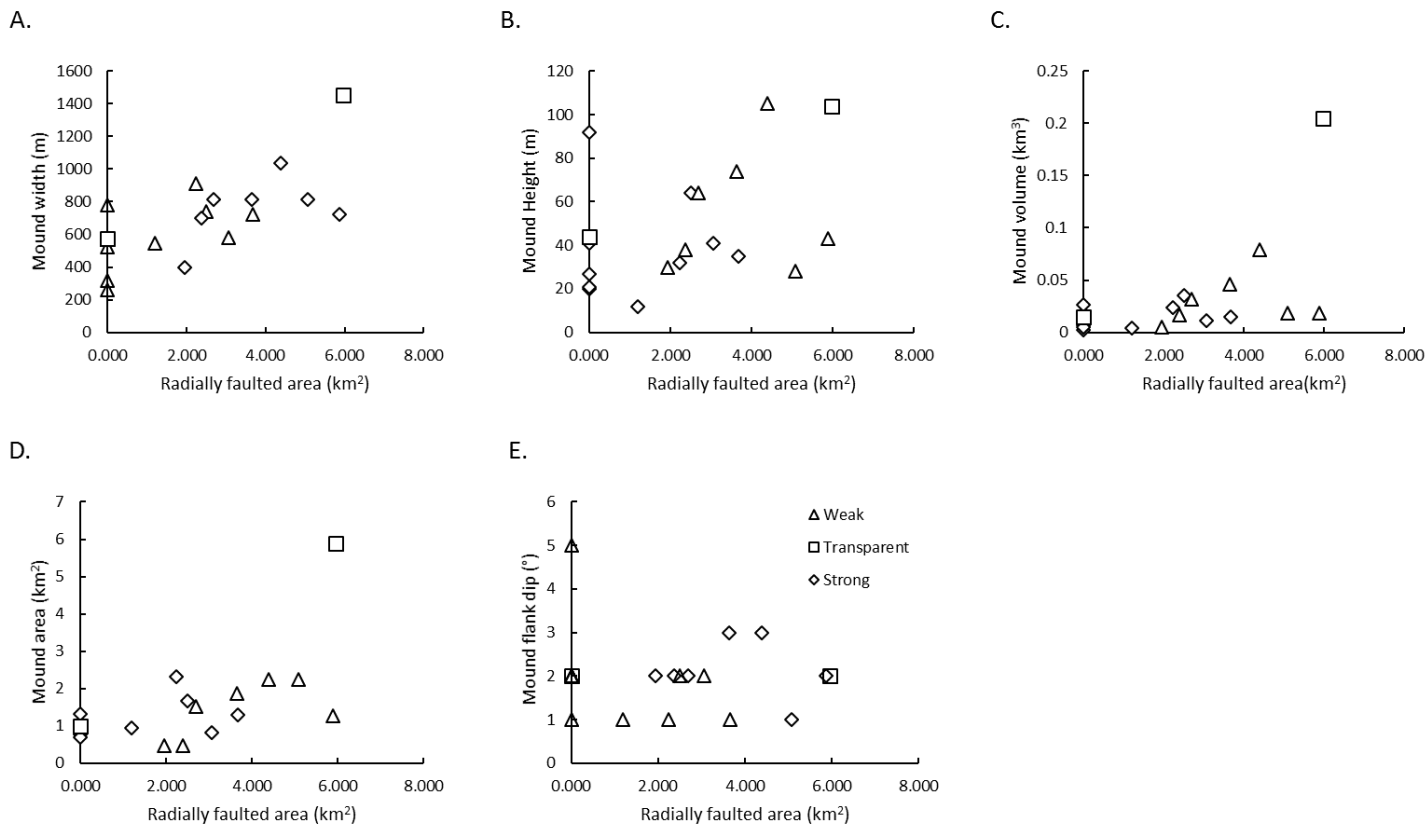


Figure 6.15: A selection of cross plots of mound attributes against the radially faulted area, (A) Vent width, (B) Vent relief, (C) Mound relief and (D) Vent volume. The data is segregated by vent internal reflection type. Vent types are (1) Strongly layered, (2) Transparent and (3) Weakly layered

<i>Vent no</i>	<i>Type</i>	<i>Radial area km²</i>	<i>Mound Rad (m)</i>	<i>Mound height (m)</i>	<i>Mound volume (km³)</i>	<i>Mound area (km³)</i>	<i>Mound Dip (°)</i>	<i>Mound width/Radial width ratio</i>
2	W	3.057	577.5	41	0.011	0.82	2	3.7
10	W	1.193	548	12	0.004	0.932	1	1.3
11	W	3.668	720.5	35	0.015	1.292	1	2.8
12	W	0.000	525	27	0.007	0.755	1	0.0
13	W	2.505	737.5	64	0.035	1.657	2	1.5
14	W	0.000	781.5	41	0.018	1.325	2	0.0
16	W	0.000	569	92	0.026	0.835	5	0.0
19	W	0.000	315.5	20	0.002	0.835	2	0.0
21	W	0.000	258	21	0.005	0.7	2	0.0
28	W	2.231	911	32	0.024	2.316	1	1.0
1	T	5.961	1454.5	104	0.205	5.898	2	1.0
3	T	0.000	574	44	0.015	0.998	2	0.0
4	S	5.879	721.5	43	0.018	1.266	2	4.6
15	S	4.387	1034.5	105	0.079	2.249	3	2.0
17	S	1.942	398.5	30	0.005	0.477	2	4.1
18	S	5.077	814.5	28	0.018	2.249	1	2.3
20	S	2.380	699.5	38	0.017	0.477	2	5.0
22	S	3.641	813.5	74	0.046	1.858	3	2.0
23	S	2.690	813.5	64	0.032	1.511	2	1.8

Table 6-1: Raw mound data used in cross-plots and statistical analysis

All vents (n=19)								
	RFZ (km²)	area	Mound width*	Mound Relief (m)	Mound volume (km³)	Mound area (km²)	area	Mound dip (°)
<i>And-Dar p-values</i>	1.068		0.229	0.016	0.00000009	0.00001334		0.00004535
<i>Spearman (rho) Stat</i>	-		0.714	0.432	0.556	0.564		-0.012
<i>Spearman (rho p)</i>	-		0.0009	0.065	0.017	0.0015		0.64
<i>Significance (Spearman)</i>			<0.005	0.1	<0.01 – 0.005	0.01 – 0.005		No correlation
Excluding vents with no radial patterns (n=12)								
<i>Spearman (r)</i>	-		0.636	0.53	0.606	0.529		0.244
<i>Spearman (p)</i>	-		0.03	0.062	0.04	0.08		0.44
<i>Significance</i>			>0.025	>0.05	>0.025	0.05		0.1
Strongly layered Vents (n=5)								
<i>Spearman (r)</i>	-		0.771	0.6	0.228	0.629		-0.125
<i>Spearman (p)</i>	-		0.042	0.23	0.631	0.131		0.789
<i>Significance</i>			<0.05	<0.1	<0.1	<0.1		<0.1
Weakly layered vents (n=7)								
<i>Spearman (r)</i>	-		0.074	0.142	0.210	-0.037		0.246
<i>Spearman (p)</i>	-		0.905	0.7	0.734	0.953		0.690
<i>Significance</i>			<0.1	<0.25	<0.1	<0.1		<0.1

Table 6-2: Table of vent statistics showing the correlation between the radially faulted area and various mound attributes

whereby the radial faults form in shallow (<200 m) burial conditions in response to an altered state of stress caused by changes in topography. 2) Late radial fault formation under deeper burial conditions (>200 m) in response to states of stress caused by differential compaction. The impact and degree of differential compaction is in turn, defined by the seismic characteristics of the vents.

6.1.1 Timing relationships between HTVCs radial faults and polygonal faults

To ascertain the origin of the radial faulting seen around HTVCs in this study, understanding the mode of emplacement (i.e. extrusive or intrusive) is critical for constraining when these vents became significant topographic features. HTVCs are typically thought to form at the palaeo-seabed through rapid flux of hydrothermal fluids and later infilled by sedimentary volcanism and flank collapse (Jamtveit et al., 2004). The reflections above the mound top show onlap and evidence of erosion that suggests that the mound had a relief during deposition in the late Tare to early Brygge formation (Fig. 6.9) and hence, was already an established feature prior to the deposition of sediments. As such the HTVCs of this survey can be constrained as having formed during the Palaeocene based on their location within the Tare Formation. This date is also consistent with widely published ages for regional igneous activity on the Norwegian Margin (Eldholm et al., 1989; Doré et al., 1999; Brekke, 2000; Berndt et al., 2001; Planke et al., 2005).

Having constrained the timing of HTVC and the mode of emplacement, the relative timing for the formation of radial faults relative to the HTVCs is considered further. An ‘early’ timing of radial fault formation was briefly suggested by Hansen et al. (2005) who noted similar radial patterns in polygonal faults around mud intrusions on the Gjallar Ridge. Hansen et al. (2005) attributed the radial perturbation patterns to mound formation occurring coeval with or preceding polygonal fault formation.

Timing of the initiation of polygonal fault growth is challenging and there are many theories as to how and when polygonal faults nucleate (see Cartwright, 2011 for review). In this study, there are no seismically resolvable growth packages in the hanging walls nor are the faults near the modern day seabed as observed in other suspected early growing polygonal fault arrays (Cartwright et al., 2004; Gay et al., 2004; Hansen et al., 2004; Watrus et al., 2003). This may indicate that these polygonal faults were undergoing blind growth and therefore offer limited constraint for fault

timing. In addition, polygonal faults show very little evidence for overprinting or linkage with radial faults. As polygonal faults, by definition, form multiple linkages and branchlines with other faults to create distinctive planform patterns, the absence of linkages between radial faults and polygonal faults would appear to indicate a strongly perturbed state of stress immediately around HTVCs (*sensu* Carruthers et al. 2013). However, the presence of a large topographic feature during the deposition of polygonal fault hosting sediments could suggest evidence that both the radial faults and polygonal faults formed during shallow burial under a perturbed state of stress (see Chapter 4).

The data presented in Chapter 4, suggest that the polygonal faults from the Angolan margin were aligned to the margins of a number of large pockmarks. These alignments were proposed to be the result of differential compaction enhanced by the local dip of the flank of the pockmark crater. The alignments of the radial faults seen in this survey are downslope striking. This orientation contrasts sharply with the results of Chapter 4. There is also a discrepancy between the more widely described convention associated within observed and modelled gravity driven systems where gravity induced faulting creates fault strikes parallel to that of the slope (Clausen et al., 1999; Higgs and McClay, 1993; Ireland et al., 2011; Mandl and Crans, 1981; Morley, 2007; Victor and Moretti, 2006). Present day slope angles on the HTVCs are between 1° and 3°. Once the effects of compaction have been removed, these dip angles could have been higher. Previous studies on the impact of slopes on faults (tectonic and polygonal) suggests that dip and relief (as a function of dip) are an important factors in the vertical polarity of faults (Mandl, 1987) but also the geometry of the faults (Morley, 2007). Given that a similar study on perturbed polygonal fault patterns found that local slopes enhanced and forced a slope-parallel alignment of perturbed polygonal faults under shallow burial conditions, the down-slope strike of the radial faults seen in this survey would appear to preclude radial fault formation in shallow burial conditions.

6.3.1 Radial fault formation through differential compaction

Previously described and modelled examples of radial features have been associated with intrusion of dikes (Ode, 1957), mantle diapirs (Janes et al., 1992; Squyres et al., 1992; Stofan et al., 1991) or salt (Withjack and Scheiner, 1982). This would indicate that models whereby one material is forcibly displacing another result in arching, uplift

or faulting. These features have been described around igneous intrusions, where forced folding around is seen above sills (Hansen and Cartwright, 2006) and salt diapirism (Rowan et al., 1999; Davison et al., 2000; Stewart, 2006). The mechanics of intrusion, particularly salt diapirs, the ratios between vertical and horizontal stresses (Luo et al., 2012) and orientation of principal stress axes (Carruthers et al., 2013) are likely to be influenced by the forces which provide the influx of material that feeds the intrusion, such as buoyancy and tectonic derived stress (Hudec and Jackson, 2007). These stress conditions may be applicable to radial faults described by Hansen et al. (2005) where the radial faults are associated with intrusive mud structures.

Nonetheless, there are obvious radial faults forming around the roof of salt domes that are geometrically similar to the radial faults observed around the HTVCs. The radial faults seen around the roof of salt domes have been widely described in seismic (Carruthers et al., 2013; Davison et al., 2000; Stewart, 2006; Yin and Groshong Jr., 2007) and by geomechanical modelling the impact salt has on its overburden (Luo et al., 2012; Poliakov et al., 1996, 1993; Schultz-Ela and Walsh, 2002). The radial faults in salt domes have been suggested to form in brittle, consolidated material within the roof complex to accommodate penetrative strain from the growing salt dome (Stewart, 2006). Yin and Groshong Jr., (2007) examined faulting over salt domes using models, balanced sections and seismic data and suggest that radial faulting over salt domes is generated by fold driven extension over the growing salt dome. More recently theoretical modelling of stresses within the material surrounding salt domes has showed that in both plastic and elastic models, salt bodies contract vertically and expand laterally (Luo et al., 2012). This vertical contraction and lateral expansion of the salt cause horizontal and vertical stresses to increase. This increase in vertical and horizontal stress perturbs the state of stress and hence the orientation of any incipient fault strikes.

Although salt and igneous/hydrothermal bodies are chemically, and in some cases, geometrically very different, the key comparison drawn from the salt-based studies is the differential response of one lithological body (salt) compared to its host rock (sediments). In the examples of salt-related deformation, the key aspect of radial pattern formation is the contrast between the response to compaction in the salt body and the surrounding sediments, whether it is through active piercement of salt by its

overburden (Yin and Groshong Jr., 2007) or passively under burial conditions (Luo et al 2011).

The suggestion here is that the HTVCs have a fundamentally different response to compaction to that of the surrounding sediments. Based on the evidence in seismic data from the Modgunn Arch, the Tare Formation, which drapes the vents, conforms closely to the geometry of the Vent top horizon. This suggests that either the Tare Formation has been compacted to conform to the geometry of the underlying vent or is a relict of depositional architecture (i.e. depositional drape). In either case, compaction over a topographic feature is likely to produce a degree of forced folding (Stearns, 1978; Cosgrove and Ameen, 1999). Differential compaction has been suggested to be the cause of forced folding in sandstone channels from the northern North sea (Cosgrove and Hillier, 1999). In the data examined by Cosgrove and Hillier (1999), sands with minor topographic highs were fluidized by the injection of gas into the sand. This migration of fluidized material and differential compaction further accentuated the existing high into its observed convex up geometry. This forced folding of the Tare Formation over the vent is much more pronounced on strongly layered and weakly layered vents (see Fig. 6.9). The radial faults are hosted within the Brygge Formation and appear to detach onto the Tare Formation (Fig. 6.14), despite both formations being comprise of fine-grained sediments. This would suggest that there is an element of mechanical stratigraphy between the Tare and Brygge Formation. The Brygge Formation is a sequence of hemipelagic oozes containing clays and bio-siliceous clays (Bryn et al., 2005; Chand et al., 2011; Eidvin et al., 2007; Hjelstuen et al., 2004). In contrast the Tare Formation consists of clays and tuffs (Brunstad et al., 2008). This would suggest that the faults formed after the Brygge and Tare Formation had different mechanical properties (i.e. degrees of compaction), prior to the establishment of the radial faults. This mechanical contrast offers some important constraint on the timing relationship. Compaction, defined as the loss of porosity in a sediment (Perrier and Quiblier, 1974), has been suggested to be an important factor in developing mechanical stratigraphy (Laubach et al., 2009). Published porosity data that shows bio-siliceous sediments and clays lose their porosities at significantly different rates after 200 m or more burial, with clays losing their porosity faster than biosiliceous ooze (Kominz et al., 2011; Praeger, 2009). This would suggest that the clays in the Tare Formation were more compacted and thus

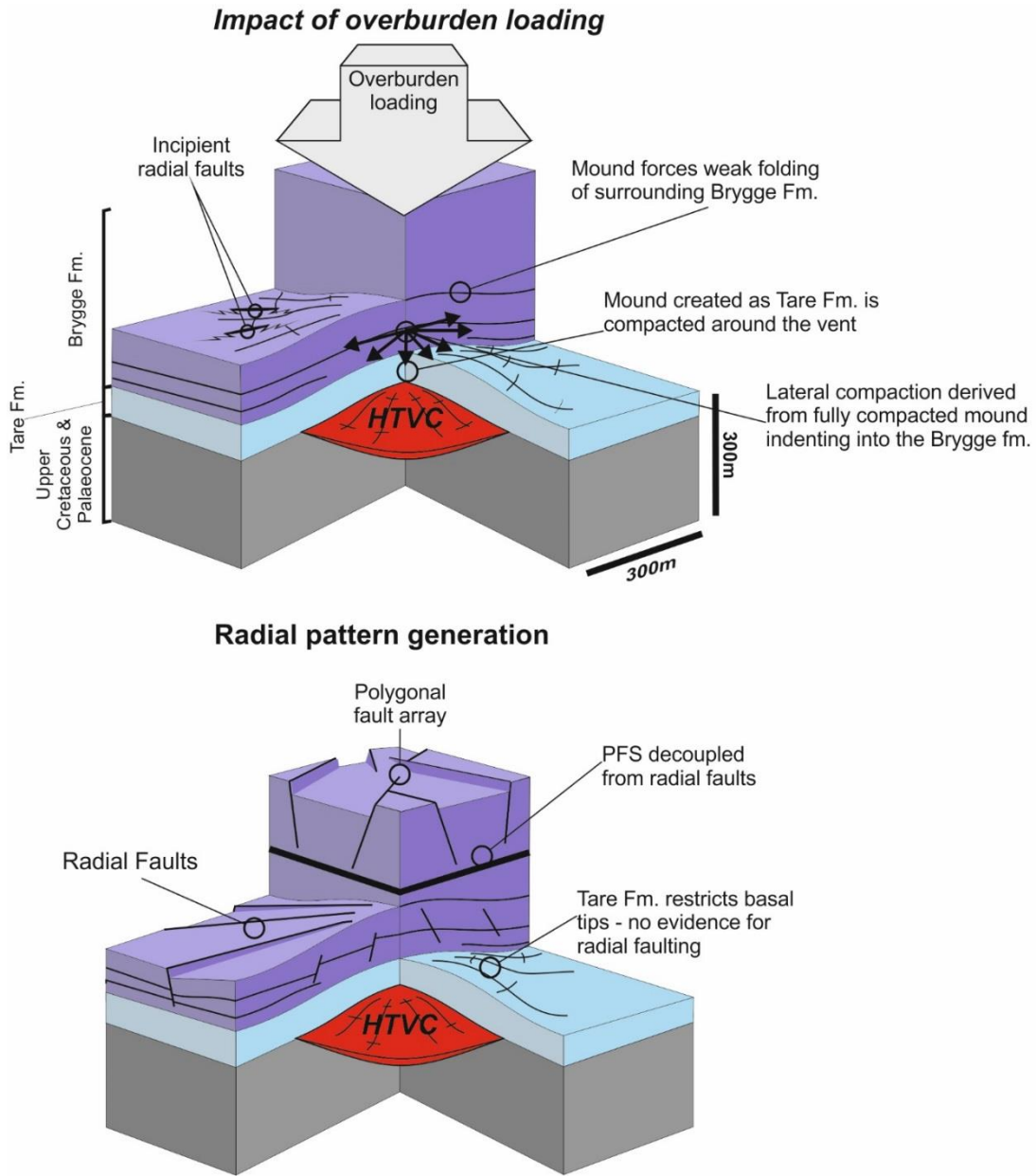


Figure 6.16: Cut away of 3D block diagrams summarizing the root cause of some of the features of the vent and the radial faults during compaction and faulting

more resistant to faulting and this is likely to have happened after burial at depths of 200 m or more.

This differential compaction between the Tare and Brygge Formations, coupled with the forced folding of the Tare Formation, generates a perturbation in similar fashion to that suggested by Luo et al., (2012) for salt. Here the HTVC creates resists compaction by vertical consolidation and lateral expansion of the vent fill. The Tare Formation undergoes forced folding due to the compaction over the vent and indents into the Brygge Formation under burial conditions. This forced folding and indentation of the Tare Formation into the Brygge Formation, forces lateral compaction of the Brygge Formation (Fig. 6.16). This alters the ratio of horizontal to vertical stress in the Brygge Formation and forces the reorientation of horizontal stress to force radial alignments (*sensu lato* Luo et al., 2012). This interpretation is supported by correlation between the dimensions of the radially fault area and mound spatial attributes (width, area and volume). These data show that wider mounds (the forced folds of the Tare Formation) produce wide radial fault zones. This would indicate that wide mounds (and hence wide vents) produce wide radially faulted zones as a product of the accommodation of strain generated by the lateral compaction response of the Brygge Formation to HTVCs. This model is underpinned by the compaction response of the HTVCs. One of the key observations regarding the vents is the apparent change in seismic characteristics. The compaction response of the vents does not produce an accurate reconstruction of the state of stress as some of the smallest vents with layered vent fill produce some of the largest radially faulted areas (i.e Vent 15, Table 6-1). Vent morphology and fill has been described previously from examples from the north-east Atlantic margin by (Hansen, 2006). Hansen (2006) describes the internal reflections of HTVCs as falling into two categories, chaotic fill and downlapping/onion-ring structure. The observations made of internal vent structure in this study broadly parallel the observations made by Hansen (2006), as such, the internal seismic characteristics are suggested here to be strongly indicative of vent fill. Based on the reflection characteristics and the response of the radial fault network to the vent types, it is clear that there are at least three different styles of venting present off a single sill. These are based on the broad reflection types set out by Avseth et al., (2010) based on the contrast between the internal reflection type and the surrounding reflections. Strongly layered vents are akin to the downlapping/onion-structure vents

of Hansen (2006) and are interpreted to represent hard reflection types. This interpretation is supported by the cross plot data which suggested that the dimensions of the radial fault zones are weakly controlled by the mound width (see Fig. 6.15A). This would suggest that the potentially hard, incompressible lithology within the vent impacts the area immediately above the vent generating a strong forced folding that extends some distance away from the vent. Weakly layered vents are equivalent to the chaotic vents of Hansen (2006). These vents are the middle member between strongly layered and transparent vents and likely represent a mixture of both venting styles. This interpretation is supported by the cross plot data, which showed a correlation to the mound radius (Table 6-2). The vent mound area (and by extension vent area) is suggested to be important in weakly layered vents as the key component in the creation of a differential compaction driven forced fold is the initial thickness and degree of compressibility of the vent. In cases where there is limited vertical consolidation of the vent, a strong forced-folding effect is generated which is reciprocated in the lateral compaction of the facies surrounding the vent. However if the vent is more susceptible to vertical consolidation by being comprised of muds or weakly cemented material, the degree of vertical consolidation and lateral compaction is significantly weaker generating a smaller radial faults (Fig. 6.17). Transparent vents are uncommon and so meaningful conclusions cannot be drawn on the limited data regarding their response to compaction, however the infilling vent material is likely to be less dense/consolidated based on the hard reflections (Avseth et al., 2010) observed at the vent top and vent base horizons.

Previous field and seismic examples make a case for a diverse arrangement for vent fill. Svensen et al., (2003) examined core taken through a hydrothermal vent from the Vøring Basin and noted seep-carbonate horizons above the vent. Svensen et al (2003) showed that the geochemical signature of the $\delta^{13}\text{C}$ within the carbonates above the vents indicated thermogenic or biogenic methane. The isotopic signature of the $\delta^{18}\text{O}$ within the calcite was also inconsistent with diagenesis. Svensen et al (2003) suggest that the carbonate cement is closely associated with the migration of thermogenic methane and/or hydrocarbons through the hydrothermal vent complex during or immediately after the emplacement of the vent. In a field based study from the Karoo basin, Svensen et al., (2006) noted the presence of either a hydrothermally emplaced zeolite cement or isolated blocks of fine grained magmatic material in vents in the

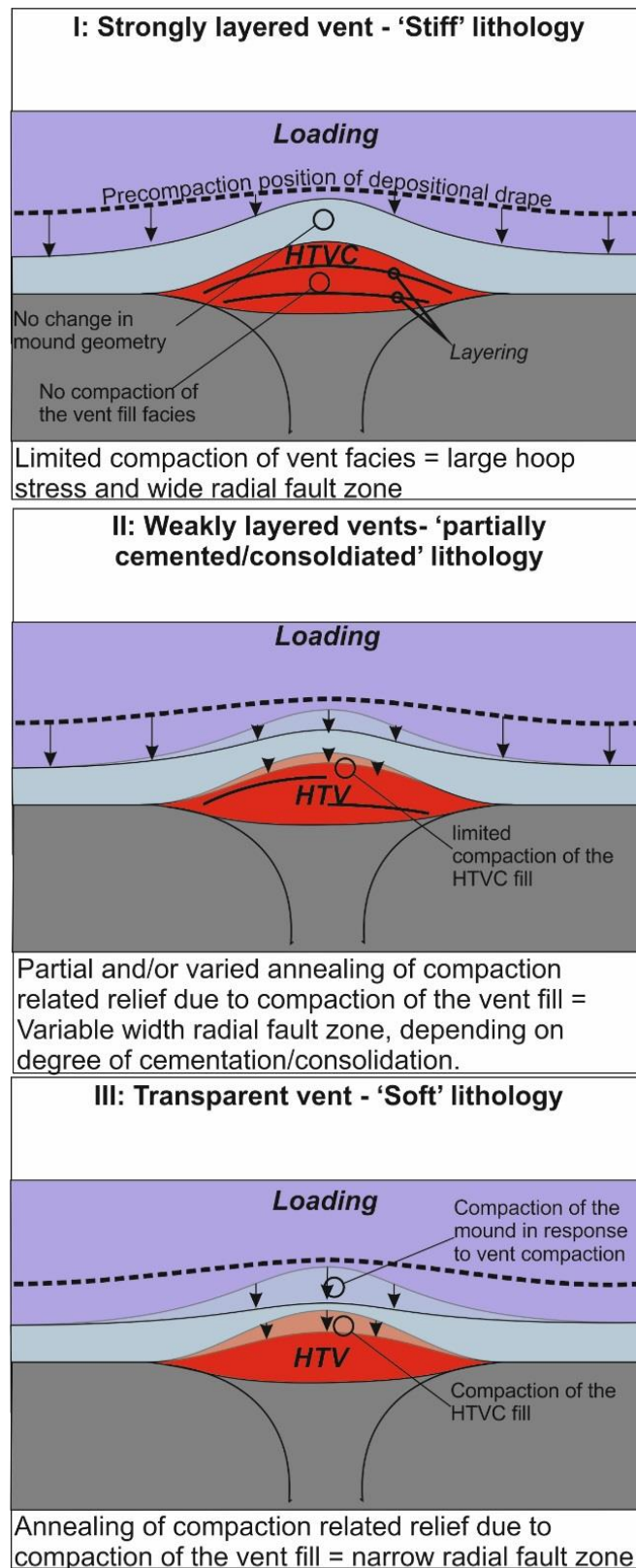


Figure 6.17: Schematic cross sections showing the impact that hard, soft and partially consolidated vent fill facies has on an incipient forced fold in the Tare Formation and the relationship between vent fill and radial fault dimensions.

Karoo basin. Integrated studies examining seismic data with well calibration show contrasting venting fills. Grove, (2012) used an integrated study of cores and seismic that demonstrated that a single mound has a mixture of sedimentary and igneous clasts, the latter showing little evidence of reworking, as would be expected from transport and weathering. Grove (2012) suggests that these angular lithic grains are in fact reworked, at depth, by hydrothermal processes and brought to the surface in sedimentary eruptions.

Seismic data has also been used to infer material properties of the HTVC's. Davis et al (2002) suggested that mounds in association with sills are made of volcanic material from the sill itself. In contrast, Hansen et al (2005) use seismic data and amplitude anomalies to distinguish three mound types on the Gjallar Ridge, Norway. These mounds comprise intrusive mud laccoliths from buried sills, as well as mud diapirs and pillows from mobilized sediment using faults as a conduit. Rollet et al (2012), use seismic and bathymetric data to map out igneous intrusions in the Capel & Faust basins, offshore Southern Australia. Line GA302/13 within the study shows a shallow sill generating a pristine example of two styles of venting from one buried sill. The northwestern side generates fluid seepage evidenced by pull down artefacts that culminate in a large pockmark at the sea bed. The southeastern side however, shows high amplitude reflection above the sill margin that has been interpreted by Rollet et al (2012) as shallow volcanics. This aptly demonstrates that not only do individual sills have a variety of styles of venting, this contrast in venting styles can be imaged in seismic data.

Both the field and seismic examples cited here show contrasting interpretations for the composition of intra-vent material driven off by migrating hydrothermal fluids as well as the utility of 3D seismic data for mapping HTVC's. It is, however, difficult to constrain exactly what lithology is causing the changing reflection types within this survey without well control. Although there is no precise lithology data available, the seismic response of the vent fill and the relationship between the spatial attributes of the mounds and the radially faulted area does suggest that there may be a link between the compaction response of vent materials and the generation of radial faults

6.4 Conclusions

This study has shown that a single sill can produce HTVCs with subtle variations in vent composition. This variation in composition can be detected and imaged in seismic data. Radial patterns around these HTVCs are the result of a differential compaction effect between the vent facies and the surrounding tier facies. The formation of radial faults is proposed to be similar to those associated with passive salt diapirs whereby in shallow unconsolidated sediments undergo differential compaction over a cemented or consolidated HTVC. The degree of cementation or percentage of ‘hard’ reflective material present in the vent itself, ultimately governs the degree of compaction and the size of the radial faults. Three reflection types are classified in this study and are tentatively proposed to be a reflection of bulk mechanical behaviour.

Strongly layered vents are harder, cemented vents and generally produce the widest radial faults. This implies that a strongly layered HTVC consists of material that has limited compressibility and resists compaction unlike the sediment surrounding it, generating a strong mechanical contrast between the two. The presence of reflections within the vent could be indicative of cemented sediments or magmatic material. Tuning could potentially increase the amplitude of the reflection but tuning in itself would suggest a vent fill composed of a layering of material (albeit potentially very thin), that has a significant acoustic impedance contrast compared with other vent types. Transparent vents are mud dominated and produce the smallest radial faults. Transparent vents generate very small to non-existent radial fault relative to their size and so are likely to represent a vent fill that has a similar compaction coefficient to that of the surrounding sediments. Although this study concludes that the formation of radial faults in this particular study is a differential compaction effect under deep burial conditions, it does not preclude early radial fault (and polygonal fault) formation as suggested by Hansen et al. (2005)

7 Origin of concentric fault patterns around pockmarks and the implications for polygonal fault growth

Abstract

Polygonal faults are layer bound arrays of normal faults, widely reported in slope and intercratonic basins. Whilst much of the research on polygonal faulting has been focussed towards the specific genesis mechanism that creates these arrays, comparatively little research has been directed towards their nucleation and early growth. This study presents evidence to constrain the earliest part of the growth history of a polygonal fault tier. Using high resolution, 3D seismic data from the West African margin, we document the interaction between a shallow buried, wedge shaped polygonal fault tier and pockmarks located at the base of the fault tier.

Detailed mapping and analysis reveals the presence of strongly curved perturbation patterns in the overlying fault network in the vicinity of pockmark craters. These perturbed patterns differ markedly from the ‘background’ polygonal pattern developed away from areas of pockmark influence. It seems most likely that the perturbation is due to local stress effects relating to residual topography of the underlying pockmarks. By analysing the thickness variations of mapped layers within the polygonally faulted tier, it can be demonstrated that any residual topography was most likely healed after approximately one third of the total tier thickness was deposited. Hence the nucleation of the polygonal faults into their perturbed propagation trajectories must have been established early in the tiers development.

From these observations, a new model of polygonal fault growth is proposed in which individual faults nucleate near the base of a tier at an early stage of burial and then propagate preferentially upwards with basal tips apparently restricted by an underlying mechanically competent unit the base of the tier. Continued growth then shifts the locus of displacement addition, such that final displacement distributions are more axio-symmetrically disposed with respect to the base and top of the tier.

Chapter 4 published in:

Morgan DA., Cartwright J.A. and Imbert P. (2015) Perturbation of polygonal fault propagation by buried pockmarks and the implications for the development of polygonal fault systems, *Marine and Petroleum Geology*, 65, pp157-171

7.1 Introduction

One of key questions remaining of polygonal faults and polygonal fault tiers is when do polygonal faults nucleate? The origin of polygonal faults is widely linked to early dewatering of fine-grained sediments, but their specific genesis is currently open to question, and has been intensely debated since they were first recognised in the early 1990s. A number of genetic mechanisms have been suggested including: (1) the process of syneresis (Cartwright and Dewhurst, 1998), (2) diagenetically induced shear failure (Shin et al., 2008); (3) silica diagenesis (Davies and Ireland, 2011), (4) differential compaction (Davies et al., 2009), (5) density inversion (Henriet et al., 1989; Watterson et al., 2000) and (6) low coefficients of friction (Goult, 2001a).

One of the major impediments to resolving this debate, is the lack of constraint on the initial growth process of the faults. It is widely observed that the maximum throw values of individual faults tend to occur close to the midpoint of the faulted interval or tier, and throw plots approximate to C or M types of Muraoka and Kamata (1983). These types of throw distribution are generally interpreted as indicating at least some degree of blind growth i.e. where part of the growth history has occurred with tiplines that do not intersect the free surface (Walsh and Watterson, 1988).

Only a few studies to date have focused explicitly on the early growth history of polygonal faults and attempted to rationalise the observed throw distributions with a kinematic model. Radial growth involving blind fault propagation from a nucleation position close to the middle of a tier has been suggested by Lonergan et al. (1998) based on a comparison of fault patterns between Miocene and Oligocene tiers of polygonal faults from the central North Sea Basin that showed cross connections between faults in the two tiers across a relatively un-faulted intervening interval. Laurent et al. (2012) described similar relationships between tiers and incorporated the effects of vertical segmentation, as inferred from interpretations of the seismic coherence attribute. In contrast, growth models in which propagation is also blind, but asymmetric, and skewed heavily towards an upward trajectory from a nucleation position somewhere close to the base of a tier have been suggested by Watterson et al. (2000), Cartwright et al. (2003) and Stuevold et al. (2003). Stuevold et al. (2003) also showed convincing evidence of dip linkage between faults propagating in vertically stacked tiers

In a study by Gay et al., (2004) suggested polygonal faults nucleated close to the seabed, and then accrued slip during progressive burial by shrinkage of the sediments, until a maximum was reached at 300 m below the seafloor, with subsequent burial (to 700 m) and shrinkage being accommodated by a system of infilling faults (Gay et al. 2004, their Fig. 14). These authors did not explicitly address the propagation history of a tier but their model conceptualises the notion of early nucleation of polygonal faults during the first stages of burial, and thus supports the early models of Henriet et al. (1989) and Cartwright (1994). Nevertheless, there is considerable uncertainty regarding the critical questions of initial nucleation position and subsequent propagation trajectory of faults within polygonally faulted tiers.

This chapter uses a high-resolution seismic survey from offshore Angola, which images a shallow polygonal fault tier, within the upper 350m of the stratigraphy below the seabed. Within this polygonal fault tier, three key areas are examined; the interaction between polygonal faults and large (150 m to 400 m wide) pockmarks; the presence of faults within a package of sediment <100 m thick and evidence for sediment trapping by the polygonal fault array. Each of these relationships will give evidence towards where polygonal faults grew in the tier (radial versus upward propagation), given evidence for early timing and differential fault nucleation, where polygonal faults within a tier nucleate and grow at different times.

7.2 Geological Background

7.2.1 Seismic stratigraphy

The interval of interest to this study is the polygonally faulted tier developed directly beneath the seafloor. The tier is hosted in a wedge-shaped unit composed of fine-grained sediments of Plio-Pleistocene age, which thickens downslope to the southwest and southeast (Fig. 7.3). Sediment thickness ranges from 80m upslope to the NE to 300m to the SW.

The seismic stratigraphy of the interval of interest is divided into two informal seismic-stratigraphic units based on gross reflection character, and demarcated by regionally mapped horizons (see Fig. 7.3). Unit 2 comprises a series of coherent, parallel reflections with mixed amplitude and high lateral continuity. This reflection package is interpreted as a hemipelagic drape deposit (Brown and Fisher, 1980) that is present below the base of the polygonally faulted tier over the entire survey. The

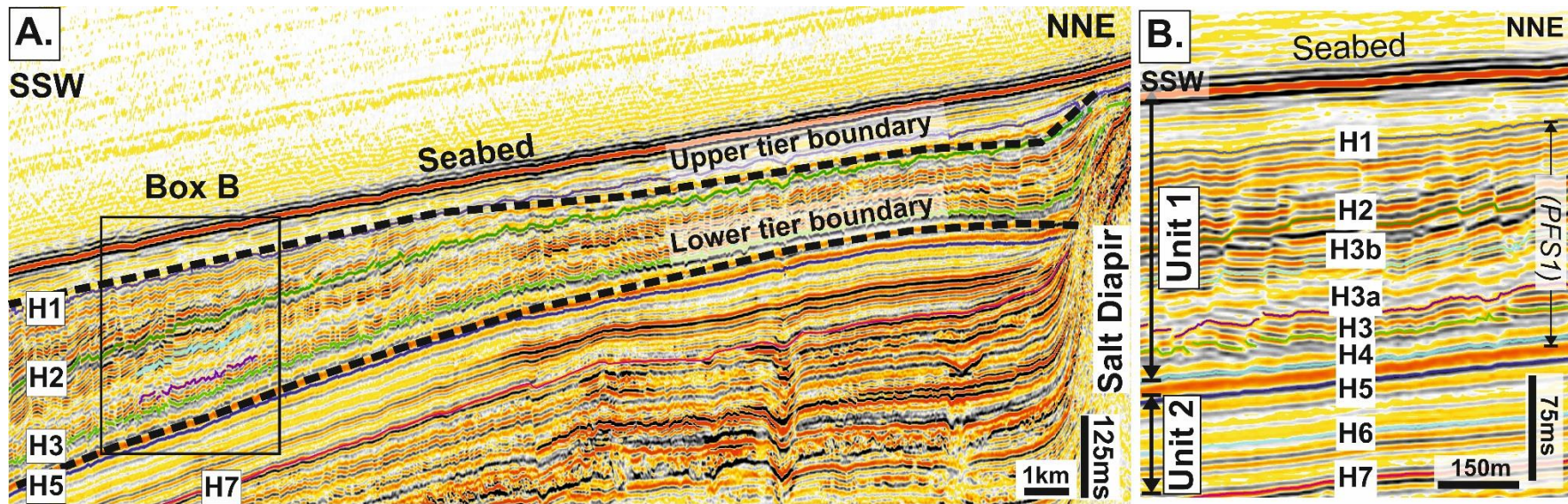


Figure 7.1: (A) A regional seismic cross section across the survey area detailing major structural elements of the survey area and location of the intervals studied. The interval studied is a wedge shaped tier containing polygonal faults just below the seabed. (B) Seismic section showing the location of the seismic units and horizons used in the study areas. PFS1 refers to the studied polygonal fault tier.

uppermost tens of metres of this unit hosts the pockmarks that form much of the focus of this study. Unit 2 is bounded at its base by a moderate to high amplitude positive reflection (H7 on Fig.. 7.3B). The upper boundary of Unit 2 is mapped consistently as Horizon H5, which is also remarkable in that it is the locus of the majority of the basal tips of the overlying polygonal fault tier. Unit 1 hosts the polygonal fault tier and consists of a series of parallel and divergent reflections of mixed coherency. The base and top of the tier are not confined to a single horizon, but instead is interpreted as exhibiting more diffuse boundaries, generally confined to a series of two to three reflections at the base and top of Unit 1. Reflections below H2 are broadly parallel, however above H2, the reflections become more divergent and the reflection packages between H1 and H2 thicken to the south-east and south-west of the survey (see Fig.. 7.3 and Fig. 7.12A). Amplitudes are variable within the units but also display a high degree of lateral continuity. Unit 1 is interpreted being dominantly composed of hemipelagites unit based on its seismic facies (Brown and Fisher, 1980). The upper and lower boundaries of Unit 1 are represented by the regionally continuous marker horizons H1 and H4, respectively

7.2.2 Pockmarks near the base of the polygonal fault tier

Eight large, sub-circular depressions have been mapped at Horizon H5, close to the base of the polygonally faulted tier. These depressions are expressed in both dip attribute and two way travel time maps of Horizon H5. These depressions are isolated occurrences, distributed randomly throughout the study area (Fig. 7.2). In section these depressions consist of a basal surface that is concave upwards and exhibit reflection geometries indicative of erosional truncation along their margins. On the basis of their sub-circular planform pattern and the evidence of erosional truncation at the depression margins, these features show similar geometric characteristics to that of large pockmarks described in many other marine and freshwater basins (Judd and Hovland, 2007). Four pockmarks were selected for detailed description here (Pocks 1, 2, 3 and 6). The case study areas were chosen for three reasons: (1) they are relatively isolated from tectonic and sedimentary features that may complicate the analysis of the polygonal fault pattern locally, (2) they are representative of diversity of stratigraphic context and geometry seen in the study area, and (3) the two study areas exhibit contrasting degrees of perturbation on the overlying polygonal fault pattern.

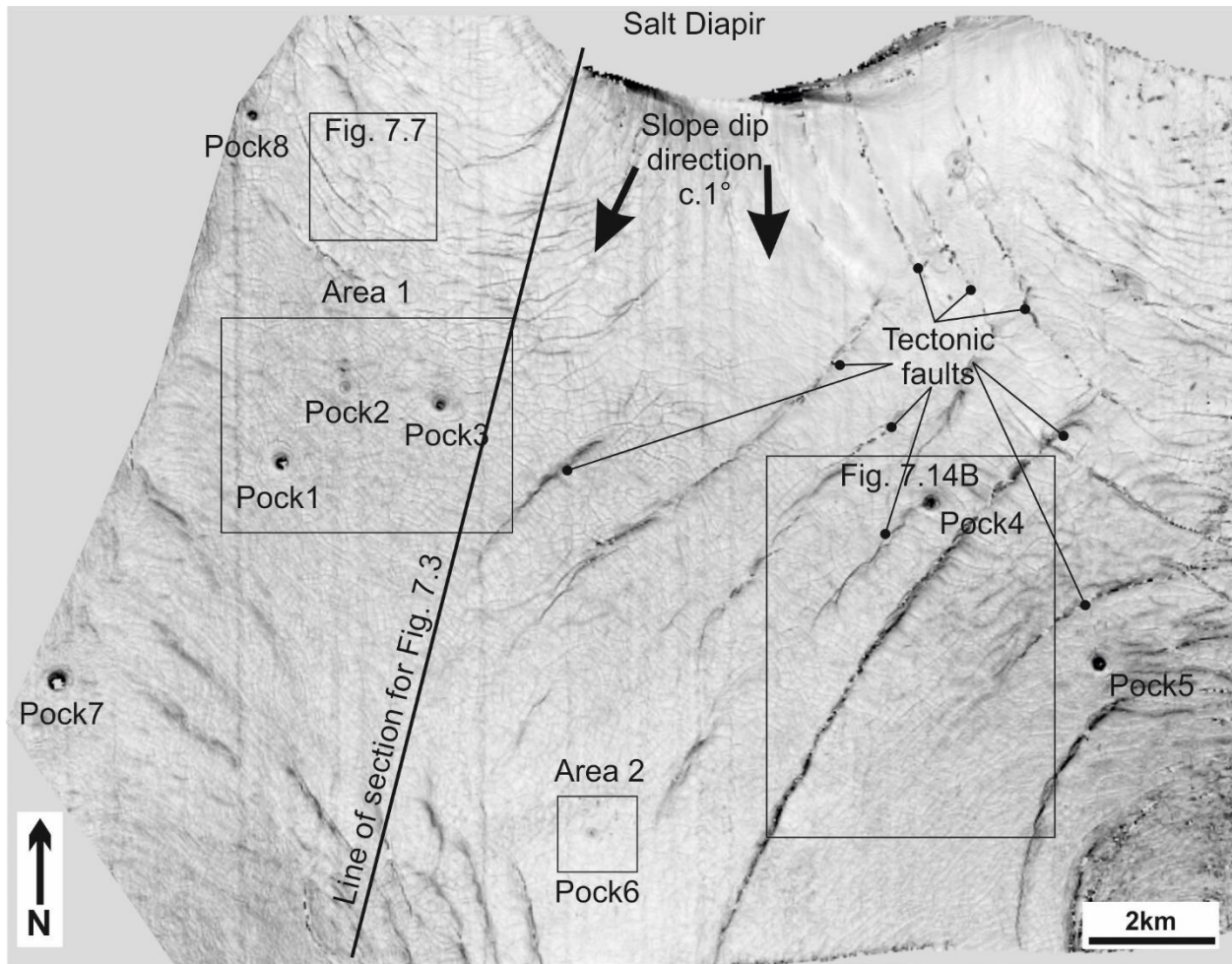


Figure 7.2: Regional time dip map of H5 detailing the spatial distribution of pockmarks (labelled with the prefix 'Pock') and the case study areas. The case study areas have been selected as they are not near tectonic faults (Pock4 and Pock5) or near the edge of the data set (Pock7 and Pock8).

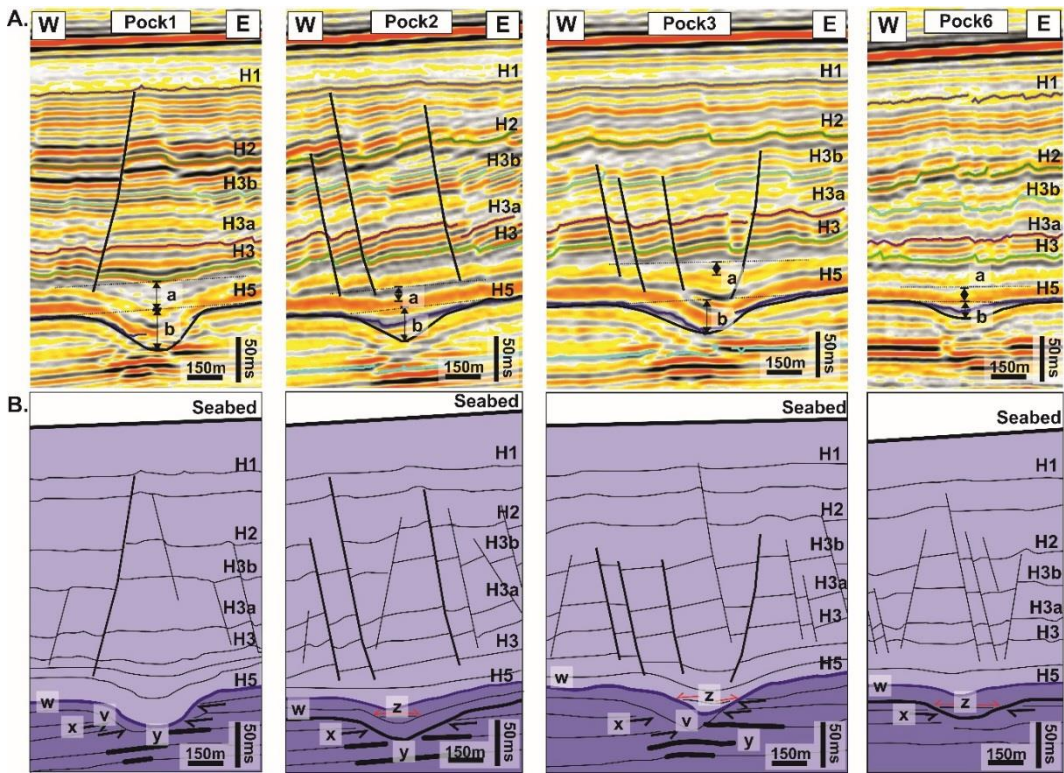


Figure 7.3: (A) Seismic cross sections across the studied pockmarks displaying the locations of initial pockmark relief (b) and residual pockmark topography (a). (B) Schematic line drawings across the studied pockmarks showing key diagnostic features of pockmarks, including evidence for polyphase pockmarks with residual craters (v), the position of the pockmark crater (w) erosional truncation (x), enhanced reflections relating to methanogenic carbonates sensu Ho et al., 2012 (y) and onlap surfaces within the pockmark infill (z). The faults highlighted in bold are the perturbed polygonal faults seen in Fig. 7.7.

Area 1 (Fig. 7.2 & Fig. 7.7A) is a cluster of three large pockmarks located on a southerly dipping slope, with a spacing of c.2 km between each one. In map view, Pock1 and Pock3 have a sub-circular shape, while Pock2 has an elliptical or ‘tear drop’ shape. The dimensions of the three pockmarks in Area 1 varies, with Pock 3 is the largest being 390 m wide and 29 ms TWT (26 m) deep, Pock2 is the smallest in this group being 300 m wide and 21 ms TWT (19 m) deep and Pock1 being 370 m wide and 24 ms TWT (22 m) deep. Area 2, is located to the south east of Area 1 and contains a single isolated pockmark (Pock6) that is 150 m wide and 14 ms TWT (12 m) deep, with gently curving flanks (c. 10°). Pock6 appears to be more irregular in planform than the sub-circular shapes of Pocks 1, 2 and 3 (Fig. 7.7B).

In cross section, the pockmarks are generally asymmetrical with a clear erosional base, defined seismically where the underlying positive reflections (e.g. labelled X in Fig. 7.3) truncate against the flank of the pockmark. The pockmarks have a combined onlap and drape infill (see Fig. 7.3 feature z and w respectively).

The base of the pockmarks is variable with some pockmark craters occurring stratigraphically higher or lower than others nearby. The pockmark craters for Pock1 and Pock3 occur stratigraphically at the H5 reflection, whereas Pock2 is one reflection cycle deeper. Beneath Pock1 and Pock3, there is a gently dipping reflection unit located on the western side of the section. These reflections have been described previously by Ho et al. (2012) as evidence for multiple phases of fluid flux and pockmark development. Ho et al. (2012) define pockmarks displaying this geometry as polyphase pockmarks. Whilst these downward bending reflections evidenced to the NW of the pockmarks suggest an earlier phase of fluid flux, synchronous with the formation of Pock2 and Pock6, it is only the most recent and youngest phase that is preserved and infilled, hence the craters of Pock1 and Pock3 are interpreted as slightly younger. It is the infill of the youngest craters that generates subtle local thickening within the overlying polygonal fault tier. Pock1 and Pock3 have an erosional truncation surface developed on the same seismic reflection and are therefore interpreted to have a similar formation age. Pock2 is slightly older with its erosional truncation surface being stratigraphically deeper than its neighbours. Pock6 is notably older than other pockmarks with a truncation surface that is at least two full reflection cycles deeper. This suggests a range of relative ages for pockmark formation, but lack of well calibration means that this range cannot be specified. Beneath some of the

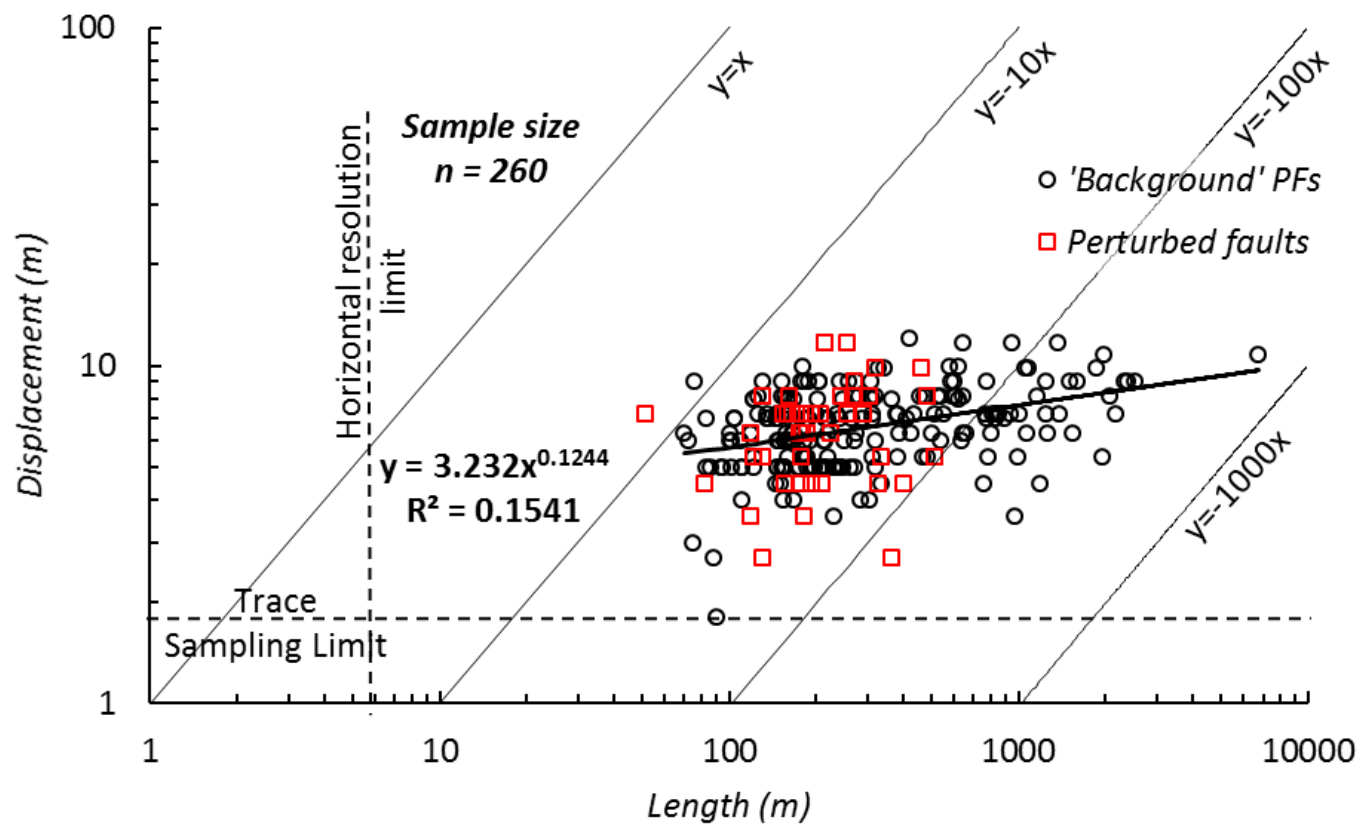


Figure 7.4: Log-log plot of displacement-length for ‘background’ and perturbed polygonal faults showing a power scaling law, with an exponent of 0.12. The scatter of data and low gradient of the best fit line are attributed to high connectivity between branchlines and the layer bound nature of the polygonal fault system which restricts displacement accumulation (Nicol et al., 2003).

depressions, there are a number of enhanced reflections (feature Y in Fig. 7.3). These enhanced reflections are usually stacked vertically over an interval of some tens of metres and have no other associated velocity artefacts, such as push down (see Ho et al., 2012 for discussion), which could indicate the presence of free gas. These enhanced reflections are interpreted in this study as the seismic expression of carbonate cemented horizons, following the interpretation of Ho et al. (2012).

7.3 Polygonal fault patterns

To understand deviations from a ‘standard’ polygonal fault pattern it is necessary to define and describe the geometries of polygonal faults in the planform and cross sectional view.

7.3.1 Plan view expression of ‘background’ polygonal faults

In general, the longest fault traces are observed in the lower third of the tier with a predominant downslope dip and an apparent orientation parallel or subparallel to the regional south-dipping slope and dip downslope. Polygonal fault trace lengths in plan-view are highly variable with fault lengths ranging from 100 m to 5 km. Fault throw is typically less than 15 m (Fig. 7.6). Generally, these shallow polygonal faults show power law scaling between displacement and length with an exponent of 0.12. The wide scatter of the data points in Fig. 7.6 may be attributed to the effects of high connectivity between within the polygonal fault array and vertical confinement of polygonal faults within a tier (Cartwright et al., 1995; Nicol et al., 2003; Cartwright, 2011). Fault height is widely variable with faults crudely scaling to tier thickness as the shortest and tallest faults are in the thinnest and thickest areas of the tier respectively.

The planform geometry of the polygonal fault array is highly variable within different stratigraphic levels of the polygonally faulted tier. Analysis of the regional horizons (H5, H3 and H2) in time dip attribute map reveals important trends in fault orientation and dip direction.

The lowest horizon (H5) shows a pattern with a strong directional influence with polygonal faults striking WNW - ESE (see Fig. 7.4D). Of all the linear dip anomalies seen in Fig. 7D, only 16 display a seismically resolvable offset (>5 m vertical offset) of the H5 reflection and hence only these faults were measured as unambiguous faults offsetting the H5 reflection. The remaining dip anomalies seen on Fig. 7.4D are at the

trace sampling limit and are associated with the basal tips of polygonal faults and may be the seismic expression of polygonal faults tipping out downwards. The dip direction of these faults is bimodal, oriented SW and NNE. All basal tips of the measured faults are unrestricted (*sensu* Nicol et al., 1996), with no apparent linkages to other faults (Fig. 7.4D).

Faults traces within H3 are of mixed geometry with linear, curvilinear or anastomosing traces present (c.f. Lonergan et al. 1998, Fig. 7.4C). Almost 230 faults are present within the 4 km² area with an average spacing of 120 m between fault traces. The strike orientations display a weak fault strike bias to those aligned NW-SE. This trend is superseded by a more dominant strike of NE-SW. These two fault sets form orthogonal linkages that give the fault array a ‘ladder’ like geometry. It should be noted that there is an inherent bias in the dataset: the faults that strike NE-SW are short (<250 m in trace length) and far more numerous. Dip directions measured at Horizon H3 display polymodal trends, with faults sets dipping NW, SE, NNE and to the south (Fig. 7.4C). The array geometry expressed at Horizon H3 shows a very high degree of connectivity between fault tips with >5 % of the observed faults displaying apparently free (unrestricted) tips (Fig. 7.4C).

Faults mapped at Horizon H2 (Fig. 7.4B) display a similar trend to those seen on Horizon H5 and the pattern is markedly different to that seen on Horizon H3. The fault traces are predominantly linear with some curvilinear traces and have an average spacing of 90 m. The orientation of the fault traces is bimodal with a trend striking broadly SW and a minor trend to the NE. Linkages between fault segments are primarily orthogonal (c.f. Lonergan et al. 1998) and free tips are common with 80% of faults having at least one unrestricted tip. Many faults tip out below Horizon H2 resulting in fault tip monoclines that are expressed as linear dip anomalies on the time dip map for H1 (Fig. 7.4A).

7.3.2 *‘Background’ polygonal faults in cross section*

The polygonal fault planes are precisely imaged by the 3D seismic data and have exclusively normal offsets within Unit 1 (Fig. 7.6A.). The polygonal faults dip both up- and down-slope with measured fault plane dips ranging from 48° to 68°. Individual faults are generally planar and there is no preferred orientation for steeply or shallowly dipping faults. The faults in section are typically observed as linked pairs, either as a conjugate fault pair (Fig. 7.6A, point A) or as a fault pair with an upslope and

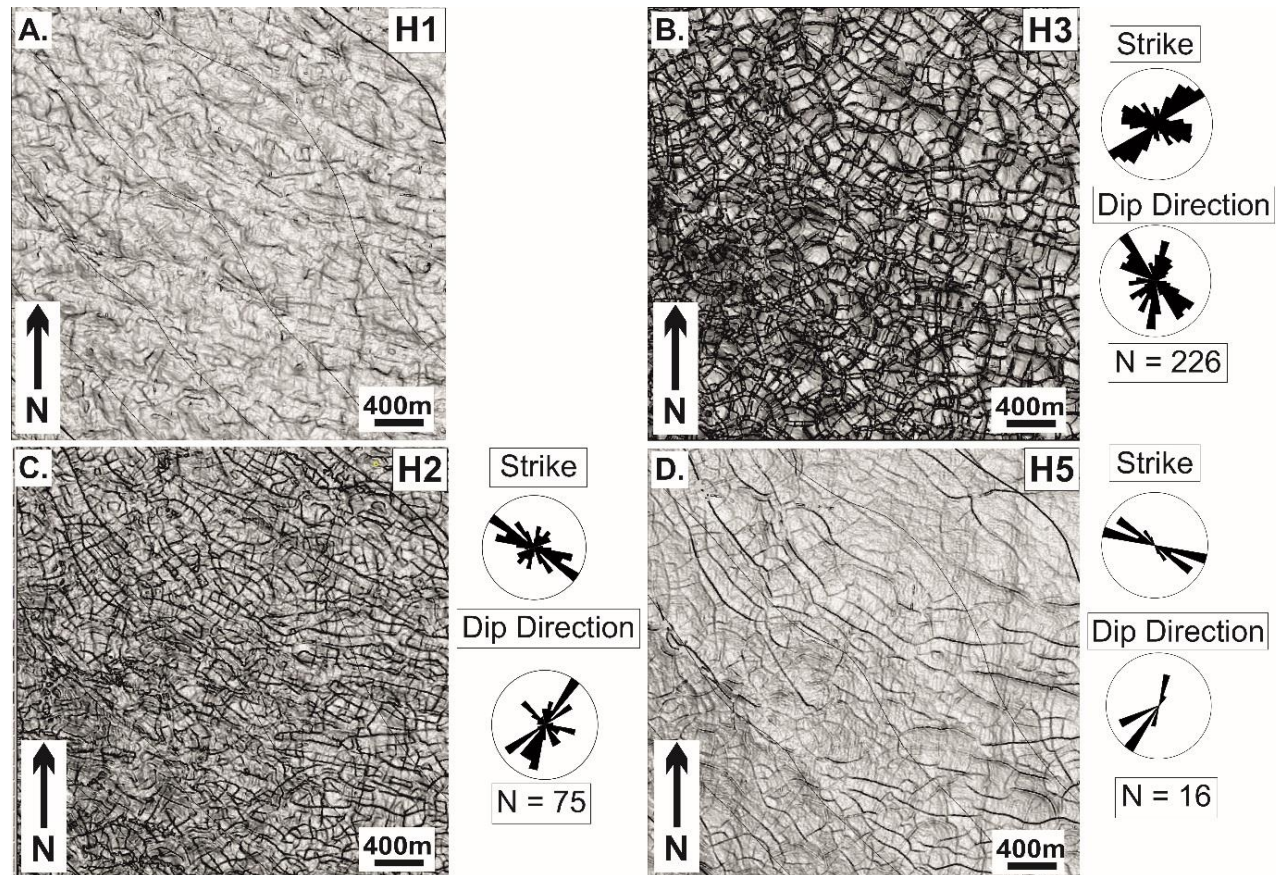


Figure 7.5: Time dip maps and rose diagrams detailing the orientation and apparent dip direction of polygonal fault traces at four different stratigraphic intervals within Unit 1. For horizon locations see Fig. 7.2. Note the low number of faults measured on H5 as only 16 of the dip anomalies expressed on the map display offsets

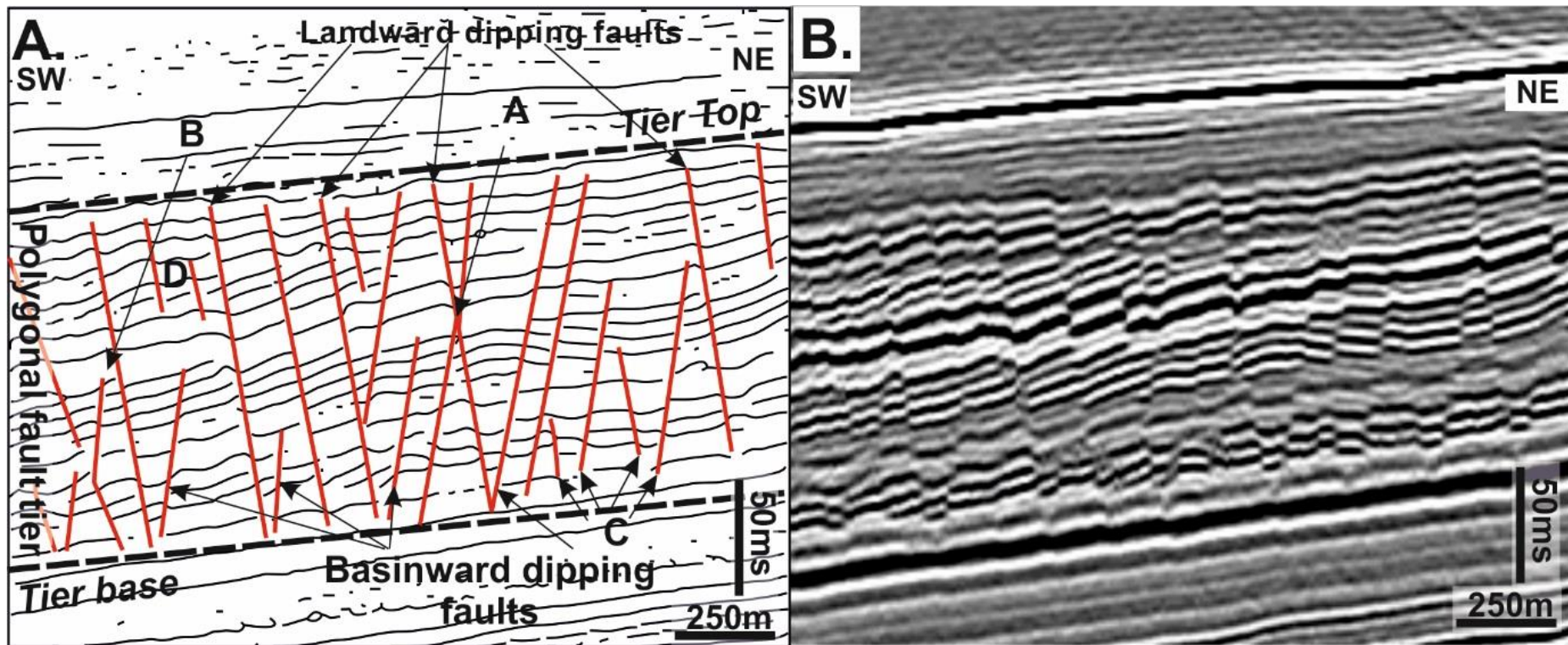


Figure 7.6: (A) Interpreted diagram of a seismic section through the polygonal fault network showing the key relationships present within the tier. (B) Raw seismic data with no interpretation

downslope fault (Fig. 7.6A). These latter faults can be classed as linked pairs because the strike and length of each fault is approximately the same. The basal tier boundary is defined as the reflection(s) within which the majority of the polygonal faults tip out. The boundary in this survey is diffuse across the tier, with basal tips confined to a series of layers and tipping out at various intervals located within three laterally extensive reflections between H3 and H5 that are within the lower third of Unit 1 and the upper third of Unit 2. Polygonal faults within the tier can interact to form conjugates where they intersect with another nearby fault (See A in Fig. 7.6A). As seen in B on Fig. 7.6A, upper fault tips also show an apparent restriction in the upper tip without abutting a nearby fault.

The polygonal faults slip sense is defined as synthetic or antithetic depending on the orientation of the fault relative to the slope (*sensu stricto* Stewart and Argent, 2000). The longest faults strike NW-SE and form an antithetic set dipping predominantly upslope, a relationship that is seen more widely in wedge-shaped tiers elsewhere (Cartwright, 2011; Clausen et al., 1999; Goult, 2001b). These faults generally have the largest maximum throw values and transect the entire tier. Their downslope dipping counterparts, occasionally reach the same height as their conjugate partners, but more commonly have their upper tips restricted by intersection. Conjugate pairs diverge upwards and in the upper half of the tier, with isolated faults occurring in the hanging walls in a manner reminiscent of the ‘space-filling’ faults of Lonergan et al. (1998)(e.g. point D, Fig. 7.6A).

Analysis of displacement profiles (i.e. throw versus depth plots) for a representative subset of these faults shows that there is no consistent pattern to vertical variation of throw on individual faults or as a group of faults (i.e. perturbed and ‘background’ faults, Fig. 7.9). The displacement profiles are highly variable from fault to fault and have no consistent position for displacement maxima (D_{max}) and minima (D_{min}), irrespective of fault height or proximity to the pockmark.

Variations in the stratigraphic position of displacement maxima and minima are known to be influenced by branch line intersections (Cowie, 1998; Cowie and Shipton, 1998; Maerten et al., 1999; Schultz, 2000; Willemse et al., 1996) as displacement and hence strain is shared across hardlinked fault branch lines (Maerten et al. 1999, Willemse et al. 1996). Dip linkage where two, initially isolated vertical fault segments

interact and coalesce into a single larger fault, typically show characteristic double displacement maxima (Baudon and Cartwright, 2008a; Cartwright et al., 1998; Childs et al., 1996; Laurent et al., 2012; Mansfield and Cartwright, 1996). Although not seismically resolved here, dip linkages may be present below the resolution limit and must be considered as a potential cause of some of the throw variations observed (Fig. 7.8). Similarly, lateral and stratigraphic changes in lithology may also be important as lithological variations, such as a transition from clay to sands, has been shown to influence the position of displacement maxima or to influence upper and lower tip positions (Gross et al., 1997; Rippon, 1984; Wilkins and Gross, 2002). Fault geometry above the buried pockmarks

The polygonal fault pattern above the pockmarks show systematic perturbation with preferential development of strongly curved fault traces that coincide with the edges of the pockmark crater (Fig. 7.9A). These perturbations are present in all the pockmarks in the study area with the exception of Pock6 (Fig. 7.9B).

Pock1, Pock2 and Pock3 are characterised by fault patterns involving a re-orientation of fault strikes from predominantly linear to curvilinear fault traces in the area immediately surrounding the pockmark. The pattern observed on dip and amplitude maps is typically a zone of curved fault traces that are crudely concentric to the edge of the pockmark crater and extend laterally up to 350 m from the pockmark crater into the surrounding tier for up to 350 m beyond the edge of the pockmark crater.

A series of time dip maps at different stratigraphic levels within the polygonal fault tier, show the location and dissipation of the perturbed fault pattern (Fig. 7.9). The pattern on horizons H5 and H3 is characterised by a zone of strongly curved faults surrounding the pockmark crater. Local horizons (H3a and H3b) show a clear zone of curved faults surrounding the pockmark crater (Fig. 7.9) with smaller faults forming at 90° to the curved faults. By H2, the curved fault pattern is much less defined, with faults displaying very little response to the pockmark, despite forming over the position of the pockmark crater. As such the perturbation of polygonal faults by the pockmark has all but disappeared from the time dip attribute map of H2 and the fault pattern over pockmark 1, 2 and 3 is almost indistinguishable from the surrounding array. Any trace of the fault pattern has ceased by H1 as the array tips out below H1.

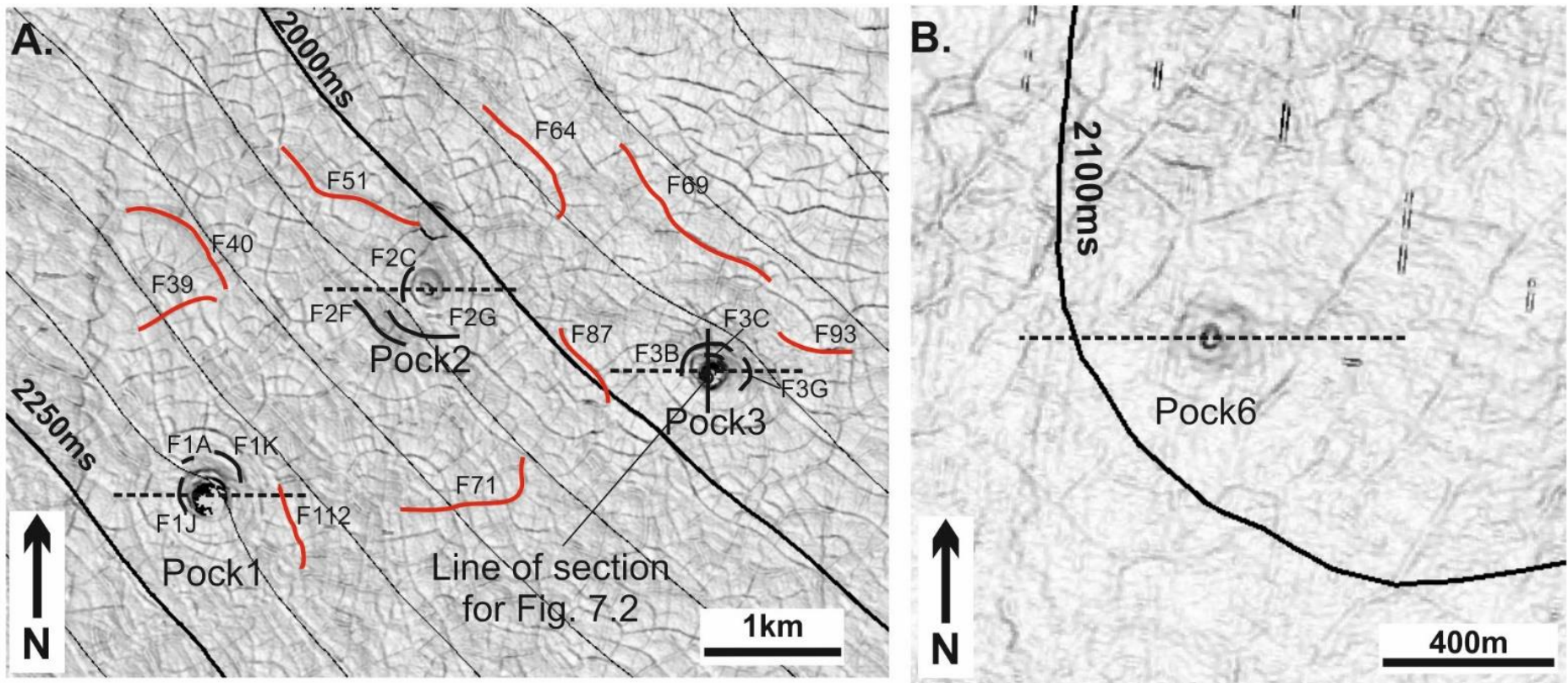


Figure 7.7: Time dip map of Horizon H5 showing the studied pockmarks and the surrounding fault patterns. (A) Shows the polygonal fault patterns in Area 1, including the faults used in the $t-z$ plots shown in Fig. 7.8 (Dashed lines indicate the line of section for Fig. 7.3A). (B) Shows Pock6 in Area 2. Note the lack of perturbed polygonal fault patterns around Pock6.

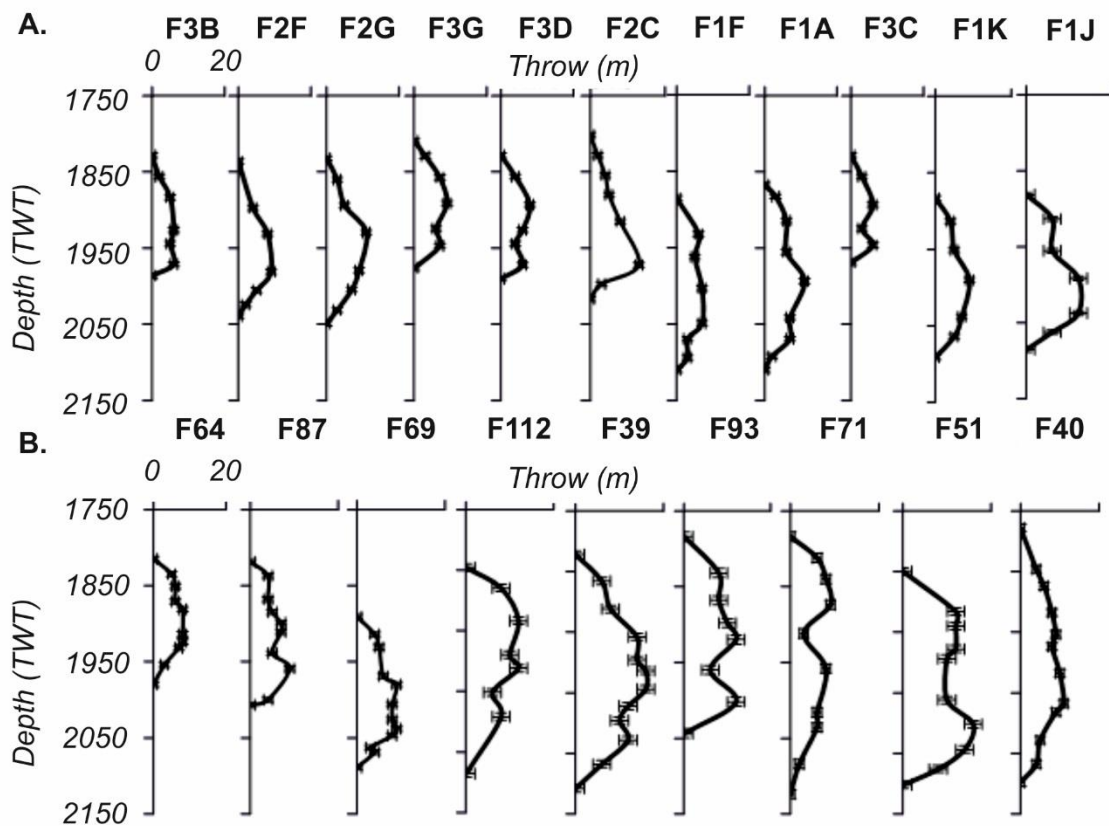


Figure 7.8: A selection of throw versus depth (t - z) plots from within the polygonal fault tier surrounding the pockmarks that show the variability in the position of displacement maxima and minima within the polygonal fault tier. (A) Refers to t - z plots from perturbed polygonal faults with the number corresponding to the pockmark. (B) T - z plots are from nearby background polygonal faults. For location of faults used in the t - z plots see Fig.7.7

In marked contrast, Pock6, displays none of the strongly curved fault patterns seen around pockmarks in Area 1. Around Pock6, the fault patterns are characterised by a ‘background’ pattern of a multi-azimuth striking fault array with no faults showing any alignment to the edge of the pockmark (Fig. 7.9).

Thickness variations expressed in the measured seismic sections (Fig. 7.10), clearly show a localised thickening focused over the pockmark crater between the H5 and H3 reflections. This residual topography in the lowest intervals in the polygonal fault tier is a function of the relief left from the initial crater formation as it was subsequently infilled. Pock1 and Pock3 are the widest and associated with the greatest residual topography on reflection between H5 and H3 reflection with both pockmarks displaying 9 m of relief change across the pockmark crater, whereas Pock2 and Pock6, and 6 m from flank to crater centre, respectively, across their pockmark craters. Moving up stratigraphy, the increase in thickness above the pockmarks generally declines (i.e. 5 m (Pock3) and 10 m (Pock1) at the level between H3 and H3a). Any thickness perturbations associated with Pock2 and Pock3 above the interval between H3 and H3a are masked by throws within the polygonal fault network. Perhaps the most striking observation is that the pockmark topography has effectively been fully annealed by the H3b-H2 isochron interval. Importantly, the annealing of residual pockmark topography between H5 and H3b coincides with the interval that contains the perturbed fault patterns seen around Pock1, Pock2 and Pock3 (see Fig. 7.9, Fig. 7.10).

It is apparent from the preceding data that there is a spatial relationship between the presence of a perturbed fault trace pattern surrounding the pockmarks and an increase in thickness across the pockmarks, associated with the residual topography of the partially infilled pockmark craters. Crucially, both the increase in thickness and the clearest perturbed fault trace pattern are localised to the lower third of the polygonal fault tier between the H5 and H3 interval (Fig. 7.9 and Fig. 7.10). With the loss of the increase in thickness across the pockmark as the topography anneals above the perturbed polygonal fault pattern rapidly dissipates back towards the ‘background’ fault pattern.

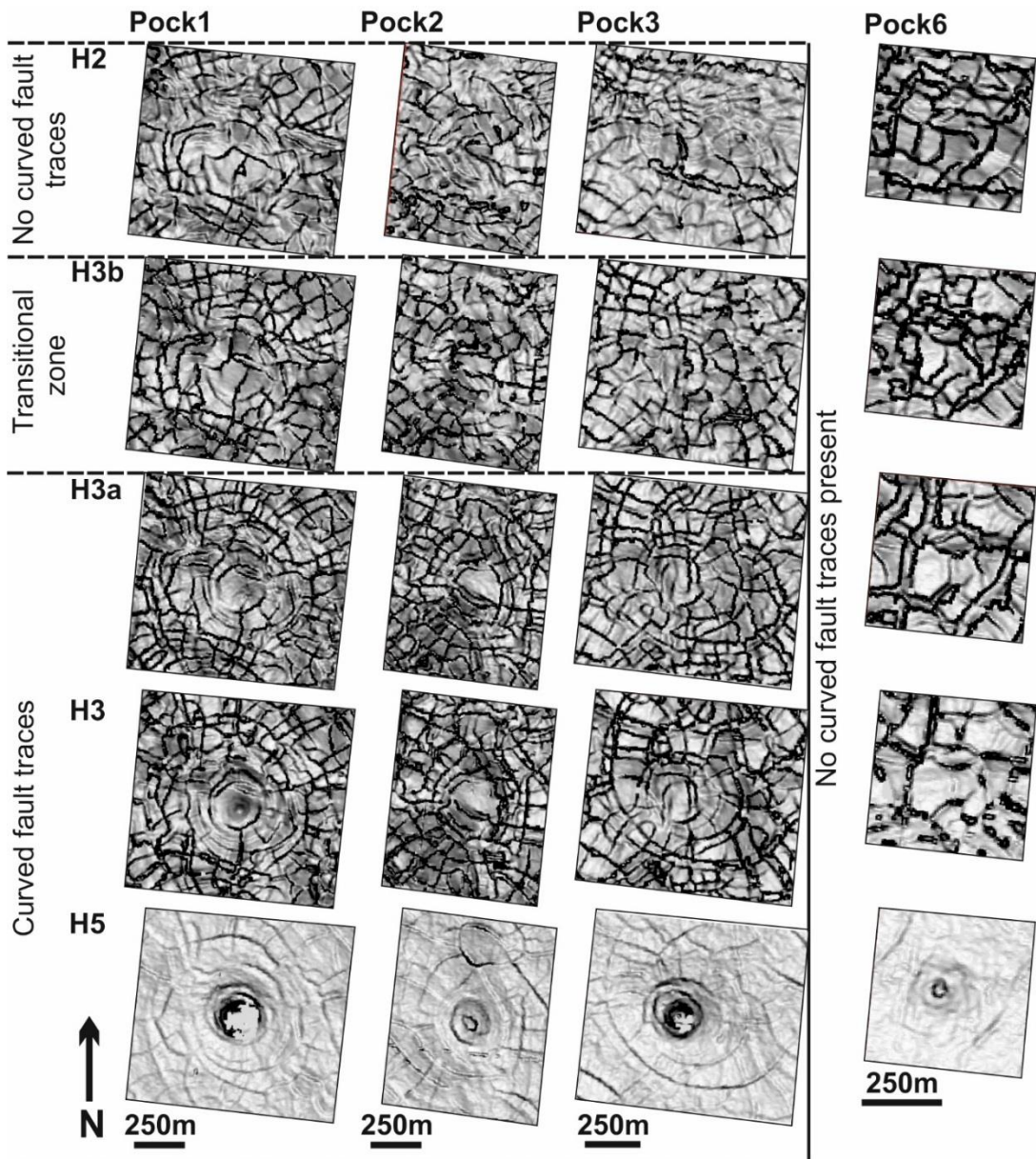


Figure 7.9: Seismic section and time dip maps of six key seismic horizons that display the change in the perturbation pattern through the stratigraphy of the polygonal fault tier overlying Pock1. The curved fault traces relate to faults that have been aligned to the edge of the pockmark crater within the lower third of the tier only. Note the absence of curved patterns around Pock6

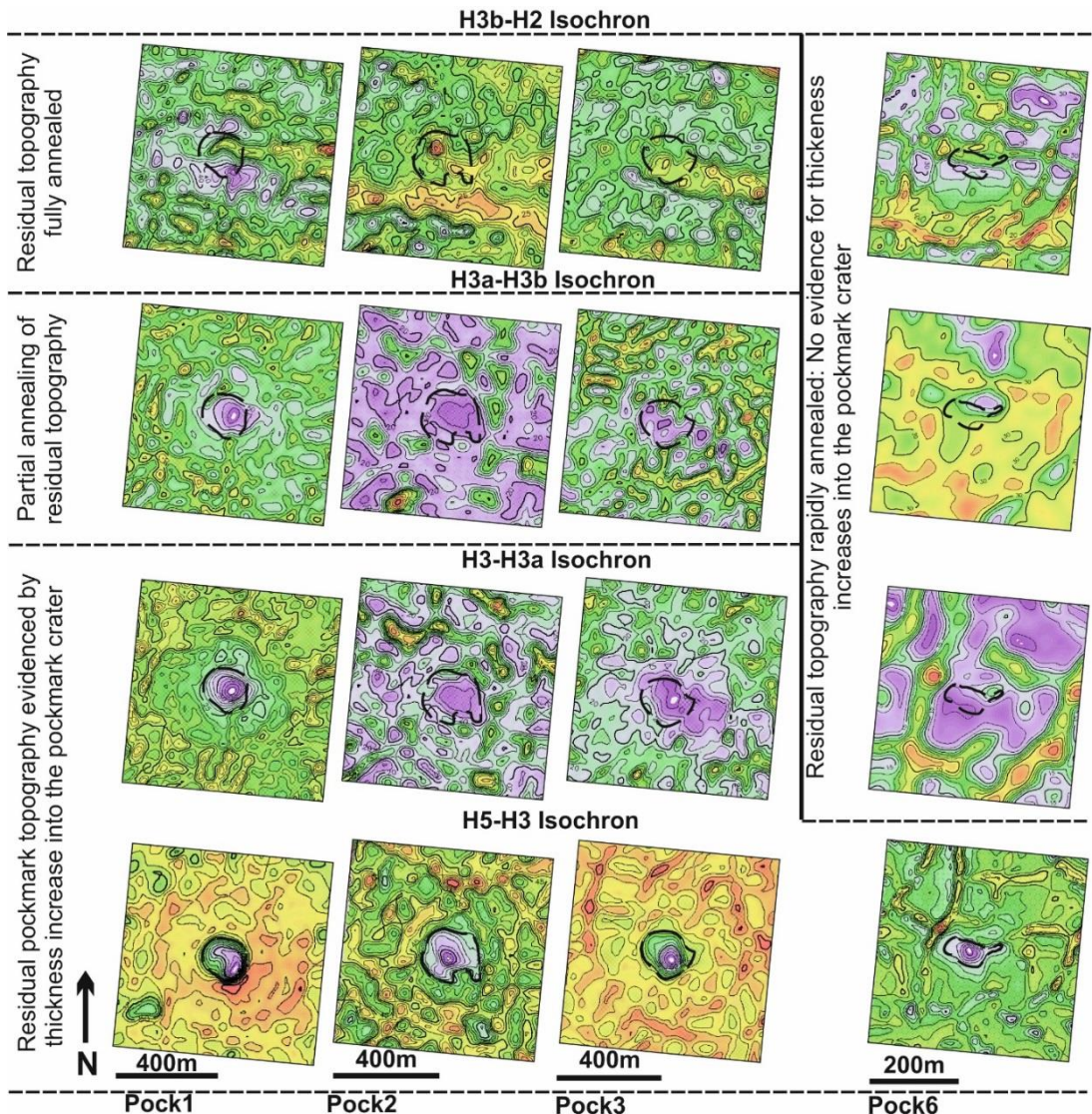


Figure 7.10: A series of TWT isochron maps across Pock1, Pock2, Pock3 and Pock6 showing increasing thicknesses (in purple) in the vicinity of the pockmark. Pock1, Pock2 and Pock3 show a thickness increase over the pockmark into the H3a-H3b isochron interval, before the residual pockmark topography is annealed at the H3b-H2 isochron interval. In contrast, Pock6 shows early residual topography in the H5-H3 isochron interval that was rapidly annealed after the H3-H3a isochron interval. The apparent patterns of thinning (yellow and red colours) within the Isochron maps coincide with the footwalls of polygonal faults as seen on the time dip maps in Fig. 7.9.

7.4 Discussion

7.4.1 *Evidence for early nucleation*

Following Carruthers et al. (2013), we suggest that there is strong evidence for perturbed local stresses as the likeliest explanation for the described changes in polygonal fault pattern around pockmarks, and we draw a loose analogy with their model of stress control of perturbed polygonal faults around salt diapirs. Secondly, and following directly from this view of local stress control on fault patterns, a strong argument can be made that the polygonal fault patterns must have been established early in the burial history of Unit 1, within the lower portion of the tier (Fig. 7.11). If fault nucleation had occurred at a level equivalent to the central portion of the tier (i.e. approximating the positions of displacement maxima) then no impact of the pockmark shape on the pattern would be observed, since the topography was fully annealed by the time the lower third of the tier thickness had been deposited. If the topography was annealed, and subsequent deposition was ‘layer-cake’ in geometry, it is difficult to see the smallest pockmarks shows the least thickness increases of 4 m what source of local stress anisotropy could have been so directly linked to the presence of the underlying, buried pockmark.

The initiation of polygonal fault growth has long been suspected to occur at relatively shallow burial depths, but estimates to date have been vague, and poorly constrained. Cartwright, (1994) argued that the 100–200 m thickness of tiers at their lateral margins in the North Sea Basin combined with recognition of small growth packages at the upper tips of some of the faults strongly suggested a shallow burial depth of less than a few hundred metres. Gay et al. (2004) also argued for a shallow burial depth based on a somewhat arguable link to ‘dewatering’ furrows developed at the seabed above polygonal faults offshore Angola. More recently, however, silica diagenesis has been suggested as a causal mechanism for fault initiation, and this would imply burial depths of perhaps >300 m owing to the specific temperature control of the silica phase boundary (Davies and Ireland, 2011). This study therefore presents strong constraints from two separate arguments (wedge geometry and buried pockmarks), that fault initiation occurred in the first 150 m or less of burial.

The observations presented in this study show that the background polygonal fault pattern of the polygonal fault tier developed within Unit 1 is locally perturbed by the presence of some, but not all the pockmark craters that formed close to the base of

Unit 1. Pock6 is a notable exception, but it differs markedly from the other seven pockmarks mapped in the study area by its small size. Interestingly, Pock2 and Pock6 are both positioned some tens of metres deeper in the stratigraphy relative to the base of the polygonal fault tier than the other 6 buried pockmarks. Despite this, a perturbation pattern is observed above Pock2 with only ca. 5 ms (4 m) of relief present at H5 whereas Pock6 with 7 ms (6 m) of relief at the same horizon (labelled a in Fig. 7.3a), displays no pattern change. The primary difference between the two areas is the relative relief of the slope on which the pockmarks occur. Pock6 occurs on a relatively flat lying region (see Fig. 7.7B), whereas Pock2 occurs on a marginally steeper slope (see Fig. 7.7A). Pock2 is also significantly wider (300 m) than Pock6 (150 m). Therefore the changes in relief associated with Pock2 are enhanced as the subtle dip changes associated with pockmark relief are over-steepened by the presence of a regional slope. The over-steepening influences the rotation of normal stress to lie perpendicular to the plane of shear stress that influences the propagation trajectory around the pockmark (Mandl, 1987). Furthermore, it is evident that central to the origin of the perturbation patterns is the depositional history of the fill of the pockmarks subsequent to the immediate crater forming phase. The pockmarks that show the clearest and longest-lived perturbed fault patterns are the largest in width and depth. The relative size of the pockmark is crucial as a large size (in terms of both width and depth) ensures that the pockmark generates and maintains bathymetric relief for a sufficient time span to be able to influence polygonal fault propagation. Pockmark longevity has been proposed to be proportional to the size of the pockmark with larger pockmarks taking longer to infill than smaller ones (Judd and Hovland, 2007) except in areas where sedimentation rates are high (Çifçi et al., 2003). Pock1 and Pock3 are large (>300 m) and as such these pockmarks would have been most likely to have residual topography for the longest time. Pock2 despite being of similar age to Pock6 and having much less relief than its younger neighbours at horizon H5, still displays a strong perturbation pattern well into the polygonal fault tier due to its large width. At this time there is insufficient data as to the actual sedimentation rate within the survey area and so it is difficult to constrain how rapidly the pockmark bathymetry was fully annealed. Nevertheless, it is important to note that Pock6 shows very subtle residual topography across the crater and would have been more easily annealed than its larger counterparts to the north.

One of the more striking observations found in the pockmarks with perturbed polygonal fault patterns is that the perturbation effect is only identifiable as being distinct from the local background polygonal pattern on horizons mapped through the lower two thirds of Unit 1 (Fig. 7.10) and that the perturbation zone extends laterally, well beyond the edges of the pockmark. This is despite the fact that the interval where thickness variation across the pockmarks is only located in the lower third in regions and directly above the buried pockmarks (Fig. 7.10).

The gradual dissipation of the perturbed pattern suggests that within shallow sections of the tier, the effect of pockmark relief is greatly reduced and horizontal stresses are also resolved to a state similar to that of regions where no pockmarks exist. Another important observation is that perturbed fault patterns are shown to gradually dissipate rather than abruptly terminate at a given horizon or reflection. It suggests that there is no discrete boundary within the tier that could be responsible for potential changes to the states of stress and hence influence changes in fault azimuth. This is also clear evidence to indicate that the sediments hosting the tier are behaving as a single mechanical unit. To account for the presence of the perturbation pattern beyond the pockmark crater the simplest conclusion to draw is that the perturbation pattern is the result of a two stages of fault development (see Fig. 7.11). The first phase of fault growth was located directly above the pockmark crater and strongly influenced by a relict topography resulting in an early forming concentric fault pattern directly above the pockmark crater. Evidence for these faults is seen where faults over the pockmark crater flanks detach slightly deeper than the surrounding faults (Fig. 7.3) and some have a D_{max} skewed towards the lower third of the tier (see Fig. 7.8, fault F1J). The second phase of faulting was perturbed by the state of stress around a pre-existing and growing fault set, confined to the area immediately above the pockmark crater.

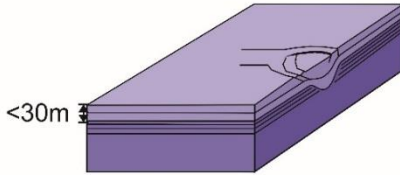
The case for early fault nucleation and growth is further strengthened when the context of this polygonally faulted tier is considered. The units hosting the polygonal faults form a wedge shaped body, offlapping the slope (Fig. 7.12A). At the upslope part of the wedge, the tier thickness decreases to less than 150 m with the upper tier boundary at or very close to the seabed. In some places, small-scale polygonal faults can be detected on this high resolution seismic at burial depths of ca.150 m (Fig. 7.12B). This implies that at least some of the polygonal faults in the study area formed at a shallow burial depth of 150 m or less. There is no geophysical reason to assume that the early

formation of polygonal faults at the shallowest end of the wedge could not apply to polygonal faults throughout the rest of the tier, as suggested here in the reconstruction presented in Fig. 7.11.

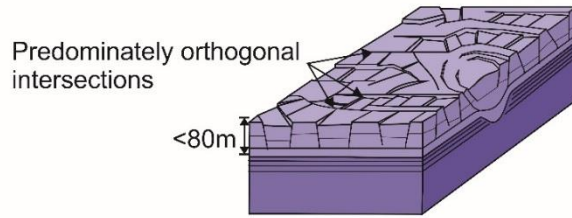
7.4.2 Stress anisotropy due to buried pockmarks

Having established a strong case that the perturbed polygonal fault patterns are directly related to the buried pockmarks, and drawn an analogy with stress control of radially and concentrically perturbed patterns of polygonal faults around salt diapirs, the question arises as to the mechanism by which a buried pockmark can produce such a localised perturbation of the background stress field? Polygonal fault patterns have been shown to be influenced by local anisotropy in the horizontal stress field. Cartwright (2011) reviewed a number of studies where polygonal faults were shown to be influenced by subtle changes in surface topography (slopes, or local topographic features due to differential compaction), and also by tectonic structures including salt diapirs and normal faults. Most recently, Carruthers et al., (2013) quantified the geometry of the perturbed horizontal stress field around salt diapirs by careful examination of the perturbed polygonal fault patterns, thus demonstrating the great potential to use polygonal fault patterns to infer palaeo-stress states associated with actively growing structures. Perturbed polygonal faults associated with buried pockmarks near the bases of tiers were described by Cartwright (2011) and the mid to lower third of tiers by Andresen and Huuse (2011). These latter authors linked the perturbed patterns to differential compaction across the pockmarks that in turn produced ‘subtle stress perturbations’ that were responsible for the observed relationships. Differential compaction can certainly modify local stress states in shallow burial conditions to the extent that shear failure and fault nucleation can occur (Price and Cosgrove, 1990). An excellent example of this process is presented by Davies et al. (2009) where irregularities in a silica diagenetic front induce surface topography by differential compaction folding, and faults then develop on crests or flanks of these folds. Differential compaction folds above buried sand-filled channels are well known in the petroleum industry both as subtle traps for hydrocarbons and as a means of generating local arrays of normal faults (Carver, 1968) and are often aligned above channel margins (Lonergan and Cartwright, 1999). Buried slope channels can even be identified by their impact on polygonal fault patterns, as exemplified by the Eocene slope channel systems of the North Sea Basin (Cartwright,

I. Early, compaction related concentric fault formation (H4)



II. Polygonal fault growth and early intersection (H3 - H3a)



III. Loss of concentric pattern near the upper tips (H2)

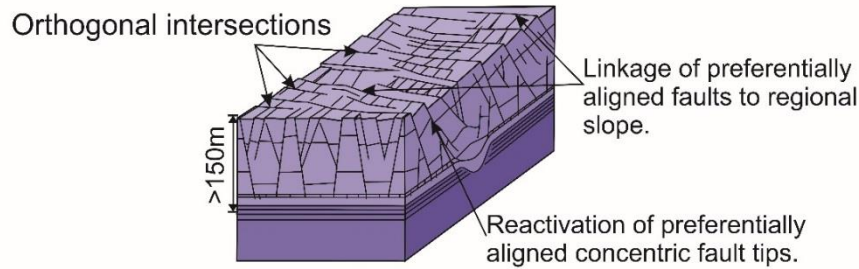


Figure 7.11: (I) Evolution of an early forming concentric fault pattern around the edge of the pockmark. The concentric fault is initially influenced by the presence of a slope, a relic from the infill of the pockmark. (II) Polygonal fault growth is influenced by the pre-existing concentric fault pattern present around the pockmark. Polygonal faults form early linkages between various branchlines, this is characterised by the lack of free tips and high connectivity between faults. (III) The perturbed polygonal fault pattern gradually dissipates with new space filling faults forming between pre-existing and preferentially aligned polygonal faults growing preferentially upwards from the lower third of the tier

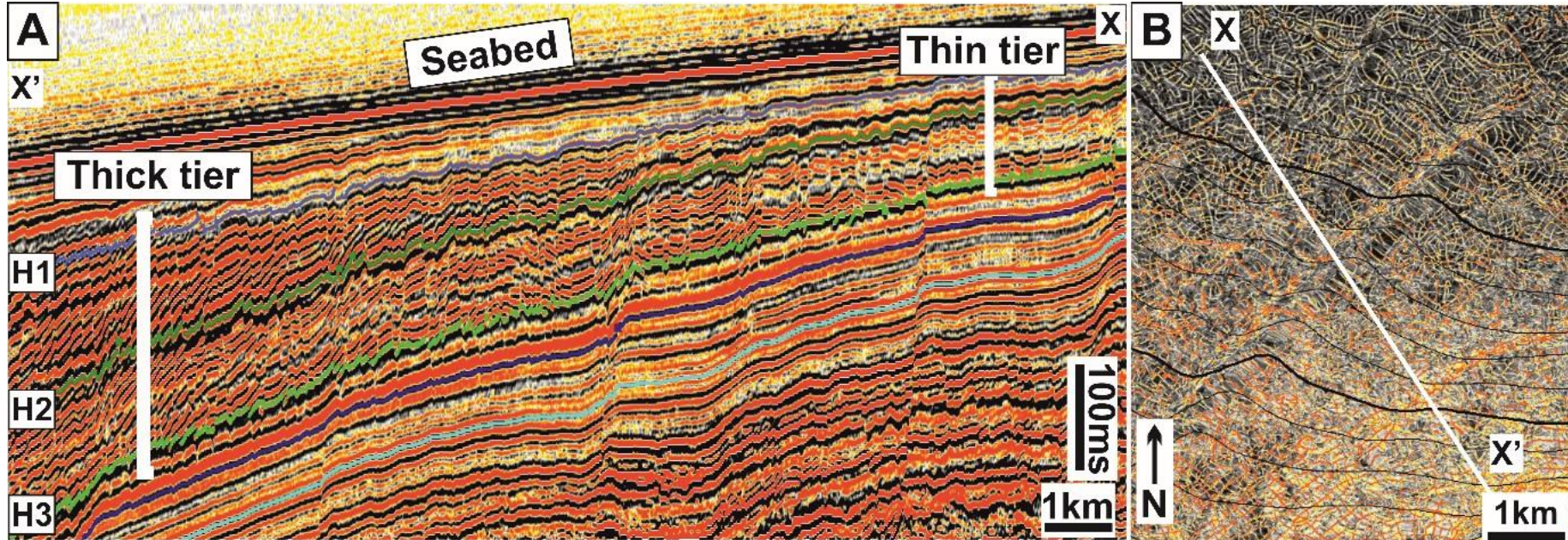


Figure 7.12: (A) A vertically exaggerated seismic cross section with high gain showing the wedge shape of the polygonal fault tier. Note the proximity of the thin faults to the sea bed near X, where the upper tips of polygonal faults die out at the H2 reflection. Where the tier thickens (X') the upper tips of the polygonal faults die out above the H1 reflection. (B) Time dip map of horizon H2 showing the geometry of the polygonal fault array seen to the SW of side of the survey.

2011). So it seems reasonable to consider that differential compaction would be at least partly responsible for the continued growth of the strongly curved faults that develop above the buried pockmarks as Andresen and Huuse (2011) suggested.

A second contributory factor that should be considered is the impact of local bathymetric relief on horizontal stress anisotropy. It has been widely observed that subtle topographic slopes of less than a few degrees exert a considerable influence on both strike and dip of polygonal fault systems, often skewing them considerably from a classical randomly oriented set into an array where the slope parallel strikes are dominant (Ireland et al., 2011). This skewing of fault strike is also seen in the current study area, in the preferential elongation of faults generally oriented NW-SE i.e. parallel to slope contours (Fig. 7.4B). This slope effect has been linked to simple gravity-induced stress anisotropy (Cartwright, 2011). Carruthers et al. (2013) discussed the possible impact of seafloor relief on the development of their perturbed patterns and also argued that stress anisotropy due to slope could have played a significant role. Given that pockmarks are by definition associated with localised gradient changes in near surface sediments, and that drape of the pockmarks can lead to persistence of the initial relief for considerable periods of time after their initial formation (Moss et al., 2012), it is suggested here that this topographic-gravitational effect arising from local changes in surface slope may have been a significant factor in the development of a gross horizontal stress anisotropy above the buried pockmark. In summary, it is suggested here that the presence of a slope from residual pockmark topography was sufficient to alter the state of stress by a subtle rotation of σ_2 to lie parallel to the edge of the pockmark crater, resulting in the curved fault pattern. A subtle change in dip could have had a profound influence on the strike of an incipient fault pattern (see Fig. 7.7 and Fig. 7.9), as seen more widely in the slope parallel elongation of the background polygonal faults (Fig. 7.4).

7.4.3 Implications for polygonal fault growth

The conceptualised growth history presented in Fig. 13 raises some interesting questions of wider relevance to the development of polygonally faulted tiers. Polygonal faults are classically seen as being excellent examples of blind faults, nucleating at depth, and then propagating radially from the nucleation site (e.g. Lonergan et al. 1998; Stuevold et al. 2003). However, the throw data for the faults in the study area show general maxima close to the centre of the tier, and some way above

the likely nucleation sites near the base of the tier, in the immediate post-pockmark infill succession (Fig. 7.8).

The traditional model for fault growth is suggested to be radial with growth nucleating from a central point of the fault, the D_{max} position (Barnett et al., 1987; Walsh and Watterson, 1988). It has also been suggested that radial growth can be modulated by other factors such as fault restriction or lithological variation (c.f. Nicol et al. 1996). Growth models for polygonal faults focussing on preferential upward propagation have been suggested previously (Cartwright et al., 2003; Imbert, 2009; Stuevold et al., 2003; Watterson et al., 2000). The evidence for some of these models has been based on conjugate pairs of faults showing the same or similar detachment positions (Imbert, 2009; Nicol et al., 2003) and D_{max} skewed towards the base of the tier (Watterson et al., 2000).

We propose a skewed radial fault growth model for this particular polygonal fault tier, that follows Nicol et al. (1996) and Wilkins and Gross (2002) in recognising the impact of strength variation due to burial depth and lithology as a major factor in throw distribution. As established in the previous section, the polygonal faults have been shown to have nucleated at very shallow depth. In this instance, there are two suggested mechanical boundaries to fault growth, the free surface near the seabed and the basal unit (Unit 2). Basal tip propagation is partially restricted by a mechanical boundary at the base of the tier, evidenced as a gradual tipping out of faults in the interval between H3 and H5. This is interpreted as evidence for a gradational change in mechanical properties with sediments becoming progressively stronger. This change in mechanical property may be partially evidenced by the increase in amplitude of the positive reflection between H4 and H5, which may be indicating a slightly harder lithology (see Fig. 7.2B, Fig. 7.3A and Fig. 7.12A). This boundary leads to the restriction of downward propagation. Given that fault height crudely scales to the height of the tier, it is not unreasonable to infer that there is a mechanical boundary present near the seabed. The sediments near the seabed become less consolidated and more porous (Kominz et al., 2011; Velde, 1996). This represents a zone of weak, unconsolidated sediments that would be unable to support shear offsets, arresting the vertical growth of upper fault tips. The presence of the two mechanical boundaries in the upper and lower tip positions could force faults to propagate preferentially laterally (Wilkins and Gross, 2002).

Initial fault growth occurs preferentially along the lateral tips, with the upper tips impeded by the seabed with basal tip propagation impeded by a mechanical layer at the base of the tier (Wilkins and Gross, 2002). The upper tip position is constrained by the position of the seabed and the mechanical properties of the units below it. This is best evidenced in Fig. 7.12 where the upper tip position cuts discordantly across the seismic reflections and lies parallel to the seabed. As subsequent layers of sediment are added and buried, polygonal fault upper tips are able to propagate towards the modern seabed in regions where sedimentation rate are highest, inferred here by the increased thickness of the wedge to the south-east and south west. Vertical growth is presumed to be blind as no seismically resolvable growth packages are evident at any level within the tier. Subsequent branchline linkages form the distinctive ‘ladder’ pattern very early on in the tier development to form the high degree of connectivity observed at the base of the tier. This model of growth has wider implications for other tiers with bathymetric features at their base. It also adds considerable constraint to the early history of polygonal fault tiers. This may be of vital importance when considering the role of polygonal faults in fluid flow within a basin. A recent field based study showed clear evidence of fluid within a potential polygonal fault planes from a polygonal fault array in Egypt (Tewksbury et al., 2014). This supports a growing body of evidence from seismic based studies which indicate that polygonal faults may be conduits for fluid flow within a basin (Berndt et al., 2003; Stuevold et al., 2003; Gay et al., 2004; Möller et al., 2004; Gay et al., 2006; Gay and Berndt, 2007; Hustoft et al., 2007; Sun et al., 2010; Seebeck et al., 2015). Therefore, constraining when polygonal faults nucleate and begin to grow is potentially an important consideration for the assessment of the integrity of regional top seals and hence hydrocarbon plays (Cartwright et al., 2007).

The upward growth model advocated here has implications for the genesis of polygonal fault systems, but a fuller discussion on genesis is beyond the scope of this paper. The conclusions of this study are in part limited by a lack of a widely accepted mechanism to create the initial fault array nucleating in the basal part of the tier.

7.5 Conclusions

1. From the observations of perturbed polygonal fault patterns above pockmarks developed at the base of the tier, the polygonal fault array in the study area initiated shortly after the deposition of H3.

2. The presence of polygonal faults in the thinnest part (c. 100 m thick) of the wedge-shaped tier implies that this is a maximum burial depth for initiation of these faults, and is therefore a valuable additional constraint for the inference of early burial nucleation elsewhere in the tier.
3. The perturbation of polygonal fault patterns is attributed to horizontal stress anisotropy due to the effects of reflect topography from the formation of the pockmarks.
4. Within the zone of perturbation, fault strike directions are polarised to propagate parallel to the edge of the pockmark and this perturbation zone is wider than the pockmark crater itself.
5. Stress anisotropy generated by slopes from residual topography from the infilling pockmark and growth may have been maintained by differential compaction across the crater of the pockmark.
6. This subtle stress anisotropy is confined to the lower third of the tier and is sufficient to alter the strike of incipient polygonal faults nucleating nearby.
7. A model for polygonal fault growth is presented consisting of three stages:(1) an initial lateral propagation phase, forced by mechanical boundaries at the top and base of the thin tier, (2) an early linkage phase as lateral tips interact and abut, followed by (3) a preferentially upward growth phase with basal tips restricted by a mechanical unit.

8 Discussion

8.1 Introduction

From the preceding chapters, there are a number of important observations in young and mature tiers that can be expanded on further to constrain how and when polygonal fault tiers grow and organise.

This section is divided into three parts, part one considers the significance and impact of localised perturbation patterns on polygonal fault tiers, assesses the utility of perturbed patterns in relative timing polygonal fault growth and finally considers the implications for polygonal fault growth and tier organisation. Part two examines the organisation of polygonal fault tiers by comparing and contrasting data from a young (West Africa) and mature (Norwegian Margin) survey. The final section examines the tier boundaries and considers the impact of changing mechanical conditions on tier organisation. This chapter concludes with a brief overview of the economic implications for polygonal faults.

8.2 The significance of small-scale perturbation patterns in polygonal fault tiers

Localised perturbation of polygonal faults patterns have been widely documented around hydrothermal vent complexes, salt diapirs, turbidite channels, tectonic faults and pockmarks. Previous authors have used the utility of using such perturbation patterns in polygonal faults to deduce timing, strain and mechanical stratigraphy of the units in which the polygonal faults are hosted (Hansen et al., 2005; Carruthers et al., 2013). To date, one study has used the perturbed polygonal fault pattern to comment on the timing of the polygonal fault array relative to hydrothermal mound (Hansen et al., 2005).

Chapters 6 and 7 explored this supposition further and examined the perturbation patterns surrounding pockmarks and hydrothermal vent complexes. Data in Chapter 6 shows perturbation patterns surrounding pockmarks slowly dying out in conjunction with the annealing of the pockmark crater. From this it is suggested that the polygonal faults formed very early within a hundred metres of burial and the perturbation around the pockmarks record a propagation trajectory of polygonal faults that is skewed preferentially upward.

In contrast, the perturbation patterns around the hydrothermal vent complexes (HTVCs) showed a different relationship. Statistical analysis of the dimensions of the

radially faulted area and various HTVC attributes inferred that the mound within the HTVC has a primary control on the dimensions of the radial faults. The majority of the radial patterns surrounding the 19 studied vents are constrained within a single 150 ms thick interval and many have displacements that are on or below the vertical resolution limit (4 ms or less). This results in a more ambiguous timing relationship between the perturbation pattern and the HTVC and ultimately leads to a conclusion that the radial patterns around the HTVC are more likely to be the result of a later compaction effect as opposed to an early forming perturbation.

8.2.1 Sources of anisotropy

In both the studied examples presented in Chapter 4 and 6, the key to generation of the perturbation pattern was horizontal stress anisotropy generated by either the pockmark or HTVC. Horizontal stress anisotropy is more typically associated with study of the perturbation of fractures in close proximity to faults (Cloos, 1955; Dyer, 1988; Rawnsley et al., 1992; Peacock, 2001). However, given that polygonal fault arrays are thought to form in broadly isotropic states of horizontal stress (Cartwright and Lonergan, 1996; Goult, 2001) there is a paucity in studies that explicitly tackle the root cause of horizontal stress anisotropy.

A study by Hansen et al. (2004) noted an interaction between polygonal and tectonic fault sets in a polygonal fault tier from offshore Canada. Hansen et al. (2004) suggest that the horizontal stress anisotropy is generated by a synchronous timing between tectonic and polygonal fault growth resulting in a stress perturbation. This study also noted that perturbation was best observed in high throw regions of the tectonic faults. Despite these observations, no further discussion on a stress perturbation mechanism was undertaken in this study. A more recent example of the perturbation of polygonal fault patterns was undertaken by Carruthers et al. (2013), who examined the origin of layer-bound radial faults around salt stocks in the Central Graben of the North Sea. Carruthers et al. (2013) suggest that the origin of the radial faulting seen around salt stocks is attributed to the horizontal loading of the sediment in the immediate vicinity of the salt/sediment interface, with the extent of the radial faults varying with the mechanical properties of the overburden.

Alternatively, stress perturbations have been suggested to be derived from differential compaction. A study by Andresen and Huuse, (2011) examined the perturbation of

fault strike in relation to a series of stacked pockmarks. The presence of perturbed fault patterns around the pockmarks was suggested to be linked to differential compaction across the pockmark crater.

Horizontal stress anisotropy generated by tectonically induced changes in local stress fields by either faults (c.f. Bai et al., 2002; Maerten et al., 2002; Hansen et al., 2004) or salt stocks (Davison et al., 2000; Stewart, 2006; Carruthers et al., 2013) is reasonably well constrained. However, differential compaction derived horizontal stress anisotropy (*sensu* Andresen and Huuse, 2011) is far more subtle and, whilst differential compaction is widely described in seismic (Williams, 1987; Xu et al., 2015; Alves, 2010) and field studies (Saller, 1996; Hunt et al., 1996; Rusciadelli and Di Simone, 2007), the mechanisms for creating horizontal stress anisotropy via differential compaction is poorly understood. From the previous studies on polygonal fault pattern perturbations and the work presented in Chapters 4 and 6, differential compaction is proposed to be a major contributing factor in generating horizontal stress anisotropy either through the warping and folding of sediments over relict topography or through creation and attenuation of slopes.

8.2.1.1 Differential compaction

In both examples of perturbed polygonal fault arrays around pockmarks and HTVCs, there is evidence for downwarping and bending of reflections over inherited topographic relief. The style of folding is paramount to the generation of any incipient fault or fracture pattern as the folding mechanism ultimately defines the states of stress (Withjack and Scheiner, 1982). A forced fold is defined as a fold which has its shape and trend defined by a pre-existing feature beneath it (Stearns, 1978; Cosgrove and Ameen, 1999). In contrast, buckle folds are formed during layer parallel compression (Cosgrove, 1999). To generate the differential compaction effect, as implied by the definition of Stearns (1978), there is a prerequisite for a mechanical stratigraphy between the polygonal fault hosting unit and the unit with residual topography. In offshore Angola, the perturbed polygonal fault array overlie pockmarks contained within an unfaulted hemipelagite whereas on the Modgunn Arch, the biosiliceous ooze hosted radial faults around the HTVCs are found above the tuffaceous clays of the Tare formation. These mechanical stratigraphies are important for two reasons. Firstly, they resist the compaction from overburden and maintain residual topography and

secondly, they force the overlying reflections to downwarp due to the differential compaction effect (Fig. 8.1).

Laubach et al. (1999), described structures within coal seams and noted the shift from sub-vertical (Mode I) coal cleat to (Mode II) normal faults, localised above sandstone lenses in field outcrops from the Cretaceous and Tertiary coal beds of the Western USA. From these observations, Laubach et al. (1999) generated a 2D finite element model to examine the stresses and strains imparted on a coal seam which is partially underlain by a sandstone body during compaction. They note that the shear stress and strains that favour normal fault formation are localised in seam above the edge of the sandstone body. From this model and the field observations, Laubach et al. (1999) indicate that the geometry of the sandstone lens is a controlling factor and that the bending of a coal seam during compaction is more pronounced where the sandbody abruptly terminates. As indicated by Laubach et al. (1999), lithology is an important factor in differential compaction, in particular is the rate at which the pore space collapses. Porosity reduction is dependent on bulk lithology (Velde, 1996; Hunt et al., 1996; Kominz et al., 2011) and depositional architecture (Praeger, 2009), with compaction triggered by loading (Rusciadelli and Di Simone, 2007). In instances where lithology changes, for example transitions between sandstone to shale, compaction coefficients can vary enormously and can be sufficient to either generate shear failure (Carver, 1968) or differential stress (Bjørlykke and Høeg, 1997). Differential compaction can also be influenced by the distribution of sediments. As shown by Williams (1987) in a study from the Madeira Abyssal plain, vertical shear stresses arise as a result of differential compaction between sediments of different thicknesses (Fig. 8.2).

8.3 Nucleation and evolution of tiers

Having discussed the implications for small-scale perturbations in polygonal fault pattern and how they relate to timing polygonal fault nucleation, it is necessary to describe and account for the development of polygonal fault tiers, specifically, the internal organisation of polygonal faults within a tier.

As described in Chapter 4 polygonal faults in the West African Margin formed soon after burial with complex branchline linkages forming within the first 150 m of burial with a high degree of connectivity within the array. One of the key observations from

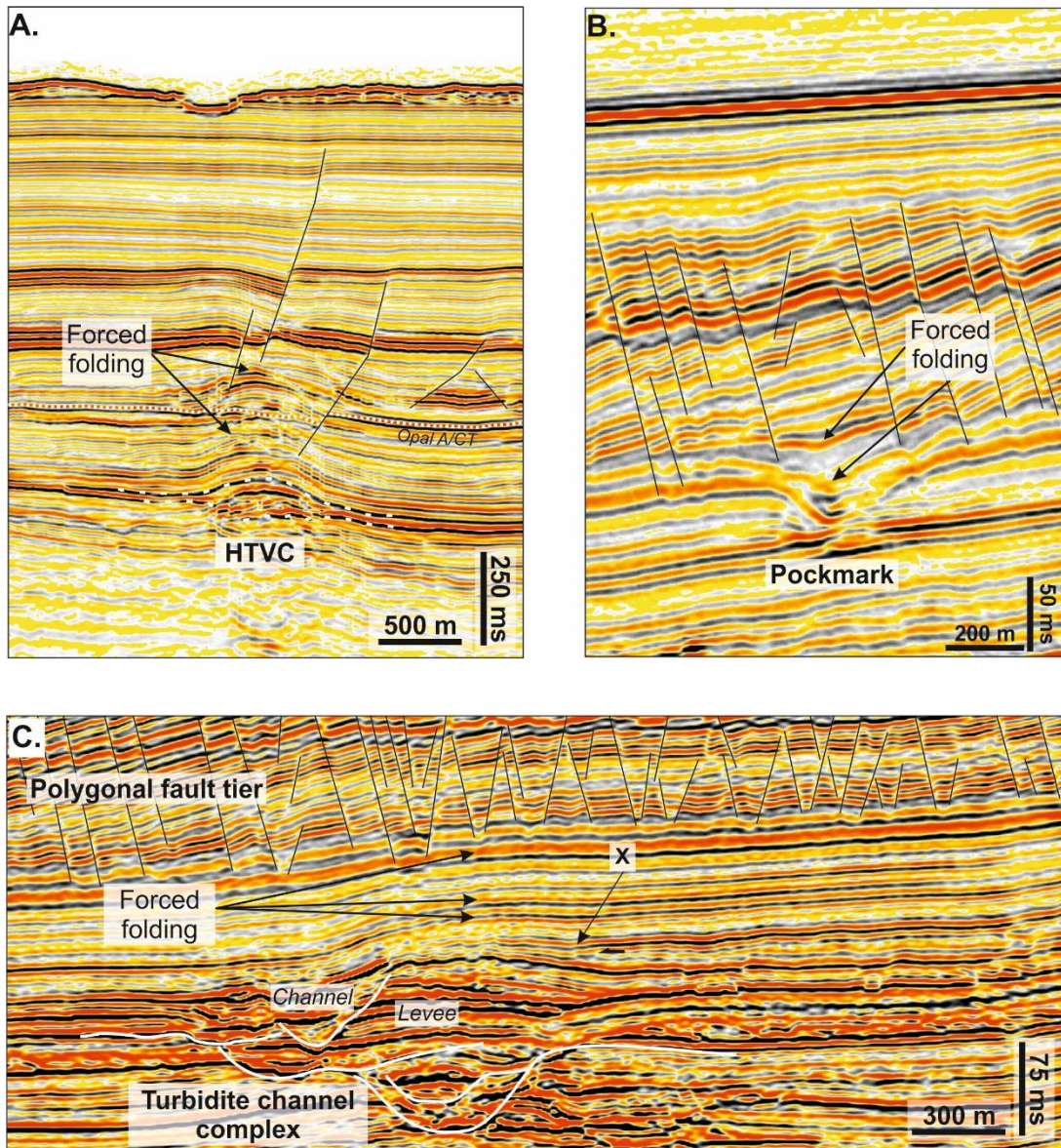


Figure 8.1: (A) Seismic cross section across a hydrothermal vent from the Norwegian Margin showing the forced fold above the vent. (B) Seismic cross-section across a pockmark from the Angolan Margin showing subtle folding above the pockmark crater (C) A seismic cross-section across turbidite channel from the Angolan Margin showing weak folding of hemipelagic drape by differential compaction. Evidence for folding over the turbidite is seen in feature X, whereby a reflections above a small onlap are downwarped in response to the overburden

this tier was the description of proto-master faults; these proto-master faults are precursors to the full size master faults of Cartwright (2011) that help constrain the upper and lower tier boundaries and are the largest faults in the array. Accompanying the proto-master faults was the increase in the variability in tier height where polygonal faults in the shallowest section of the tier are almost homogeneous in terms of their height and become increasingly more heterogeneous with increasing burial. In Chapter 4, the deeply buried mature tier of the Norwegian margin was used to examine the organisation of polygonal faults after significant burial and during diagenesis. This study noted a number of key spatial organisational differences within the tier. Integral to these organisational differences was how master faults exert a local influence the array and how diagenetic changes alter the accruement of displacement and restrict upper tip positions.

These studies together create a composite model for tier evolution through time from shallow to deep burial. The preceding sections now examine the commonalities between both tiers and comment on the implications for the development of polygonal fault tiers through time

8.3.1 Nucleation

One of the primary difficulties in establishing when polygonal fault nucleation occurs is the lack of constraint on the actual genesis mechanism. To date there are five main mechanisms including the process of syneresis (Dewhurst et al., 1999), diagenetically induced shear failure (Shin, 2009), silica diagenesis (Davies and Ireland, 2011), differential compaction (Davies et al., 2009) and density inversion (Henriet et al., 1989; Watterson et al., 2000). Each of these mechanisms operates under potentially very different diagenetic and burial conditions. Many of these studies are derived from observations in seismic data, in tiers that are hundreds of metres thick, where the sedimentology and diagenetic pathways are often inferred. These studies offer limited options for a constrained temporal interpretation of polygonal fault nucleation.

Most polygonal fault genesis mechanisms would appear to imply a degree of burial, which is an implicit part of many of the conceptual diagrams on polygonal fault nucleation (see discussions in James et al., 2000; Cartwright et al., 2003; James et al., 2006; Goult, 2008; Cartwright, 2011). Burial is necessary to either reach a minimum geothermal condition to start diagenesis (Davies and Ireland, 2011; Davies et al., 2009)

or to generate under-compaction overpressure in a particular unit (Henriet et al., 1989; Watterson et al., 2000). However, the amount of burial required for polygonal fault formation is at present unknown. The numerical models of Shin et al. (2008) suggested that mineral dissolution strain softens the sediment column and permits shear failure. The DEM models of Shin et al. (2010) could apply to other diagenetic processes that could produce strain softening such as mineral phase changes, particle size redistribution and authigenic mineral growth. However, many of these diagenetic processes such as mineral dissolution and authigenic mineral growth occur under specific burial conditions. The specific burial conditions (pressure temperature, solubility, mineral concentration etc.) needed to force mineral dissolution and authigenesis will vary for clays, siliceous oozes and chalks, as well as from basin to basin.

Additionally, the diagenetic reactivity of sediments can be enhanced by the presence of volcanic glass, organic material and biogenic silica (Opal A), which are some of the most reactive components (Hesse and Schacht, 2011). Volcanic ash is highlighted in a number of studies that examine various aspects of the stratigraphic sequence that hosts polygonal fault tiers in the Nankai trough (Heffernan et al., 2004). These shallow polygonal faults are hosted within a sequence of smectite rich clays with interbedded ash layers, minor turbiditic sands and silts and siliceous claystones (Moore et al., 2001; Wilson et al., 2003; Spinelli et al., 2007; Praeger, 2009). Wilson et al. (2003) noted that the ash layers, found in the Upper Shikoku basin facies, have undergone varying degrees of alteration, with deeper ash layers showing more alteration than shallow layers. Praeger, (2009), observed a close association between the throw maxima on polygonal faults and diagenetically altered ash layers. As noted by Cartwright, (2011) the diagenetic sequence is unknown within the Shikoku Basin facies but many of the siliceous claystones found in the Lower Shikoku basin facies, show minor amounts of volcanic glass as well as zeolites and opal CT suggesting a potential volcanic origin (Wilson et al., 2003; Cartwright, 2011). Indeed, Cartwright (2011) reviewed the Nankai trough polygonal faults along with a case study from Norway to suggest that ‘early’ diagenesis can cause shear offsets in buried sediments. Cartwright (2011) proposes three candidate reactions; dissolution of detrital carbonates, the dissolution of cement phases and the mineralisation of organic material.

8.3.1.1 Shallow versus deep nucleation?

Early polygonal fault growth was first suggested by (Cartwright, 1994) based on the presence of faults in thin sediment accumulations near the margins of polygonal fault tiers. Gay et al. (2004) also presented reconstructions of a polygonal fault tier in the Lower Congo Basin that suggested polygonal fault growth could occur within 70 m of the present day seabed. Other studies use the presence of growth strata in the lower third of the polygonal fault tier to infer shallow growth (Hansen et al., 2004). Sub-seismic scale polygonal faults, with centimetre scale displacements have also been observed in pinger data, within glacio-lacustrine clays, a few metres below the bottom of Lake Superior (Cartwright et al., 2004; Watrus et al., 2003) as well as in biosiliceous sediments 30 – 50 m below the seabed in the Hatton Basin, NE Atlantic (Berndt et al., 2012).

The polygonal fault tier described in Chapters 4 and 5 strongly indicates that polygonal faults can, in some instances, nucleate under very shallow burial conditions (see Chapter 4 for more detail). At the upslope part of the wedge, the wedge thickness decreases to less than 120 m with the upper tier boundary at or very close to the seabed, and in some places, small-scale polygonal faults can be detected on this high resolution seismic data at burial depths of ca.70 m. This implies that at least some of the polygonal faults in the study area formed at a shallow (<100 m) burial depths (see Chapter 4). However, whilst polygonal fault arrays can clearly be hosted at shallow depth, at present there are few polygonal fault genesis mechanisms that can account for their presence at such depths.

Diagenesis, in the context of polygonal faulting, is proposed to be a continuum in which the changes in the chemistry and structure of the sediment are manifold. Particular aspects of diagenesis, such as mineral dissolution (Davies et al., 2009; Davies and Ireland, 2011; Shin et al., 2010) have been interpreted as causative mechanism for polygonal fault nucleation. Mineral dissolution is part of a gamut of chemical reactions and processes that operate in and near the water-sediment interface but to date, only mineral dissolution as a diagenetic process is explicitly considered in polygonal fault genesis studies (Davies et al., 2009; Shin et al., 2010; Cartwright, 2011; Davies and Ireland, 2011; Roberts, 2014). It is also important to note that all studies that consider mineral dissolution as a causative mechanism are based in either calibrated seismic data (Davies et al., 2009; Davies and Ireland; 2011) or numerical

	Temp (°C)		Material source reactions in mudstones				
	10°C	70°C	Clay mineral changes	Minerals destroyed	Organic Matter	Pore space	Pore water expulsion curve
Surface -			Ion exchange reactions	Amorphous materials $\text{Fe}_2\text{O}_3\text{nH}_2\text{O}$, $\text{Al}_2\text{O}_3\text{nH}_2\text{OSiO}_2$ Unstable in pore waters	Microbal O_2 and SO_4^{2-} Fermentation and microbial CH_4 production	ca. 70%-80% porosity	Carbonate saturated; calcite, dolomite, siderite cements
ca.1 km -			Smectite/Illite conversion		Organic acids CO_2 , H_2O , H_2S	Mechanical compaction	ca. 20% porosity

Figure 8.3: Modified from Worden and Burley 2003. A summary table of shallow diagenetic processes within mudstones

modelling (Shin et al., 2010), without direct observation from core samples taken from within the polygonal fault tier. Despite this, mineral dissolution has been submitted as a causative mechanism for polygonal fault nucleation.

8.3.1.2 *Nucleation position*

Having established that polygonal faults can be hosted in comparatively thin sediment accumulations (<150 m) and that low temperature diagenesis has a range of volume reducing mechanisms that could accommodate faulting, it is necessary to examine the distribution of nucleation points within an incipient polygonal fault tier.

Based on observations made in Angola, polygonal faults are distributed fairly uniformly within a particular sequence of reflections at the base of the tier at shallow depth (See Fig 5.7 Chapter 5). This would suggest that the nucleation position is focussed towards the base of the tier (synonymous with the Trigger interval of Goult, 2001). In contrast, polygonal faults of the Modgunn Arch have faults distributed through a number of formations with numerous displacement maxima positions. This geometry could support either; a) single nucleation positions (as seen in the Angolan Margin) or alternatively, could support a dispersed nucleation model possibly with displacement maxima corresponding to the nucleation points (*sensu* Barnett et al. 1987).

These models imply very different growth mechanisms for polygonal faults. The nucleation of faults in the dispersed nucleation model is suggested to be more akin to radial faulting where faults can grow radially through the sediment from a fixed position (i.e. the displacement maximum, after Barnett et al., 1987). The focussed model suggests nucleation in the lower third of the tier with fault preferential tip propagation (usually the upper tip).

Whilst it is important to note that these are end member models and natural datasets may have a combination of both mechanisms, the proposed nucleation geometry is suggested to be more aligned to a focussed nucleation position, typically towards the lower third of the tier. This is evidenced from natural and modelled datasets. As demonstrated in Chapters 4 and 5, from the Angolan Margin, polygonal faults can nucleate in the lower third of the tier whereby examination of polygonal faults at different wedge thicknesses (analogous to burial depths) showed progressive upward growth with increasing burial. Crucially, the increasing burial also shows progressive

restriction of upper tips as fault tips converge, creating triangular abutments between faults with opposing dips. In the mature tier of the Modgunn Arch, similar triangular abutments are also found in the lower third of the tier. Using the geometries of the Angolan margin and applying them to a mature tier, it is suggested that there is a strong case for focussed tier nucleation.

Additionally, recent work by Roberts, 2014, numerically modelled polygonal fault nucleation undergoing gravitational loading, hemipelagic sedimentation, chemically induced porosity reduction and high geothermal gradients, conditions which are analogous to those found in the Nankai trough polygonal faults (see Heffernan et al., 2004). The models of Roberts (2014) show that polygonal fault nucleation occurs in the lower third of the polygonal fault tier, near the base of the tier with polygonal faults showing broadly consistent fault heights (Fig. 8.4), These faults evolve through time to form an array akin to what has been widely described in polygonal fault literature.

8.3.2 *Tier boundaries*

Tier boundaries are fundamental aspects of polygonal faults tiers for defining and constraining their stratigraphic position. The upper tip position of polygonal faults is defined as the first horizon at which there is no seismically resolvable deformation (either by offset or fault tip monoclines, see Chapter 2). Upper tier boundaries are either constrained by a single reflection or contained within several reflection cycles.

Tier 1 polygonal faults in the Modgunn Arch region terminate at the Plio-Pleistocene unconformity (PPU). Well data that intersects the southern half of the survey shows that the unconformity is characterised by a thin shale horizon. Above the PPU sedimentation switches from biosiliceous oozes of the Kai formation to glaciogenic clays and minor sands of the Naust formation, characterised by increases in gamma and density (Bøe et al., 2000; Bünz et al., 2003; Chand et al., 2011; Dalland et al., 1995; Eidvin et al., 2007; Swiecicki et al., 1998). The significance of upper tip restriction at regional unconformities has been proposed to indicate the cessation of polygonal fault activity (James et al., 2006; Neagu et al., 2010) or where polygonal faults cross an unconformity surface, they can be interpreted to be reactivated (Baudon and Cartwright, 2008; Neagu et al., 2010). Subsequently, the polygonal faults in Tier 1 of the Modgunn Arch survey can be interpreted as inactive and thus temporally constrained by the unconformity surface.

Multi horizon upper tip terminations are only observed in Tier 1, Lower Congo basin. The upper tip position of Tier 1 covers a series of reflections from H5 where the wedge thins to 150 m to H9 where the wedge thickness is 350 m. The upper tip position is generally less than 60 m from the present day seabed, although some polygonal fault upper tips are within 30 m of the seabed. Clearly, this polygonal fault tier is not defined by lithological variation within the tier or temporally by a single horizon and was interpreted in Chapter 4 that the polygonal fault tips reach mechanically incompetent unit that cannot support shear offset located below the seabed.

A comparison of upper tip gradients of polygonal faults in both the Norwegian and West Africa Margins reveals that the upper tips of both fault sets, despite the differences in geometry and configuration compare well and the majority have basal tip gradients of <0.3. This would indicate that the upper tips of polygonal faults despite the obvious differences in burial depth and lithology share similar displacement characteristics.

One of the impediments to resolving the upper tip position is the question of whether polygonal faults have active or inactive tips. James et al. (2006) discuss polygonal fault tip activity in the North Sea and briefly consider the uncertainty as to whether polygonal fault tips in the region are presently active. Given the proximity of the Angolan polygonal faults to the modern day seabed, it seems likely that they are active and undergoing blind growth, especially when seismic resolution limitations are factored in (see 8.3.3.1 for further discussion on seismic resolution). In contrast, the polygonal faults of the Modgunn Arch are likely to be inactive as many of the faults are buried by up to 300 m of unfaulted glaciogenic clays of the Naust formation.

Basal tier boundaries are the reflection(s) underlying a polygonal fault array that contain the basal tips of a polygonal fault array. From the two tiers described in this thesis, only two types of basal tip boundary are recorded those with single reflection tier boundaries and those tiers with basal tips with in a package,

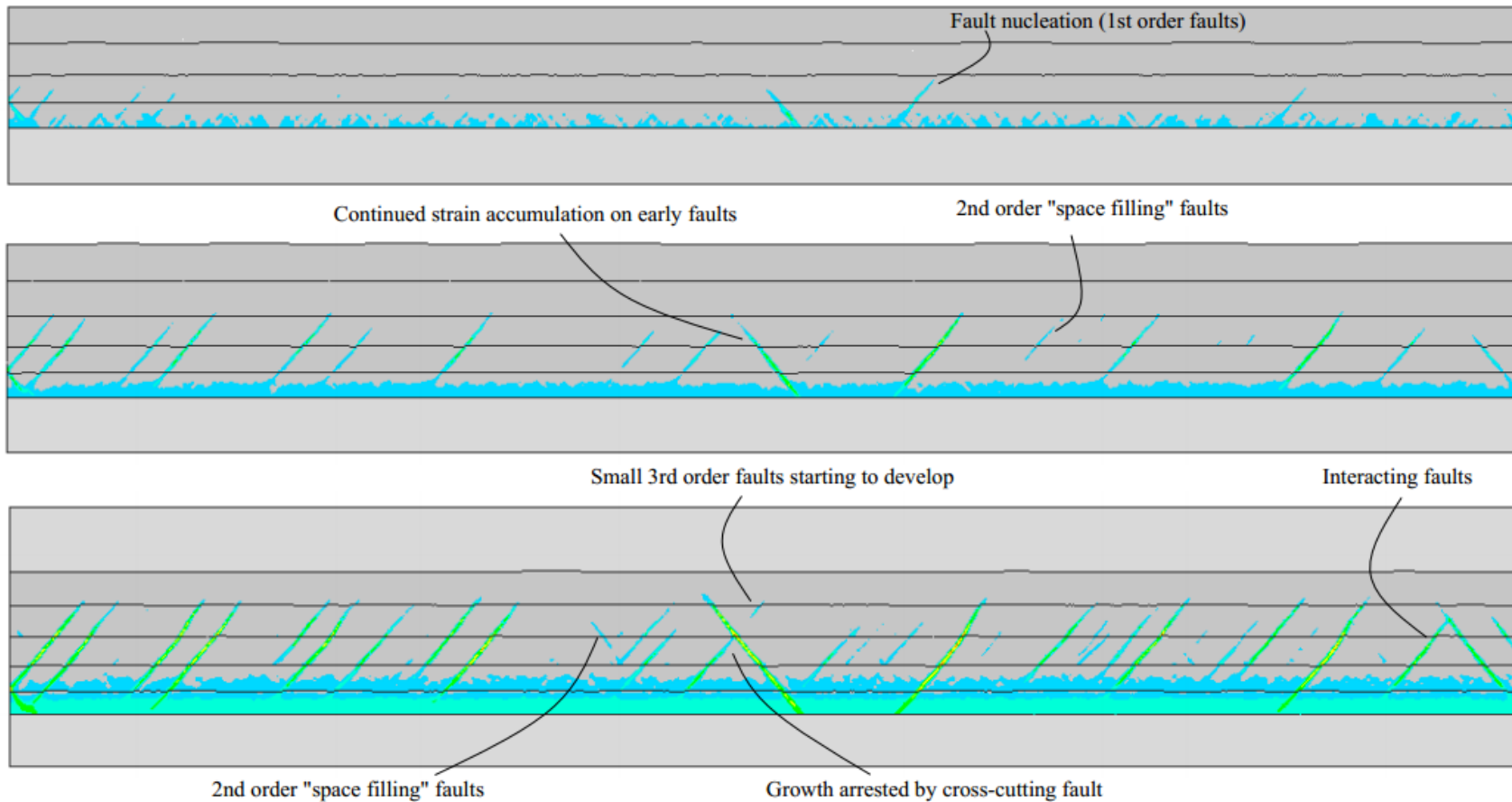


Figure 8.4: From Roberts (2014) A 2D numerical model of polygonal fault evolution simulating fault growth over several million years in diatomaceous mudstone (darker grey). The light blue areas simulate plastic strain from chemically reactive zones (a proxy for shallow silica diagenesis) and the light grey non-reactive sediments. Note the natural formation of an ordered hierarchy of polygonal fault growth as well as triangular abutments

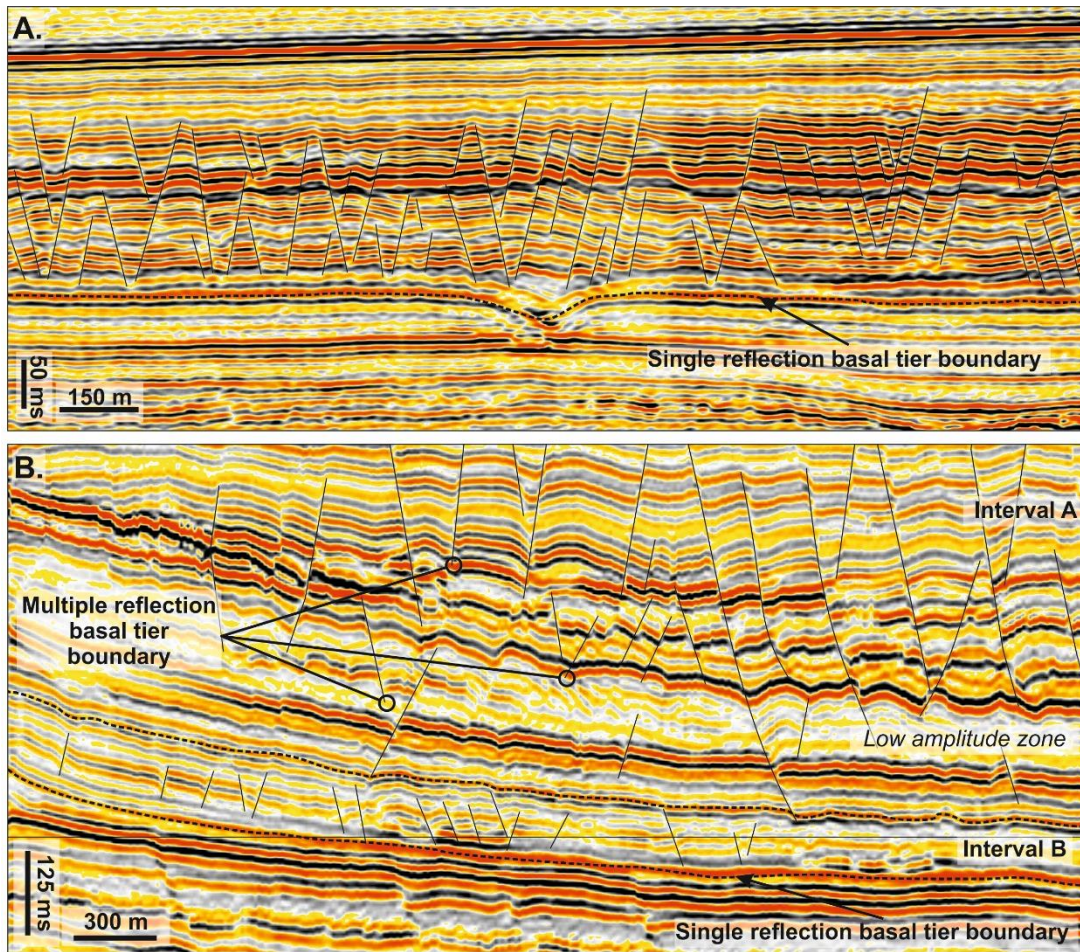


Figure. 8.5: (A) Seismic section showing the basal tier configuration of the polygonal fault tier from the Angolan Margin. (B) Seismic section from the Modgunn Arch showing different basal tip terminations within a single polygonal fault tier. The multiple reflection configuration within Interval A shows basal tips located above and within a low amplitude zone, whilst Interval B faults terminate at a single high amplitude hard event.

spanning several reflection cycles (see Fig.. 8.5). Single reflection tier boundaries are observed in the Lower Congo Basin and in Interval B, Tier 1 in the Modgunn Arch survey. Single reflection tier boundaries are high amplitude, laterally extensive, coherent reflections. Polygonal fault basal tips are hosted above this reflection but can also cross this reflection boundary. The basal tier horizon in the Angolan Margin Survey is a medium to high amplitude reflection at the base of the tier and demarcates the boundary between polygonally faulted and un-faulted hemipelagites. No well data exists for this tier boundary so lithology cannot be constrained but the seismic character of the reflection may be an expression of its mechanical properties. The low basal tip gradients coupled with the seismic characteristics could indicate a rise in Young's modulus (Bürgmann et al., 1994; Cowie and Scholz, 1992a; Schultz and Fossen, 2002) and hence increased mechanical strength of the basal layer.

The base of Interval B, Tier 1 does have well control and the basal tier reflection marks the junction between the Palaeocene age Tare and Tang formations. The Tang formation is comprised of smectite rich marine clays (Thyberg et al., 2000) and show gradually increasing tuff content into the Tare formation (Brekke, 2000; Brunstad et al., 2008; Dalland et al., 1995; Storvoll et al., 2005).

Multiple reflection tier boundary is defined as a package of reflections containing the basal tips of polygonal faults with a discrete base and top. This package ideally would have a different seismic character to the rest of the tier. The best example of a multi-reflection tier boundary is seen at the base of Interval A, Modgunn Arch tier 1 (Fig.. 8.5).

In seismic, the unit hosting the basal tip (defined as Unit II in Chapter 5 is defined by two prominent 'hard' reflections (Avseth et al., 2010) suggesting the basal tip hosting unit exhibits a strong acoustic contrast between the underlying and overlying units. The intervening reflections are low amplitude incoherent reflections, contained in the lower third of the Brygge formation. There are no nearby wells that intersect the low amplitude package so the lithology and state of compaction remain unknown. However, in addition to the seismic character change within the unit, Unit II has important kinematic indicators that suggest it is behaving in a different manner to the surrounding seismic packages. Analysis of H5N at the top of Unit II reveals a series of fault displacements related folds that are exclusive to this horizon. The

horizons above and below show only minor folding that can clearly be attributed to fault drag. Furthermore, this unit accentuates fault displacement through differential compaction, giving large displacement maxima that are localised to the lower third of the faulted interval. This suggests that Unit II is mechanically different and is deforming in response to downward propagating tips from the overlying fault tier. Similar low amplitude zones that also skewed displacements to the lower third of the tier have been reported in an Australian polygonal fault tier in the Lake Hope region where a low density interval occurred at the base of a polygonal fault tier comprised of unconsolidated muds (Watterson et al., 2000).

8.3.3 Tier boundary classification

Previous studies have attempted to classify polygonal faults on the basis of planform pattern (Lonergan et al., 1998) or on tier geometry (Cartwright, 2011). Cartwright (2011) provides schematic diagrams of an idealised, complex and wedge shaped tier as a basis for describing tier geometry (Fig. 8.6). Whilst these geometric configurations of tiers are useful descriptive tools, they are not a useful classification scheme for tiers. For example, the data presented in the Modgunn Arch survey would suggest that polygonal faults in the tier are contained within a wedge shaped tier or a complex tier, depending on the orientation of the seismic line. As evidenced in Chapter 7 the intensity and complexity of fault arrays is variable, even over comparatively small distances (15 km) in a single tier. This could potentially suggest that a single tier may have both the idealised and complex fault arrangements, complicating the classification of tiers on this basis. Furthermore, tier geometry is more complex as on a regional 2D seismic line the tier strongly conforms to the geometry of the reflection package between the Hellan Hansen and Modgunn arches. This aptly highlights that for any given survey, the polygonal faults and the geometry of the tier expressed therein, are potentially biased by the orientation of the line of section used to analyse the tier and also inherently limited by the extent to which the tier is imaged during the acquisition phase of the data, where only a fraction of the tier is could be captured. Due to the layer-bound nature of polygonal fault arrays, the overall geometry of a

Classification of polygonal fault tiers as seen in a single survey (Example from the Modgunn Arch Survey Offshore, Norway)

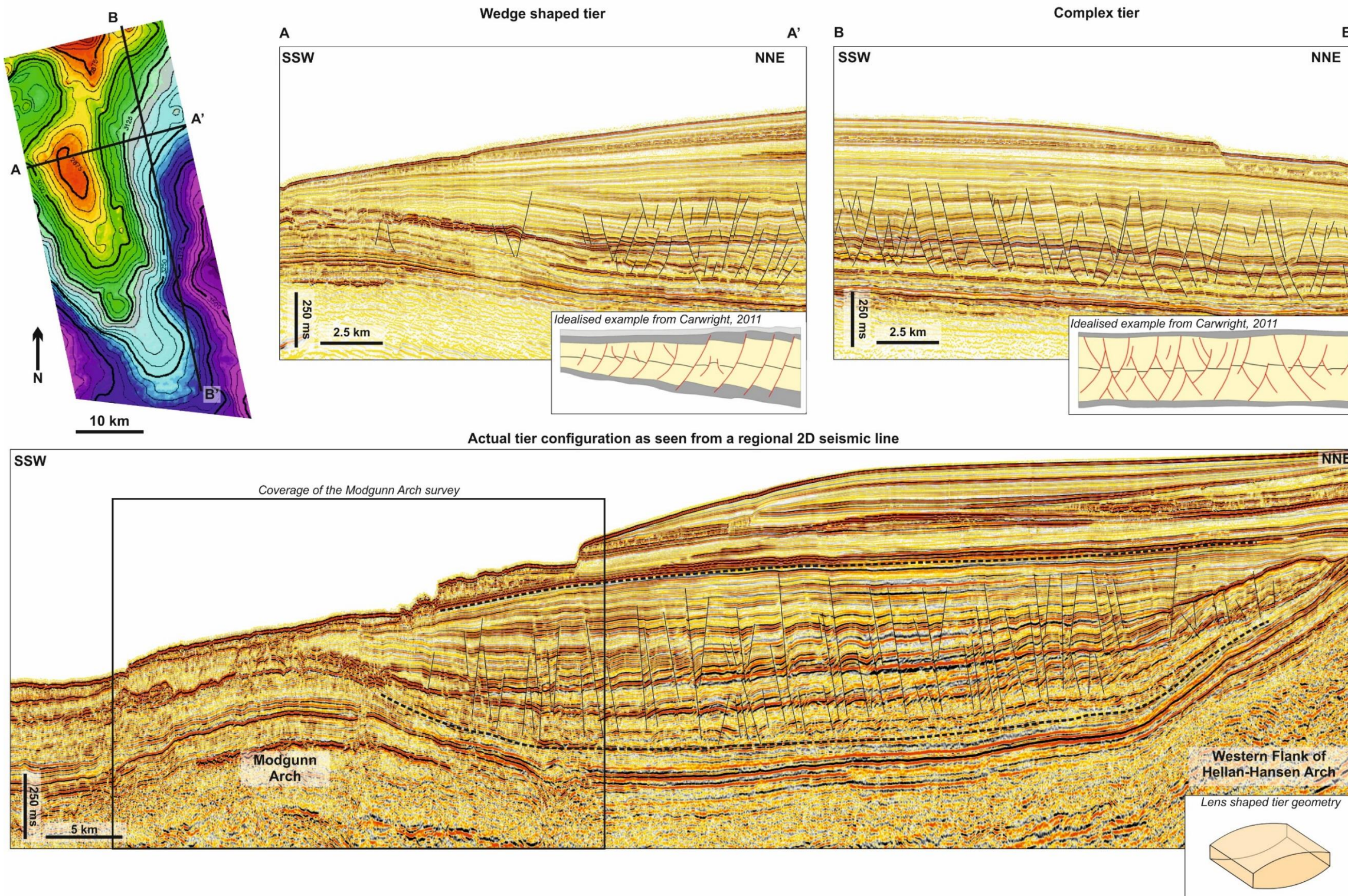


Figure 8.6: A summary of the caveats to the tier classification proposed by Cartwright, 2011. (Top) The two interpreted seismic sections show that for a single polygonal fault tier, the geometry of the tier can be classified as both the wedge and complex geometries creating conflicting descriptors of polygonal fault tier configuration. (Bottom) The regional seismic line also highlights that the geometry of the tier is entirely dependent on which portion of the tier is imaged in the seismic acquisition process. This would suggest that geometry based descriptors of polygonal fault tier geometry offer limited and incomplete view of polygonal fault tier geometry.

polygonal fault tier is likely to broadly conform to the reflection geometries defined by Mitchum et al. (1977) (Fig. 8.6). Instances where this is not case, would suggest that polygonal faults have breached their upper tip boundaries and further highlights the importance of mechanical stratigraphy within polygonal fault tiers.

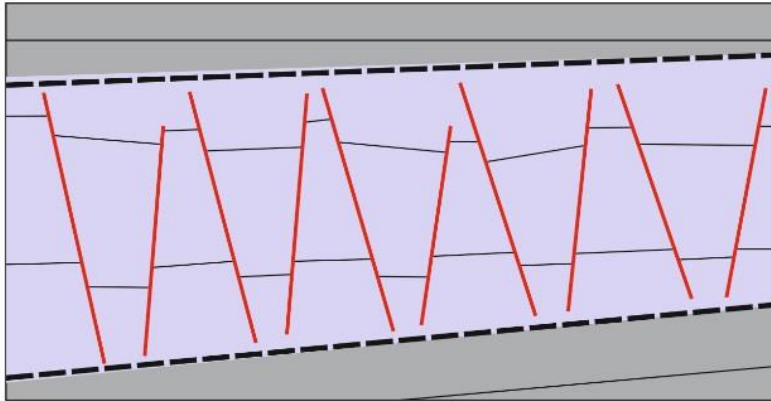
This study proposes that the classification of polygonal fault tiers should be on the basis of the interaction between polygonal faults and their upper and lower boundaries (Fig. 8.7). This change would reflect and comment on the mechanical stratigraphy inherent within a polygonal fault tier and is independent of both tier configuration, the amount of the tier imaged in the seismic data and the intensity of faulting. From the description of polygonal fault tier boundaries submitted in the preceding sections, tier geometries are classified on the basis of ‘strong’ and ‘weak’ mechanical stratigraphy. The basis of strength classification would ideally be corroborated with the geophysical expression of the horizon(s) hosting the tip and, where available, use well data to constrain lithology. It is proposed that polygonal faults with a strong mechanical stratigraphy have sharp tier boundaries, confined to a single reflection at the top and base (Fig. 8.7). The upper and lower tier boundary is concordant and conforms to the geometry of the unfaulted, surrounding reflections. In contrast mechanically weak tiers will have evidence for upper and lower tips spread over several reflection cycles resulting in a diffuse tier boundary. Break-out faults are relatively common and unless they become more than isolated examples for example >25% of the fault observed tips in the study area(s), break-out faults can be considered to be isolated examples and not representative of the mechanical stratigraphy. Tier boundaries in tiers with weak mechanical stratigraphy are suggested to be discordant, when compared to un-faulted reflections surrounding the tier. As seen in Tier 1, Lower Congo basin, the reflections within the tier are insufficient to impact fault propagation until the faults reach seabed. This simple classification system can apply to tiers as a whole or to sections (see Fig. 8.7) of the tier, and provide a simple descriptive tool for the spatial changes to mechanical stratigraphy in any fault system.

8.3.3.1 Caveats to the tier boundaries and classification

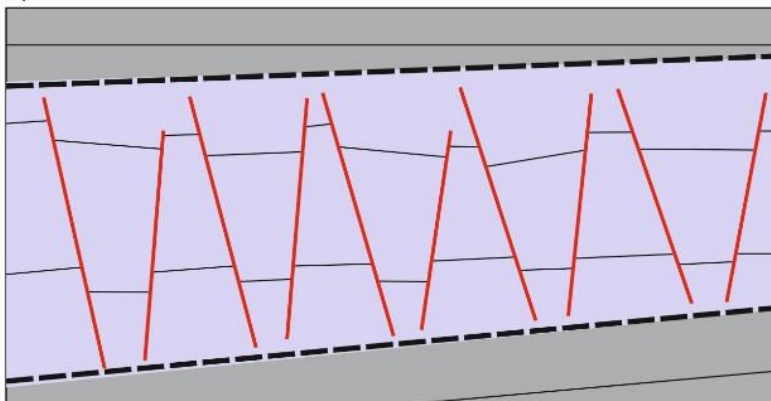
The major and significant caveat to the position of the upper and lower tier boundaries is the seismic resolution limit. Although care was taken at the outset of this study to ensure a range of seismic resolutions (see Chapter 2), the seismic resolution remains a significant source of uncertainty within the classification schemes and the overall tip

Strong Mechanical Stratigraphy

a) Sharp tier boundaries

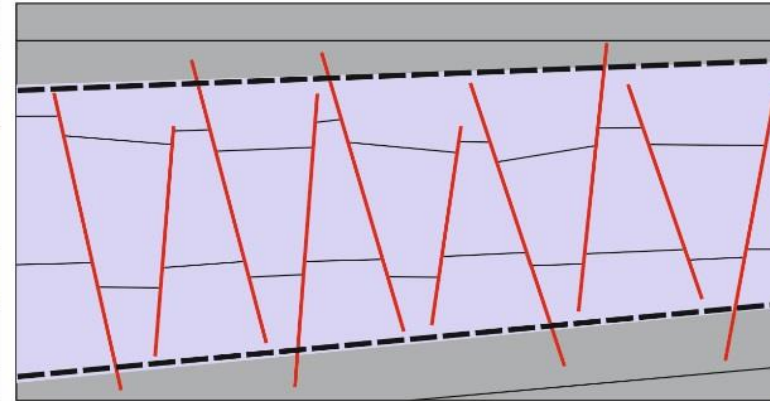


c) Concordant tier boundaries



Weak Mechanical Stratigraphy

b) Diffuse tier boundaries



d) Discordant tier boundaries

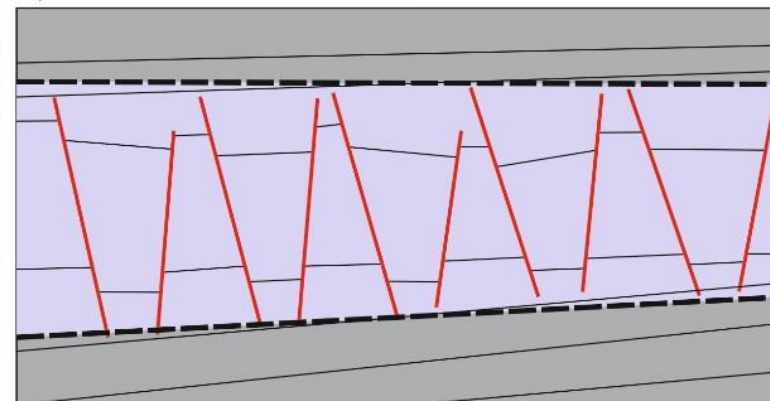


Figure 8.7: Schematic diagrams summarising the different styles of tier boundary observed within the two study areas and the implication for mechanical stratigraphy

geometry. Previous studies that examined data with a resolution limit (geophysical or otherwise) have attempted to circumvent the resolution issue by the addition of the estimated below resolution extent of the fault (Walsh and Watterson, 1988). This method was applied in coalfield data where an additional 50m was added to the fault dimensions to account for the resolution limit of 15cm (6 inches). Such a technique may not be appropriate in seismic datasets where tens of metres of fault are potentially omitted by resolution limits. Numerous studies suggest that steep upper tip gradients are diagnostic of restriction of upper tips due to mechanical stratigraphy (Roche et al., 2012; Schultz and Fossen, 2002; Soliva and Benedicto, 2005; Wilkins and Gross, 2002). However, when dealing with metres to tens of metres of unseen fault tip, displacement gradients alone are insufficient to predict the full extent of faults. Ultimately, displacement gradients in seismic are proxies for the likelihood that fault tips are restricted as opposed to being *actually* restricted. This is because displacement gradients cannot account for termination geometry between the fault tip and barrier (Hibscher et al., 2003; McGrath and Davison, 1995; Roche et al., 2012; Wilkins and Gross, 2002) or below resolution variation in tip gradients near the tip (Soliva and Benedicto, 2005). Such observations are at present, purely in the domain of field based studies (Henriet et al., 1989; Hibscher et al., 2003; Tewksbury et al., 2014) or from sonar based studies (Cartwright et al., 2004; Wattrus et al., 2003) of polygonal faults.

However this study proposes that a useful proxy for mechanical restriction may be to examine the spread of tip gradients. For example, where tip gradients fall in a narrow range it is possible to attribute the narrow distribution to a mechanical boundary as the displacement gradient decreases due to changing rheology. In contrast those tips that have a ‘seismic’ cut-off due to vertical resolution limits will likely have a much wider range of tip values. It is also important to consider that the resolution limit at the top of a polygonal fault tier is intrinsically better than the resolution at the base of the tier, especially deeply buried tiers (<1 km or more), due to progressive attenuation of the seismic signal (Brown, 2004).

Therefore the tier classification and boundary conditions must be defined as the seismically resolvable tip position and the actual upper tip position is likely to be higher in the stratigraphy, depending on the geometry and lithology of the units hosting the tips. Interpretation of the mechanical boundaries must respect that the

geophysical expression of fault tips is potentially very different to the physical tip position.

8.3.4 *Polygonal fault scaling*

Displacement-length and displacement-height plots of both the immature (Angola) and mature (Norway) polygonal fault data sets were analysed in log-log space. Displacement-height plots for both Norwegian and the Angolan Margins show different scaling properties (Fig. 8.8). The displacement height plots of the Angolan Margin show a linear scaling ($R^2 = 0.42$) whereas the polygonal faults of the Norwegian Margin show an exponential scaling ($R^2 = 0.55$). When both polygonal fault sets are analysed together the overall scaling has a strong exponential trend ($R^2=0.7$).

Displacement length plots (Fig. 8.9) for the Angolan Margin show weak power law trends ($R^2=0.41$) whereas the dataset for Norway shows a moderate linear trend ($R^2=0.55$) and the dataset overall shows a fractal (power law) scaling where;

$$\& L^{-0.7}$$

Equation 8.1

The transition of the displacement length scaling could be due to a number of factors. Previously fault length/displacement scaling relationships have been suggested to be linear (Cowie and Scholz, 1992a; Walsh and Watterson, 1988) or power law (Needham and Yielding, 1996; Yielding et al., 1996). In addition, analysis of fault populations has shown that through time fault arrays can deviate from linear to exponential to power law scaling. These transitions have been calibrated in seismic data (Walsh et al., 2003) where the smallest faults in the population die out and the largest faults subsequently become more interconnected. There are also a number of numerical and geometric models that predict transitions from power law to linear scaling, which may be influenced by the thickness of the mechanical unit (Ackermann et al., 2001) and the connectivity of the array (Spyropoulos et al., 1999). Field based studies also show the effect of the mechanical properties of the material hosting the fault array on fault scaling (Gross et al., 1997; Steen and Andresen, 1999; Wilkins and Gross, 2002).

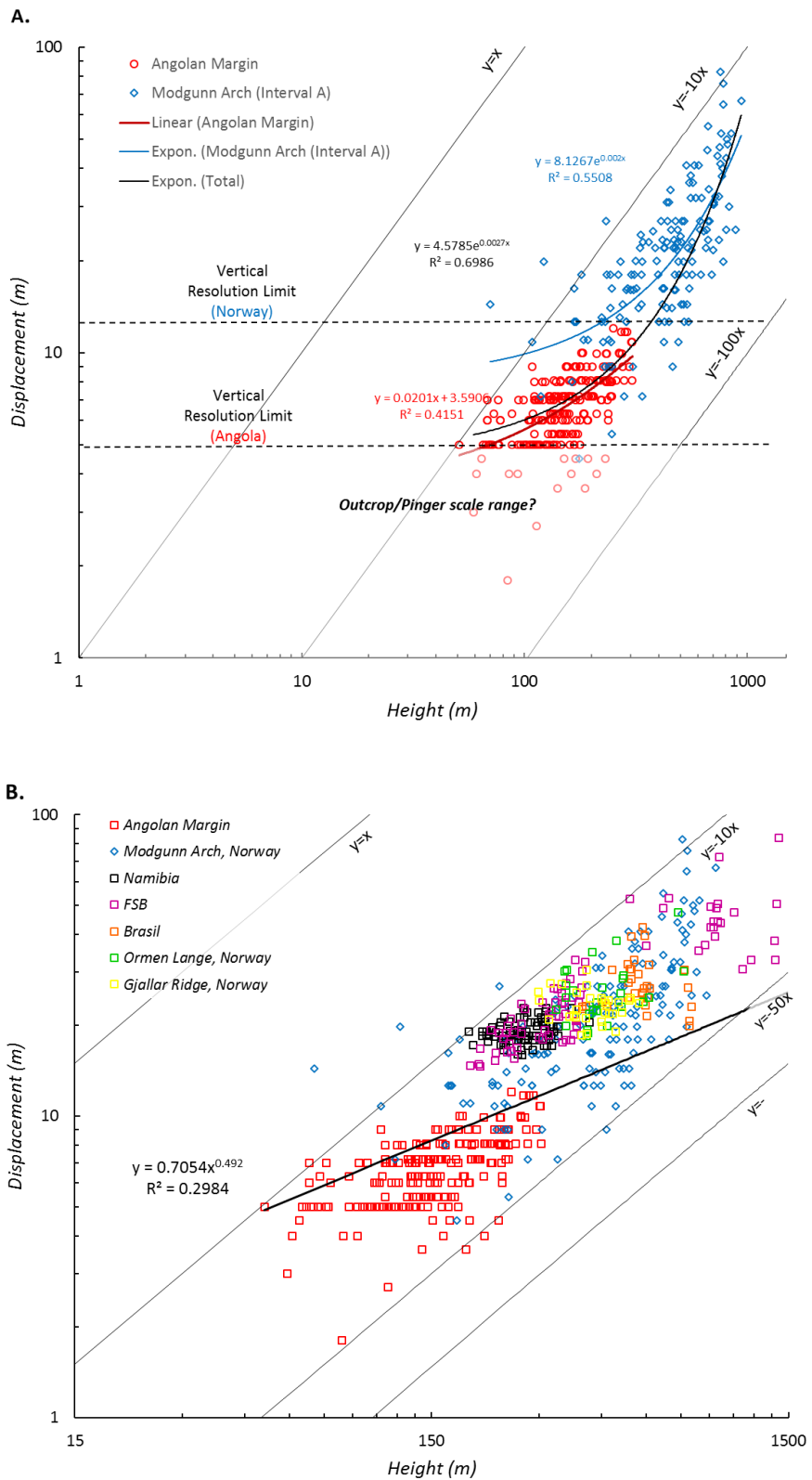


Figure 8.8: (A) displacement-height plot in log-log space detailing the scaling laws of the polygonal faults of the Angolan and Norwegian Margins (B) The same data cross-plotted with additional data from Shin et al., 2008 showing a power law scaling

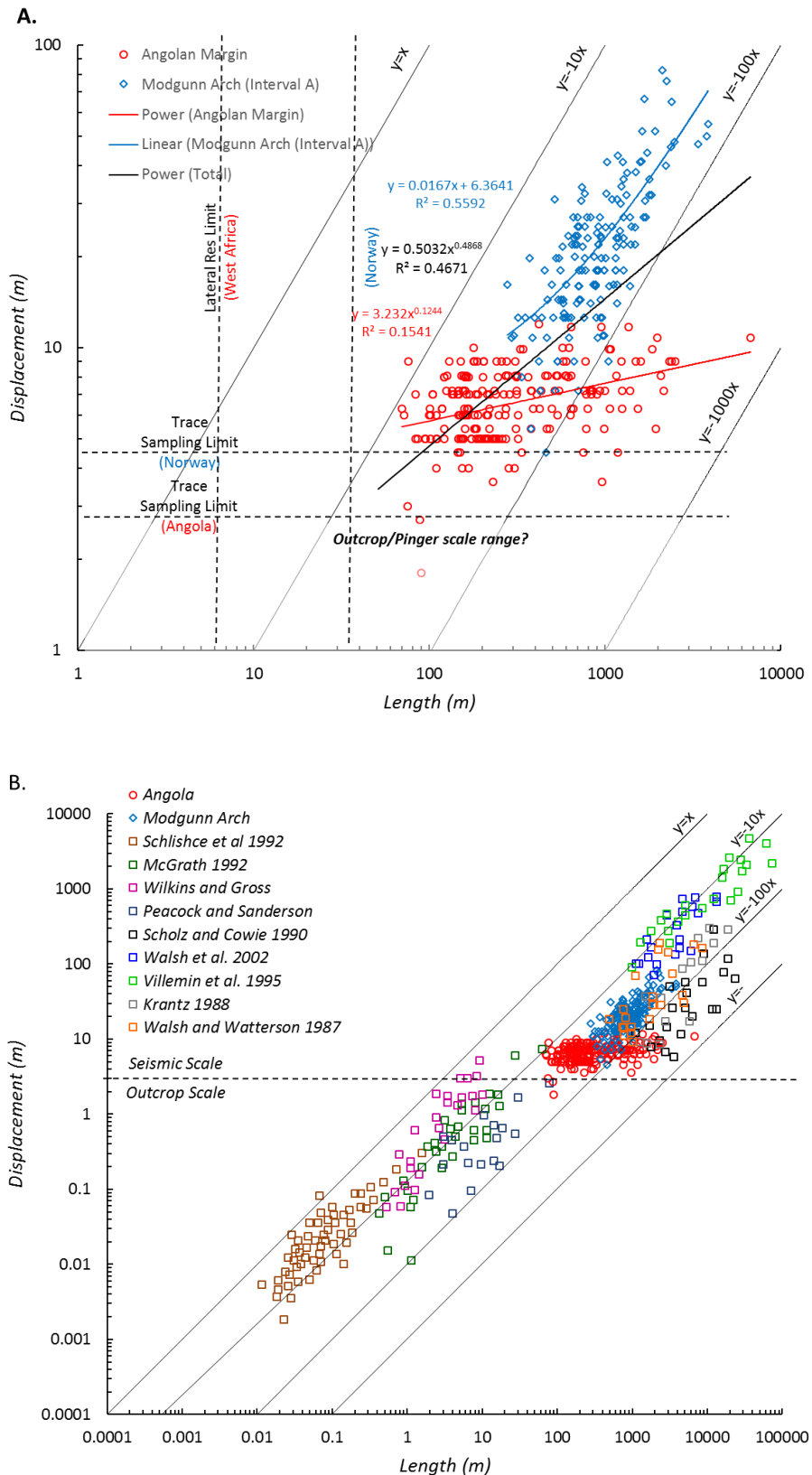


Figure 8.9: (A) displacement-length plot in log-log space detailing the scaling laws of the polygonal faults of the Angolan and Norwegian Margins (B) The same data cross-plotted with additional data from Kim and Sanderson, 2005 to compare polygonal faults with tectonic fault scaling

There has been considerable debate as to whether transitions for power-law to linear scaling are natural trends or artefacts of sampling. A number of studies have suggested that the sampling parameters are critical for the estimation of fault scaling relationships (Marrett and Allmendinger, 1991; Yielding et al., 1996) and indicated potential problems with comparing local and regional scale faulting as well as potential issues with estimating from displacement maxima. A study by Nicol et al. (1996), examined fault populations over seven orders of magnitude, from outcrop to seismic scale and noted that whilst the exponent for fault scaling changed, the overall fault scaling was still power-law. Nicol et al. (1996) conclude that the examination of power scaling laws over too wide or too narrow a range of displacements and lengths impacts the exponent value and ultimately the overall scaling relationship. This data set examines fault displacements over two orders of magnitude and fault lengths over four orders of magnitude for length. Comparison between the data presented here and metadata presented by Kim and Sanderson, (2005), show that the polygonal faults of this study compare well with their tectonic counterparts and fall within the lower limit of the tectonic scaling range of ($y=-10x$ to $y=-100x$).

The data also broadly conforms to the previous works of Spyropoulos et al. (1999) Gupta and Scholz, (2000a) and Ackermann et al. (2000). The modelled based work of Spyropoulos et al. (1999) and Ackermann et al. (2000) as well as the observed changes of Gupta and Scholz (2000a), all report changes in scaling relationships within fault populations from power law to exponential scaling. The change in scaling relationship was attributed to increased coalescence between individual fractures which coincides with a decreased the rate of fracture nucleation (Spyropoulos et al., 1999). Additionally Ackermann et al. (2000) contend that the mechanical thickness may contribute to the scaling relationships by suppressing fault interactions. In the context of the polygonal fault data presented in the results chapter, many of the observations made by Spyropoulos et al. (1999) and Ackermann et al. (2000) can be made in the polygonal fault dataset. There are clear changes in scaling between polygonal faults at different developmental stages with changes in scaling of both displacement height and displacement length. This would suggest that the changes in scaling are likely to be the representative of polygonal fault growth at different developmental stages rather than artefacts of sampling bias.

Numerous studies have related the scaling properties to the strain of a sediment column (Ackermann et al., 2001; Cladouhos and Marrett, 1996; Marrett and Allmendinger, 1991; Scholz et al., 1993). This data set supports some of the conclusions of Nicol et al. (1996) in that, for a single tier of faults where the range of displacement and length varies by one and two orders of magnitude, the power law scaling is lost as the sample range is too narrow. This also encapsulates fault geometry and dimensions at a fixed temporal point in the tier evolution, either late or early formation and hence a sample of only part of the faults on a scaling curve. This issue is largely circumvented in tectonic faults as they are often widely distributed over a large area and are much larger spatially, offsetting units at a variety of scales. Polygonal faults by definition are heavily constrained in their lateral extent and much smaller and prone to spatial clustering (Nicol et al., 1996), which masks the power-law curve. Therefore, the comparison of two related datasets at the seismic scale, at two different stages of evolution produces the widely accepted power-law distribution by sampling a wider range of fault dimensions.

Whilst the power law scaling of displacement-length in normal faults and the caveats and pitfalls of sampling are well understood and documented (see Nicol et al., 1996 for discussion), the displacement-height scaling parameter of normal faults is less well understood. It is inferred here that the change in scaling relationships in displacement-height space between mature and immature polygonal fault arrays is a function of strain generated by the compaction of sediment.

Displacement-height has been seldom described in seismic or field datasets. In this study a metadata analysis was undertaken (Fig. 8.8B) to compare the results of the two tiers studied here with other tiers from a published dataset in Shin et al. (2010). Analysis of the linear regression trends (R^2) within the data suggests that a power law curve best fits the polygonal fault displacement-height metadata with a weak correlation ($R^2 = 0.29$) where;

$$\text{displacement} \propto \text{height}^{4.2}$$

Equation 8.2

The significance of the power law curve for fault height-displacement scaling is suggested here to be indicative of the strain pathway within polygonal fault arrays. Work by Fossen and Gabrielsen, (1996) showed that within an analogue model of a

fault array within plaster, the smallest faults accommodated the smallest amount of extension and the largest faults accommodate the majority of extension and hence strain. In the polygonal fault data it is suggested that the evolution of polygonal fault organisational hierarchies is also indicative of strain within a polygonal fault tier. Within polygonal fault arrays, the greatest number of faults (as a proxy for fault intensity) is located in the lower third to lower half of the tier, across all tiers studied. Fault numbers and fault spacing progressively increases up sequence and fault numbers are low near the top of a tier. The presence of high fault numbers at the base of the tier would suggest a higher strain at the base, the variability in strikes of faults in the base of the tier would also suggest that the strain is heterogeneous.

As discussed in Chapter 7, polygonal fault heights vary with numerous fault families present in a single tier. These fault families show increasing spatial dimensions as well as increasing displacements. Furthermore, they show an orientation to the ‘background’ stress field either to topography or far field stress, depending on the package geometry. As faults families grow and evolve, it is proposed that the strain is accommodated on fewer faults, resulting in higher displacements. The gradual dissipation of a ‘polygonal fault prone’ stress field manifested as a re-orientation of fault strike to regional stress, either to regional tectonic stress (Modgunn Arch) or to stress fields influenced by slopes (Angolan Margin). The impact of this strain partitioning onto larger faults results in the exponential curve. Additionally, this could explain why displacement maxima are axio-symmetrically aligned with respect to the centre of the tier. The gradual dissipation of displacement towards the upper tips also reflecting the gradual dissipation of strain derived from the base of the tier.

8.4 Polygonal fault tier evolution

In summary, the evolution of polygonal fault tiers is a function of the timing between nucleation of faults and the diagenetic history within a sediment body. The development of a polygonal fault tier is proposed to be the result of three evolutionary stages, of growth, restriction and break-out (Fig. 8.10).

8.4.1 Stage 1: Growth

Polygonal fault growth (post nucleation) is Stage 1 of a polygonal fault tier development. Growth can occur early, within the first 100m of burial and is

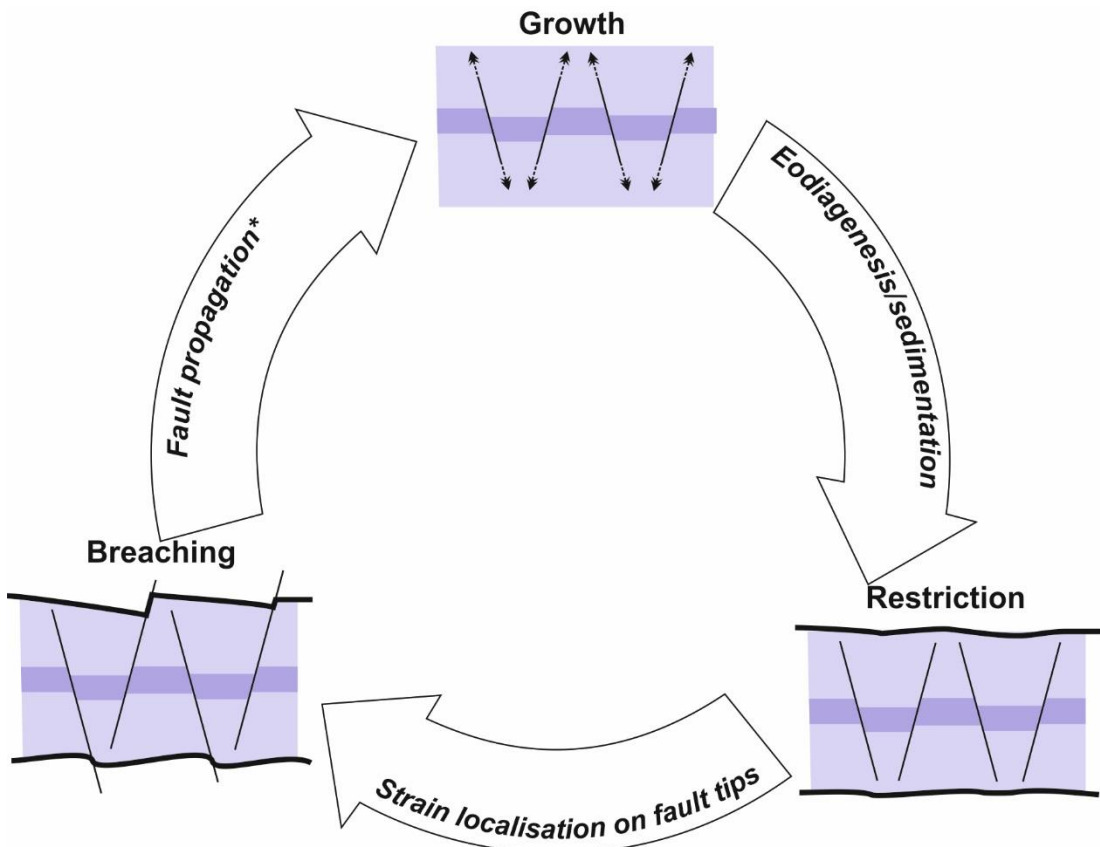


Figure 8.10: A process diagram showing the key processes operating within a polygonal fault tier that drives tier evolution

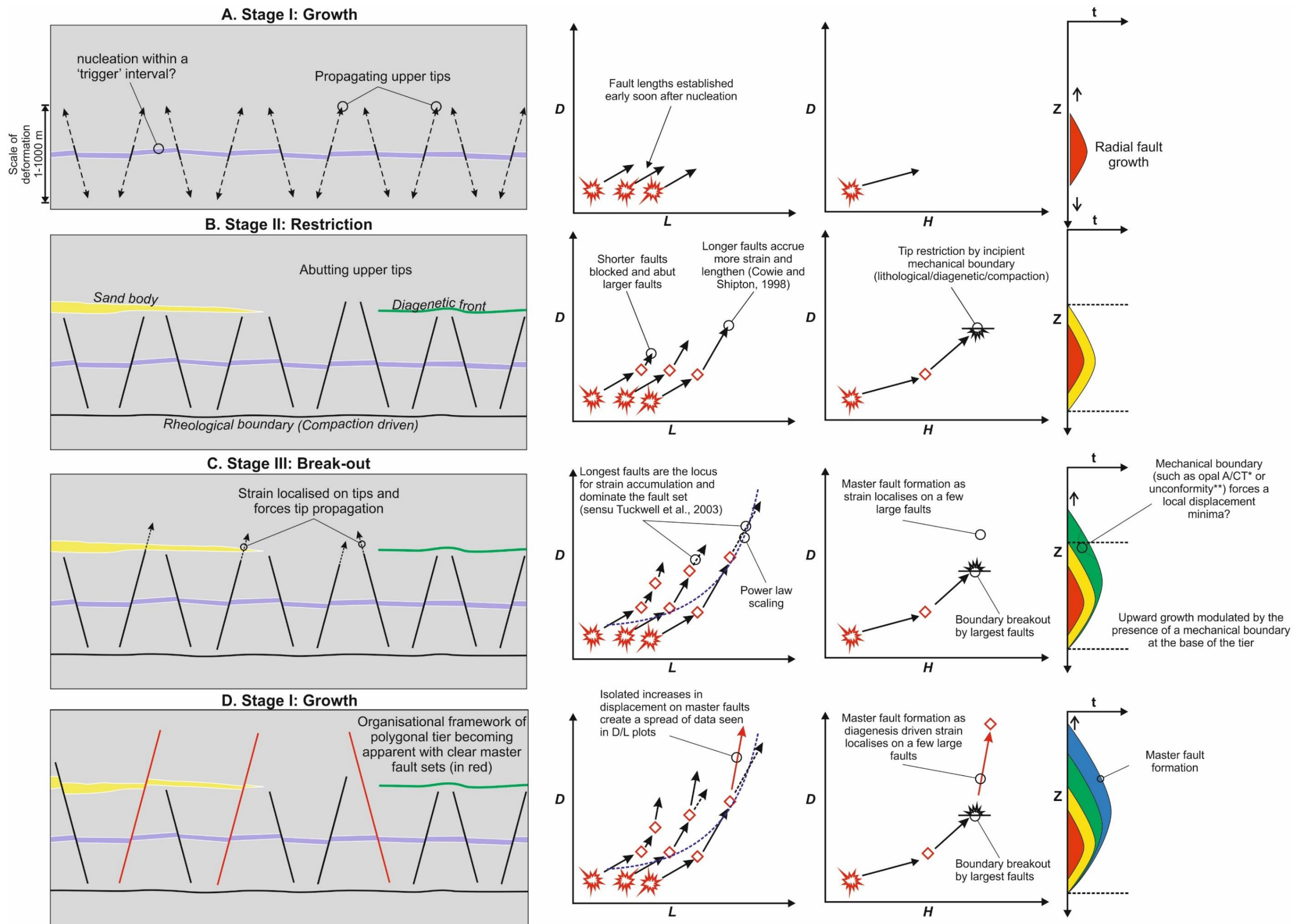


Figure 8.11: A schematic diagram detailing the evolution of a polygonal fault tier at each stage and offers an explanation for the scaling relationships (both displacement-length and displacement-height) that exist between different tiers. (A) Stage I is nucleation and growth of the initial polygonal fault array (B) the restriction stage can be driven by a variety of factors (summarised in B) that prevent upward propagation of faults, (C) The break-out stage occurs when faults accrue sufficient strain to break a boundary , usually localised on the largest faults. (D) The largest faults continue to grow and form the organisation relationships (Master faults, sub-tiers etc.) described in Chapter 4 and 5.

governed by low coefficients of friction during compaction and early diagenetic processes (see 8.3.1.1). Growth can deviate between radial and non-radial growth, modulated by the timing between the nucleation and the development of the basal tier boundary (Stage 2).

8.4.2 Stage 2: Restriction

Basal tier boundaries fall into two categories, the ‘hard’ basal reflection which consists of a hard lithology or tip zones made where mechanical properties gradually preclude fault propagation (Fig. 8.11). The formation of these tip zones is likely to be in the early diagenetic domain and as such dominated by mass transfer reactions and mechanical compaction (Gier et al., 2008; Worden and Burley, 2003; Worden and Morad, 2003). As these reactions are strongly controlled by the inherent sedimentology of the sediments (Worden and Burley, 2003), the formation of tier boundaries at major breaks in sedimentation such as unconformities are likely to be an important factor in defining a basal tip as sediment provenance changes. The restriction of basal tips coupled with early interaction between fault branchlines, may provide the catalyst for forcing a change in the propagation trajectory from radial to asymmetrically skewed growth (upwards, laterally etc.) (Wilkins and Gross, 2002). The restriction of radially propagating tip(s) by mechanical stratigraphy has been demonstrated to force preferential lateral tip propagation (Wilkins and Gross, 2002), lower tip gradients (Ferrill and Morris, 2001; Muraoka and Kamata, 1983; Roche et al., 2012; Wibberley et al., 2007), influence the distribution of displacement (Morris et al., 2009), influence the position of displacement maxima and minima (Rippon, 1984) and influence the frequency of faults at a given interval (Morris et al., 2009). Continued fault propagation results in the organisation of fault architecture as propagating upper tips interact and abut, potentially influenced by the local dip (Mandl, 1987; Mandl and Crans, 1981) and the basal boundary lithology (Stewart and Argent, 2000). Upper tip restriction can also occur at major unconformities where polygonal fault growth can switch from blind (Lonergan et al., 1998) to syn-sedimentary (Hansen et al., 2004; Möller et al., 2004) as faults reach the seabed or cease entirely where grain sizes increase (Cartwright, 2011; Jackson et al., 2014).

8.4.3 Stage 3: Break-out

These tier boundary types described in section 8.3.2 represent end-members of tip configurations. In all the tiers documented in this study, there are isolated examples of

basal and upper tips breaching their respective boundaries. Break-out faults occur in all tier boundary types and there is at least one example of a break-out fault in each survey. Mechanical impediments to continued fault growth have been widely documented in outcrop (Gross et al., 1997; Peacock, 1991; Rippon, 1984; Roche et al., 2012; Wilkins and Gross, 2002) and in numerical models (Bürgmann et al., 1994).

There are numerous studies that suggest barriers to fault growth are temporary. In conditions whereby loading parameters remain unchanged through geologic time, strain localisation occurs near the fault tip that can eventually lead to breaching of the barrier (Cowie and Scholz, 1992b; Gupta and Scholz, 2000b). Alternatively, faults can breach a mechanical barrier if the slip patch, the active region of fault where slip localises, is proportional to fault dimensions (Cowie and Scholz, 1992c). This mechanism assumes that energy required to create a new fault segment scales to the dimension of the slip patch of a given fault. In essence, a fault barrier will no longer impede fault propagation if the fault length increases (Cowie and Shipton, 1998). In multi-layer sequences of rocks with a strength contrast, faults propagating fault tips often show preferential nucleation in the stronger mechanical units due to high volumetric strains (Schöpfer et al., 2006). The faults in the multi-layer sequence form in three stages, faults in the stronger units initially form due to monoclonal flexure and develop into tensile fractures that later develop a shear component. The final stage of growth is a through-going fault as the individual segments in the stronger units link (Schöpfer et al., 2006).

In the context of the polygonal fault arrays studied here, it is a crucial observation for the development of polygonal fault arrays that barriers to polygonal fault growth in both upper and lower boundaries are temporary. It is suggested here that breaching faults may represent early stages of polygonal faults overcoming mechanical barriers to growth by one or a combination of the mechanisms described in previous studies (Fig. 8.11). Break-out of polygonal fault tier boundaries may be an important process for the continued activity of a polygonal fault array and development of a fault hierarchies in mature polygonal fault tier.

As suggested by (Cowie and Scholz, 1992b; Cowie and Shipton, 1998), fault dimensions may be a key factor in governing the break-out of tier barriers. Observations from Tier 1, Lower Congo Basin, displacement-length plots show that

Polygonal fault length can be established early on in a tier's history, within 200m of burial. Comparison between displacement-length data from the Lower Congo Basin and Interval B Modgunn Arch suggests that the range of fault lengths between the two tiers are similar. From this, a stepped model for polygonal fault growth is proposed where faults undergo periods of lengthening and displacement accumulation (Cartwright et al., 1995; Cowie and Shipton, 1998; Kim et al., 2001; Kim and Sanderson, 2005).

The evolution of master polygonal faults in Interval B, Tier 1 of the Modgunn Arch survey are suggested to be derived from restricted faults (Brygge faults) confined below the Mid-Miocene unconformity (MMU). Brygge faults in both CSS and CSN of the Modgunn arch surveys have steep upper tips that lie below the MMU, suggesting that the Brygge faults are pinned by the MMU. Evolution from formation faults to Master and tier faults is inferred to be due to the largest faults in the array overcoming the restriction on the MMU by strain localisation in the upper tip regions (Cowie and Scholz, 1992b; Gupta and Scholz, 2000b).

9 Conclusions

9.1 Introduction

The overall aim of this thesis was to examine the growth and development of polygonal fault tiers. This thesis examined three concepts; the interaction between faults and features within a tier; the propagation of polygonal faults and the polygonal fault organisation.

9.2 The interaction between polygonal faults and features at the base of the tier.

The results in Chapters 6 and 7 show that polygonal faults strongly interact with features at the base of a tier, forming perturbed fault patterns, forming radial and concentric patterns around the features. There is evidence to suggest that perturbation patterns can be used as an analogue for inferring the nucleation position of faults. This is based on the strong spatial relationship between the extent of the perturbed faults and the thickness variation associated with pockmarks, as described in Chapter 7. However, similar perturbation patterns can be derived from differential compaction. In the case of HTVCs, the compaction response of the underlying vents is crucial and this modulates the extent of the radial fault zone, as the largest radial fault zones relative to vent dimensions are typically related to HTVCs with a layered vent fill. The differences in vent fill are responsible for the scatter in the cross plots of the radially faulted area. Based on the presence of radial faults and the correlation between HTVC width and the radius of the radial polygonal faults, this study concludes that the perturbation polygonal faults around HTVCs is a later differential compaction event and therefore cannot be linked to the nucleation position of polygonal faults in the Modgunn Arch survey.

The data presented in Chapter 7, demonstrates a clear link between thickness changes across the pockmark and the position of perturbed polygonal fault arrays. However, this observation is much less well defined in the polygonal faults of the Norwegian margin. The nucleation position of perturbed, and by extension, non-perturbed polygonal faults is important. Polygonal fault nucleation within 100 m of burial suggests an ‘early’ nucleation timing, providing an important indicator of the genesis of polygonal faults soon after deposition. Such an important observation is difficult to elucidate in seismic data and, given its significance to polygonal fault genesis, needs very careful interpretation. Consequently, there are a number of criteria proposed for the use of perturbed polygonal faults as a proxy for nucleation position,

- *Feature type*: The feature which generates the perturbation must be a static feature at the base of the tier such as a pockmark, or channel levee and represent a single ‘event’. ‘Active’ features such as diapirs (mud or salt) and tectonic faults that move or displace the sub-surface over several phases obfuscate when nucleation occurs due to the possibility of reactivation or active deformation (i.e. folding).
- *Feature numbers*: Ideally, there would be multiple examples of this feature throughout the tier, preferably across the range of tier thicknesses. An isolated (one or two) or clustered examples would be insufficient to draw conclusions from.
- *Burial context*: Are the basal features shallowly or deeply buried? More deeply buried features are more subjective as nucleation during burial induced differential compaction must be considered as a factor.
- *Fault height*: The perturbed faults must extend well into the tier and cannot be confined to a single thin interval at the base.
- *Dissipation*: The change from perturbed to non-perturbed state must be observed to link any thickness changes to the dissipation of the perturbed pattern.
- *No mechanical boundaries*: The dissipation of the perturbed pattern must be seen to gradually dissipate and not terminate at a mechanical boundary. Such a boundary could suggest decoupling within the tier and limit the extent of the perturbation geometry.

9.3 Propagation and organisation of polygonal faults

This study proposes an alternative growth model for polygonal faults whereby polygonal fault propagation occurs under shallow burial conditions (<150 m) and is focussed preferentially upwards. This is based on two independent observations; firstly, this study documents a fully developed polygonal fault array in sediment accumulations as low as 150 m from the West African Margin; secondly by examining fault patterns through a single wedge shaped tier, it can be demonstrated that polygonal fault upper tips propagate upwards whereas the basal tips become pinned by a mechanical boundary. This study reveals that polygonal fault arrays, with fully linked branchlines are established at <150m burial. The subsequent growth is focussed upwards from in the tier, with a basal tier boundary also established at <150 m burial.

Crucially polygonal faults of West Africa show triangular abutments, where two faults with opposing dips begin to interact. Triangular abutments are also observed in the Modgunn Arch survey where they are found in the lower third of the tier. These abutments in both West Africa and the Norwegian Margin, are suggested to be indicators to the nucleation position for the polygonal fault tier. It is interpreted here as indicating that in both tiers, the original seed location for polygonal faulting is in the lower third of the tier.

9.4 Fault Organisation

Leading on from propagation and the triangular abutments, tier organisation, particularly the growth and formation of master faults, is suggested here to be the result of competition for space to grow between competing fault branchlines. As seen in Chapter 5, at 300 m burial, there is evidence for fault hierarchies beginning to form with some polygonal faults obviously larger than others in the same tier. During the evolution of a tier, it can be demonstrated that there are two potential pathways for Master polygonal faults to form. Master polygonal faults can form in highly connected arrays through preferential alignment to regional stresses. Alternatively, in relatively unconnected or isolated arrays, some polygonal faults are predisposed to form Master polygonal faults as they are the largest polygonal faults in the local array and form the locus for strain accumulation.

Furthermore, this study describes polygonal fault tier boundaries in three dimensional context and suggests that polygonal fault tier boundaries are re-classified, not on the basis of the faults within the tier, but on the geometry of the polygonal fault boundary itself. As described in Chapter 8, it is suggested here that polygonal faults tier boundaries can indicate ‘strong’ or ‘weak’ mechanical stratigraphy within a tier based on the definition of the upper and lower tip positions. Where upper and lower tier boundaries are concordant with regional seismic reflections, this would indicate a ‘strong’ mechanical stratigraphy as polygonal faults are restricted to a specific package of reflections. Discordant upper and lower tier boundaries cross several reflection cycles, and indicates a ‘weak’ mechanical stratigraphy as faults are able to propagate freely. This is proposed to be more informative with respect to the controls on the formation of tier boundaries and less prone to directional sampling as with the geometries suggested by Cartwright (2011).

9.5 Recommendations for future work

The results of this thesis offers important constraint on the timing of polygonal fault nucleation as the presence of polygonal faults in sediment packages of <150 m strongly indicates that the genesis mechanism of polygonal faults must potentially account for low states of stress and partially consolidated sediments. This study concludes that there is a strong case for polygonal fault nucleation via the Cam-Clay model. It is suggested here that the polygonal fault nucleation is initiated during the consolidation of clays under burial. This consolidation coupled with the precipitation of early diagenetic cements promotes shear offsets without the changes in stress or volume. However, the Cam-Clay model is unsubstantiated for polygonal faults and lacks primary observations on mineralogy, pore fluid pressure, compaction and background regional stresses.

This study suggests that future polygonal fault studies be conducted with well control. To date very few polygonal fault studies can quantify the material properties of the tier-hosting materials. At present, the material properties of a polygonal fault tier, particularly at their upper and lower boundaries, are largely unknown and would give vital constraint on the lithological or rheological controls on the upper and lower tier boundaries. A suite of petrophysical logs, with side wall or conventional cores, tied to seismic data, would generate new insight into polygonal fault tiers, particularly the state of compaction, pore-fluid pressure, and mineralogy. These observations would help constrain whether polygonal fault nucleation and growth via a Cam-Clay model is possible.

References

- Ackermann, R.V., Schlische, R.W., 1997. Anticlustering of small normal faults around larger faults. *Geology* 25, 1127–1130.
- Ackermann, R.V., Schlische, R.W., Withjack, M.O., 2001. The geometric and statistical evolution of normal fault systems: an experimental study of the effects of mechanical layer thickness on scaling laws. *J. Struct. Geol.* 23, 1803 – 1819.
- Allen, P.A., Allen, J.R., 2005. Basin Analysis: Principles and applications, 2nd ed. Blackwell Publishing, Oxford.
- Alves, T.M., 2010. 3D Seismic examples of differential compaction in mass-transport deposits and their effect on post-failure strata. *Mar. Geol.* 271, 212–224. doi:10.1016/j.margeo.2010.02.014
- Andersen, T.B., Jamveit, B., 1990. Uplift of deep crust during orogenic extensional collapse: A model based on field studies in the Sogn-Sunnifjord Region of western Norway. *Tectonics* 9, 1097–1111.
- Andersen, T.B., Osmundsen, P.T., Jolivet, L., 1994. Deep crustal fabrics and a model for the extensional collapse of the southwest Norwegian Caledonides. *J. Struct. Geol.* 16, 1191–1203.
- Anderson, J.E., Cartwright, J.A., Drysdall, S.J., Vivian, N., 2000. Controls on turbidite sand deposition during gravity driven extension of a passive margin: examples from Miocene sediments in Block 4, Angola. *Mar. Pet. Geol.* 17, 1165 – 1203.
- Andresen, K.J., Huuse, M., 2011. “Bulls-eye” pockmarks and polygonal faulting in the Lower Congo Basin: Relative timing and implications for fluid expulsion during shallow burial. *Mar. Geol.* 279, 111–127. doi:10.1016/j.margeo.2010.10.016
- Anka, Z., Séranne, M., Lopez, M., Scheck-Wenderoth, M., Savoye, B., 2009. The long-term evolution of the Congo deep-sea fan: A basin-wide view of the interaction between a giant submarine fan and a mature passive margin (ZaiAngo project). *Tectonophysics* 470, 42–56. doi:10.1016/j.tecto.2008.04.009
- Ashcroft, W., 2011. A petroleums geologists guide to seismic reflection, 1st ed. Wiley - Blackwell, Oxford, UK.
- Avseth, P., Mukerji, T., Mavko, G., 2010. 4. Common techniques for quantitative seismic interpretation, in: Quantitative Seismic Interpretation: Applying Rock Physics Tools to Reduce Interpretation Risk. Cambridge University Press, pp. 168–211.
- Babonneau, N., Savoye, B., Cremer, M., Bez, M., 2004. Multiple terraces within the deep incised Zaire Valley (ZaiAngo Project): are they confined levees, in: Lomas, S.A., Joseph, P. (Eds.), Confined Turbidite Systems. Geological Society of London, Special publications, pp. 91–114.
- Bahorich, M., Farmer, S., 1995. 3D seismic discontinuity for faults and stratigraphic features: The coherence cube. *Lead. Edge* 14, 1053 – 1058.
- Bai, T., Maerten, L., Gross, M.R., Aydin, A., 2002. Orthogonal cross joints: do they imply a regional stress rotation? *J. Struct. Geol.* 24, 77–88.
- Bally, A.W., 1988. Thoughts on the tectonics of folded belts s. *Struct. Concepts Tech. Basic Concepts Fold. Struct. Tech.* 1, 183.
- Barnett, J.A., Mortimer, J., Rippon, J.H., Walsh, J.J., Watterson, J., 1987. Volume Containing a Single Normal Fault 71, 925 – 937.

- Baudon, C., Cartwright, J., 2008a. Early stage evolution of growth faults: 3D seismic insights from the Levant Basin, Eastern Mediterranean. *J. Struct. Geol.* 30, 888–898. doi:10.1016/j.jsg.2008.02.019
- Baudon, C., Cartwright, J., 2008b. The kinematics of reactivation of normal faults using high resolution throw mapping. *J. Struct. Geol.* 30, 1072–1084. doi:10.1016/j.jsg.2008.04.008
- Baudon, C., Cartwright, J.A., 2008c. 3D seismic characterisation of an array of blind normal faults in the Levant Basin, Eastern Mediterranean. *J. Struct. Geol.* 30, 746–760. doi:10.1016/j.jsg.2007.12.008
- Bell, B., Butcher, H., 2002. On the emplacement of sill complexes: evidence from the Faroe-Shetland Basin, in: Jolley, D.W., Bell, B.R. (Eds.), *The North Atlantic Igneous Province: Stratigraphy, Tectonic, Volcanic, Magmatic Processes*. Geological Society of London, Special publications, pp. 307–329.
- Berndt, C., Bunz, S., Mienert, J., 2003. Polygonal fault systems on the mid-Norwegian margin: a long-term source for fluid flow. *Geol. Soc. Lond. Spec. Publ.* 216, 283–290. doi:10.1144/GSL.SP.2003.216.01.18
- Berndt, C., Jacobs, C., Evans, A., Gay, A., Elliott, G., Long, D., Hitchen, K., 2012. Kilometre-scale polygonal seabed depressions in the Hatton Basin, NE Atlantic Ocean: Constraints on the origin of polygonal faulting. *Mar. Geol.* 332-334, 126–133. doi:10.1016/j.margeo.2012.09.013
- Berndt, C., Planke, S., Alvestad, E., Tsikalas, F., Rasmussen, T., 2001. Seismic volcanostratigraphy of the Norwegian Margin: constraints on the tectonomagmatic break-up process. *J. Geol. Soc.* 151, 413–426.
- Berner, R.A., 1980. *Early Diagenesis: A theoretical approach*. Princeton University Press.
- Binks, R.M., Fairhead, J.D., 1992. A plate tectonic setting for Mesozoic rifts of West and Central Africa. *Tectonophysics* 213, 141–151.
- Bjørlykke, K., Høeg, K., 1997. Effects of burial diagenesis on stresses, compaction and fluid flow in sedimentary basins. *Mar. Pet. Geol.* 14, 267–276.
- Blystad, P., Brekke, H., Færseth, R.B., Larsen, B.T., Skogseid, J.T., Tørrudbakken, B., 1995. Structural elements of the Norwegian margin. *Nor. Pet. Dir. Bull.* 8.
- Bøe, R., Hovland, M., Instanes, A., Rise, L., Vasshus, S., 2000. Submarine slide scars and mass movements in Karmsundet and Skudeneshavn, southwestern Norway: morphology and evolution. *Mar. Geol.* 167, 147–165.
- Bohrmann, G., Abelmann, A., Gersonde, R., Hubberten, H., Kuhn, G., 1994. Pure siliceous ooze, a diagenetic environment for early chert formation. *Geology* 22, 207–210.
- Bolton, A., Maltman, A., Clennell, M., 1998. The importance of overpressure timing and permeability evolution in fine grained sediments undergoing shear. *J. Struct. Geol.* 20, 1013 – 1022.
- Brekke, H., 2000. The tectonic evolution of the Norwegian Sea Continental Margin with emphasis on the Vøring and Møre Basins. *Geol. Soc. Lond. Spec. Publ.* 167, 327–378. doi:10.1144/GSL.SP.2000.167.01.13
- Brekke, H., Dahlgren, S., Nyland, B., Magnus, C., 1999. The prospectivity of the Vøring and Møre basins on the Norwegian Sea continental margin, in: *Petroleum Geology of Northwest Europe: Proceedings of the 5th Conference*. Geological Society of London, pp. 261–274.
- Brekke, H., Sjukstad, H.I., Magnus, C., Williams, R.W., 2001. Sedimentary environments offshore Norway—an overview, in: *Norwegian Petroleum Society Special Publications*. pp. 7–37.

- Broucke, O., Temple, F., Rouby, D., Robin, C., Calassou, S., Nalpas, T., Guillocheau, F., 2004. The role of deformation processes on the geometry of mud-dominated turbiditic systems, Oligocene and Lower–Middle Miocene of the Lower Congo basin (West African Margin). *Mar. Pet. Geol.* 21, 327–348. doi:10.1016/j.marpetgeo.2003.11.013
- Brown, A.R., 2004. Interpretation of three-dimensional seismic data, 6th ed, AAPG Memoir. American Association of Petroleum Geologists, Society of Exploration Geophysicists, Tulsa, OK.
- Brownfield, M.E., Charpentier, R.R., 2006. Geology and total petroleum systems of the West-Central Coastal province (7203), West Africa, U.S. Geological Survey Bulletin 2207-B. US Department of the Interior, US Geological Survey.
- Brown, L.F., Fisher, W.L., 1980. Seismic stratigraphic interpretation and petroleum exploration. AAPG Department of Education.
- Brun, J.-P., Fort, X., 2004. Compressional salt tectonics (Angolan margin). *Tectonophysics* 382, 129–150. doi:10.1016/j.tecto.2003.11.014
- Brunstad, H., Gradstein, F., Vergara, L., Lie, J.E., Hammer, Ø., 2008. A Revision of the Rogaland Group, Norwegian North Sea [WWW Document]. Nor. Stratigr. Lex. URL <http://nhm2.uio.no/norges/litho/rogaland.php> (accessed 6.5.14).
- Bryn, P., Berg, K., Forsberg, C.F., Solheim, A., Kvalstad, T.J., 2005. Explaining the Storegga Slide. *Mar. Pet. Geol.* 22, 11–19. doi:10.1016/j.marpetgeo.2004.12.003
- Bryn, P., Berg, K., Stoker, M.S., Haflidason, H., Solheim, A., 2005. Contourites and their relevance for mass wasting along the Mid-Norwegian Margin. *Mar. Pet. Geol.* 22, 85–96. doi:10.1016/j.marpetgeo.2004.10.012
- Bünz, S., Mienert, J., Berndt, C., 2003. Geological controls on the Storegga gas-hydrate system of the mid-Norwegian continental margin. *Earth Planet. Sci. Lett.* 209, 291–307. doi:10.1016/S0012-821X(03)00097-9
- Bürgmann, R., Pollard, D.D., Martel, S.J., 1994. Slip distributions on faults: effects of stress gradients, inelastic deformation, heterogeneous host-rock stiffness, and fault interaction. *J. Struct. Geol.* 16, 1675–1690.
- Burley, S.D., 1984. Patterns of diagenesis in the Sherwood Sandstone Group (Triassic), United Kingdom. *Clay Miner.* 19, 403–440.
- Burwood, R., 1999. Angola: source rock control for the Lower Congo Coastal and Kwanza Basin petroleum systems, in: Cameron, N.R., Bate, R.H., Clure, V.S. (Eds.), Oil and Gas Habitats of the South Atlantic. Geological Society of London, Special publications, London, pp. 181 – 194.
- Bussmann, I., Suess, E., 1998. Groundwater seepage in Eckernförde Bay (Western Baltic Sea): Effect on methane and salinity distribution of the water column. *Cont. Shelf Res.* 18, 1795–1806.
- Calassou, S., Moretti, I., 2003. Sedimentary flattening and multi-extensional deformation along the West African margin. *Mar. Pet. Geol.* 20, 71–82. doi:10.1016/S0264-8172(02)00134-4
- Carruthers, D., Cartwright, J., Jackson, M.P.A., Schutjens, P., 2013. Origin and timing of layer-bound radial faulting around North Sea salt stocks: New insights into the evolving stress state around rising diapirs. *Mar. Pet. Geol.* 48, 130–148. doi:10.1016/j.marpetgeo.2013.08.001
- Cartwright, J., 2011. Diagenetically induced shear failure of fine-grained sediments and the development of polygonal fault systems. *Mar. Pet. Geol.* 28, 1593–1610. doi:10.1016/j.marpetgeo.2011.06.004

- Cartwright, J.A., 1994a. Episodic basin-wide fluid expulsion from geopressured shale sequences in the North Sea basin. *Geology* 22, 447–450.
- Cartwright, J.A., 1994b. Episodic basin-wide hydrofracturing of overpressured Early Cenozoic mudrock sequences in the North Sea Basin. *Mar. Pet. Geol.* 11, 587–607.
- Cartwright, J.A., 1994c. Episodic basin-wide fluid expulsion from geopressured shale sequences in the North Sea basin. *Geology* 22, 447. doi:10.1130/0091-7613(1994)022<0447:EBWFEF>2.3.CO;2
- Cartwright, J.A., Dewhurst, D.N., 1998. Layer-bound compaction faults in fine-grained sediments. *Geol. Soc. Am. Bull.* 110, 1242–1257. doi:10.1130/0016-7606(1998)110<1242:LBCFIF>2.3.CO;2
- Cartwright, J.A., Lonergan, L., 1996. Volumetric contraction during the compaction of mudrocks: A mechanism for the development of regional-scale polygonal fault systems. *Basin Res.* 8, 183–193.
- Cartwright, J.A., Trudgill, B.D., Mansfield, C.S., 1995. Fault growth by segment linkage: an explanation for scatter in maximum displacement and trace length data from the Canyonlands Grabens of SE Utah. *J. Struct. Geol.* 17, 1319–1326.
- Cartwright, J., Bouroulliec, R., James, D., Johnson, H., 1998. Polycyclic motion history of some Gulf Coast growth faults from high-resolution displacement analysis. *Geology* 26, 819. doi:10.1130/0091-7613(1998)026<0819:PMHOSG>2.3.CO;2
- Cartwright, J., Huuse, M., 2005. 3D seismic technology: the geological “Hubble.” *Basin Res.* 17, 1–20. doi:10.1111/j.1365-2117.2005.00252.x
- Cartwright, J., Huuse, M., Aplin, A., 2007. Seal bypass systems. *AAPG Bull.* 91, 1141–1166. doi:10.1306/04090705181
- Cartwright, J., James, D., Bolton, A., 2003. The genesis of polygonal fault systems: a review. *Geol. Soc. Lond. Spec. Publ.* 216, 223–243. doi:10.1144/GSL.SP.2003.216.01.15
- Cartwright, J., Wattrus, N., Rausch, D., Bolton, A., 2004a. Recognition of an early Holocene polygonal fault system in Lake Superior: Implications for the compaction of fine-grained sediments. *Geology* 32, 253. doi:10.1130/G20121.1
- Cartwright, J., Wattrus, N., Rausch, D., Bolton, A., 2004b. Recognition of an early Holocene polygonal fault system in Lake Superior: Implications for the compaction of fine-grained sediments. *Geology* 32, 253. doi:10.1130/G20121.1
- Carver, R.E., 1968. Differential compaction as a cause of regional contemporaneous faults. *Am. Assoc. Pet. Geol. Bull.* 52, 414 – 419.
- Castelltort, S., Pochat, S., Van den Driessche, J., 2004a. How reliable are growth strata in interpreting short-term (10 s to 100 s ka) growth structures kinematics? *Comptes Rendus Geosci.* 336, 151–158. doi:10.1016/j.crte.2003.10.020
- Castelltort, S., Pochat, S., Van Den Driessche, J., 2004b. Using T-Z plots as a graphical method to infer lithological variations from growth strata. *J. Struct. Geol.* 26, 1425–1432. doi:10.1016/j.jsg.2004.01.002
- Chand, S., Rise, L., Knies, J., Haflidason, H., Hjelstuen, B.O., Bøe, R., 2011. Stratigraphic development of the south Vørings margin (Mid-Norway) since early Cenozoic time and its influence on subsurface fluid flow. *Mar. Pet. Geol.* 28, 1350–1363. doi:10.1016/j.marpgeo.2011.01.005

- Childs, C., Nicol, A., Walsh, J.J., Watterson, J., 2003. The growth and propagation of synsedimentary faults. *J. Struct. Geol.* 25, 633–648.
- Childs, C., Nicol, A., Walsh, J.J., Watterson, J., 1996. Growth of vertically segmented normal faults. *J. Struct. Geol.* 18, 1389–1397.
- Cladouhos, T.T., Marrett, R., 1996. Are fault growth and linkage models consistent with power-law distributions of fault length? *J. Struct. Geol.* 18, 281 – 293.
- Clausen, J.A., Gabrielsen, R.H., Reksnes, P.A., Nyseather, E., 1999. Development of intraformational (Oligocene - Miocene) faults in the northern North Sea: influence of remote stresses and doming of Fennoscandia. *J. Struct. Geol.* 21, 1457 – 1475.
- Cloos, E., 1955. Experimental analysis of fracture patterns. *Geol. Soc. Am. Bull.* 66, 241–256. doi:10.1130/0016-7606(1955)66[241:EAOFP]2.0.CO;2
- Cohen, H.A., McClay, K., 1996. Sedimentation and shale tectonics of the northwestern Niger Delta front. *Mar. Pet. Geol.* 13, 313–328.
- Cole, D., Stewart, S.A., Cartwright, J.A., 2000. Giant irregular pockmark craters in the Palaeogene of the outer Moray Firth basin, UK North Sea. *Mar. Pet. Geol.* 17, 563–577.
- Cosgrove, J.W., 1999. Forced folds and fractures: An introduction. *Geol. Soc. Lond. Spec. Publ.* 169, 1–6. doi:10.1144/GSL.SP.2000.169.01.01
- Cosgrove, J.W., Ameen, M.S., 1999. A comparison of the geometry, spatial organization and fracture patterns associated with forced folds and buckle folds. *Geol. Soc. Lond. Spec. Publ.* 169, 7–21. doi:10.1144/GSL.SP.2000.169.01.02
- Cosgrove, J.W., Hillier, R.D., 1999. Forced-fold development within Tertiary sediments of the Alba Field, UKCS: evidence of differential compaction and post-depositional sandstone remobilization. *Geol. Soc. Lond. Spec. Publ.* 169, 61–71. doi:10.1144/GSL.SP.2000.169.01.05
- Coward, M.P., Purdy, E.G., Ries, A.C., Smith, D.G., 1999. The distribution of petroleum reserves in basins of the South Atlantic margins, in: Cameron N.R., Bate R.H., & Clure V.S. (Eds) Oil and Gas Habitats of the South Atlantic. Geological Society of London, Special publications, pp. 101–131.
- Cowie, P.A., 1998. A healing-reloading feedback control on the growth rate of seismogenic faults. *J. Struct. Geol.* 20, 1075–1087.
- Cowie, P.A., Scholz, C.H., 1992a. Displacement-length scaling relationship for faults: data synthesis and discussion. *J. Struct. Geol.* 14, 1149–1156.
- Cowie, P.A., Scholz, C.H., 1992b. Physical explanation for the displacement-length relationship of faults using a post-yield fracture mechanics model. *J. Struct. Geol.* 14, 1133–1148.
- Cowie, P.A., Scholz, C.H., 1992c. Growth of faults by accumulation of seismic slip. *J. Geophys. Res. Solid Earth* 1978–2012 97, 11085–11095.
- Cowie, P.A., Shipton, Z.K., 1998. Fault tip displacement gradients and process zone dimensions. *J. Struct. Geol.* 20, 983 – 997.
- Cramez, C., Jackson, M.P.A., 2000. Superposed deformation straddling the continental-oceanic transition in deep-water Angola. *Mar. Pet. Geol.* 17, 1095–1109.
- Dalland, A., Worsley, D., Ofstad, K., 1995. A lithostratigraphic scheme for the Mesozoic and Cenozoic Succession offshore mid- and northern Norway. *Nor. Pet. Dir. Bull.* 4, 65.
- Davies, R., Bell, B.R., Cartwright, J.A., Shoulders, S., 2002. Three-dimensional seismic imaging of Paleogene dike-fed submarine volcanoes from the

- northeast Atlantic margin. *Geology* 30, 223. doi:10.1130/0091-7613(2002)030<0223:TDSIOP>2.0.CO;2
- Davies, R.J., Cartwright, J., 2002. A fossilized Opal A to Opal C/T transformation on the northeast Atlantic margin: support for a significantly elevated Palaeogeothermal gradient during the Neogene? *Basin Res.* 14, 467–486.
- Davies, R.J., Ireland, M.T., 2011. Initiation and propagation of polygonal fault arrays by thermally triggered volume reduction reactions in siliceous sediment. *Mar. Geol.* 289, 150–158. doi:10.1016/j.margeo.2011.05.005
- Davies, R.J., Ireland, M.T., Cartwright, J.A., 2009. Differential compaction due to the irregular topology of a diagenetic reaction boundary: a new mechanism for the formation of polygonal faults. *Basin Res.* 21, 354–359. doi:10.1111/j.1365-2117.2008.00389.x
- Davison, I., Alsop, I., Birch, P., Elders, C., Evans, N., Nicholson, H., Rorison, P., Wade, D., Woodward, J., Young, M., 2000. Geometry and late-stage structural evolution of Central Graben salt diapirs, North Sea. *Mar. Pet. Geol.* 17, 499 – 522.
- Dawers, N.H., Anders, M.H., 1995. Displacement-length scaling and fault linkage. *J. Struct. Geol.* 17, 607–614.
- Dehandschutter, B., Gaviglio, P., Sizun, J.P., Sintubin, M., Vandycke, S., Vandenberghe, N., Wouters, L., 2005a. Volumetric matrix strain related to intraformational faulting in argillaceous sediments. *J. Geol. Soc.* 162, 801–813. doi:10.1144/0016-764904-093
- Dehandschutter, B., Gaviglio, P., Sizun, J.P., Sintubin, M., Vandycke, S., Vandenberghe, N., Wouters, L., 2005b. Volumetric matrix strain related to intraformational faulting in argillaceous sediments. *J. Geol. Soc.* 162, 801–813. doi:10.1144/0016-764904-093
- Dewhurst, D.N., Cartwright, J.A., Lonergan, L., 1999. The development of polygonal fault systems by syneresis of colloidal sediments. *Mar. Pet. Geol.* 793 – 810.
- Dickinson, G., 1954. Subsurface interpretation of intersecting faults and their effects upon stratigraphic horizons. *AAPG Bull.* 38, 854–877.
- Doré, A.G., Lundin, E.R., Jensen, L.N., Birkeland, Ø., Eliassen, P.E., Fichler, C., 1999. Principal tectonic events in the evolution of the northwest European Atlantic margin, in: Geological Society, London, Petroleum Geology Conference Series. Geological Society of London, pp. 41–61.
- Droz, L., Rigaut, F., Cochonat, P., Tofani, R., 1996. Morphology and recent evolution of the Zaire turbidite system (Gulf of Guinea). *Geol. Soc. Am. Bull.* 108, 253–269.
- Dumke, I., Berndt, C., Crutchley, G.J., Krause, S., Liebetrau, V., Gay, A., Couillard, M., 2014. Seal bypass at the Giant Gjallar Vent (Norwegian Sea): Indications for a new phase of fluid venting at a 56-Ma-old fluid migration system. *Mar. Geol.* 351, 38–52. doi:10.1016/j.margeo.2014.03.006
- Duval, B., Cramez, C., Jackson, M.P.A., 1992. Raft tectonics in the Kwanza Basin, Angola. *Mar. Pet. Geol.* 9, 389–404.
- Dyer, R., 1988. Using joint interaction to estimate paleostress ratios. *J. Struct. Geol.* 10, 685 to 699.
- Eichenseer, H.T., Walgenwitz, F.R., Biondi, P.J., 1999. Stratigraphic control on facies and diagenesis of dolomitized oolitic siliciclastic ramp sequences (Pinda Group, Albian, offshore Angola). *AAPG Bull.* 83, 1729–1758.
- Eidvin, T., Bugge, T., Smelror, M., 2007. The Molo Formation, deposited by coastal progradation on the inner Mid-Norwegian continental shelf, coeval with the

- Kai Formation to the west and the Utsira Formation in the North Sea. *Nor. Geol. Tidsskr.* 87, 75.
- Eldholm, O., Thiede, J., Taylor, E., 1989. The Norwegian continental margin: Tectonic, volcanic, and paleoenvironmental framework, in: Proceedings of the Ocean Drilling Program, Scientific Results. pp. 5–26.
- Ellis, M.A., Dunlap, W.J., 1988. Displacement variation along thrust faults: implications for the development of large faults. *J. Struct. Geol.* 10, 183 – 192.
- Fabricius, I.L., 2007. Chalk: composition, diagenesis and physical properties. *Geol. Soc. Den. Bull.* 55, 97–128.
- Fader, G.B., 1991. Gas-related sedimentary features from the eastern Canadian continental shelf. *Cont. Shelf Res.* 11, 1123–1153.
- Ferrill, D.A., Morris, A.P., 2008. Fault zone deformation controlled by carbonate mechanical stratigraphy, Balcones fault system, Texas. *AAPG Bull.* 92, 359–380. doi:10.1306/10290707066
- Ferrill, D.A., Morris, A.P., 2001. Displacement gradient and deformation in normal fault systems. *J. Struct. Geol.* 23, 619–638.
- Ferrill, D.A., Stamatakos, J.A., Sims, D., 1999. Normal fault corrugation: implications for growth and seismicity of active normal faults. *J. Struct. Geol.* 21, 1027 – 1038.
- Folkestad, A., Steel, R.J., 2001. The alluvial cyclicity in HorneLEN Basin (Devonian western Norway) revisited: a multiparameter sedimentary analysis and stratigraphic implications, in: Norwegian Petroleum Society Special Publications. pp. 39–50.
- Fossen, H., Gabrielsen, R.H., 1996. Experimental modeling of extensional fault systems by use of plaster. *J. Struct. Geol.* 18, 673–687. doi:10.1016/S0191-8141(96)80032-0
- Fossen, H., Schultz, R.A., Rundhovde, E., Rotevatn, A., Buckley, S.J., 2010. Fault linkage and graben stepovers in the Canyonlands (Utah) and the North Sea Viking Graben, with implications for hydrocarbon migration and accumulation. *AAPG Bull.* 94, 597–613. doi:10.1306/10130909088
- Gay, A., Berndt, C., 2007. Cessation/reactivation of polygonal faulting and effects on fluid flow in the Voring Basin, Norwegian Margin. *J. Geol. Soc.* 164, 129–141. doi:10.1144/0016-76492005-178
- Gay, A., Lopez, M., Cochonat, P., Levaché, D., Sermondadaz, G., Seranne, M., 2006a. Evidences of early to late fluid migration from an upper Miocene turbiditic channel revealed by 3D seismic coupled to geochemical sampling within seafloor pockmarks, Lower Congo Basin. *Mar. Pet. Geol.* 23, 387–399. doi:10.1016/j.marpgeo.2006.02.004
- Gay, A., Lopez, M., Cochonat, P., Séranne, M., Levaché, D., Sermondadaz, G., 2006b. Isolated seafloor pockmarks linked to BSRs, fluid chimneys, polygonal faults and stacked Oligocene–Miocene turbiditic palaeochannels in the Lower Congo Basin. *Mar. Geol.* 226, 25–40. doi:10.1016/j.margeo.2005.09.018
- Gay, A., Lopez, M., Cochonat, P., Sermondadaz, G., 2004. Polygonal faults-furrows system related to early stages of compaction - upper Miocene to recent sediments of the Lower Congo Basin. *Basin Res.* 16, 101–116. doi:10.1111/j.1365-2117.2003.00224.x
- Gay, A., Lopez, M., Ondreas, H., Charlou, J.-L., Sermondadaz, G., Cochonat, P., 2006c. Seafloor facies related to upward methane flux within a Giant Pockmark of the Lower Congo Basin. *Mar. Geol.* 226, 81–95. doi:10.1016/j.margeo.2005.09.011

- Gernigon, L., Ringenbach, J.-C., Planke, S., Le Gall, B., 2004. Deep structures and breakup along volcanic rifted margins: insights from integrated studies along the outer Vøring Basin (Norway). *Mar. Pet. Geol.* 21, 363–372. doi:10.1016/j.marpetgeo.2004.01.005
- Gernigon, L., Ringenbach, J.C., Planke, S., Le Gall, B., Jonquet-Kolstø, H., 2003. Extension, crustal structure and magmatism at the outer Vøring Basin, Norwegian margin. *J. Geol. Soc.* 160, 197–208.
- Gier, S., Worden, R.H., Johns, W.D., Kurzweil, H., 2008. Diagenesis and reservoir quality of Miocene sandstones in the Vienna Basin, Austria. *Mar. Pet. Geol.* 25, 681–695. doi:10.1016/j.marpetgeo.2008.06.001
- Gómez, M., Vergés, J., Fernàndez, M., Torne, M., Ayala, C., Wheeler, W., Karpuz, R., 2004. Extensional geometry of the Mid Norwegian Margin before Early Tertiary continental breakup. *Mar. Pet. Geol.* 21, 177–194. doi:10.1016/j.marpetgeo.2003.11.017
- Goult, N.R., 2008. Geomechanics of polygonal fault systems: a review. *Pet. Geosci.* 14, 389–397. doi:10.1144/1354-079308-781
- Goult, N.R., 2001a. Mechanics of layer-bound polygonal faulting in fine-grained sediments. *J. Geol. Soc.* 159, 239–246. doi:10.1144/0016-764901-111
- Goult, N.R., 2001b. Polygonal fault networks in fine-grained sediments—an alternative to the syneresis mechanism. *First Break* 19, 69–73.
- Goult, N.R., Swarbrick, R.E., 2005. Development of polygonal fault systems: a test of hypotheses. *J. Geol. Soc.* 162, 587–590. doi:10.1144/0016-764905-004
- Gross, M.R., Bai, T., Wacker, M.A., Collinsworth, K.B., Behl, R.J., 1997. Influence of mechanical stratigraphy and kinematics on fault scaling relations. *J. Struct. Geol.* 19, 171–183.
- Grove, C., 2012. Submarine hydrothermal vent complexes in the Paleocene of the Faroe-Shetland Basin: Insights from three-dimensional seismic and petrographical data. *Geology* 41, 71–74. doi:10.1130/G33559.1
- Guiraud, R., Maurin, J.-C., 1992. Early Cretaceous rifts of Western and Central Africa: an overview. *Tectonophysics* 213, 153–168.
- Gupta, A., Scholz, C.H., 2000a. A model of normal fault interaction based on observations an theory. *J. Struct. Geol.* 22, 865–879.
- Gupta, A., Scholz, C.H., 2000b. Brittle strain regime transition in the Afar depression: Implications for fault growth and seafloor spreading. *Geology* 28, 1087–1090.
- Haflidason, H., Sejrup, H.P., Nygård, A., Mienert, J., Bryn, P., Lien, R., Forsberg, C.F., Berg, K., Masson, D., 2004. The Storegga Slide: architecture, geometry and slide development. *Mar. Geol.* 213, 201–234. doi:10.1016/j.margeo.2004.10.007
- Hansen, D.M., 2006. The morphology of intrusion-related vent structures and their implications for constraining the timing of intrusive events along the NE Atlantic margin. *J. Geol. Soc.* 163, 789–800. doi:10.1144/0016-76492004-167
- Hansen, D.M., Cartwright, J., 2006. The three-dimensional geometry and growth of forced folds above saucer-shaped igneous sills. *J. Struct. Geol.* 28, 1520–1535. doi:10.1016/j.jsg.2006.04.004
- Hansen, D.M., Cartwright, J., 2006. Saucer-shaped sill with lobate morphology revealed by 3D seismic data: implications for resolving a shallow-level sill emplacement mechanism. *J. Geol. Soc.* 163, 509–523. doi:10.1144/0016-764905-073

- Hansen, D.M., Cartwright, J.A., Thomas, D., 2004. 3D Seismic Analysis of the Geometry of Igneous Sills and Sill Junction Relationships. *Geol. Soc. Lond. Mem.* 29, 199–208. doi:10.1144/GSL.MEM.2004.029.01.19
- Hansen, D.M., Shimeld, J.W., Williamson, M.A., Lykke-Andersen, H., 2004. Development of a major polygonal fault system in Upper Cretaceous chalk and Cenozoic mudrocks of the Sable Subbasin, Canadian Atlantic margin. *Mar. Pet. Geol.* 21, 1205–1219. doi:10.1016/j.marpgeo.2004.07.004
- Hansen, J.P.V., Cartwright, J.A., Huuse, M., Clausen, O.R., 2005. 3D seismic expression of fluid migration and mud remobilization on the Gjallar Ridge, offshore mid-Norway. *Basin Res.* 17, 123–139. doi:10.1111/j.1365-2117.2005.00257.x
- Hasiotis, T., Papatheodorou, G., Kastanos, G., Ferentinos, G., 1996. A pockmark filed in the Patras Gulf (Greece) and its activation during the 14/7/93 seismic event. *Mar. Geol.* 130, 333 – 344.
- Heffernan, A.S., Moore, J.C., Bangs, N.L., Moore, G.F., Shipley, T.H., 2004. Initial Deformation in a Subduction Thrust System: Polygonal Normal Faulting in the Incoming Sedimentary Sequence of the Nankai Subduction Zone, Southwestern Japan. *Geol. Soc. Lond. Mem.* 29, 143–148. doi:10.1144/GSL.MEM.2004.029.01.14
- Heidbach, O., Tingay, M., Barth, A., Reinecker, J., Kurfeß, D., Müller, B., 2008. The World Stress Map. doi:10.1594/GFZ.WSM.Rel.2008
- Hein, J.R., Scholl, D.W., Barron, J.A., Jones, M.G., Miller, J., 1978. Diagenesis of late Cenozoic diatomaceous deposits and formation of the bottom simulating reflector in the southern Bering Sea. *Sedimentology* 25, 155–181.
- Henriet, J.P., De Batist, M., Van Vaerenburgh, W., Verschuren, M., 1989. Seismic facies and clay tectonic fatures of the Ypresian Clay in the southern North Sea. *Bull. Belg. Geol. Soc.* 97, 457 – 472.
- Henriet, J.P., De Batist, M., Verschuren, M., 1991. Early fracturing of Palaeogene clays, southernmost North Sea: relevance to mechanisms of primary hydrocarbon migration, in: Spencer A.M. (ed.) Generation, Accumulation and Production of Europe's Hydrocarbons, Special Publication of the European Association of Petroleum Geologists. pp. 217 – 227.
- Hesse, R., Schacht, U., 2011. Early Diagensis of Deep-Sea Sediments, in: Hunke, H., Mulder, T. (Eds.), *Deep-Sea Sediments, Developments in Sedimentology*. Elsevier, Amsterdam, pp. 557–714.
- Hibsch, C., Cartwright, J., Hansen, D.M., Gaviglio, P., Andre, G., Cushing, M., Bracq, P., Juignet, P., Benoit, P., Allouc, J., 2003. Normal faulting in chalk: tectonic stresses vs. compaction-related polygonal faulting. *Geol. Soc. Lond. Spec. Publ.* 216, 291–308. doi:10.1144/GSL.SP.2003.216.01.19
- Higgs, W.G., McClay, K.R., 1993. Analogue sandbox modelling of Miocene extensional faulting in the Outer Moray Firth. *Geol. Soc. Lond. Spec. Publ.* 71, 141–162. doi:10.1144/GSL.SP.1993.071.01.07
- Hjelstuen, B.O., Eldholm, O., Skogseid, J., 1997. Vøring Plateau diapir fields and their structural and depositional settings. *Mar. Geol.* 144, 33–57.
- Hjelstuen, B.O., Sejrup, H.P., Haflidason, H., Berg, K., Bryn, P., 2004. Neogene and Quaternary depositional environments on the Norwegian continental margin 62°N–68°N. *Mar. Geol.* 213, 257–276.
- Holbourn, A., Kuhnt, W., El Albani, A., Pletsch, T., Luderer, F., Wagner, T., 1999. Upper Cretaceous palaeoenvironments and benthonic foraminiferal

- assemblages of potential source rocks from the western African margin, Central Atlantic. *Geol. Soc. Lond. Spec. Publ.* 153, 195–222.
- Ho, S., Carruthers, D.T., Imbert, P., Cartwright, J.A., 2013. Spatial Variations in geometries of polygonal faults due to stress perturbations and interplay with fluid venting structures, in: *Sedimentary Basin Evolution*. Presented at the 75th EAGE Conference and Exhibition, London. doi:10.3997/2214-4909.20131054
- Ho, S., Cartwright, J.A., Imbert, P., 2012. Vertical evolution of fluid venting structures in relation to gas flux, in the Neogene-Quaternary of the Lower Congo Basin, Offshore Angola. *Mar. Geol.* 332-334, 40–55. doi:10.1016/j.margeo.2012.08.011
- Ho, S., Cartwright, J.A., Imbert, P., 2012. The Formation of Advancing Pockmarks Arrays: An Interplay between Hydrocarbon Leakage and Slope Sedimentation, in: *AAPG Annual Convention and Exhibition*.
- Hovland, M., Gardner, J.V., Judd, A.G., 2002. The significance of pockmarks to understanding fluid flow processes and geohazards. *Geofluids* 2, 127–136.
- Hovland, M., Heggland, R., De Vries, M.H., Tjelta, T.I., 2010. Unit-pockmarks and their potential significance for predicting fluid flow. *Mar. Pet. Geol.* 27, 1190–1199. doi:10.1016/j.marpetgeo.2010.02.005
- Hudec, M.R., Jackson, M.P., 2004. Regional restoration across the Kwanza Basin, Angola: Salt tectonics triggered by repeated uplift of a metastable passive margin. *AAPG Bull.* 88, 971–990.
- Hudec, M.R., Jackson, M.P., 2002. Structural segmentation, inversion, and salt tectonics on a passive margin: Evolution of the Inner Kwanza Basin, Angola. *Geol. Soc. Am. Bull.* 114, 1222–1244.
- Hudec, M.R., Jackson, M.P.A., 2007. Terra infirma: Understanding salt tectonics. *Earth-Sci. Rev.* 82, 1–28. doi:10.1016/j.earscirev.2007.01.001
- Hunt, D., Allsop, T., Swarbrick, R.E., 1996. Compaction as a primary control on the architecture and development of depositional sequences: conceptual framework, applications and implications. *Geol. Soc. Lond. Spec. Publ.* 104, 321–345. doi:10.1144/GSL.SP.1996.104.01.18
- Hustoft, S., Mienert, J., Bünz, S., Nouzé, H., 2007. High-resolution 3D-seismic data indicate focussed fluid migration pathways above polygonal fault systems of the mid-Norwegian margin. *Mar. Geol.* 245, 89–106. doi:10.1016/j.margeo.2007.07.004
- Imbert, P., 2009. Seismic-scale expression of fluid sourcing, circulation and expulsion in sedimentary series. Presented at the International Petroleum Technology Conference, Doha, Qatar.
- Ireland, M.T., Goult, N.R., Davies, R.J., 2011a. Influence of stratigraphic setting and simple shear on layer-bound compaction faults offshore Mauritania. *J. Struct. Geol.* 33, 487–499. doi:10.1016/j.jsg.2010.11.005
- Ireland, M.T., Goult, N.R., Davies, R.J., 2011b. Influence of stratigraphic setting and simple shear on layer-bound compaction faults offshore Mauritania. *J. Struct. Geol.* 33, 487–499. doi:10.1016/j.jsg.2010.11.005
- Ireland, M.T., Goult, N.R., Davies, R.J., 2010. Influence of pore water chemistry on silica diagenesis: evidence from the interaction of diagenetic reaction zones with polygonal fault systems. *J. Geol. Soc.* 167, 273–279. doi:10.1144/0016-76492009-049
- Ishii, E., Sanada, H., Iwatsuki, T., Sugita, Y., Kurikami, H., 2011. Mechanical strength of the transition zone at the boundary between opal-A and opal-CT zones in siliceous rocks. *Eng. Geol.* 122, 215–221. doi:10.1016/j.enggeo.2011.05.007

- Jackson, C.A.-L., 2012. Seismic reflection imaging and controls on the preservation of ancient sill-fed magmatic vents. *J. Geol. Soc.* 169, 503–506. doi:10.1144/0016-76492011-147
- Jackson, C.A.L., Carruthers, D.T., Mahlo, S.N., Briggs, O., 2014. Can polygonal faults help locate deep-water reservoirs? *AAPG Bull.* 98, 1717–1738. doi:10.1306/03131413104
- Jackson, C.A.L., Gawthorpe, R.L., Sharp, I.R., 2006. Style and sequence of deformation during extensional fault-propagation folding: examples from the Hammam Faraun and El-Qaa fault blocks, Suez Rift, Egypt. *J. Struct. Geol.* 28, 519–535. doi:10.1016/j.jsg.2005.11.009
- James, D.M.D., Goultby, N.R., Swarbrick, R.E., 2006. Discussion on development of polygonal fault systems: a test of hypotheses. *J. Geol. Soc.* 163, 221–223. doi:10.1144/0016-764905-111
- James, D.M.D., Watterson, J., Walsh, J.J., Nicol, A., Nell, P.A.R., Bretan, P.G., 2000. Discussion on geometry and origin of a polygonal fault system. *J. Geol. Soc.* 157, 1261 – 1264.
- Jamtveit, B., Svensen, H., Podaldchikov, Y.Y., Planke, S., 2004. Hydrothermal vent complexes associated with sill intrusions in sedimentary basins, in: Breitkreuz C., Petford, N. (eds). *Physical Geology of High-Level Magmatic Systems*. Geological Society of London, Special publications, London, pp. 233 – 241.
- Janes, D.M., Squyres, S.W., Bindschadler, D.L., Baer, G., Schubert, G., Sharpton, V.L., Stofan, E.R., 1992. Geophysical models for the formation and evolution of coronae on Venus. *J. Geophys. Res. Planets* 1991–2012 97, 16055 – 16067.
- Judd, A.G., Long, D., Sankey, M., 1994. Pockmark formation and activity, UK block 15/25, North Sea. *Bull Geol Soc Den.* 41, 34–49.
- Judd, A., Hovland, M., 2007. *Seabed Fluid Flow The Impact on Geology, Biology, and the Marine Environment*. Cambridge University Press.
- Karner, G.D., Driscoll, N.W., 1999. Tectonic and stratigraphic development of the West African and eastern Brazilian Margins: insights from quantitative basin modelling, in: Cameron N.R., Bate R.H., & Clure V.S. (Eds) *Oil and Gas Habitats of the South Atlantic*. Geological Society of London, Special publications, pp. 11 – 40.
- Karner, G.D., Driscoll, N.W., Barker, D.H.N., 2003. Syn-rift regional subsidence across the West African continental margin: the role of lower plate ductile extension. *Geol. Soc. Lond. Spec. Publ.* 207, 105–129.
- Karner, G.D., Driscoll, N.W., McGinnis, J.P., Brumbaugh, W.D., Cameron, N.R., 1997. Tectonic significance of syn-rift sediment packages across the Gabon-Cabinda continental margin. *Mar. Pet. Geol.* 14, 973–1000.
- Karner, G.D., Gamboa, L.A.P., 2007. Timing and origin of the South Atlantic pre-salt sag basins and their capping evaporites. *Geol. Soc. Lond. Spec. Publ.* 285, 15–35. doi:10.1144/SP285.2
- Karner, M., Keene, J.B., Gieskes, J.M., 1977. Diagenesis of siliceous oozes - I. Chemical controls on the rate of opal-A to opal-CT transformation - an experimental study. *Geochim. Cosmochim. Acta* 41, 1041 – 1059.
- Kearey, P., Brooks, M., Hill, I., 2002. *An Introduction to Geophysical Exploration*, 3rd ed. Blackwell Pub., Malden.
- Kim, Y.-S., Andrews, J.R., Sanderson, D.J., 2001. Reactivated strike-slip faults: examples from north Cornwall, UK. *Tectonophysics* 340, 173–194.

- Kim, Y.-S., Sanderson, D.J., 2005. The relationship between displacement and length of faults: a review. *Earth-Sci. Rev.* 68, 317–334. doi:10.1016/j.earscirev.2004.06.003
- Kominz, M.A., Patterson, K., Odette, D., 2011. Lithology Dependence of Porosity In Slope and Deep Marine Sediments. *J. Sediment. Res.* 81, 730–742. doi:10.2110/jsr.2011.60
- Kristensen, M.B., Childs, C.J., Korstgård, J.A., 2008. The 3D geometry of small-scale relay zones between normal faults in soft sediments. *J. Struct. Geol.* 30, 257–272. doi:10.1016/j.jsg.2007.11.003
- Kvalstad, T.J., Andresen, L., Forsberg, C.F., Berg, K., Bryn, P., Wangen, M., 2005. The Storegga slide: evaluation of triggering sources and slide mechanics. *Mar. Pet. Geol.* 22, 245–256. doi:10.1016/j.marpetgeo.2004.10.019
- Larson, R.L., Ladd, J.W., 1973. Evidence for the opening of the South Atlantic in the Early Cretaceous. *Nature* 246, 209 – 212.
- Laubach, S.E., Olson, J.E., Gross, M.R., 2009. Mechanical and fracture stratigraphy. *AAPG Bull.* 93, 1413–1426. doi:10.1306/07270909094
- Laubach, S.E., Schultz-Ela, D.D., Tyler, R., 1999. Differential compaction of interbedded sandstone and coal. *Geol. Soc. Lond. Spec. Publ.* 169, 51–60. doi:10.1144/GSL.SP.2000.169.01.04
- Laurent, D., Gay, A., Baudon, C., Berndt, C., Soliva, R., Planke, S., Mourguès, R., Lacaze, S., Pauget, F., Mangue, M., Lopez, M., 2012. High-resolution architecture of a polygonal fault interval inferred from geomodel applied to 3D seismic data from the Gjallar Ridge, Vørings Basin, Offshore Norway. *Mar. Geol.* 332-334, 134–151. doi:10.1016/j.margeo.2012.07.016
- Lavier, L.L., Steckler, M.S., Brigaud, F., 2001. Climatic and tectonic control on the Cenozoic evolution of the West African margin. *Mar. Geol.* 178, 63–80.
- Lima, R.D., De Ros, L.F., 2002. The role of depositional setting and diagenesis on the reservoir quality of Devonian sandstones from the Solimões Basin, Brazilian Amazonia. *Mar. Pet. Geol.* 19, 1047–1071. doi:10.1016/S0264-8172(03)00002-3
- Liu, J.-P., Pan, X., Tian, Z., Chen, Y., Wan, L., 2008. Petroleum geology and resources in West Africa: An overview. *Pet. Explor. Dev.* 35, 378–384.
- Lonergan, L., Cartwright, J.A., 1999. Polygonal faults and their influence on deep-water sandstone reservoir geometries, Alba Field, United Kingdom Central North Sea. *AAPG Bull.* 83, 410–432.
- Lonergan, L., Cartwright, J.A., Jolly, R., 1998. The geometry of polygonal fault systems in Tertiary mudrocks pf the North Sea. *J. Struct. Geol.* 20.
- Løseth, H., Henriksen, S., 2005. A Middle to Late Miocene compression phase along the Norwegian passive margin, in: *Petroleum Geology: North-West Europe and Global Perspectives – Proceedings of the 6th Petroleum Geology Conference*. Geological Society of London, pp. 845–859.
- Lundin, E., 1992. Thin-skinned extensional tectonics on a salt detachment, northern Kwanza Basin, Angola. *Mar. Pet. Geol.* 9, 405 – 411.
- Lundin, E., Doré, A.G., 2002. Mid-Cenozoic post-breakup deformation in the “passive”margins bordering the Norwegian–Greenland Sea. *Mar. Pet. Geol.* 19, 79–93.
- Lundin, E.R., Doré, A.G., 1997. A tectonic model for the Norwegian passive margin with implications for the NE Atlantic: Early Cretaceous to break-up. *J. Geol. Soc.* 154, 545–550.

- Luo, G., Nikolinakou, M.A., Flemings, P.B., Hudec, M.R., 2012. Geomechanical modeling of stress adjacent to salt bodies: Part 1 - Uncoupled models. *AAPG Bull.* 96, 43 – 64.
- Maerten, L., Gillespie, P., Pollard, D.D., 2002. Effects of local stress perturbation on secondary fault development. *J. Struct. Geol.* 24, 145 – 153.
- Maerten, L., Willemse, E.J., Pollard, D.D., Rawnsley, K., 1999. Slip distributions on intersecting normal faults. *J. Struct. Geol.* 21, 259–272.
- Magee, C., Duffy, O.B., Purnell, K., Bell, R.E., Jackson, C.A.-L., Reeve, M.T., 2015. Fault-controlled fluid flow inferred from hydrothermal vents imaged in 3D seismic reflection data, offshore NW Australia. *Basin Res.* n/a–n/a. doi:10.1111/bre.12111
- Magee, C., Jackson, C.A.-L., Schofield, N., 2014. Diachronous sub-volcanic intrusion along deep-water margins: insights from the Irish Rockall Basin. *Basin Res.* 26, 85–105. doi:10.1111/bre.12044
- Mandl, G., 1987. Tectonic deformation by rotating parallel faults: the “bookshelf” mechanism. *Tectonophysics* 141, 277–316.
- Mandl, G., Crans, W., 1981. Gravitational gliding in deltas. *Geol. Soc. Lond. Spec. Publ.* 9, 41–54. doi:10.1144/GSL.SP.1981.009.01.05
- Mansfield, C., Cartwright, J., 2001. Fault growth by linkage: observations and implications from analogue models. *J. Struct. Geol.* 23, 745–763.
- Mansfield, C.S., Cartwright, J.A., 1996. High resolution fault displacement mapping from three-dimensional seismic data: evidence for dip linkage during fault growth. *J. Struct. Geol.* 18, 249–263.
- Mansurbeg, H., Morad, S., Salem, A., Marfil, R., El-ghali, M.A.K., Nystuen, J.P., Caja, M.A., Amorosi, A., Garcia, D., La Iglesia, A., 2008. Diagenesis and reservoir quality evolution of palaeocene deep-water, marine sandstones, the Shetland-Faroes Basin, British continental shelf. *Mar. Pet. Geol.* 25, 514–543. doi:10.1016/j.marpgeo.2007.07.012
- Marrett, R., Allmendinger, R.W., 1991. Estimates of strain due to brittle faulting: sampling fault populations. *J. Struct. Geol.* 13, 735 – 738.
- Mascle, J., Phillips, J.D., 1972. Magnetic smooth zones in the South Atlantic. *Nature* 240, 80 – 84.
- McGinnis, J.P., Driscoll, N.W., Karner, G.D., Brumbaugh, W.D., Cameron, N., 1993. Flexural response of passive margins to deep-sea erosion and slope retreat: implications for relative sea-level change. *Geology* 21, 893–896.
- McGrath, A.G., Davison, I., 1995. Damage zone geometry around fault tips. *J. Struct. Geol.* 17, 1011 – 1024.
- Meadows, D., Davies, R.J., 2007. Morphological development of basin-scale silica diagenetic fronts revealed with 2D seismic reflection data: offshore Sakhalin, Russian Far East. *J. Geol. Soc.* 164, 1193–1206. doi:10.1144/0016-76492006-163
- Miles, A., Cartwright, J., 2010. Hybrid flow sills: A new mode of igneous sheet intrusion. *Geology* 38, 343–346. doi:10.1130/G30414.1
- Mitchum, R., Vail, P.R., Sangree, J.B., 1977. Seismic stratigraphy and global changes of sea level, Part 6: Stratigraphic interpretation of seismic reflection patterns in depositional sequences., in: Payne C.M (eds) *Seismic Stratigraphy: Application to Hydrocarbon Exploration*. American Association of Petroleum Geologists Memoir, pp. 117 – 133.

- Möller, N.K., Gjelberg, J.G., Martinsen, O., Charnock, M.A., Færseth, R.B., Sperrevik, S., Cartwright, J.A., 2004. A geological model for the Ormen Lange hydrocarbon reservoir. *Nor. J. Geol. Geol. Foren.* 84.
- Monnier, D., Imbert, P., Gay, A., Mourguès, R., Lopez, M., 2014. Pliocene sand injectites from a submarine lobe fringe during hydrocarbon migration and salt diapirism: a seismic example from the Lower Congo Basin. *Geofluids* 14, 1–19. doi:10.1111/gfl.12057
- Moore, G.F., Taira, A., Klaus, A., Becker, L., Boeckel, B., Cragg, B.A., Dean, A., Fergusson, C.L., Henry, P., Hirano, S., Hisamitsu, T., Hunze, S., Kastner, M., Maltman, A.J., Morgan, J.K., Murakami, Y., Saffer, D.M., Sánchez-Gómez, M., Scream, E.J., Smith, D.C., Spivack, A.J., Steurer, J., Tobin, H.J., Ujiie, K., Underwood, M.B., Wilson, M., 2001. New insights into deformation and fluid flow processes in the Nankai Trough accretionary prism: Results of Ocean Drilling Program Leg 190: DEFORMATION AND FLUID FLOW PROCESSES. *Geochem. Geophys. Geosystems* 2, n/a–n/a. doi:10.1029/2001GC000166
- Morad, S., Al-Ramadan, K., Ketzer, J.M., De Ros, L.F., 2010. The impact of diagenesis on the heterogeneity of sandstone reservoirs: A review of the role of depositional facies and sequence stratigraphy. *AAPG Bull.* 94, 1267–1309.
- Morad, S., Ketzer, J.R.M., De Ros, L.F., 2000. Spatial and temporal distribution of diagenetic alterations in siliciclastic rocks: implications for mass transfer in sedimentary basins. *Sedimentology* 47, 95–120.
- Moreau, J., Ghienne, J.F., Hurst, A., 2012. Kilometre-scale sand injectites in the intracratonic Murzuq Basin (South-west Libya): an igneous trigger? *Sedimentology* 59, 1321–1344. doi:10.1111/j.1365-3091.2011.01308.x
- Morley, C.K., 2007. Development of crestal normal faults associated with deepwater fold growth. *J. Struct. Geol.* 29, 1148–1163. doi:10.1016/j.jsg.2007.03.016
- Morley, C.K., 2003. Mobile shale related deformation in large deltas developed on passive and active margins, in: Van Rensbergen, P., Hilis, R.R., Maltman, A.J., Morley, C.K. (Eds.), *Subsurface Sediment Mobilization*, Special Publications. The Geological Society of London, London, pp. 335 – 357.
- Morris, A.P., Ferrill, D.A., McGinnis, R.N., 2009. Mechanical stratigraphy and faulting in Cretaceous carbonates. *AAPG Bull.* 93, 1459 – 1470.
- Moss, J.L., Cartwright, J., Moore, R., 2012. Evidence for fluid migration following pockmark formation: Examples from the Nile Deep Sea Fan. *Mar. Geol.* 303–306, 1–13. doi:10.1016/j.margeo.2012.01.010
- Munro, M.A., Blenkinsop, T.G., 2012. MARD—A moving average rose diagram application for the geosciences. *Comput. Geosci.* 49, 112–120. doi:10.1016/j.cageo.2012.07.012
- Muraoka, H., Kamata, H., 1983. Displacement distribution along minor fault traces. *J. Struct. Geol.* 5, 483–495.
- Naturhistorisk Museum, U.I.O., 2015. <http://www.nhm2.uio.no/norlex/stratchart.php> [WWW Document]. Nor. Interact. Offshore Stratigr. Lex.
- Neagu, R.C., Cartwright, J.A., Davies, R.J., Jensen, L., 2010a. Fossilisation of a silica diagenesis reaction front on the mid-Norwegian Margin. *Mar. Pet. Geol.* 27, 2141 – 2155.
- Neagu, R.C., Cartwright, J., Davies, R., 2010b. Measurement of diagenetic compaction strain from quantitative analysis of fault plane dip. *J. Struct. Geol.* 32, 641–655. doi:10.1016/j.jsg.2010.03.010

- Needham, D.T., Yielding, G., 1996. Fault population description and prediction using examples from the offshore U.K. *J. Struct. Geol.* 18, 155–167.
- Nelson, M.A., 2007. 3D geometry and kinematics of non-colinear fault intersections (Unpublished PhD Thesis). Cardiff University.
- Nicol, A., Walsh, J.J., Watterson, J., Gillespie, P.A., 1996a. Fault size distributions - are they really power law? *J. Struct. Geol.* 18, 191 – 197.
- Nicol, A., Walsh, J.J., Watterson, J., Nell, P.A.R., Bretan, P., 2003. The geometry, growth and linkage of faults within a polygonal fault system from South Australia. *Geol. Soc. Lond. Spec. Publ.* 216, 245–261. doi:10.1144/GSL.SP.2003.216.01.16
- Nicol, A., Watterson, J., Walsh, J.J., Childs, C., 1996b. The shapes, major axis orientations and displacement patterns of fault surfaces. *J. Struct. Geol.* 18, 235–248.
- Ode, H., 1957. Mechanical analysis of the dike pattern of the Spanish Peaks area, Colorado. *Geol. Soc. Am. Bull.* 58, 567 – 576.
- Omosanya, K.O., Alves, T.M., 2014. Mass-transport deposits controlling fault propagation, reactivation and structural decoupling on continental margins (Espírito Santo Basin, SE Brazil). *Tectonophysics* 628, 158–171. doi:10.1016/j.tecto.2014.04.045
- Osborne, M.J., Swarbrick, R.E., 1997. Mechanisms for generating overpressure in sedimentary basins: a reevaluation. *AAPG Bull.* 81, 1023–1041.
- Ostanin, I., Anka, Z., di Primio, R., Bernal, A., 2012. Identification of a large Upper Cretaceous polygonal fault network in the Hammerfest basin: Implications on the reactivation of regional faulting and gas leakage dynamics, SW Barents Sea. *Mar. Geol.* 332-334, 109–125. doi:10.1016/j.margeo.2012.03.005
- Peacock, D.C.P., 2001. The temporal relationship between joints and faults. *J. Struct. Geol.* 23, 329–341.
- Peacock, D.C.P., 1991. Displacement and segment linkage in strike-slip fault zones. *J. Struct. Geol.* 13, 721 – 733.
- Peacock, D.C.P., Sanderson, D.J., 1991. Displacements, segment linkage and relay ramps in normal fault zones. *J. Struct. Geol.* 13, 721–733.
- Peltonen, C., Marcussen, O., Bjorlykke, K., Jahren, J., 2008. Mineralogical control on mudstone compaction: a study of Late Cretaceous to Early Tertiary mudstones of the Voring and More basins, Norwegian Sea. *Pet. Geosci.* 14, 127–138. doi:10.1144/1354-079308-758
- Perrier, R., Quiblier, J., 1974. Thickness changes in sedimentary layers during compaction history; methods for quantitative evaluation. *AAPG Bull.* 58, 507–520.
- Pilcher, R., Argent, J., 2007. Mega-pockmarks and linear pockmark trains on the West African continental margin. *Mar. Geol.* 244, 15–32. doi:10.1016/j.margeo.2007.05.002
- Planke, S., Rasmussen, T., Rey, S.S., Myklebust, R., 2005a. Seismic characteristics and distribution of volcanic intrusions and hydrothermal vent complexes in the Vøring and Møre basins, in: Geological Society, London, Petroleum Geology Conference Series. Geological Society of London, pp. 833–844.
- Planke, S., Rasmussen, T., Rey, S.S., Myklebust, R., 2005b. Seismic characteristics and distribution of volcanic intrusions and hydrothermal vent complexes in the Vøring and Møre basins, in: Geological Society, London, Petroleum Geology Conference Series. Geological Society of London, pp. 833–844.

- Planke, S., Symonds, P.A., Alvestad, E., Skogseid, J., 2000. Seismic volcanostratigraphy of large-volume basaltic extrusive complexes on rifter margins. *J. Geophys. Res.* 105, 19335 – 19351.
- Poliakov, A.N.B., Podladchikov, Y.Y., Dawson, E.C., Talbot, C.J., 1996. Salt diapirism with simultaneous brittle faulting and viscous flow. *Geol. Soc. Lond. Spec. Publ.* 100, 291–302. doi:10.1144/GSL.SP.1996.100.01.19
- Poliakov, A.N.B., Van Balen, R., Podladchikov, Y., Daudre, B., Cloetingh, S., Talbot, C., 1993. Numerical analysis of how sedimentation and redistribution of surficial sediments affects salt diapirism. *Tectonophysics* 226, 199–216.
- Polteau, S., Mazzini, A., Galland, O., Planke, S., Malthe-Sørensen, A., 2008. Saucer-shaped intrusions: Occurrences, emplacement and implications. *Earth Planet. Sci. Lett.* 266, 195–204. doi:10.1016/j.epsl.2007.11.015
- Praeger, T., 2009. Heterogeneities in fine-grained slope systems and their impact on seal quality (Unpublished Ph. D Thesis). Cardiff University.
- Pratt, B.R., 1998. Syneresis cracks: subaqueous shrinkage in argillaceous sediments caused by earthquake-induced dewatering. *Sediment. Geol.* 117, 1–10.
- Price, N., Cosgrove, J., 1990. Analysis of Geological Structures. Cambridge University Press, Cambridge.
- Rawnsley, K.D., Rives, T., Petti, J.-P., Hencher, S.R., Lumsden, A.C., 1992. Joint development in perturbed stress fields near faults. *J. Struct. Geol.* 14, 939–951.
- Rippon, J.H., 1984. Contoured patterns of the throw and hade of normal faults in the Coal Measures (Westphalian) of north-east Derbyshire. *Proc. Yorks. Geol. Soc.* 45, 147–161. doi:10.1144/pygs.45.3.147
- Rise, L., Saettem, J., Fanavoll, S., Thorsnes, T., Ottesen, T.G., Bøe, R., 1999. Sea-bed pockmarks related to fluid migration from Mesozoic bedrock strata in the Skagerrak offshore Norway. *Mar. Pet. Geol.* 16, 619 – 631.
- Ritter, U., Zielinski, G.W., Weiss, H.M., Zielinski, R.L.B., Saettem, J., 2004. Heat flow in the Voring Basin, Mid-Norwegian Shelf. *Pet. Geosci.* 10, 353–365. doi:10.1144/1354-079303-616
- Roberts, D., 2003. The Scandinavian Caledonides: event chronology, palaeogeographic settings and likely modern analogues. *Tectonophysics* 365, 283–299. doi:10.1016/S0040-1951(03)00026-X
- Roberts, D.T., 2014. A geomechanical analysis of the formation and evolution of polygonal fault systems (Unpublished Ph. D Thesis). Cardiff University.
- Roche, V., Homberg, C., Rocher, M., 2012. Fault displacement profiles in multilayer systems: from fault restriction to fault propagation: Evolution of the fault displacement profile. *Terra Nova* 24, 499–504. doi:10.1111/j.1365-3121.2012.01088.x
- Rollet, N., McGiveron, S., Hashimoto, T., Hackney, R., Petkovic, P., Higgins, K., Grosjean, E., Logan, G.A., 2012. Seafloor features and fluid migration in the Capel and Faust basins, offshore eastern Australia. *Mar. Pet. Geol.* 35, 269–291. doi:10.1016/j.marpgeo.2012.03.011
- Rowan, M.G., Jackson, M.P., Trudgill, B.D., 1999. Salt-related fault families and fault welds in the northern Gulf of Mexico. *AAPG Bull.* 83, 1454–1484.
- Rusciadelli, G., Di Simone, S., 2007. Differential compaction as a control on depositional architectures across the Maiella carbonate platform margin (central Apennines, Italy). *Sediment. Geol.* 196, 133–155. doi:10.1016/j.sedgeo.2006.06.006

- Saller, A.H., 1996. Differential compaction and basinward tilting of the prograding capitan reef complex, Permian, west Texas and southeast New Mexico, USA. *Sediment. Geol.* 101, 21–30. doi:10.1016/0037-0738(95)00115-8
- Sapin, F., Ringenbach, J.-C., Rives, T., Pubellier, M., 2012. Counter-regional normal faults in shale-dominated deltas: Origin, mechanism and evolution. *Mar. Pet. Geol.* 37, 121–128. doi:10.1016/j.marpetgeo.2012.05.001
- Savoye, B., Babonneau, N., Dennielou, B., Bez, M., 2009. Geological overview of the Angola–Congo margin, the Congo deep-sea fan and its submarine valleys. *Deep Sea Res. Part II Top. Stud. Oceanogr.* 56, 2169–2182. doi:10.1016/j.dsr2.2009.04.001
- Schlumberger, 1999. GeoFrame Basic Seismic Interpretation using ISEX: Training and Exercise Guide.
- Scholz, C.H., Dawers, N.H., Yu, J.-Z., Anders, M.H., 1993. Fault Growth and Fault Scaling Laws: Preliminary Results. *J. Geophys. Res.* 98, 21951 – 21961.
- Schöpfer, M.P.J., Childs, C., Walsh, J.J., 2006. Localisation of normal faults in multilayer sequences. *J. Struct. Geol.* 28, 816–833. doi:10.1016/j.jsg.2006.02.003
- Schultz-Ela, D.D., Walsh, P., 2002. Modeling of grabens extending above evaporites in Canyonlands National Park, Utah. *J. Struct. Geol.* 24, 247–275.
- Schultz, R.A., 2000. Fault-population statistics at the Valles Marineris Extensional Province, Mars: implications for segment linkage, crustal strains and its geodynamical development. *Tectonophysics* 16, 169 – 193.
- Schultz, R.A., Fossen, H., 2002. Displacement-length scaling in three dimensions: importance of aspect ratio and application to deformation bands. *J. Struct. Geol.* 24, 1389– 1411.
- Seebeck, H., Tenthorey, E., Consoli, C., Nicol, A., 2015. Polygonal faulting and seal integrity in the Bonaparte Basin, Australia. *Mar. Pet. Geol.* 60, 120–135. doi:10.1016/j.marpetgeo.2014.10.012
- Segall, P., Pollard, D.D., 1980. Mechanics of discontinuous faults. *J. Geophys. Res.* 85, 4337 – 4350.
- Seranne, M., 1999. Early Oligocene stratigraphic turnover on west Africa continental margin: a signature of the Tertiary greenhouse to icehouse transition? *Terra Nova* 11.
- Séranne, M., Anka, Z., 2005. South Atlantic continental margins of Africa: A comparison of the tectonic vs climate interplay on the evolution of equatorial west Africa and SW Africa margins. *J. Afr. Earth Sci.* 43, 283–300. doi:10.1016/j.jafrearsci.2005.07.010
- Shin, H., 2009. Development of discontinuities in granular media. PhD Thesis Georgia Institute of Technology.
- Shin, H., Santamarina, J.C., Cartwright, J.A., 2010. Displacement field in contraction-driven faults. *J. Geophys. Res.* 115. doi:10.1029/2009JB006572
- Sibson, R.H., 2000. Fluid involvement in normal faulting. *J. Geodyn.* 29, 469–499.
- Skogseid, J., Planke, S., Faleide, J.I., Pedersen, T., Eldholm, O., Neverdal, F., 2000. NE Atlantic continental rifting and volcanic margin formation. *Geol. Soc. Lond. Spec. Publ.* 167, 295–326.
- Smallwood, J.R., Maresh, J., 2002. The properties, morphology and distribution of igneous sills: modelling, borehole data and 3D seismic from the Faroe-Shetland area. *Geol. Soc. Lond. Spec. Publ.* 197, 271–306. doi:10.1144/GSL.SP.2002.197.01.11

- Smith, G.N., Smith, I.G., 1998. Elements of Soil Mechanics. Blackwell Publishing, Oxford, UK.
- Solheim, A., Berg, K., Forsberg, C., Bryn, P., 2005. The Storegga Slide complex: repetitive large scale sliding with similar cause and development. *Mar. Pet. Geol.* 22, 97–107. doi:10.1016/j.marpetgeo.2004.10.013
- Soliva, R., Benedicto, A., 2005. Geometry, scaling relations and spacing of vertically restricted normal faults. *J. Struct. Geol.* 27, 317–325. doi:10.1016/j.jsg.2004.08.010
- Soliva, R., Benedicto, A., 2004. A linkage criterion for segmented normal faults. *J. Struct. Geol.* 26, 2251–2267. doi:10.1016/j.jsg.2004.06.008
- Sommaruga, A., Bøe, R., 2002. Geometry and subcropmaps of shallow Jurassic basins along the Mid-Norway coast. *Mar. Pet. Geol.* 19, 1029–1042.
- Soter, S., 1999. Macroscopic seismic anomalies and submarine pockmarks in the Corinth–Patras rift, Greece. *Tectonophysics* 308, 275–290.
- Spathopoulos, F., 1996. An insight on salt tectonics in the Angola Basin, South Atlantic. *Geol. Soc. Lond. Spec. Publ.* 100, 153–174. doi:10.1144/GSL.SP.1996.100.01.11
- Spinelli, G.A., Mozley, P.S., Tobin, H.J., Underwood, M.B., Hoffman, N.W., Bellew, G.M., 2007. Diagenesis, sediment strength, and pore collapse in sediment approaching the Nankai Trough subduction zone. *Geol. Soc. Am. Bull.* 119, 377–390.
- Spyropoulos, C., Griffith, W.J., Scholz, C.H., Shaw, B.E., 1999. Experimental Evidence for Different Strain Regimes of Crack Populations in a Clay Model. *Geophys. Res. Lett.* 26, 1081 – 1084.
- Squyres, S.W., Janes, D.M., Baer, G., Bindschadler, D.L., Schubert, G., Sharpton, V.L., Stofan, E.R., 1992. The morphology and evolution of coronae on Venus. *J. Geophys. Res. Planets* 1991–2012 97, 13611–13634.
- Stearns, D.W., 1978. Faulting and forced folding in the Rocky Mountains foreland. *Geol. Soc. Am. Mem.* 151, 1 – 38.
- Steen, Ø., Andresen, A., 1999. Effects of lithology on geometry and scaling of small faults in Traissic sandstones, East Greenland. *J. Struct. Geol.* 21, 1351 – 1368.
- Stewart, S.A., 2006. Implications of passive salt diapir kinematics for reservoir segmentation by radial and concentric faults. *Mar. Pet. Geol.* 23, 843 – 853. doi:10.1016/j.marpetgeo.2006.04.001
- Stewart, S.A., Argent, J.D., 2000. Relationship between polarity of extensional fault arrays and presence of detachments. *J. Struct. Geol.* 22, 693–711.
- Stofan, E.R., Bindschadler, D.L., Head, J.W., Parmentier, E.M., 1991. Corona structures on Venus: models of origin. *J. Geophys. Res. Planets* 1991–2012 96, 20933 – 20496.
- Storvoll, V., Bjørlykke, K., Mondol, N.H., 2005. Velocity-depth trends in Mesozoic and Cenozoic sediments from the Norwegian Shelf. *AAPG Bull.* 89, 359–381. doi:10.1306/10150404033
- Stuevold, L.M., Faerseth, R.B., Arnesen, L., Cartwright, J., Moller, N., 2003. Polygonal faults in the Ormen Lange Field, More Basin, offshore Mid Norway. *Geol. Soc. Lond. Spec. Publ.* 216, 263–281. doi:10.1144/GSL.SP.2003.216.01.17
- Sundby, B., 2006. Transient state diagenesis in continental margin muds. *Mar. Chem.* 102, 2–12. doi:10.1016/j.marchem.2005.09.016

- Sun, Q., Wu, S., Lü, F., Yuan, S., 2010. Polygonal faults and their implications for hydrocarbon reservoirs in the southern Qiongdongnan Basin, South China Sea. *J. Asian Earth Sci.* 39, 470–479. doi:10.1016/j.jseaes.2010.04.002
- Svensen, H., Jamtveit, B., Planke, S., Chevallier, L., 2006. Structure and evolution of hydrothermal vent complexes in the Karoo Basin, South Africa. *J. Geol. Soc.* 163, 671–682.
- Svensen, H., Planke, S., Chevallier, L., Malthe-Sørenssen, A., Corfu, F., Jamtveit, B., 2007. Hydrothermal venting of greenhouse gases triggering Early Jurassic global warming. *Earth Planet. Sci. Lett.* 256, 554–566. doi:10.1016/j.epsl.2007.02.013
- Svensen, H., Planke, S., Jamtveit, B., Pedersen, T., 2003. Seep carbonate formation controlled by hydrothermal vent complexes: a case study from the Vøring Basin, the Norwegian Sea. *Geo-Mar. Lett.* 23, 351–358. doi:10.1007/s00367-003-0141-2
- Svensen, H., Planke, S., Malthe-Sørenssen, P.T., Jamtveit, B., Myklebust, R., Rasmussen, T., Rey, S.S., 2004. Release of methane from a volcanic basin as a mechanism for initial Eocene global warming. *Nature* 429, 542–545. doi:10.1038/nature02575
- Svensen, H., Planke, S., Polozov, A.G., Schmidbauer, N., Corfu, F., Podladchikov, Y.Y., Jamtveit, B., 2009. Siberian gas venting and the end-Permian environmental crisis. *Earth Planet. Sci. Lett.* 277, 490–500. doi:10.1016/j.epsl.2008.11.015
- Swiecicki, T., Gibbs, P.B., Farrow, G.E., Coward, M.P., 1998. A tectonostratigraphic framework for the Mid-Norway region. *Mar. Pet. Geol.* 15, 245–276.
- Tari, G., Molnar, J., Ashton, P., 2003. Examples of salt tectonics from West Africa: a comparative approach, in: Cameron, N.R., Bate, R.H., Clure V.S. (Eds.), *Oil and Gas Habitats of the South Atlantic*. Geological Society of London, Special publications, London, pp. 85–104.
- Tewksbury, B.J., Hogan, J.P., Kattenhorn, S.A., Meertens, C.J., Tarabees, E.A., 2014. Polygonal faults in chalk: Insights from extensive exposures of the Khoman Formation, Western Desert, Egypt. *Geology* 42, 479–482. doi:10.1130/G35362.1
- Thiede, J., Myhre, A.M., 1996. 36. The palaeoceanographic history of the North Atlantic-Arctic gateways: synthesis of the Leg 151 drilling results, in: *Proceedings of the Ocean Drilling Program, Scientific Results*. pp. 645–658.
- Thyberg, B., Jordt, H., Bjørlykke, K., Faleide, J.I., 2000. Relationships between sequence stratigraphy, mineralogy and geochemistry in Cenozoic sediments of the northern North Sea. *Spec. Publ.-Geol. Soc. Lond.* 167, 245–272.
- Trude, J., Cartwright, J., Davies, R.J., Smallwood, J., 2003. New technique for dating igneous sills. *Geology* 31, 813. doi:10.1130/G19559.1
- Tuckwell, G.W., Lonergan, L., Jolly, R.J.H., 2003. The control of stress history and flaw distribution on the evolution of polygonal fracture networks. *J. Struct. Geol.* 25, 1241 – 1250.
- Uchupi, E., 1989. The tectonic style of the Atlantic Mesozoic rift system. *J. Afr. Earth Sci.* 8, 143–164.
- Valle, P.J., Gjelberg, J.G., Helland-Hansen, W., 2001. Tectonostratigraphic development in the eastern lower Congo Basin, offshore Angola, West Africa. *Mar. Pet. Geol.* 18, 909–927.
- Velde, B., 1996. Compaction trends of clay-rich deep sea sediments. *Mar. Geol.* 133, 193–201.

- Victor, P., Moretti, I., 2006. Polygonal fault systems and channel boudinage: 3D analysis of multidirectional extension in analogue sandbox experiments. *Mar. Pet. Geol.* 23, 777–789. doi:10.1016/j.marpetgeo.2006.06.004
- Walgenwitz, F., Pagel, M., Meyer, A., Maluski, H., Monie, P., 1990. Thermo-Chronological approach to reservoir diagenesis in the offshore Angola Basin: a fluid inclusion, 40Ar - 39Ar and K - Ar investigation. *Bull. Am. Assoc. Pet. Geol.* 74, 547 – 563.
- Walsh, J.J., Bailey, W.R., Childs, C., Nicol, A., Bonson, C.G., 2003a. Formation of segmented normal faults: a 3-D perspective. *J. Struct. Geol.* 25, 1251–1262.
- Walsh, J.J., Childs, C., Imber, J., Manzocchi, T., Watterson, J., Nell, P.A.R., 2003b. Strain localisation and population changes during fault system growth within the Inner Moray Firth, Northern North Sea. *J. Struct. Geol.* 25, 307–315.
- Walsh, J.J., Nicol, A., Childs, C., 2002. An alternative model for the growth of faults. *J. Struct. Geol.* 24, 1669–1675.
- Walsh, J.J., Watterson, J., 1989. Displacement gradients on fault surfaces. *J. Struct. Geol.* 11, 307–316.
- Walsh, J.J., Watterson, J., 1988. Analysis of the relationship between displacements and dimensions of faults. *J. Struct. Geol.* 10, 239–247.
- Walsh, J.J., Watterson, J., 1987. Distributions of cumulative displacement and seismic slip on a single normal fault surface. *J. Struct. Geol.* 9, 1039 – 1046.
- Watterson, J., Walsh, J.J., Nicol, A., Bretan, P.G., 2000. Geometry and origin of a polygonal fault system. *J. Struct. Geol.* 151 – 162.
- Watrus, N.J., Rausch, D.E., Cartwright, J., 2003. Soft-sediment deformation in Lake Superior: evidence for an immature Polygonal Fault System? *Geol. Soc. Lond. Spec. Publ.* 216, 323–334.
- White, R.S., Smallwood, J.R., Fliedner, M.M., Boslaugh, B., Maresh, J., Fruehn, J., 2003. Imaging and regional distribution of basalt flows in the Faeroe-Shetland Basin. *Geophys. Prospect.* 51, 215–231.
- Wibberley, C.A.J., Petit, J.-P., Rives, T., 2007. The effect of tilting on fault propagation and network development in sandstone-shale sequences: a case study from the Lodeve Basin, southern France. *J. Geol. Soc.* 164, 599–608. doi:10.1144/0016-76492006-047
- Wilkins, S.J., Gross, M.R., 2002. Normal fault growth in layered rocks at Split Mountain, Utah: influence of mechanical stratigraphy on dip linkage, fault restriction and fault scaling. *J. Struct. Geol.* 24, 1413 – 1429.
- Willemse, E.J., Pollard, D.D., Aydin, A., 1996. Three-dimensional analyses of slip distributions on normal fault arrays with consequences for fault scaling. *J. Struct. Geol.* 18, 295–309.
- Williams, S.R.J., 1987. Faulting in abyssal-plain sediments, Great Meteor East, Madeira Abyssal Plain. *Geol. Soc. Lond. Spec. Publ.* 31, 87–104. doi:10.1144/GSL.SP.1987.031.01.08
- Wilson, M.E.J., Hirano, S., Fergusson, C.L., Steurer, J., Underwood, M.E., 2003. 2. DATA REPORT: SEDIMENTOLOGICAL AND PETROGRAPHIC CHARACTERISTICS OF VOLCANIC ASHES AND SILICEOUS CLAYSTONES (ALTERED ASHES) FROM SITES 1173, 1174, AND 1177, LEG 190, in: Mikada, H., Moore, G.F., Taira, A., Becker, K., Moore, J.C., Klaus, A. (Eds.), *Proceedings of the Ocean Drilling Program, Scientific Results.* p. 196.
- Withjack, M.O., Scheiner, C., 1982. Fault patterns associated with domes - an experimental and analytical study. *AAPG Bull.* 66, 302 – 316.

- Worden, R.H., Burley, S.D., 2003. Sandstone diagenesis: from sand to stone, in: Burley S. D. & Worden R.H. (eds) Clastic Diagenesis: Recent and Ancient, Reprint Series of the International Association of Sedimentologists. Blackwell Pub., Oxford, UK, pp. 3–44.
- Worden, R.H., Morad, S., 2003. Clay minerals in sandstones: controls on formation distribution and evolution, in: Worden R.H. & Morad S. (eds) Clay Mineral Cements in Sandstones, Special Publication of the International Association of Sedimentologists. International Association of Sedimentologists, Oxford, UK, pp. 3 – 41.
- Xu, S., Hao, F., Xu, C., Wang, Y., Zou, H., Gong, C., 2015. Differential compaction faults and their implications for fluid expulsion in the northern Bohai Bay Basin, China. Mar. Pet. Geol. 63, 1–16. doi:10.1016/j.marpetgeo.2015.02.013
- Yielding, G., Needham, D.T., Jones, H., 1996. Sampling of fault populations using sub-surface data: a review. J. Struct. Geol. 18, 135 – 146.
- Yin, H., Groshong Jr., R.H., 2007. A three-dimensional kinematic model for the deformation above an active diapir. AAPG Bull. 91, 343 – 363.
- Zhao, F., Wu, S., Sun, Q., Huuse, M., Li, W., Wang, Z., 2014. Submarine volcanic mounds in the Pearl River Mouth Basin, northern South China Sea. Mar. Geol. 355, 162–172. doi:10.1016/j.margeo.2014.05.018
- Ziegler, P.A., 1988. Evolution of the Arctic-North Atlantic and the Western Tethys. AAPG Mem. 43, 164–196.
- Çifçi, G., Dondurur, D., Ergün, M., 2003. Deep and shallow structures of large pockmarks in the Turkish shelf, Eastern Black Sea. Geo-Mar. Lett. 23, 311–322. doi:10.1007/s00367-003-0138-x

Nad ydych yn gallu sglein yn turd ond gallwch ei rolio mewn glitter